https://ntrs.nasa.gov/search.jsp?R=19790001854 2020-03-22T02:30:35+00:00Z

NASA CR-152128

STUDY OF AERODYNAMIC TECHNOLOGY FOR A VSTOL FIGHTER/ATTACK AIRCRAFT

VOLUME I - UNCLASSIFIED

by J. R. Lummus

Prepared Under Contract NAS2-9769
by
General Dynamics
Fort Worth Division

for

AMES RESEARCH CENTER

NATIONAL AERONAUTICS AND SPACE ADMINISTRATION

1. Report No.	2. Government Accession No.	3. Recipient's Catalog No.
NASA CR-152128		

4. Title and Subtitle	5. Report Date
STUDY OF AERODYNAMIC TECHNOLOGY FOR VSTOL FIGHTER/ATTACK AIRCRAFT	May 1978
	6. Performing Organization Code
7. Author(s)	8. Performing Organization Report No.
J. R. Lummus	
	10. Work Unit No.
9. Performing Organization Name and Address General Dynamics/Fort Worth Division P. O. Box 748 Fort Worth, Texas 76101	11. Contract or Grant No. NAS2-9769
	13. Type of Report and Period Covered Contractor Final Report Nov 1, 77 - May 31, 78
12. Sponsoring Agency Name and Address NASA, Ames Research Center, Moffett Field,Ca 94035 David Taylor Naval Ship Research & Development Center, Bethesda, Md 20084	14. Sponsoring Agency Code

15. Supplementary Notes

Ames Research Center Technical Monitor - W.P. Nelms (415) 965-5855
NSRDC Point of Contact - R.L. Schaeffer (202) 227-1180

16. Abstract

An assessment has been made of the aerodynamic uncertainties associated with the design of a cold-deck-environment Navy VSTOL fighter/attack aircraft utilizing jet-diffuser ejectors for vertical lift and vectored-engine-over-wing blowing for supercirculation benefits. The critical aerodynamic uncertainties have been determined as those associated with the constraints which size the aircraft to a specified set of requirements. A wind tunnel model and test programs are recommended for resolving these uncertainties.

17. Key Words (Suggested by Author(s))	18. Distribution Statement
EJECTOR, Vectored-Engine-Over Wing, VSTOL, SUPERCIRCULATION, POWERED LIFT	

19. Security Classif. (of this report)	20. Security Classif. (of this page)	21. No. of Pages	22. Price*
Unclassified	Unclassified		

*For sale by the National Technical Information Service, Springfield, Virginia 22161

FOREWORD

The Study of Aerodynamic Technology for VSTOL Fighter/Attack Aircraft was conducted by General Dynamics' Fort Worth Division under NASA AMES Research Center Contract NASA2-9769. The contract monitor was Mr. W. P. Nelms of NASA Ames. The overall objective of this study was to assess the aerodynamic uncertainties associated with designing a Navy VSTOL ejector/vectored-engine-over-wing (VEO-Wing) fighter/attack aircraft. This volume (Volume I) of a two-volume final report contains unclassified data; Volume II contains General Dynamics proprietary data.

The study was conducted within the Fort Worth Division's Aerodynamics Section, with Mr. J. R. Lummus serving as Program Manager. The author wishes to acknowledge the assistance provided by Mr. Nelms of NASA Ames and by R. G. Bradley, D. Lobrecht, W. H. Foley, C. B. Snyder, G. T. Joyce, and H. J. Sherrer of General Dynamics.

TABLE OF CONTENTS

		PAGE
1.	SUMMARY	1
2.	INTRODUCTION	2
	2.1 Background	2
	2.2 Study Objectives	2
	2.3 Concept Selection	3
	2.4 Study Plan	5
3.	AIRCRAFT DESCRIPTION	14
	3.1 Design Philosophy	14
	3.2 Sizing Groundrules	19
	3.3 Physical Description	20
4.	AERODYNAMIC CHARACTERISTICS	31
	4.1 Longitudinal Aerodynamics	31
	4.1.1 Minimum Drag Buildup	36
	4.1.2 Lift, Drag, and Pitching Moment Estimates Including Trim Effects	40
	4.1.3 Stability Analysis	83
	4.1.4 High Lift Characteristics	91
	4.1.5 Control Schemes and Effectiveness	94
	4.2 Lateral Directional Characteristics	98
	4.3 Propulsion Induced Effects	104
	4.3.1 Induced Aerodynamics	104
	4.3.2 Reingestion Losses	108
	4.3.3 Footprints	108
5.	PROPULSION CHARACTERISTICS	110
	5.1 System Description	110
	5.2 System Performance	113
	5.3 Installation Losses	115
	5.4 Jet Diffuser Ejector	122
	5.5 Reaction Controls	129

TABLE OF CONTENTS, (Continued)

		PAGE
6.	AIRCRAFT DESIGN	133
	6.1 Mass Properties	133
	6.2 Structural Design	138
	6.3 Flight Controls	140
	6.3.1 Conceptual Design	140
	6.3.2 Physical Design	142
	6.4 Crew Station and Escape System	143
	6.5 Subsystems	145
	6.5.1 Avionics Subsystem	145
	6.5.1.1 Architecture	148
	6.5.1.2 Functional Descriptions	150
	6.5.1.3 Packaging	153
	6.5.1.4 Environmental Control	154
	6.5.2 Vehicle Equipment and Power	154
7.	AIRCRAFT PERFORMANCE	161
	7.1 Aircraft Sizing	161
	7.2 Mission Performance	165
	7.3 Combat Performance	165
	7.4 VTO Transition Studies	165
	7.5 STOL Takeoff Performance	176
	7.6 Single Engine Recovery	190
	7.7 Design Sensitivities and Tradeoffs	190
8.	AERODYNAMIC UNCERTAINTIES	208
	8.1 Selection	208
	8.2 Description	211
9.	PROPOSED RESEARCH PROGRAM	216
10.	CONCLUSIONS	224
11.	REFERENCES	227
12.	APPENDICES	230
	A. VEO/RALS VSTOL Fighter/Attack Aircraft Concept	231
	B. Aero-Only Aerodynamic Coefficients Predictions	234

LIST OF FIGURES

Figure		Page
2-1	VEO-Wing Development Program	4
2-2	E205 Three-View Drawing	6
2-3	R104 Three-View Drawing	7
2-4	Ejector Configuration in VTOL Mode	8
2-5	Ejector Configuration in Cruise Mode	9
2-6	RALS Configuration in Cruise Mode	10
2-7	Study Plan	11
3-1	VEO-Wing Fighter Concept	15
3-2	VEO-Wing Drag-Polar Improvements	16
3-3	VEO-Wing Experimental Data Base	17
3-4	3/4-Scale Powered VEO-Wing Fighter Model	18
3-5	DLI Mission Profile	21
3-6	E205 Inboard Profile	22
3-7	External Store Locations	25
3-8	E205 Cross-Sectional Area Distribution	29
4-1	Longitudinal Forces Acting on E205	32
4-2	E205 Minimum Trimmed Drag Versus Mach Number	37
4-3	Store Drag Increments for DLI Mission	38
4-4	STOL Store Loading	39
4-5	VSTOL Aerodynamic Data, Aero-Only	
	a. coefficients power off, $\delta_F = 0^o$, Mach = .4	41
	b. coefficients power off, $\delta_F = 15^o$, Mach = .4	43
	c. coefficients power off, $\delta_F = 30^o$, Mach = .4	45
	d. C_T (total) = 2.0, C_T(VEO-wing nozzle) = 2.0, C_T (ejector) = 0, $\delta_F = 0^o$, Mach = .13	47
	e. C_T (total) = 2.0, C_T (VEO-wing nozzle)= 2.0, C_T (ejector) = 0, $\delta_F = 15^o$, Mach = .105	49
	f. C_T (total) = 2.0, C_T(VEO-wing nozzle) = 2.0, C_T (ejector) = 0, $\delta_F = 30^o$, Mach = .10	51
	g. C_T (total) = 5.0, C_T(VEO-wing nozzle) = 5.0, C_T (ejector) = 0, $\delta_F = 0^o$, Mach = .09	53
	h. C_T (total) = 5.0, C_T(VEO-wing nozzle) = 5.0, C_T (ejector) = 0, $\delta_F = 15^o$, Mach = .08	55
	i. coefficients, C_T (total) = 5.0, C_T (VEO-wing nozzle) = 5.0, C_T (ejector) = 0, $\delta_F = 30^o$, Mach = .09	57

LIST OF FIGURES (CONT'D)

Figure		Page
4-6	VSTOL Aerodynamic Data, Equivalent	
	a. Coefficients, C_T(total) = 2.0, C_T(VEO-wing nozzle) = 2.0, C_T(ejector) = 0 , $\delta_F = 0^o$, Mach = .13	59
	b. Coefficients, C_T(total) = 3.0, C_T(VEO-wing nozzle) = 2.0, C_T(ejector) = 1.0, $\delta_F = 15^o$, Mach = .105	61
	c. Coefficients, C_T(total) = 3.7, C_T(VEO-wing nozzle) = 2.0, C_T(ejector) = 1.7 $\delta_F = 30^o$, Mach = .10	63
	d. Coefficients, C_T(total) = 5.0, C_T(VEO-wing nozzle) = 5.0, C_T(ejector) = 0, $\delta_F = 0^o$, Mach = .09	65
	e. Coefficients, C_T(total) = 7.4, C_T(VEO-wing nozzle) = 5.0, C_T(ejector) = 2.4, $\delta_F = 15^o$, Mach = .08	67
4-7	VSTOL Aerodynamics Data, Total	
	a. Coefficients, C_T(total) = 2.0, C_T(VEO-wing nozzle) = 2.0, C_T(ejector) = 0, $\delta_F = 0^o$, Mach = .13	69
	b. Coefficients, C_T(total) = 3.0, C_T(VEO-wing nozzle) = 2.0, C_T(ejector) = 1.0, $\delta_F = 15^o$, Mach = .105	71
	c. Coefficients, C_T(total) = 3.7, C_T(VEO-wing nozzle) = 2.0, C_T(ejector) = 1.7, $\delta_F = 30^o$, Mach = .10	73
	d. Coefficients, C_T(total) = 5.0, C_T(VEO-wing nozzle) = 5.0, C_T(ejector) = 0, $\delta_F = 0^o$, Mach = .09	75
	e. Coefficients, C_T(total) = 7.4, C_T(VEO-wing nozzle) = 5.0 C_T(ejector) = 2.4, $\delta_F = 15^o$, Mach = .09	77

LIST OF FIGURES (CONT'D)

Figure		Page
4-8	VSTOL Trimmed Lift Curve, Aerodynamic Plus Ejector Trim	80
4-9	VEO-Wing Trim Method for Maneuver	81
4-10	E205 Trimmed Span Efficiency	82
4-11	E205 Trimmed Cruise/Maneuver Drag Polars	84
4-12	a. E205 Lift and Pitching Moment Curves at M = 1.2 with Canard Deflection	85
	b. E205 Drag Polars at M = 1.2 with Canard Deflection.	86
4-13	a. E205 Lift and Pitching Moment Curves at M = 1.6 with Canard Deflection	87
	b. E205 Drag Polars at M = 1.6 with Canard Deflection.	88
4-14	Aerodynamic Center Test/Theory Correlation	89
4-15	E205 Predicted Aerodynamic Center	90
4-16	E205 Trimmed $C_{L_{Max}}$ vs Mach No.	93
4-17	E205 Buffet-Onset Angle of Attack	96
4-18	E205 Hover-Control Thrusting Devices	97
4-19	E205 Lateral-Directional Characteristics	
	a. C_{Y_β} vs α and Mach No.	99
	b. C_{n_β} vs α and Mach No.	100
	c. C_{l_β} vs α and Mach No.	101
	d. Vertical-Tail Effectiveness	102
	e. Aileron Effectiveness	103

LIST OF FIGURES (CONT'D)

Figure		Page
4-20	E205 Propulsion-Induced Normal Force and Pitching Moment in Ground Effect	106
4-21	Variation of E205 Ejector Augmentation Ratio with Ground Height	107
4-22	Ground Temperature Footprints	109
4-23	Ground Velocity Footprints	109
4-24	Deck Pressure Footprints	109
5-1	Typical Operating Modes of VEO-Wing Two-Dimensional Wedge/CD Nozzle	111
5-2	Jet Turning Angle vs Geometric Nozzle Deflection for VEO-Wing Two-Dimensional Wedge/CD Nozzle	112
5-3	Baseline Inlet and Nozzle Definition	114
5-4	Estimated Inlet Pressure Recovery	117
5-5	Estimated Inlet Spillage Drag Coefficient	118
5-6	Measured Nozzle Pressure Drag on VEO-Wing Conceptual Model	120
5-7	External Nozzle Boattail Drag Increments	121
5-8	Jet-Diffuser Ejector Design	123
5-9	AJDE Augmentation Ratio Performance	124
5-10	Variable-Area Primary Ejector Nozzles	126
5-11	Packaging Scheme for Jet-Diffuser Ejector	128
5-12	General Dynamics Ejector Model Geometry	130
5-13	Reaction Control System Thrust Requirements for Variations in VTOGW	132

LIST OF FIGURES (CONT'D)

Figure		Page
6-1	Functional Longitudinal Control Schematic	141
6-2	Avionic Weights Forecast	147
6-3	Digital Hardware Weight Reduction	147
6-4	Subsystem Integration	149
6-5	Advanced Digital System Architecture	149
6-6	Avionics Packaging Concept	155
7-1	Aircraft/Engine Sizing Carpet, E205	162
7-2	Specific Excess Power, P_S vs	
	a. Sustained Normal Load Factor, N_Z, Altitude = 10,000 ft	167
	b. Sustained Normal Load Factor, N_Z, Altitude = 20,000 ft	168
	c. Sustained Normal Load Factor N_Z, Altitude = 30,000 ft	169
7-3	Max A/B Flight Envelope	170
7-4	VTO Transition Flight Profile Segments	171
7-5	Schedules of Engine Airflow Split vs VEO Nozzle Deflection for Max Axial Thrust	172
7-6	Ejector Configuration E205 VTO Transition Time Histories	173
7-7	Control System Models for STOL Analysis	177
7-8	Deck Edge Relative (Inertial) Velocity Requirements for Desired Lift-Off Conditions	179

LIST OF FIGURES (CONT'D)

Figure		Page
7-9	Approximate Deck Run Velocity Profiles Requirements for Desired Lift-Off Conditions	180
7-10	Comparison of (STO) Takeoff Methods Studied	182
7-11	E205 Deck Run Requirements for Conventional VEO STOL Takeoff Method	184
7-12	E205 Deck Run Requirements for VTO/VEO-Wing STOL Takeoff Method	185
7-13	Climb Out Corridor for VTO/VEO-Wing STO Takeoff Method	186
7-14	After-Deck-Edge STO Time History for Conventional VEO-Wing Takeoff Method	187
7-15	Flight Trajectory After Lift-Off for Conventional VEO Takeoff Method	189
7-16	Single-Engine-Out Minimum Lateral Control Speeds	191
7-17	Sizing Carpet with 5% Increased Fuel Flow	192
7-18	Landing Gear Length Sensitivity	195
7-19	SFC Sensitivity	196
7-20	Engine Thrust-to-Weight-Ratio Sensitivity	197
7-21	Minimum Drag Sensitivity	198
7-22	Trim Drag Sensitivity	199
7-23	Span Efficiency (e) Sensitivity	200
7-24	DLI Mission Radius Sensitivity	201
7-25	Specific Excess Power Sensitivity, P_S, at Mach 0.9, 10,000 ft	202

LIST OF FIGURES (CONT'D)

Figure		Page
7-26	Sustained Load Factor Sensitivity, N_Z at Mach 0.6, 10,000 ft	203
7-27	Acceleration Time Sensitivity, Time from Mach 0.8 to 1.6, 35,000 ft	204
7-28	Sensitivities to Max A/B, S.L., Static, Uninstalled Thrust/Weight Required for Hover in Ground Effect	205
7-29	Dry Weight Sensitivity	207
9-1	Approach for Simulating the RALS Configuration for Use of the E205 Wind Tunnel Model	221
BB-1	Power-Off Wing Body Life, Drag, and Pitching Moment Characteristics for the VEO-Wing fighter model of Reference 4	236
BB-2	Supercirculation Lift, Drag, and center-of-Pressure-Location Increments due to Veo-Wing Flap Deflection and Blowing from General Dynamics' Powered Research Model of Reference 3	
	a. ΔC_{L_Γ} vs C_T, $\delta_{T_E} = 0^\circ$	237
	b. ΔC_{D_Γ} vs C_T, $\delta_{T_E} = 0^\circ$	237
	c. ΔC_{L_Γ} vs C_T, $\delta_{T_E} = 15^\circ$	238
	d. ΔC_{D_Γ} vs C_T, $\delta_{T_E} = 15^\circ$	238
	e. $\bar{X} C_{P_\Gamma}$ vs C_T, $\delta_{T_E} = 15^\circ$	238
	f. ΔC_{L_Γ} vs C_T, $\delta_{T_E} = 30^\circ$	239
	g. ΔC_{D_Γ} vs C_T, $\delta_{T_E} = 30^\circ$	239
	h. $\bar{X} C_{P_\Gamma}$ vs C_T, $\delta_{T_E} = 30^\circ$	239

LIST OF FIGURES (CONT'D)

Figure		Page
BB-2	Supercirculation Lift, Drag, and Center-of-Pressure-Location Increments due to VEO-Wing Flap Deflection and Blowing from General Dynamic's Powered Research Model of Reference 3 — with Spanwise Blowing	
	i. ΔC_{L_Γ} vs C_T, $\delta_{T_E} = 30^\circ$	240
	j. $\overline{X}C_{P_\Gamma}$ vs C_T, $\delta_{T_E} = 30^\circ$	240
BB-3	Lift, Drag, and Pitching-Moment Increments due to Canard Deflection from General Dynamics' Powered Research Model of Reference 3.	
	a. $\Delta C_{L_{Canard}}$ vs δ_C	241
	b. $\Delta C_{D_{Canard}}$ vs δ_C	241
	c. $\Delta C_{M_{Canard}}$ vs δ_C	241

LIST OF TABLES

Table		Page
2-1	Sized Ejector Aircraft (E205) Performance Summary	13
3-1	Dimensional and Design Data for Ejector E205 Configuration	26
3-2	E205 Center-of-Gravity Locations	30
4-1	Methods Summary	33
4-2	E205 Minimum Trimmed Drag Buildup	35
4-3	E205 Control Rates In and Out of Ground Effect	95
4-4	Ejector Efflux Exit Conditions	108
5-1	Pratt & Whitney 325-25-2800 Parametric Engine Installed Performance Data, ESF=1.0	116
6-1	E205 Mass Properties Summary	134
6-2	E205 Weight Statement	135
6-3	E205 Materials Breakdown	136
6-4	E205 Weight Sensitivity Derivatives	137
6-5	Avionics Predictions for VSTOL-B Projected to 1995	146
7-1	Sized Ejector Airplane Characteristics	164
7-2	Mission Segment Performance	166
7-3	Summary of VTO Transition Cases Studied	175
8-1	Aerodynamic Parameters Associated with Various Airplane Requirements	209

LIST OF TABLES, (Continued)

Table		Page
8-2	Sizing Constraints for Various Airplane Requirements	210
9-1	Proposed Wind Tunnel Test Program	222
AA-1	RALS Sized Airplane Characteristics	232
AA-2	Comparison of DLI Mission Fuel Usage for RALS and Ejector Configurations	233

LIST OF SYMBOLS

A	axial force, lb (N)
A_o	ejector primary + wall nozzle area, in.^{2} (cm^2)
A_2	ejector throat area, in.^{2} (cm^2)
a.c.	aerodynamic center, $\%\bar{c}$
AR	aspect ratio
b	span, in. (m)
$\bar{c}$, MAC	mean aerodynamic chord, in. (m)
$C_{A_{ejector}}$	axial force coefficient due to ejector
C_D	drag coefficient
$C_{D_{AERO}}$	aero-only drag coefficient (no thrust increments included)
$C_{D_{min}}$	minimum drag coefficient
C_{D_E}	equivalent drag coefficient
$C_{D_{RAM}}$	ram-drag coefficient (engine inlet)
C_{D_t}	total drag coefficient
C_L	lift coefficient
$C_{L_{buffet}}$	buffet-onset lift coefficient
$C_{L_{max}}$	maximum-lift coefficient
$C_{L_{aero}}$	aero-only lift coefficient (no thrust increments included)
C_{L_E}	equivalent lift coefficient
C_{L_t}	total lift coefficient
C_{N_I}	propulsion-induced normal-force coefficient, $\frac{\Delta N}{T}$

LIST OF SYMBOLS, (Continued)

$C_{M_{X\bar{c}}}$	pitching moment about X percent $\bar{c}$
C_{M_I}	propulsion-induced pitching-moment coefficient, $\frac{\Delta M}{T\bar{c}}$
C_{M_O}	zero-lift pitching-moment coefficient
C_{M_E}	equivalent pitching-moment coefficient
C_R	root chord
C_{R_I}	propulsion-induced rolling moment coefficient, $\frac{RM}{Tb}$
C_T	thrust coefficient, $\frac{T}{qS_{REF}}$
c_t	tip chord
CMU, C_μ	ideal thrust coefficient, $\dot{w}\ Vj/gqS_{REF}$
D	drag, lb(N)
D_E	equivalent diameter of circle having area equal to total ejector throat area, ft(m)
e	span efficiency factor
ESF	engine scale factor, $\frac{T}{T_{ESF} = 1.0}$
G	main landing gear length, ft(m), with oleo extended for VTO = 5.71 ft(trunion to ground = H - .5 ft.)
H	height of ejector flap trailing edges above the ground, ft(m)
IGE	in ground effect

L	lift, lb(N)
L_R	reaction lift, lb(N)
L_Γ	lift due to supercirculation lb(N)
L_o	power-off lift, lb(N)
M	Mach number
M	pitching moment ft lb(NM)
NPR	nozzle pressure ratio, $\frac{\text{Total Pressure}}{P_\infty}$
N	normal force, lb(kg)
OGE	out of ground effect
P_∞	freestream static pressure, lb/ft^2 $(\frac{N}{m^2})$
P_o	freestream total pressure, lb/ft^2, $(\frac{N}{m^2})$
q	freestream dynamic pressure, lb/ft^2 $(\frac{N}{m^2})$
RM	rolling moment
SOB	sink over bow, ft(m)
S_C	canard exposed area, ft^2 (m^2)
S_{ref}	reference area, $ft^2(m^2)$ (usually equal to S_W)
STOL	short takeoff or landing
S_W	area of trapezoidal wing extended to centerline, $ft^2(m^2)$
S_{V_T}	exposed area of vertical tail, $ft^2(m^2)$
T	thrust, lb(N)
V_∞	freestream velocity, ft/sec, knots (m/sec)

V_R	relative (inertial) velocity = $V_{VEHICLE} + V_{WOD}$
V_j	jet velocity based on isentropic expansion from nozzle camber total pressure to freestream static pressure, ft/sec (m/sec)
VSTOL	vertical or short takeoff or landing
VTOL	vertical takeoff or landing
VEO-Wing	vectored engine over wing
$\dot{w}$	weight flow, lb/sec (kg/sec)
$\bar{X}_{cp_\Gamma}$	action point of circulation lift relative to leading edge of MAC
$\bar{Y}$	spanwise location of MAC
WOD	velocity of wind over deck, knots (m/sec)
α, alpha	angle of attack, deg
β, beta	angle of sideslip, deg
C_l	rolling-moment coefficient
C_n	yawing-moment coefficient
C_Y	side-force coefficient
ΔC_{L_Γ}	incremental circulation lift coefficient due to flap deflection and blowing (VEO-Wing nozzles)
ϕ	ejector measured thrust/isentropic supply thrust (where isentropic supply thrust is the thrust which would be obtained from supplied air at the nozzle exit of pressures and flow rates expanded at isentropically to ambient pressure)
δ_C	canard deflection (positive, leading-edge up), deg
δ_{TE}, δ_F	VEO-Wing nozzle and outboard flaperon deflection, deg ; except for aileron action the flaperons and VEO-Wing nozzle flaps always deflect together.

θ	pitch attitude angle, deg
θ_j	jet thrust deflection out of VEO-Wing nozzles when deflected, $_{TE}$, deg
γ	flight path angle, deg
λ	taper ratio, $\frac{\text{tip chord}}{\text{root chord}}$
Λ_{LE}	leading-edge sweep angle, deg

1. SUMMARY

This document presents the conceptual analysis phase of a study conducted by General Dynamics to investigate the aerodynamic technology of a promising new supersonic vertical short takeoff and landing (VSTOL) fighter/attack aircraft for the U.S. Navy. The study configuration combines a jet-diffuser-ejector concept for vertical lift with a vectored-engine-over-wing (VEO-Wing) concept for improved maneuver and short takeoff and landing (STOL) performance. The objectives of the study were to subjectively assess the aerodynamic uncertainties affecting the sizing and design of this ejector VSTOL fighter/attack concept and to recommend a wind tunnel test plan to resolve these uncertainties. The assessment was made by sizing the concept to perform a selected design mission, achieve specified combat performance, hover, perform VTOL transitions, and demonstrate STOL performance with an overload capability. The sized VEO-Wing ejector configuration successfully achieves the performance goals while providing a cold-deck environment for VSTOL operations. Comparisons between the ejector concept and another VEO-Wing-derivative VSTOL concept, the Remote Augmented Lift System (RALS), are also presented. The use of the VEO-Wing concept in conjunction with a forward located vertical lift system yields a configuration with superior STOL performance capability. Wind tunnel test programs to resolve the critical aerodynamic uncertainties associated with this concept are recommended.

2. INTRODUCTION

2.1 Background

Many potential advantages for incorporating VSTOL capability into future Navy fighter/attack aircraft have been perceived by both the government and the aerospace industry. Among the advantages are tactical benefits resulting from dispersal of air strength through operation from ships smaller than aircraft carriers, improved combat tactics via in-flight use of vertical-lift propulsive systems, reduced costs from requirements for construction of smaller ships, and improved close support through short takeoff and landing. Presently, the integration of a vertical-lift propulsive system penalizes subsonic cruise performance and supersonic dash capability, degrades the ship-board deck environment, and imposes additional operational requirements. However, innovative aircraft design, including advances in propulsive system, flight control, structural, and aerodynamic technologies projected to the 1990 time period, has led to the emergence of VSTOL concepts with significant transonic maneuver and supersonic performance potential. Nevertheless, detailed configuration design of these VSTOL aircraft concepts is generally lacking, and only limited experimental data to define the aerodynamic/propulsive characteristics of such vehicles are available. Therefore, studies have been commissioned by the Navy and NASA Ames to investigate the aerodynamic technology associated with various VSTOL fighter/attack aircraft concepts.

2.2 Study Objectives

The conceptual analysis phase (Phase I) of this study had the following objectives:

1. Identify and analyze a unique high-performance VSTOL concept that has potential to fulfill the Navy fighter/attack role.

2. Estimate the aerodynamic characteristics of this configuration and identify those aerodynamic uncertainties requiring additional research.

3. Define a wind-tunnel program for Ames Research Center's Unitary and 12-foot wind tunnels. This program should explore as many of the uncertainties as possible and provide an initial high-quality aerodynamic data base for DOD, NASA, and industry use.

In Phase II of this study, a wind tunnel model of the aircraft analyzed during Phase I will be designed and fabricated. The model will provide parametric variations so that as many as possible of the critical aerodynamic uncertainties identified in Phase I can be explored.

2.3 Concept Selection

Two promising VSTOL concepts were identified from General Dynamics' in-house VSTOL fighter research programs. Both configurations are derivatives of General Dynamics' Vectored-Engine-Over-Wing (VEO-Wing) concept (in development for several years (see Figure 2-1)). This concept achieves improved transonic maneuvering and short takeoff and landing (STOL) performance by utilizing the full engine momentum from over-wing-mounted engines to augment the external aerodynamics through a jet-flap effect and vortex augmentation. The major difference between the two candidate concepts is the propulsive systems utilized for vertical lift. These propulsive systems are the jet diffuser ejector and the General Electric-developed Remote Augmentation Lift System (RALS). These systems represent the range of cold-vs-hot deck environments currently being considered for vertical propulsion concepts. Both systems afford thrust/lift augmentation, which allows reduced engine/vehicle size for a given payload capability. The aerodynamic lift augmentation achieved from the VEO-Wing nozzles through supercirculation also leads to reduced vehicle size.

The contracted scope of this study limited the scope of the analysis to only one concept, the jet-diffuser-ejector concept. This concept was selected after discussions with NASA and Navy personnel because it offered more potential shipboard operations due to its benign footprint. Further, it represents more areas of aerodynamic uncertainty and differs more from the existing experimental data base than does the RALS. The RALS configuration more closely resembles the VEO-Wing fighter for which an unpowered experimental data base already exists. General Dynamics has continued to pursue the RALS configuration through an in-house funding in a somewhat parallel study program; in fact, the RALS and

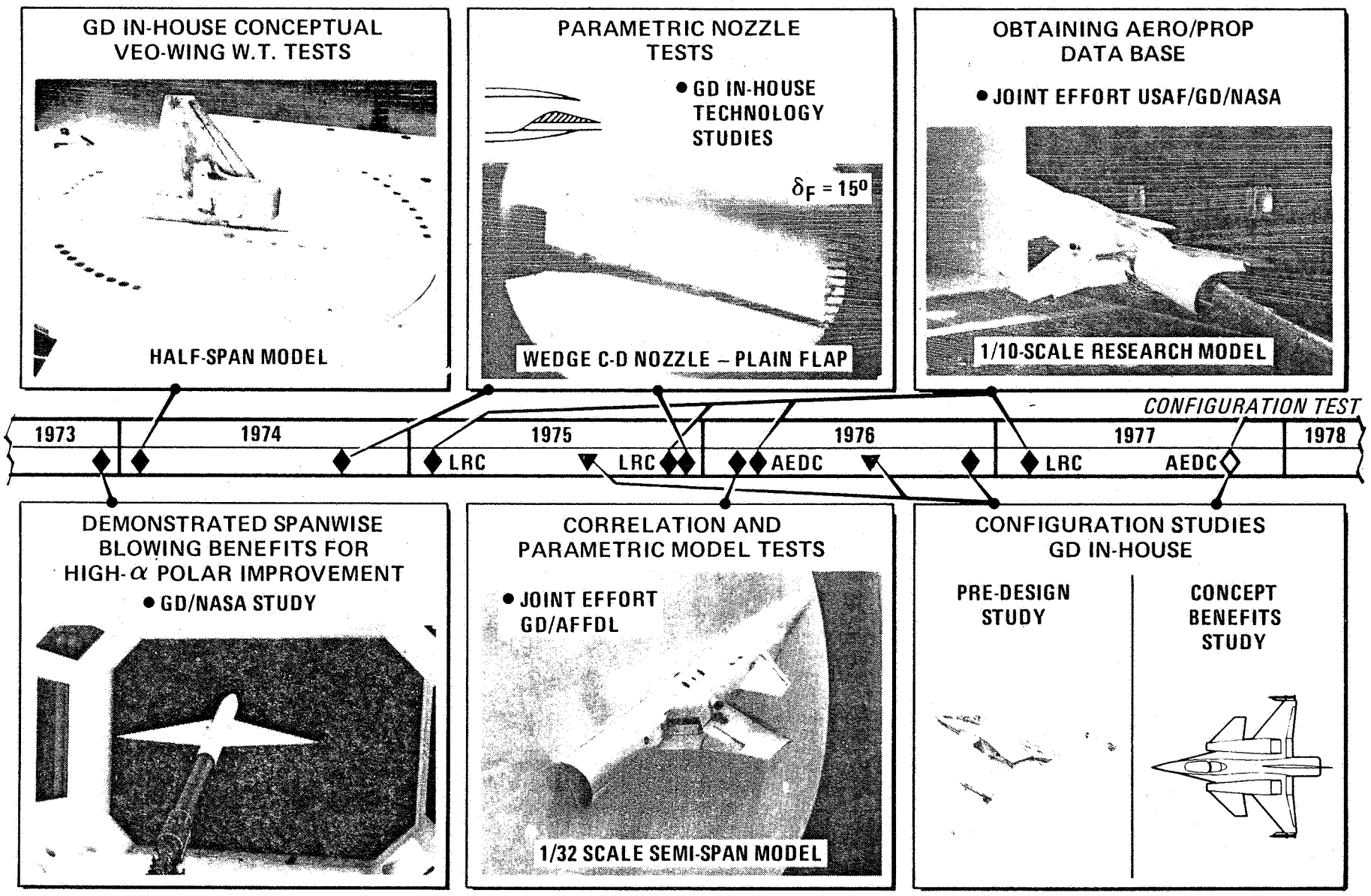

Figure 2-1 VEO-Wing Development Program

ejector configurations have been compared by use of NAVAIR-supplied groundrules in a study conducted for NAVAIR (Reference 1). Comparisons between the ejector and RALS configurations sized to the groundrules of this NASA Ames study are given in Appendix A. Three-view drawings of these two configurations, E205 and R104, are shown in Figures 2-2 and 2-3. The RALS R104 configuration does not represent an aircraft exactly sized to meet any of the combination of requirements but, instead, serves as a sizing baseline configuration for synthesis studies. Artist sketches are shown for the ejector airplane in VTOL and cruise modes in Figures 2-4 and 2-5 and for the RALS concept in cruise mode in Figure 2-6. Many of the areas of aerodynamic uncertainty pursued in this study are applicable to both concepts, since both configurations are derivatives of the VEO-Wing designs. The recommended test program to resolve the aerodynamic uncertainties for the E205 ejector configuration indicates that the wind tunnel model could be built, at a nominal added cost, to parametrically develop an experimental data base for the VEO-Wing RALS configuration as well as for the VEO-Wing ejector configuration.

The ejector and RALS concepts are representative of two alternatives among many for achieving vertical flight in a high-performance fighter. They should not be construed as necessarily being preferred approaches of General Dynamics but, rather, as part of a larger effort to evaluate competitive propulsion/configuration concepts from which a preferred concept can be selected.

2.4 Study Plan

The manner in which the study was accomplished is shown schematically in Figure 2-7. The selected jet-diffuser-ejector concept was designed and sized to meet certain mission, hover, and combat performance (maneuvering) requirements (described in Section 3). The sizing approach involved the development of constraint lines for the combat and hover requirements on a mission carpet plot (takeoff gross weight vs engine-scale factor and wing area) to establish the minimum-TOGW airplane satisfying these requirements. Since the VTO transition and STO performance requirements are not well defined, the final sized airplane for this study, E205, was sized to meet the hover, mission, and combat performance requirements defined in Section 3. The fallout VTO transition and STO performance for this sized airplane have been determined, as well as sizing

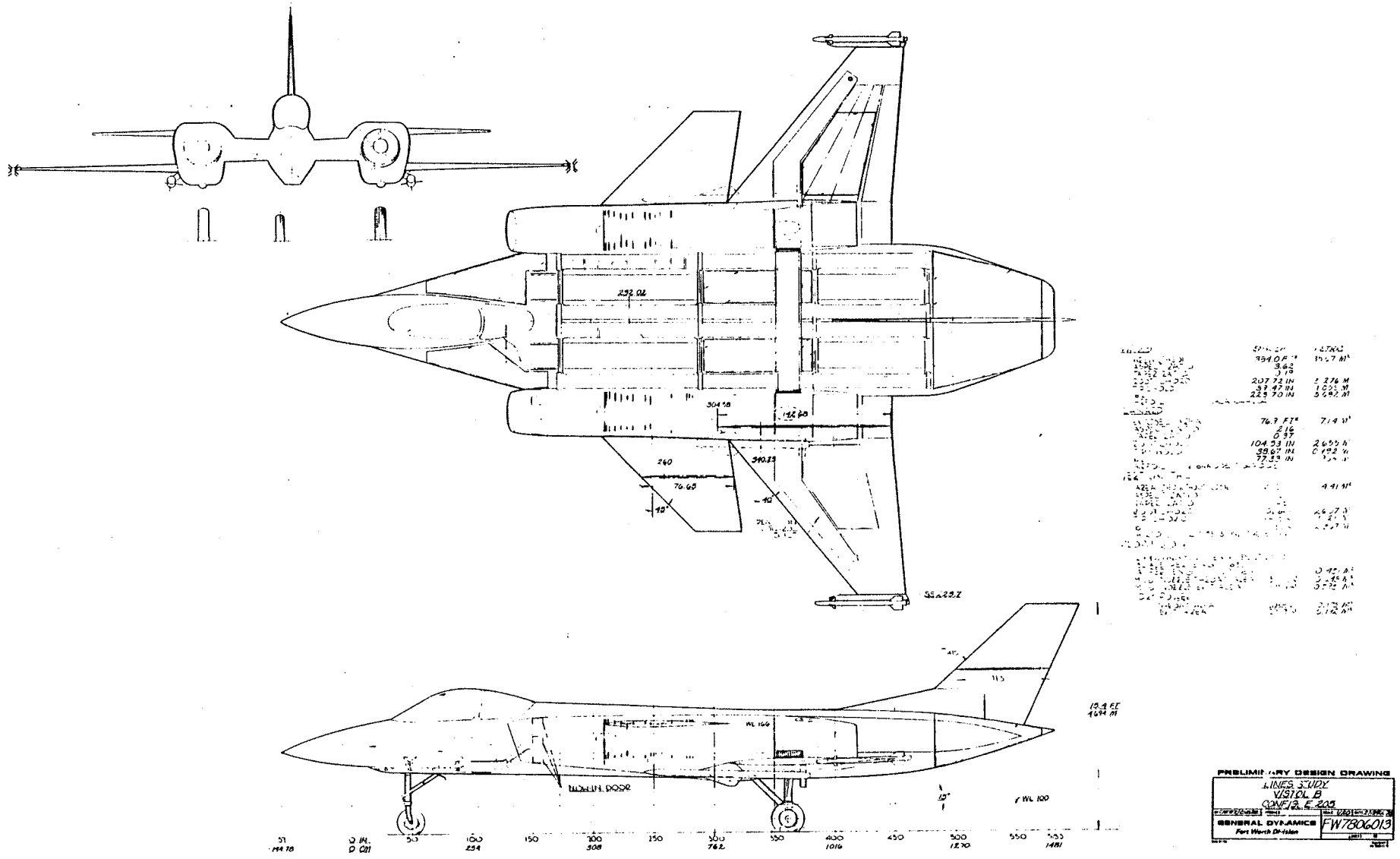

Figure 2-2 E205 Three-View Drawing

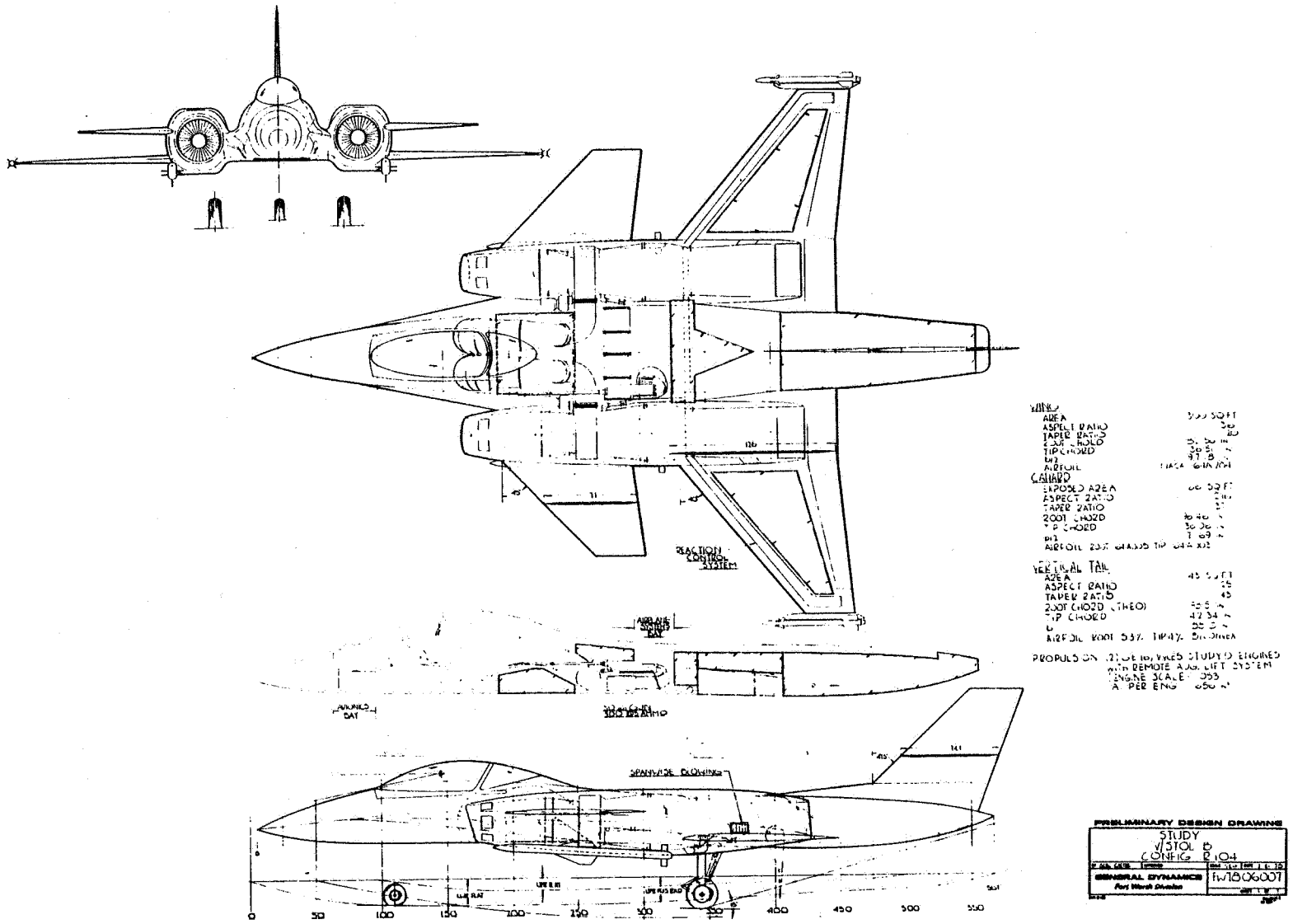

Figure 2-3 R104 Three-View Drawing

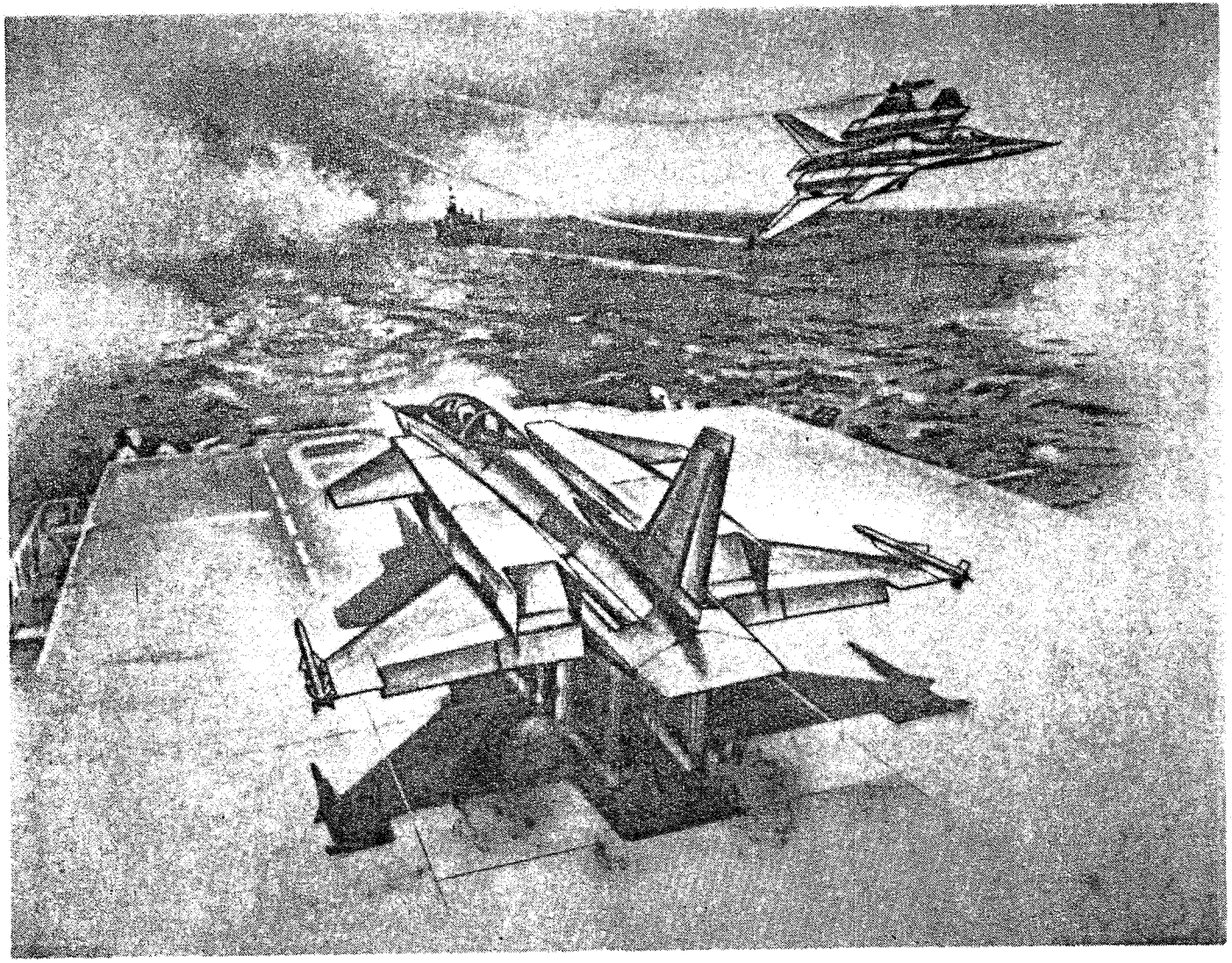

Figure 2-4 Ejector Configuration in VTOL Mode

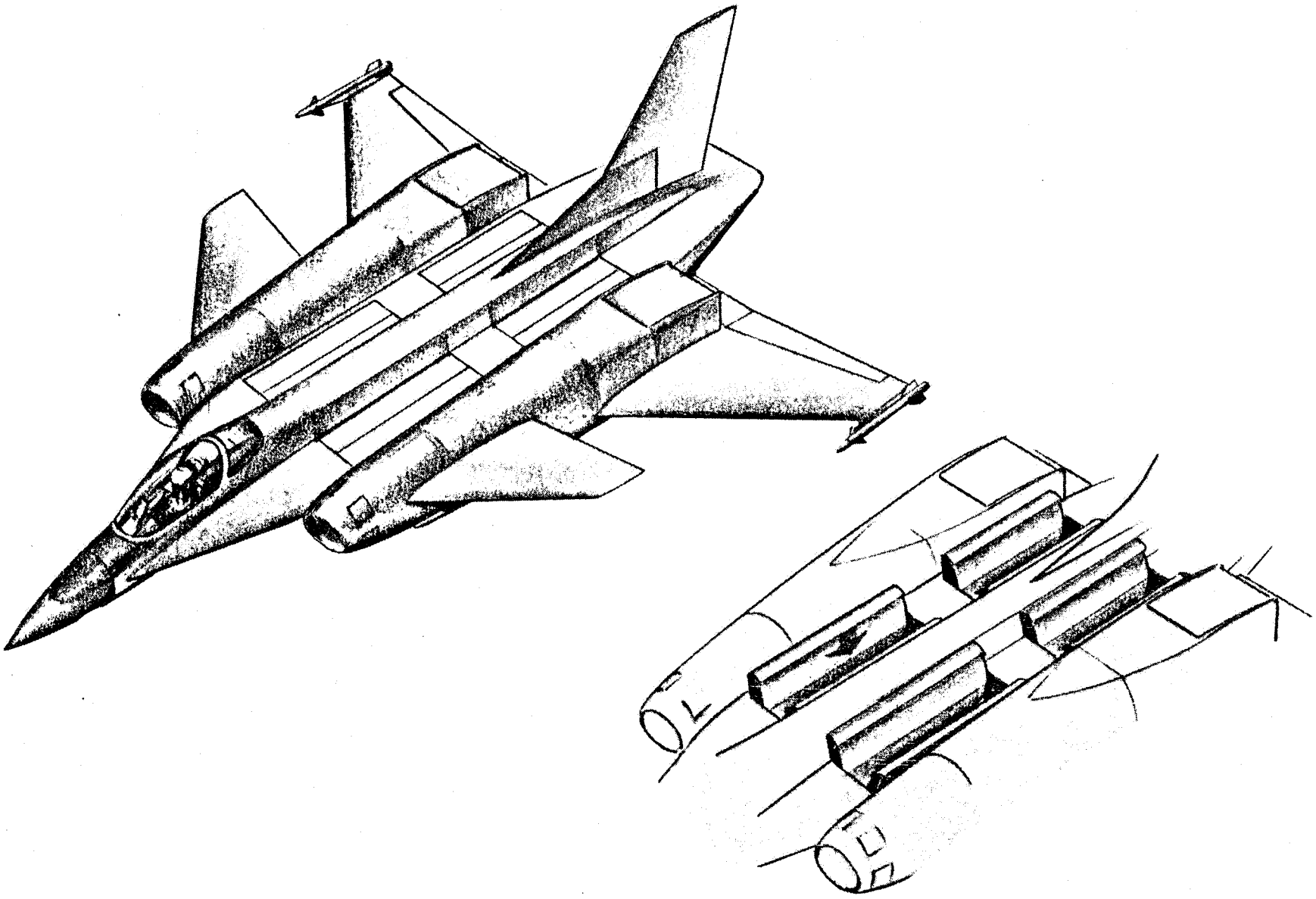

Figure 2-5 Ejector Configuration in Cruise Mode

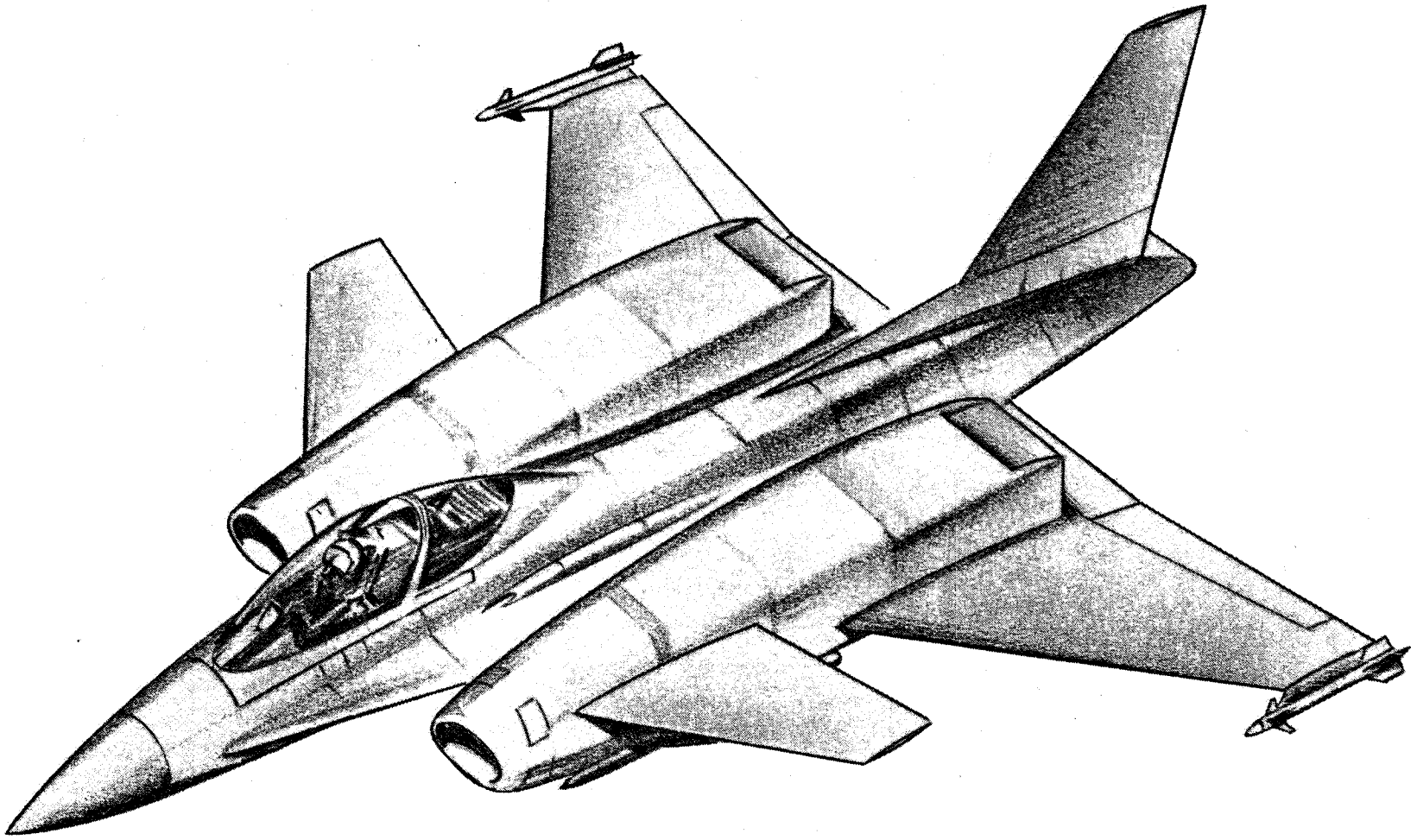

Figure 2-3 RALS Configuration in Cruise Mode

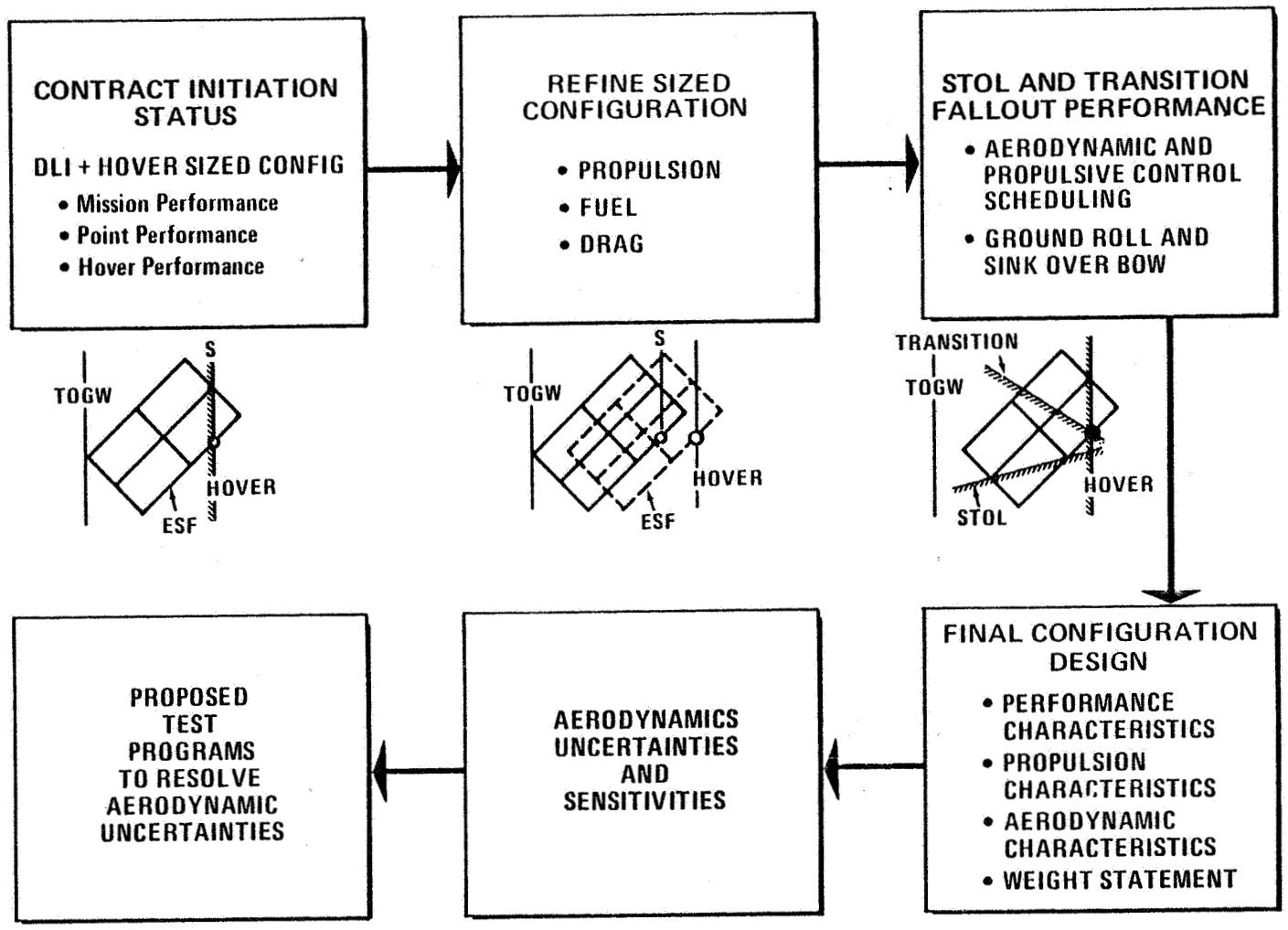

Figure 2-7 Study Plan

sensitivities for the STO requirements. The performance characteristics of the E205 configuration are shown in Table 2-1. No vertical or short landing analysis of this aircraft has been performed.

The critical aerodynamic uncertainties were identified as those aerodynamic parameters which are associated with the design requirements that size the aircraft and which could not be confidently estimated by analytical or experimental means.

Please note that the reader will be referred to a second volume for proprietary material. This second volume is for government use only since it also contains General Dynamics Proprietary data.

TABLE 2-1 SIZED EJECTOR AIRCRAFT (E205) PERFORMANCE SUMMARY

Item	Performance
Deck Launch Intercept (DLI) Mission Takeoff Gross Weight - lb(kg)	34,987(15,867)
Combat Weight (88% Fuel) - lb(kg)	30,789(13,963)
P_S (M.9/10kft/1G) - fps(mps)	938(285.9)
N_Z (M.6/10kft/P_S=0) - g	6.2
Accel Time (M.8 - 1.6/35kft) - sec	76.8
Max Mach Number	1.83
STOL TOD (VTOGW + 10klb/at +20kt WOD and 0 ft SOB) - ft(M)	400(122)
Transition Time - sec	27

3. AIRCRAFT DESCRIPTION

3.1 Design Philosophy

The design philosophy of the VEO Wing ejector configuration is the successful integration of a promising vertical-lift concept, the Alperin jet diffuser ejector (Reference 2), into the VEO-Wing fighter configuration concept already developed at General Dynamics. The VEO-Wing fighter concept (Figure 3-1) was selected as a configuration starting point because

1. Combat maneuvering and STOL performance benefits are achieved with the concept by use of the full engine momentum from over-wing-mounted engines to augment the external aerodynamics through a jet-flap effect and vortex augmentation. Curves in Figure 3-2 illustrate the polar improvements provided by the VEO-Wing fighter relative to a very similar conventional fighter configuration.

2. An experimental data base is available from several years of General Dynamics/Air Force research (Figures 2-1 and 3-3) in on-going complementary test and study programs, including the NASA/Ames Research Center 3/4-scale powered VEO-Wing model soon to be tested in the NASA Ames 40-ft by 80-ft tunnel (Figure 3-4). The powered General Dynamics Research model and the AFFDL unpowered VEO-Wing model shown in Figure 3-3 form the data base for the ejector and RALS configuration.

3. The VEO-Wing configuration with its widely spaced engines and flat strake is readily adaptable to house the ejectors.

The Alperin jet diffuser ejector was selected as the vertical-lift concept for the study because (1) it holds the promise of achieving VSTOL fighter/attack capability in a cold-deck environment; (2) there are more aerodynamic uncertainties associated with the resulting wide-body configuration; (3) the Alperin-type jet diffuser ejector concept offers the highest experimental ejector augmentation ratios demonstrated to date.

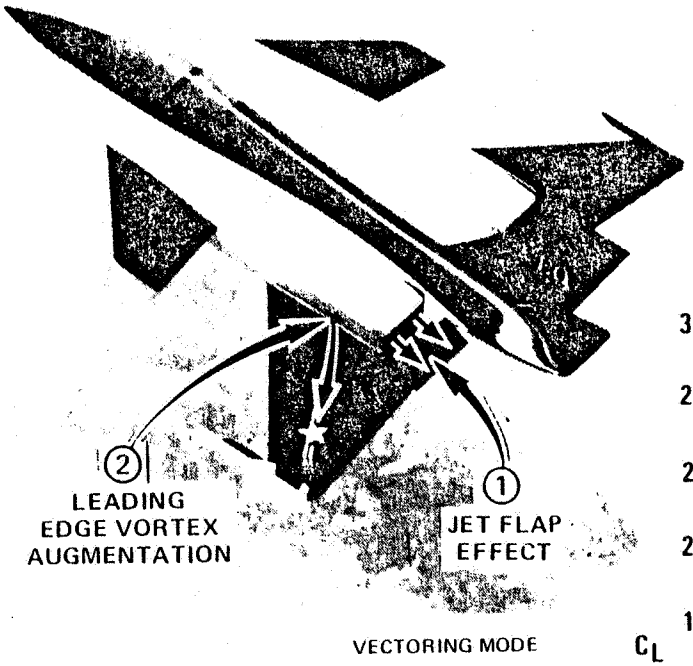

- COMBINES SUPERCIRCULATION FROM OVER-WING-MOUNTED ENGINES WITH LEADING EDGE VORTEX AUGMENTATION TO OBTAIN
  - Increased Maneuver g's (Sustained and Instantaneous)
  - Full α -Range Polar Improvement
  - High Angle of Attack Directional Stability
  - STOL

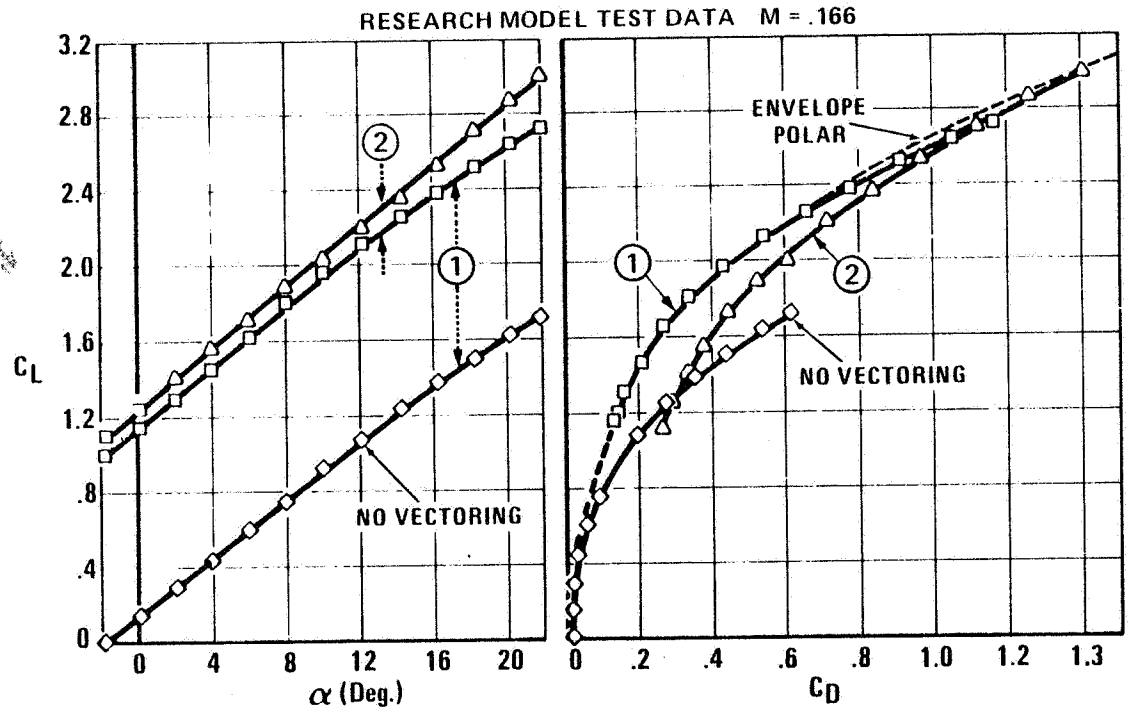

- UTILIZES FULL ENGINE MOMENTUM (No Bleed)
  - Current Engines
  - No Internal Ducting (Thin Wings for Supersonic Performance)

Figure 3-1 VEO-Wing Fighter Concept

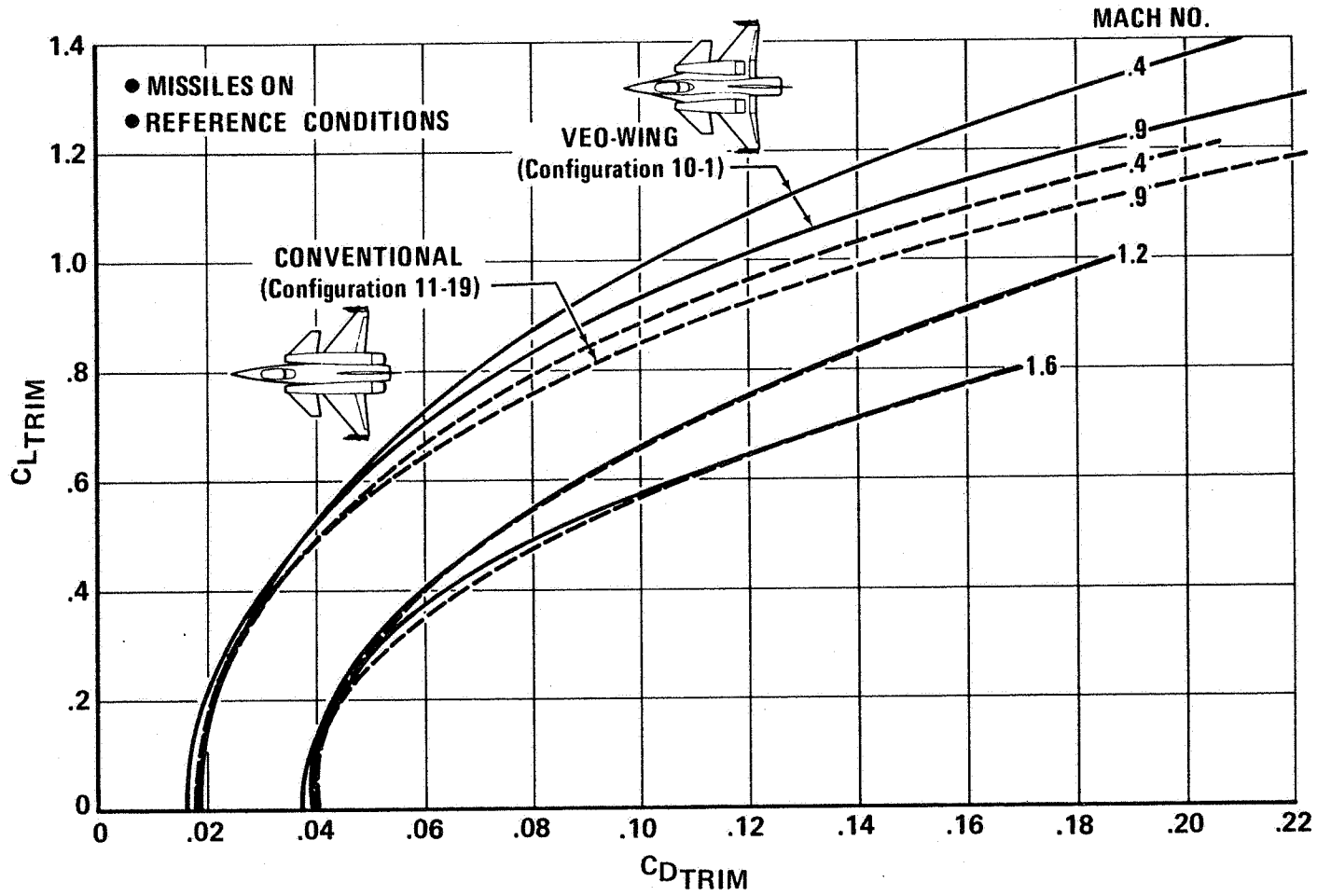

Figure 3-2 VEO-Wing Drag-Polar Improvements

GD/NASA/AFFDL RESEARCH MODEL
(Ref. 3)

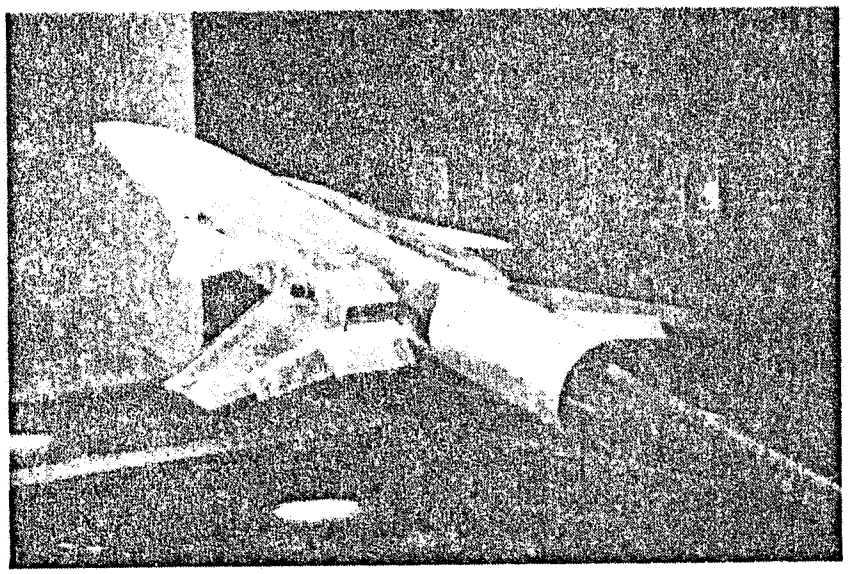

- POWERED MODEL
  Tested Subsonic to Supersonic
  α's to 40° Subsonic
- PROVIDES–Power Effects
  –Canard Effects (Subsonic)
  –Transonic e's

FOR THIS STUDY

AFFDL VEO FIGHTER MODEL AEDC TEST
(Ref. 4)

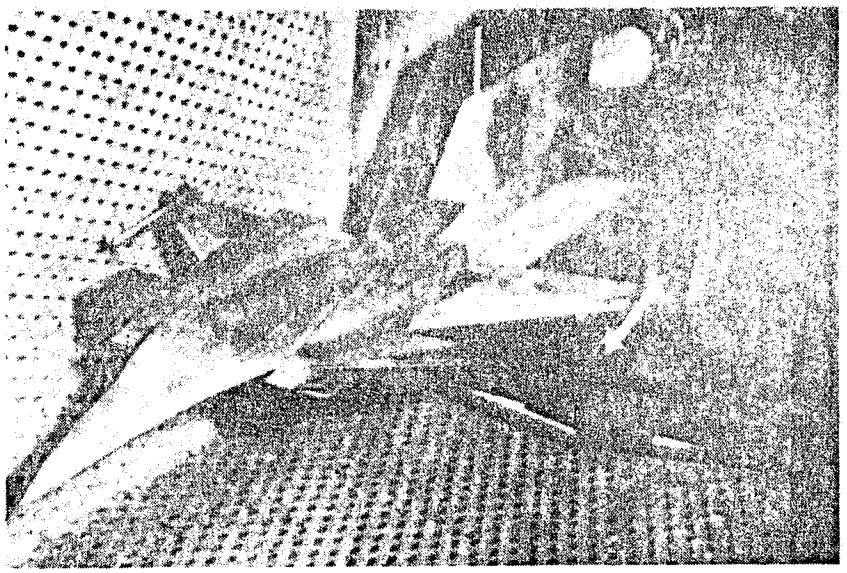

- UNPOWERED FLOW THROUGH MODEL
- PROVIDES–Power Off Baseline for VSTOL Aero Buildup
  –Supersonic Trimmed Polar Shapes

FOR THIS STUDY

Figure 3-3 VEO-Wing Experimental Data Base

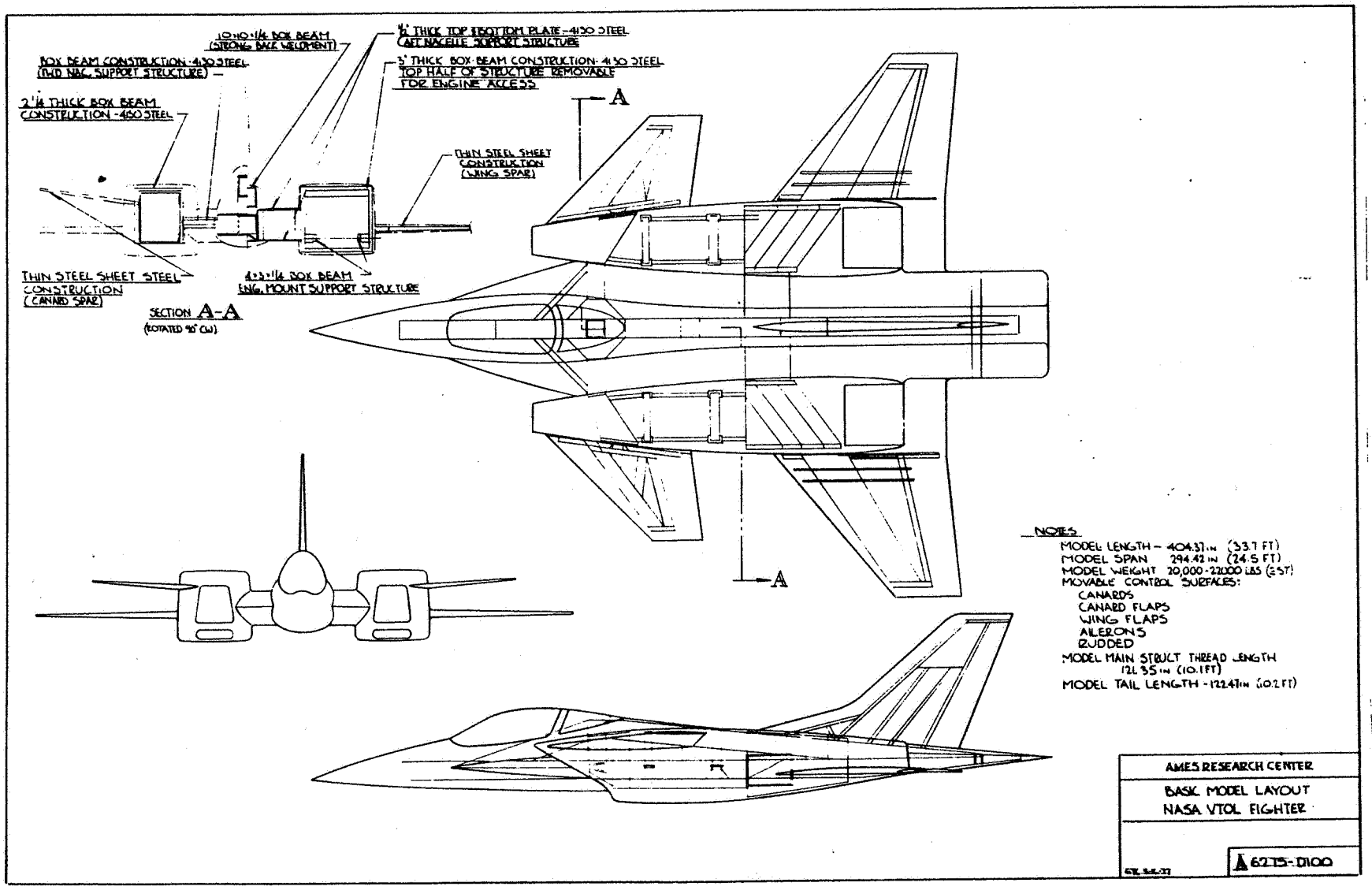

Figure 3-4 3/4-Scale Powered VEO-Wing Fighter Model

The VEO-wing ejector fighter/attack configuration layout has been influenced heavily by the necessity to meet the following three criteria simultaneously:

1. Static margin variation (center of gravity-aerodynamic center) with Mach no. from approximately -18% (unstable) subsonically to +10% (stable) supersonically. The maximum allowable instability of -18% static margin subsonically is a constraint set by the aerodynamic control and control system response capability expected in the 1990 time period.

2. Center-of-gravity, wing, nozzle, and canard-location relationships (as well as static margin) to achieve the supercirculation benefits of the VEO-Wing concept for cruise maneuvering and STOL. To achieve the benefits of the VEO-Wing concept requires the c.g. to be as far aft as possible, at least +3%c or greater (with static margin as in Criteria 1). This drives the configuration very hard; it is difficult to achieve the c.g. location without getting so much "real estate" ahead of the c.g. that the resulting forward-located aerodynamic center produces more instability than can be tolerated. This point is discussed in detail in Section 4.1.3.

3. Center-of-gravity, aircraft inertias, and thruster locations which meet the hover requirements.

3.2 SIZING GROUND RULES

This study has been structured to assess the importance of the various aerodynamic uncertainties involved in the concept by actually designing and sizing the airplane to a set of requirements suggested by the NASA contract guidelines and by General Dynamics' experience in previous Navy VSTOL fighter studies. The requirements, shown below, rereflect the desire for the aircraft to have good supersonic fighter combat performance (with reasonable mission "legs") when operating in VTO and good attack-support capability when operating in STOL:

Mission: (Standard Day)	VTO Deck Launch Intercept (DLI) with radius of action = 150 n.mi and

	design dash M = 1.6 (see Figure 3-5 for detailed mission profile definition).
Combat Performance: (Standard Day)	•Sustained load factor of 6.2 at Mach 0.6, 10,000 ft of altitude at 88% VTOL gross weight. •Specific excess power of 900 fps at 1g, Mach 0.9, 10,000 ft of altitude at 88% VTOL gross weight.
VTOL: (Tropical Day)	Vertical acceleration = 1.05 g (IGE) while achieving maximum design control rates simultaneously in all axes, where maximum design control acceleration rates are Roll = .96 rad/sec^2 Pitch = .28 rad/sec^2 Yaw = .40 rad/sec^2
STOL: (Tropical Day)	Operational from land and from ships smaller than CV's without catapults and arresting gear; sea-based gross weight = VTO maximum gross weight + 10,000 lb; sea-based WOD = 20 kt for overload.
VTO Takeoff Gross Weight	Maximum = 35,000 lb.
Fuel Flow Conservatism	Use minimum engine without 5% fuel flow conservatism (approximately same as using average engine with 5% fuel flow conservatism).

3.3 Physical Description

The three-view drawing of the jet-diffuser ejector V/STOL fighter/attack conceptual design (E205) sized to meet the mission, hover, and combat performance requirements specified in Section 3.2 is presented in Figure 2-2. The inboard profile of this aircraft is shown in Figure 3-6.

MISSION DEFINITION

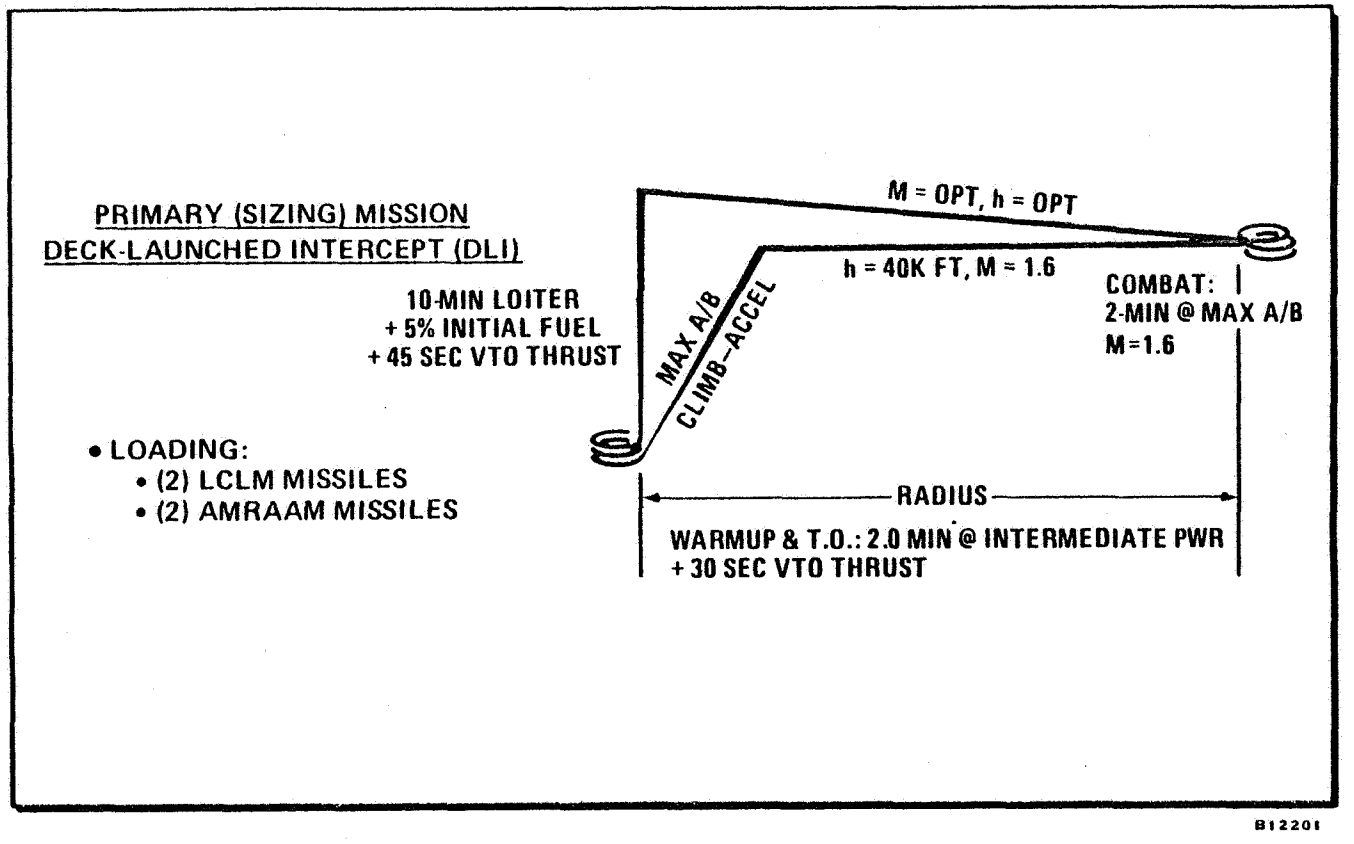

Figure 3-5 DLI Mission Profile

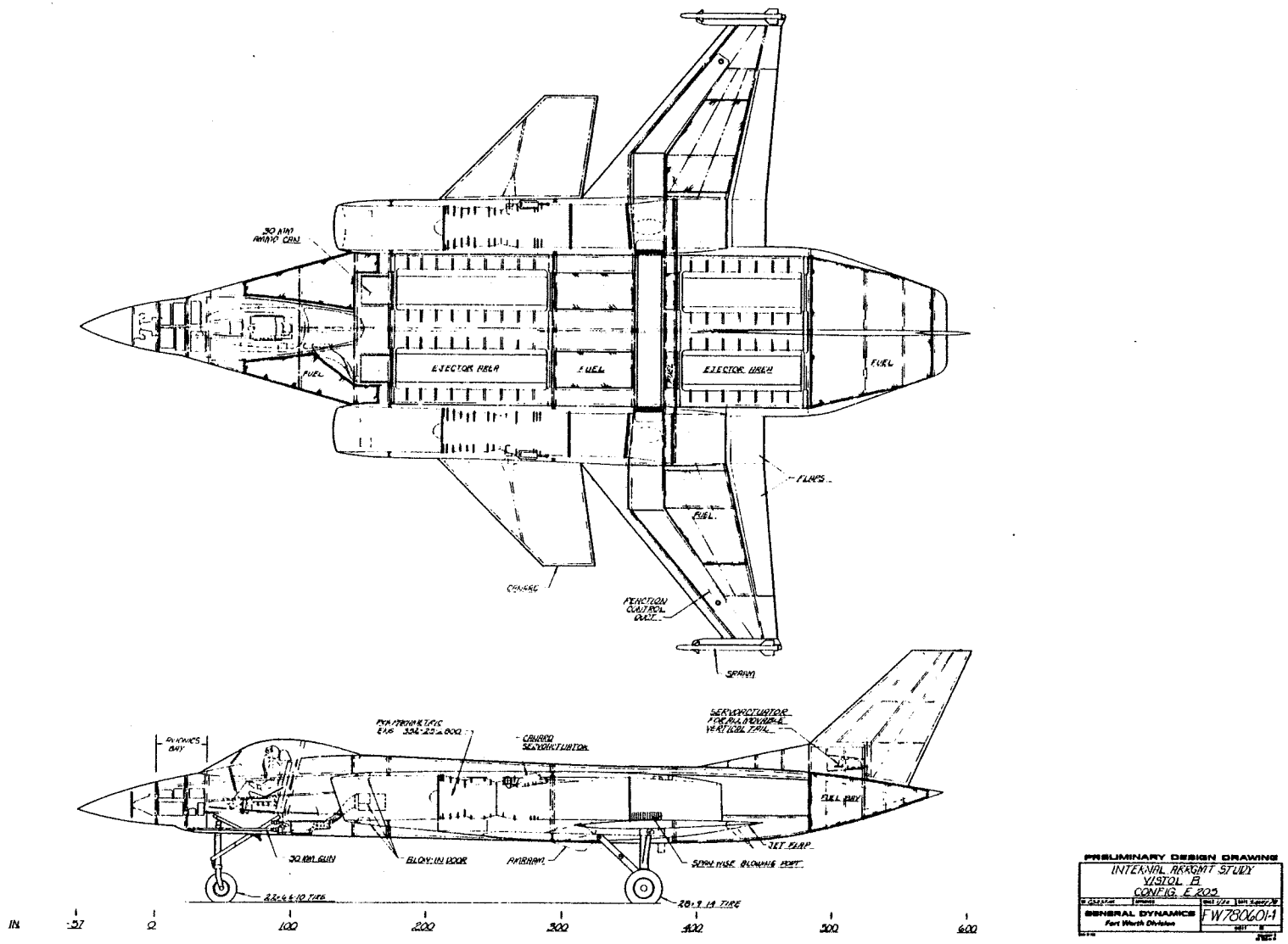

Figure 3-6 E205 Inboard Profile

It is a cool-footprint system using advanced turbofan engines in conjunction with jet diffuser ejectors. This supersonic fighter design is configured to provide propulsive enhancement of external aerodynamics by a VEO-Wing (Figure 3-1), which utilizes the full engine momentum from the over-wing-mounted engines to augment the external aerodynamics through a jet-flap effect. This unique integration of airframe and propulsion systems is combined with spanwise blowing, in which a portion of the engine exhaust is used at high angles of attack to produce leading-edge vortex augmentation. The total system is thus capable of providing lift/drag polar improvements in the full angle-of-attack range, resulting in improved maneuverability and STOL performance.[1]

The concept utilizes a high-canard, low-wing arrangement with podded engines located for over-the-wing blowing. Four chord-wise bays between the center body and nacelles (two forward and two aft) are provided for location of the jet diffuser ejectors.

Unique features of this configuration approach are the incorporation of movable doors to form the ejector nozzle and the stowable primary nozzles, which result in a relatively compact arrangement when the ejectors are not in use. A strake is extended forward and a beaver tail aft to fair off the depth of the ejectors when folded into their cruise position. The ejector design is based on application of the research reported in Reference 2 and discussed in detail in Section 5.4. The ejectors are sized to be operated with intermediate power airflow from P&WA

---

[1] Although the spanwise blowing nozzle is shown on the 3-view, the STOL and VTO-transition analysis presented in this report have not been performed using the spanwise blowing benefits because there is not enough experimental data to optimize the chordwise location of the blowing slot to complement the desired instability levels (the chordwise location has a very pronounced effect on the center of pressure of the wing which in turn affects the aerodynamic center). Since STOL and VTO transition are greatly affected by the pitch rotation rate caused by the aircraft instability, a careful experimental and performance examination of chordwise location of the spanwise blowing on this configuration will be required.

.35-25-2800 parametric engines. Air is diverted to the primary and throat nozzles through the ducting arrangement shown in Figure 2-2. The augmentation ratio is 1.98 in free air and 1.70 at lift off. Thrust modulation at the forward and aft ejectors, by varying airflow at the ejector primary nozzles, is used for pitch control during hover and transition. Yaw control is achieved by vectoring the ejector flow. Engine exhaust air is ducted to upward and downward firing thrusters for roll control. No lift is produced by this reaction control system in hover. The VEO-Wing engine nozzles can be operated in afterburner power setting with the ejectors running. IR-guided LCLMs (Low-Cost Light-Weight Missiles) are carried on the wing tip; other payload is carried on nacelle and/or wing pylon stations (Figure 3-7).

Dimensional and pertinent design data for the E205 configuration are presented in Table 3-1. The wetted area component buildup is included. The cross-sectional area distribution is shown in Figure 3-8. The c.g. location for several descriptive conditions are provided in Table 3-2. The c.g. will be maintained by fuel burn sequencing at +.03c (F.S. 308.86) as long as possible to achieve the VEO benefits for combat (until about 3000 of the 9521 lb of fuel is left).

The control devices and deflection limits are as follows:

		Max deflection
1.	VEO-Wing nozzle	-10° to $+30^{\circ}$
2.	Flaperon (outboard of VEO-Wing nozzle)	-20° to $+30^{\circ}$
3.	Canard	-25 to $+25^{\circ}$
4.	Reaction controls (discussed in section 5.3)	
5.	All-moving vertical tail	-25 to $+25^{\circ}$

The flaperon acts with the VEO-Wing nozzle for high lift but also acts as an aileron from the deflected flap position to provide roll control.

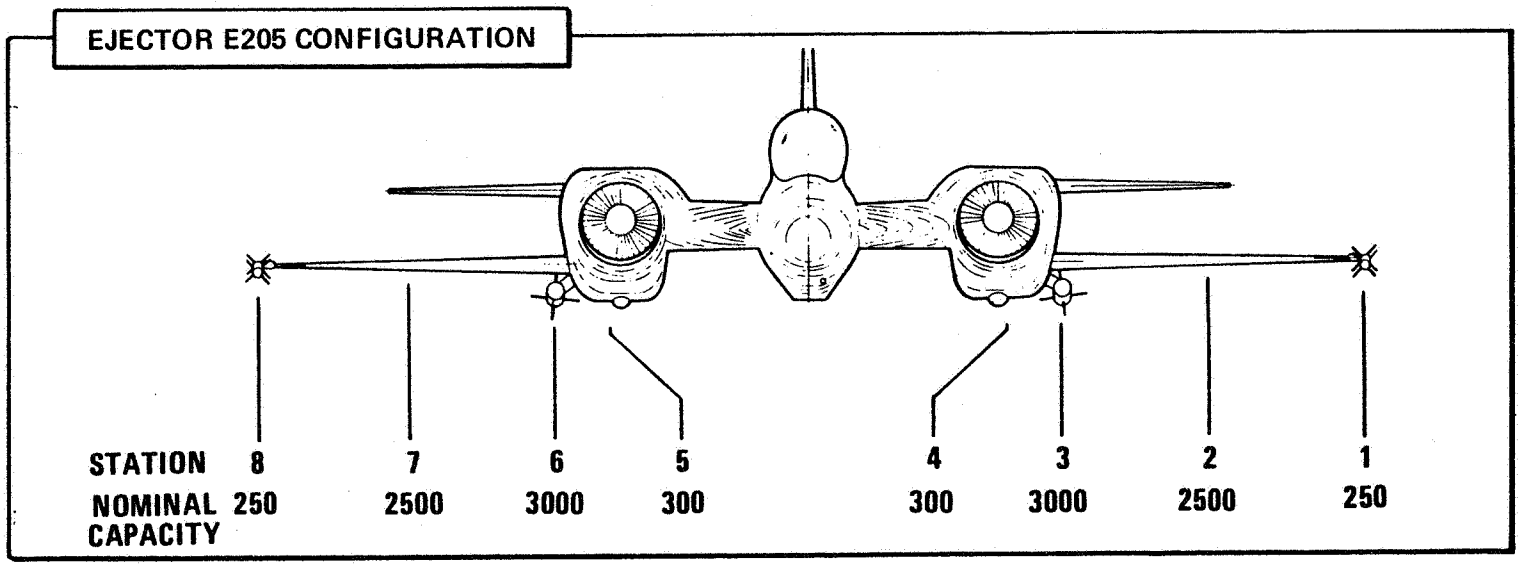

Figure 3-7 External Store Locations

TABLE 3-1 DIMENSIONAL AND DESIGN DATA FOR EJECTOR E205 CONFIGURATION

WING

Area (Ref)	384 ft^2	(35.67 m^2)
Aspect Ratio	3.62	
Taper Ratio	.19	
b	37.28 ft	(11.36 m)
b/2	223.70 in.	(5.682 m)
C_R	207.72 in.	(5.276 m)
C_T	39.47 in.	(1.003 m)
$\bar{c}$	142.680 in.	(3.624 m)
Y	86.473 in.	(2.196 m)
Airfoil Root & Tip	NACA 64A204	
Sweep-Leading Edge	40°	
Sweep - $\bar{c}/4$	32°	
Incidence	-0°	
Dihedral	0°	

CANARD

Area (Exp)	76.9 ft^2	(7.14 m^2)
Aspect Ratio	2.16	
Taper Ratio	.37	
b (Tip to Tip)	28.6 ft	(8.72 m)
b/2 (Exp)	77.33 in.	(1.96 m)
C_R (Exp)	104.58 in.	(2.655 m)
C_T	38.67 in.	(.982 m)
$\bar{c}$	76.65 in.	(1.947 m)
Y	32.74 in.	(.832 m)
Airfoil Root	NACA 64A005	
Airfoil Tip	NACA 64A003	
Sweep-Leading Edge	45°	
Sweep - $\bar{c}/4$	37°	
Incidence & Dihedral	0°	
L_c (LE $\bar{c}$ Wing to $\bar{c}/4$ Canard)	6.7 ft	(2.04 m)
V_c (Volume)	514.3 ft^3	(14.565 m^3)

Table 3-1 (Continued)

VERTICAL TAIL

Area (Exp)	47.5 ft^2	(4.41 m^2)
Aspect Ratio	1.27	
Taper Ratio	.43	
b	7.8 ft	(2.38 m)
C_R	102.6 in.	(2.606 m)
C_T	44.1 in.	(1.120 m)
$\bar{c}$	77.3 in.	(1.963 m)
Y	40 in.	(1.016 m)
Airfoil Root	5.3% Biconvex	
Airfoil Tip	4% Biconvex	
Sweep - Leading Edge	47.5°	
L_{VT} (LE $\bar{c}$ Wing to $\bar{c}$/4 VT)	17.8 ft	(5.43 m)
V_{VT} (Volume)	845.1 ft^3	(23.933 m^3)

WETTED AREAS

Fuselage	451 ft^2	(41.90 m^2)
Canopy	33 ft^2	(3.07 m^2)
Nacelle	461 ft^2	(42.83 m^2)
Wing	919.5 ft^2	(85.42 m^2)
Canard	153.8 ft^2	(14.29 m^2)
Vertical Tail	95 ft^2	(8.83 m^2)
Dorsal	8 ft^2	(.74 m^2)
Wing Aft of Nac	27.7 ft^2	(2.57 m^2)
TOTAL	2149 ft^2	(199.64 m^2)

Fineness Ratio (l/de)	7.66	
Fuel Fraction	27.2%	
Structural Fraction (w/o Ejectors)	32.4%	
Composites (% of Struct Wt) (W/O Landing Gear)	23.1%	
Advanced Metallics (Incl Ejectors) (% of Struct Wt W/O Landing Gear)	72.8%	
C G Location (% c)	3.0%	
VTO TOGW/Max TOGW	34987/44987	(15853/20384 kg)
Combat Wt (88% VTOGW)	30789 lb	(13950 kg)
Flight Design Wt (88% VTOGW)	30789 lb	(13950 kg)
Empty Wt	23402 lb	(10603 kg)
Payload (VTO/Max Overlead)	1146/11,146 lb	(520/5055 kg)
Installed Gun Sys. Weight/Ammo	521/500 lb	(236/227 kg)
Avionic Wt (Installed/Uninstalled)	1057/846 lb	(479/384 kg)
Internal Fuel Volume		
Fuselage (Bladder)	877 lb	(3974 kg)
Wing (Integral, Halon Inerted)	750 lb	(340 kg)
Total	9521 lb	(4314 kg)
Design Mission Fuel	9521 lb	(4314 kg)

Table 3-1 (Continued)

Number of Engines & Types	(2) P&W Parametric Eng FB ABTF BPR=.352 OPR=25 TIT=2800°F	(1537.8°C)
Thrust(Max A/B SLS-Uninstalled Each)	22,718 lb	(10,294 kg)
Inlet Type	Axisymmetric Normal Shock Shock	
A1 Per Engine	4.86 ft^2	(.451 m^2)
W/S At VTOGW	91 lb/ft^2	(444 kg/m^2)
T/W At VTOGW (Max A/B SLS Uninstalled Thrust)	1.3	
Max Cross Section Area Minus A1	33.2 ft^2	(3.084 m^2)
Airplane Overall Dimensions		
Overall Length	53.3 ft^2	(16.25 m)
Overall Span (Including Missiles)	39.4 ft	(12.0 m)
Overall Height	15.4 ft	(4.69 m)
Flight Design Limit Load Factor	7.5 g	
Design Rate of Sink	15 fps	(4.57 mps)

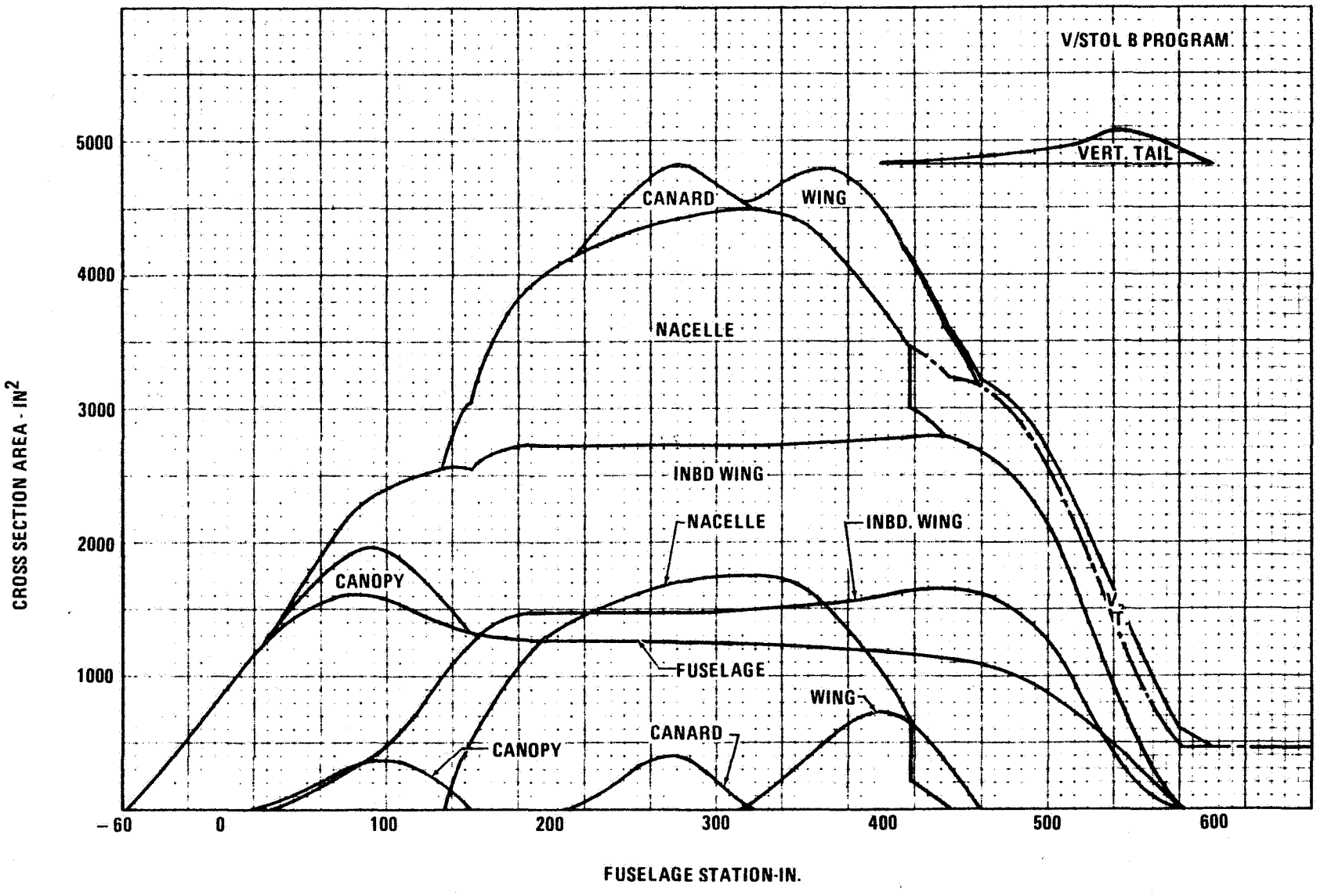

Figure 3-8 E205 Cross-Sectional Area Distribution

TABLE 3-2 E205 CENTER OF GRAVITY LOCATIONS

CONDITION	% $\bar{c}$	WEIGHT (LB)	FUSELAGE STATION	WATERLINE
WEIGHT EMPTY	-9.1	23,402	291.54	98.53
OPERATING WEIGHT	-11.9	24,550	287.65	98.45
ZERO FUEL WEIGHT	-11.8	25,466	287.75	97.64
MAX INTERNAL FUEL	+3.0	34.987	308.86	98.13

4. AERODYNAMIC CHARACTERISTICS

4.1 Longitudinal Aerodynamics

The longitudinal aerodynamics of the E205 ejector configuration are based on estimated values of minimum drag while the lift, pitching moment, and drag due to lift rely heavily on the experimental data base developed from wind-tunnel tests of the powered General Dynamics Research Model and the unpowered VEO-Wing fighter model (Figure 3-3). Figure 4-1 summarizes the longitudinal forces acting on the E205 configuration. This data base is available in Reference 3 and 4. The longitudinal aerodynamic data presented for the E205 configuration is divided into three categories of application: STOL/VTOL ($M \leq .3$), up-and-away combat/maneuver ($.3 \leq M \leq 1.0$), and supersonic dash ($M \leq 1.0$). Table 4-1 provides a summary of analysis schemes with other pertinent data included for each flight regime. Three types of data coefficients have been developed for analyzing the configuration in these flight regimes and are defined by the following equations:

1. <u>Total Coefficients</u> (Subscript t): All aerodynamic plus thrust forces included

$$C_{L_t} = C_{L_{Aero}} + C_{T_{V.N.}} \sin(\delta_F + \alpha) + C_{T_{EJ}} \cos\alpha - C_{D_{\substack{Ram \\ Ejector}}} \sin\alpha$$

$$C_{D_t} = C_{D_{Aero}} = C_T \cos\alpha(\delta_F + \alpha) + C_{T_{EJ}} \sin\alpha + C_{D_{\substack{Eng\text{-}Inlet \\ Ram\ Drag}}} + C_{D_{\substack{Ram \\ Ejector}}} \cos\alpha$$

$$C_{M_t} = C_{M_{Aero}} + C_T \cos\delta_F \left(\frac{C.G.W.L. - V.N.W.L.}{\bar{c}}\right)$$

$$+ C_{T_{V.N.}} \sin\delta_F \left(\frac{C.G.F.S. - V.N.F.S.}{\bar{c}}\right)$$

$$+ C_{T_{EJ}} \left(\frac{C.G.F.S. - EJ.F.S.}{\bar{c}}\right) + C_{D_{Eng\text{-}Inlet}} \bullet \sin\alpha \left(\frac{C.G.F.S. - Inlet\ F.S.}{\bar{c}}\right)$$

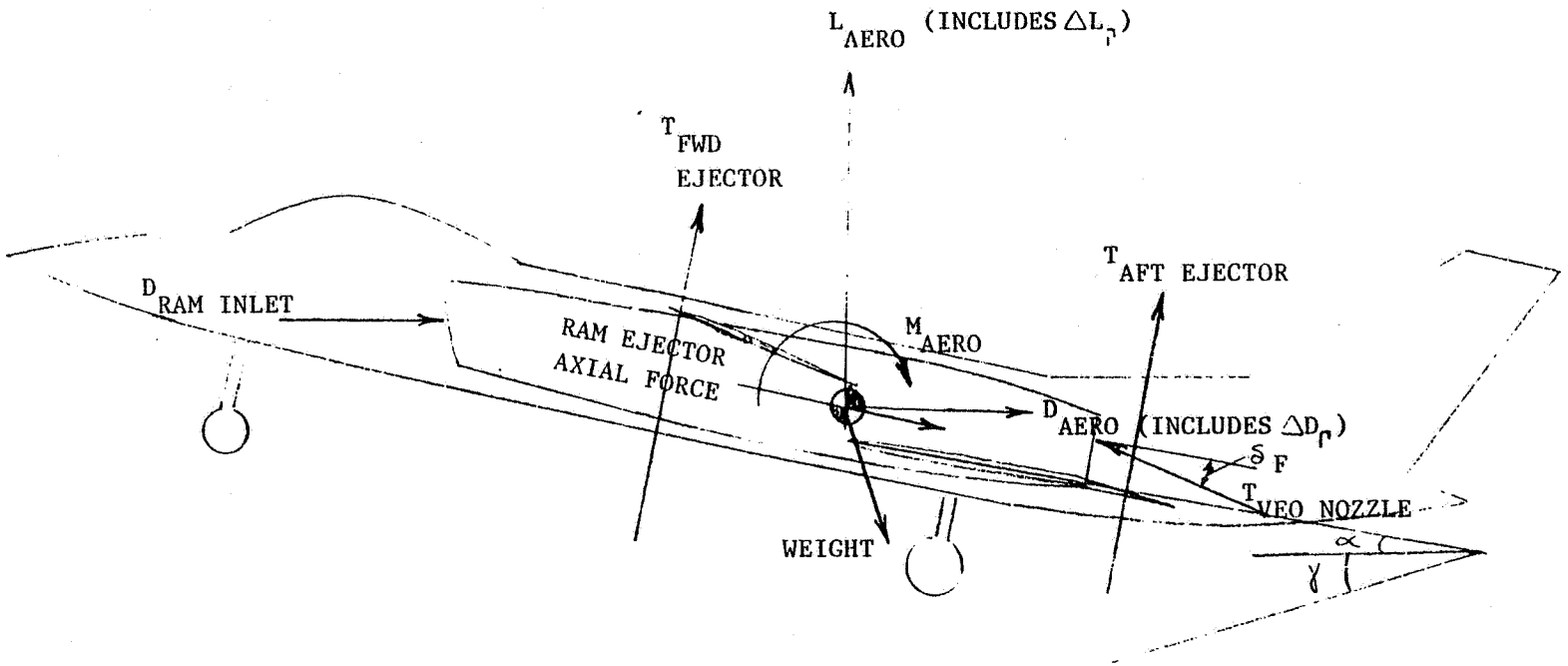

Figure 4-1 Longitudinal Forces Acting on E205

Table 4-1 Methods Summary

FLIGHT REGIME	PROPULSION SYSTEM EMPLOYED	VEO NOZZLE THRUST ANGLE	VEO NOZZLE THRUST MAGNITUDE	BOOKKEEPING AND TRIM METHODS	DATA TYPE PRESENTED
STOL, VTOL $M \leq .3$	THRUST VECT FROM VEO NOZZLE + EJECTOR THRUST + SPANWISE BLOWING (NOT USED IN REPORTED ANALYSIS BUT POSSIBLE)	$\delta_{TE} = 30^{\circ}$	$C_T \leq 7.4$	GROSS THRUST APPLIED/REMOVED IN ($+\delta_{TE}$) DIRECTION NOZZLE & INLET FORCES APPLIED EXTERNALLY TRIM w FLAPERON, CANARD, EJECTORS, VEO WING NOZZLE	AERO EQUIVALENT TOTAL
CRUISE/ MANEUVER $.3 \leq M \leq 1.0$	THRUST VECT FROM VEO NOZZLE	$\delta_{TE} = 15^{\circ}$	$C_T \leq .2$	NET THRUST APPLIED/REMOVED IN DIRECTION INDUCED & VECTORING EFFECTS INCLUDED IN "EQUIVALENT" POLAR NOZZLE & INLET FORCES IN PROP. TRIM WITH FLAPERON, CANARD, VEO WING NOZZLE	EQUIVALENT
DASH $M > 1.0$	NO THRUST VECTORING NO SPANWISE BLOWING	$\delta_{TE} = 0^{\circ}$	$C_T < .15$	CONVENTIONAL A/C METHODS (USE UNPOWERED DATA) TRIM WITH CANARD	EQUIVALENT

Where C.G.W.L. = waterline for center-of-gravity location

C.G.F.W. = fuselage station for center-of-gravity location

V.N.F.S. = fuselage station of VEO-Wing nozzle thrust vector

EJ. F.S. = fuselage station of ejector thrust vector.

Assuming ejector thrust always 90° to W.L., i.e. no thrust recovery.

2. Equivalent Coefficients (Subscript E): Aerodynamic plus thrust forces with thrust-angle-of-attack effects removed are:

$$C_{L_E} = C_{L_T} - C_{T_{V.N.}} \sin\alpha - C_{T_{EJ}} \cos\alpha + C_{\substack{DRam \\ Ejector}} \sin\alpha$$

$$C_{D_E} = C_{D_T} + C_{T_{V.N.}} \cos\alpha - C_{T_{EJ}} \sin\alpha - C_{\substack{Dram \\ Ejector}} \cos\alpha$$

$$C_{M_E} = C_{M_T} - C_{T_{V.N.}} \left(\frac{c.g.W.L. - V.N.W.L.}{\bar{c}}\right) - C_{T_{EJ}} \left(\frac{C.G.F.S. - EJ.F.S.}{\bar{c}}\right)$$

3. Aerodynamic-Only Coefficients (Subscript Aero): Longitudinal force and moment coefficients with all thrust effects removed:

$C_{L_{Aero}}$, $C_{D_{Aero}}$, $C_{M_{Aero}}$. The coefficients were developed by applying corrections (for super-circulation, VEO-Wing nozzle deflection, and canard deflections, derived from the General Dynamics Research model plus differences between the AFFDL VEO-Wing fighter model and E205 geometry) to the unpowered VEO-Wing fighter model wing-body data of Reference 4.

A detailed set of equations for developing the aero-only coefficients for the E205 configuration in the STO/VTOL regimes is presented in Appendix B. The equivalent coefficients were then developed from these data. The combat/maneuvering aero-data buildup is discussed in Subsection 4.1.2.

TABLE 4-2 E 205 MINIMUM DRAG BUILDUP

S_{ref} = 384 ft^2

DRAG COMPONENT	MACH NUMBER .2	.4	.6	.8	.9	1.2	1.6	2.0
	(Drag in Counts)							
Friction	166.5	149.3	139.0	130.4	126.5	116.0	103.0	90.8
Form	17.2	15.5	14.2	13.4	13.1	-	-	-
Interference	8.2	6.9	10.9	21.0	22.2	-	-	-
Wing Camber	2.1	2.1	2.1	2.1	6.3	9.4	10.4	14.6
Roughness + Protuberance	25.9	25.9	25.9	25.9	25.9	32.5	28.8	25.4
Flap Scrub	32.7	10.9	5.5	4.4	4.4	2.2	1.1	1.1
Wave	-	-	-	-	-	292.3	289.4	281.4
Missiles + Launchers								
(2) Wing-Tip LCLM	7.7	7.7	7.7	7.9	8.7	16.1	14.3	12.2
(2) NAC-MT'D AMRRAM	7.7	7.7	7.7	7.9	8.9	13.5	11.0	7.5
Trim	0	0	0	0	0	0	8	8
Total $C_{D_{min}}$	268	226	213	213	216	482	466	441

4.1.1 Minimum Drag Buildup

Table 4-2 presents the estimated minimum trimmed drag component buildup for the E205 configuration ($.2 \leq M \leq 2.0$) (with canard, VEO-Wing nozzle, and flaperons at a zero-degree deflection). Trimmed minimum drag is plotted versus Mach number in Figure 4-2. The subsonic and supersonic friction, form, wing camber, and interference drag were estimated by an empirical aircraft aerodynamic prediction method developed by General Dynamics for AFFDL (Reference 5). The supersonic wave drag was estimated by a modified version of the Harris area-rule procedure. The roughness-plus-protuberance drag was estimated as 18% of the friction plus form drag subsonically and 28% of friction drag supersonically based on F-16 flight test experience. The flap scrub drag was estimated by the following equation from Reference 6 for a nominal engine condition (Max A/B).

$$C_{D_{\substack{\text{Scrub}\\ \text{Drag}}}} = C_f \frac{A_{wet}}{S_{Ref}} \times \frac{q_{\text{Local Cooled}}}{q_\infty}$$

where A_{wet} = wetted area of flap washed by VEO-nozzle jet

S_{ref} = reference wing area

$q_{\text{Local Cooled}}$ = film-cooling dynamic pressure (VEO-Wing nozzle has a fan air liner that puts out a sheet of film-cooling airflow over the flap to prevent burning up the flap)

q_∞ = free-stream dynamic pressure

C_f = turbulent skin friction coefficient at the R_N of the film-cooling flow.

The incremental drag of the installed missiles and launchers for the DLI mission (Figure 4-3) was estimated by use of the semi-empirical method of reference 7. By this same method, the minimum drag increment the STOL store-loading of Figure 4-4 (2 LCLMs, 4 guided advanced 1000-lb bombs, and two 370-gallon external fuel tanks + pylons and racks) is estimated as 125

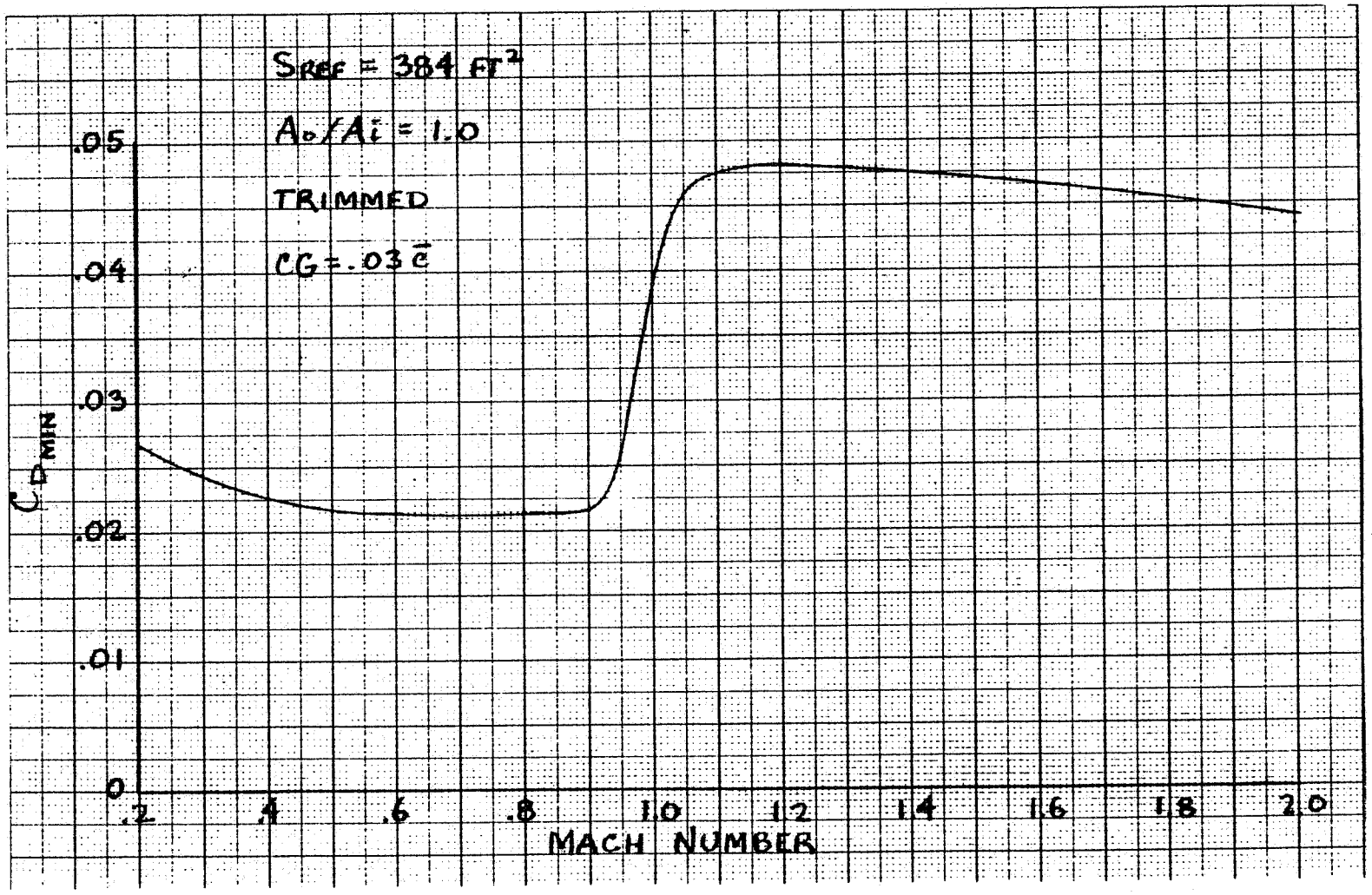

Figure 4-2 E205 Minimum Trimmed Drag Versus Mach Number

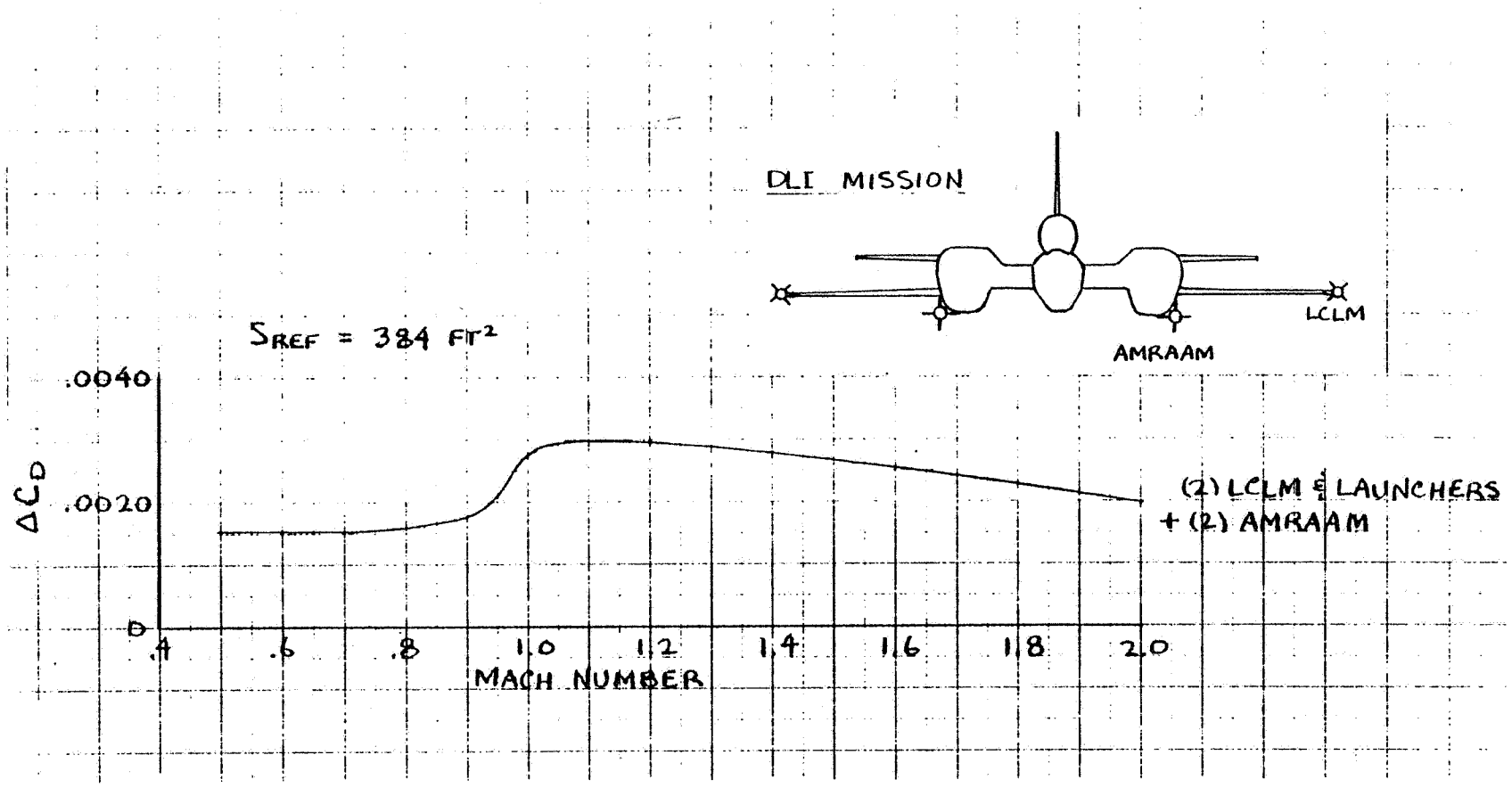

Figure 4-3 Store Drag Increments for DLI Mission

V/STOL B CONFIG E205

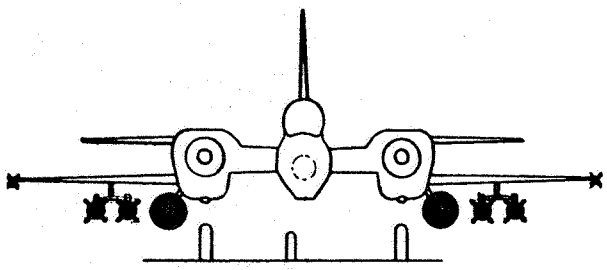

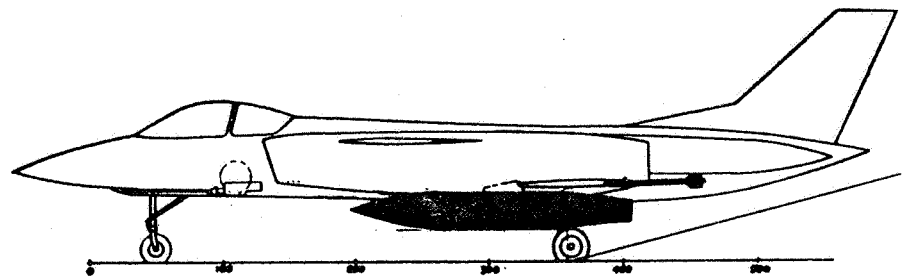

STOL TAKEOFF LOADING
- 2 LCLM
- 4 Guided Advance General Purpose Bombs (1000 Lb)
- 2 370 Gallon Fuel Tanks

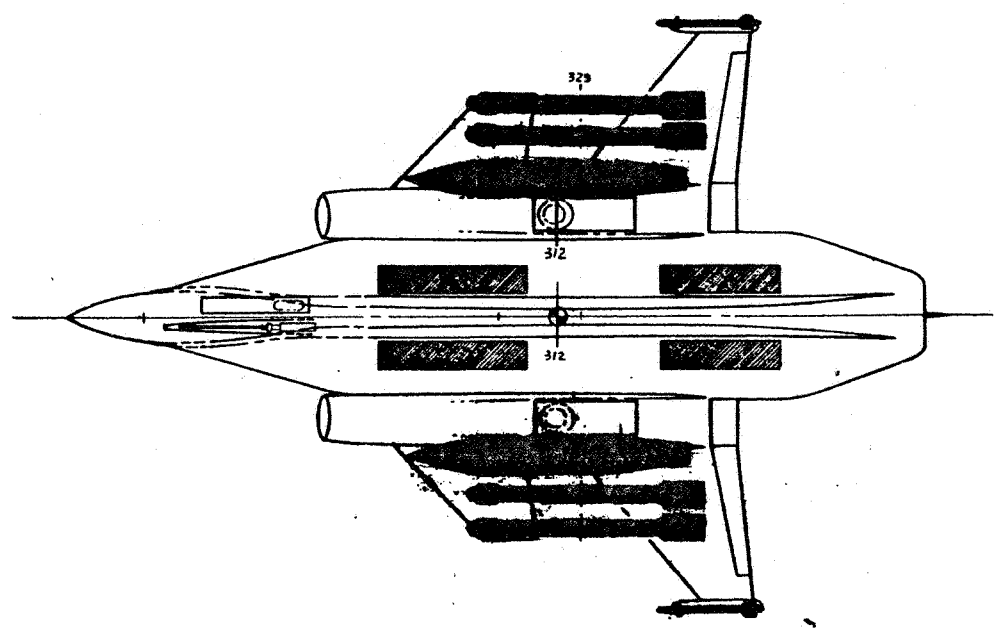

Figure 4-4 STOL Store Loading

counts (.0125). The minimum drag increment of the landing gear and ejector doors is estimated to be .0350 using the method of Reference 8, which correlates gear and gear-door drag (frontal area) with airplane type and takeoff gross weight.

The airplane also experiences an ejector ram drag penalty when the ejector is activated. It is calculated by the following equation, which simply brings the entrained mass of air to rest:

$$D_{\substack{\text{Ram}\\ \text{Ejector}}} = RK \left(\frac{\dot{w}}{g_c} \right) V_\infty \cos \alpha$$

where $R = \dfrac{\text{Ejector Primary + Ejector Secondary + Entrained Airflow}}{\text{Airflow Supplied by Engine to Ejector - Ducting Losses}}$

$\approx$ 15 for Alperin ejector

K = % of total engine air diverted to the ejector

$\frac{\dot{w}}{g_c}$ = total engine airflow at engine exit

V_∞ = free stream velocity

4.1.2 Lift, Drag, and Pitching Moment Estimates Including Trim Effects

Figures 4-5, 4-6, and 4-7 present examples of the three types of VSTOL aerodynamic coefficient data discussed previously: aero-only, equivalent and total lift, drag, and pitching moment coefficient curves for the matrix: C_T = 0, 2.0, 5.0; $\delta_{TE} = 0^o$, 15°, 30° and canard deflections ranging from -8° to $+20^o$ deflection. Estimates of the aero data for all of these combinations were required because the STOL analysis computer routine employed in this study performs the trim process internally according to specified flight laws. Since the ejector can be used for a trim device in STOL/VTOL operations, the equivalent and total aero data are presented with variations in forward (only) ejector thrust to illustrate how this trim process can be accomplished at low speeds. This aero data includes supercirculation, canard, and VEO-Wing nozzle deflection increments derived from the General Dynamics' research model test data, as described and displayed in Appendix B. Example data is also presented for the effects of spanwise blowing on the supercirculation increments (although not employed in the STOL/VTOL analysis presented in this report).

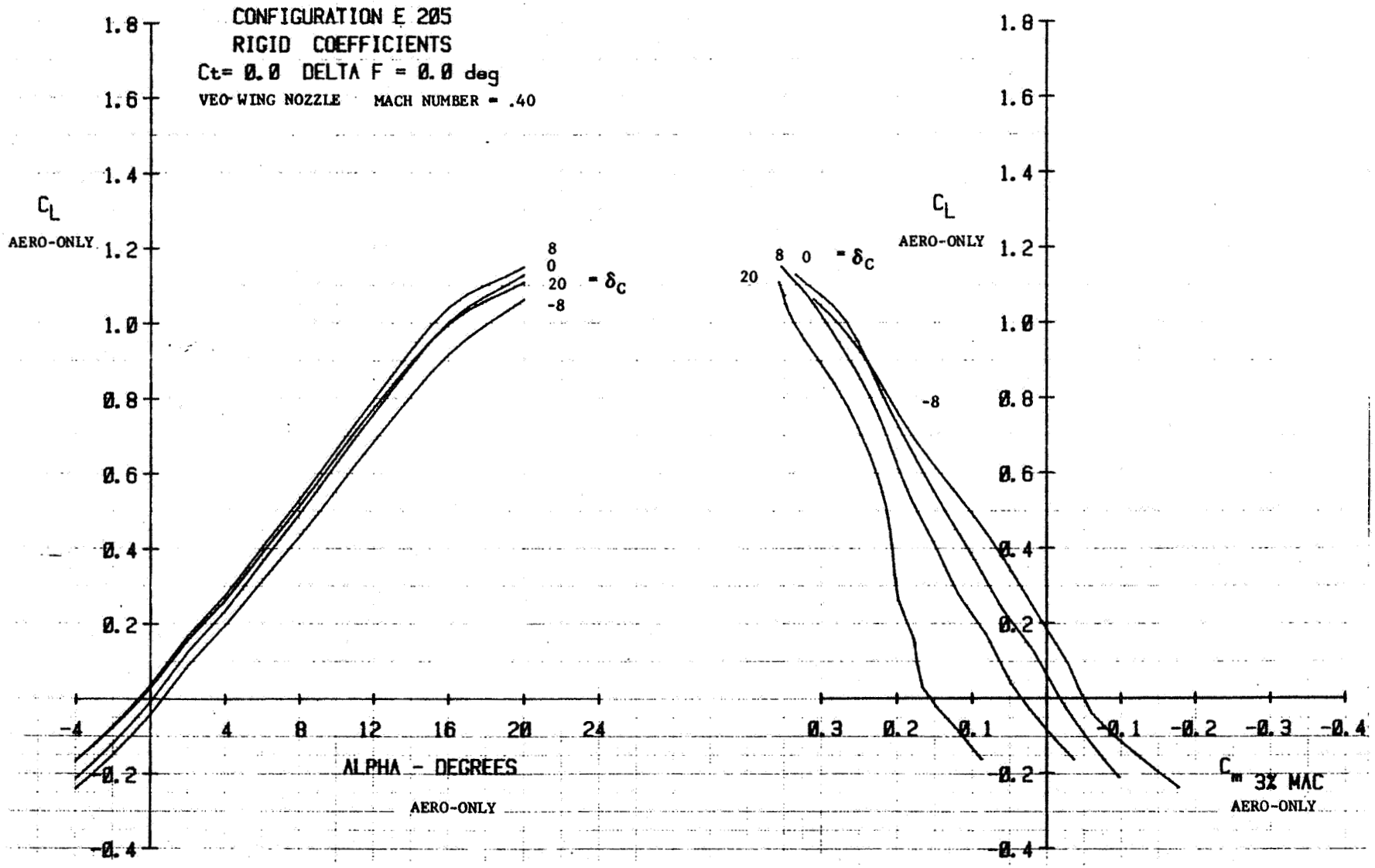

Figure 4-5a. V/STOL aerodynamic data, aero-only coefficients power off, $\delta_F = 0^o$, Mach = .4

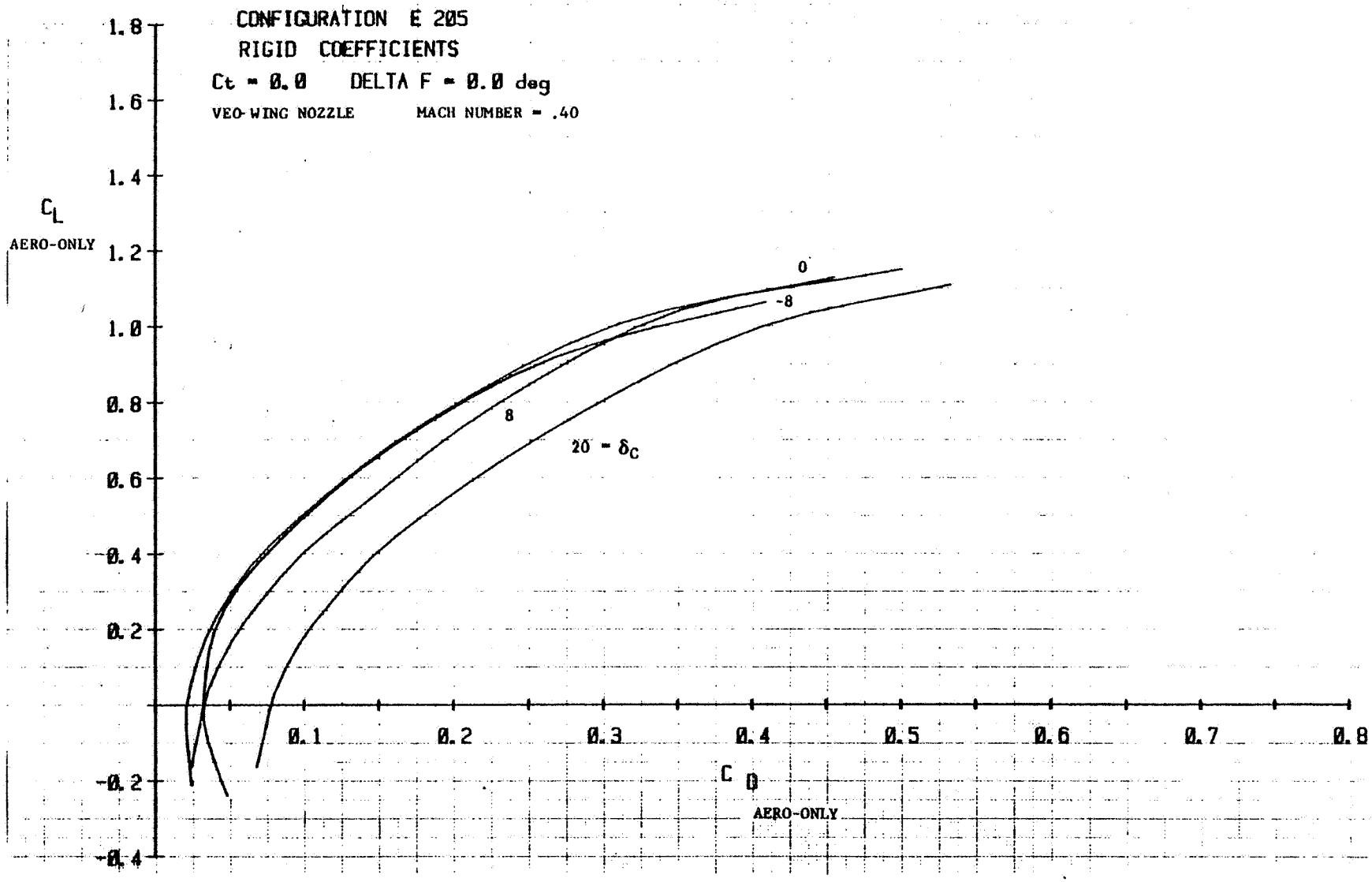

Figure 4-5a. (con't) V/STOL aerodynamic data, aero-only coefficients power off, $\delta_F = 0^o$, Mach = .4

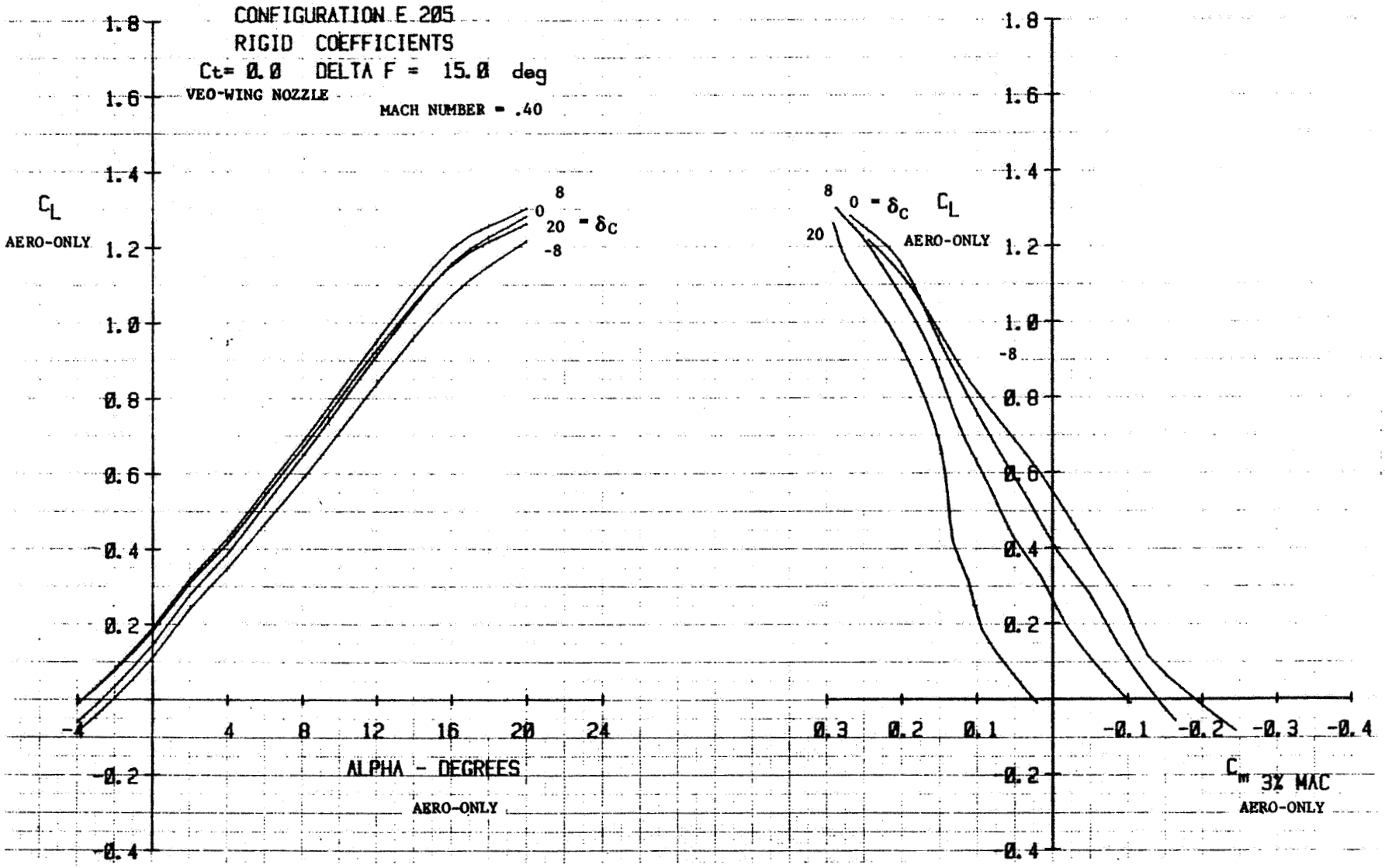

Figure 4-5b. V/STOL aerodynamic data, aero-only coefficients power off, $\delta_F = 15^o$, Mach = .4

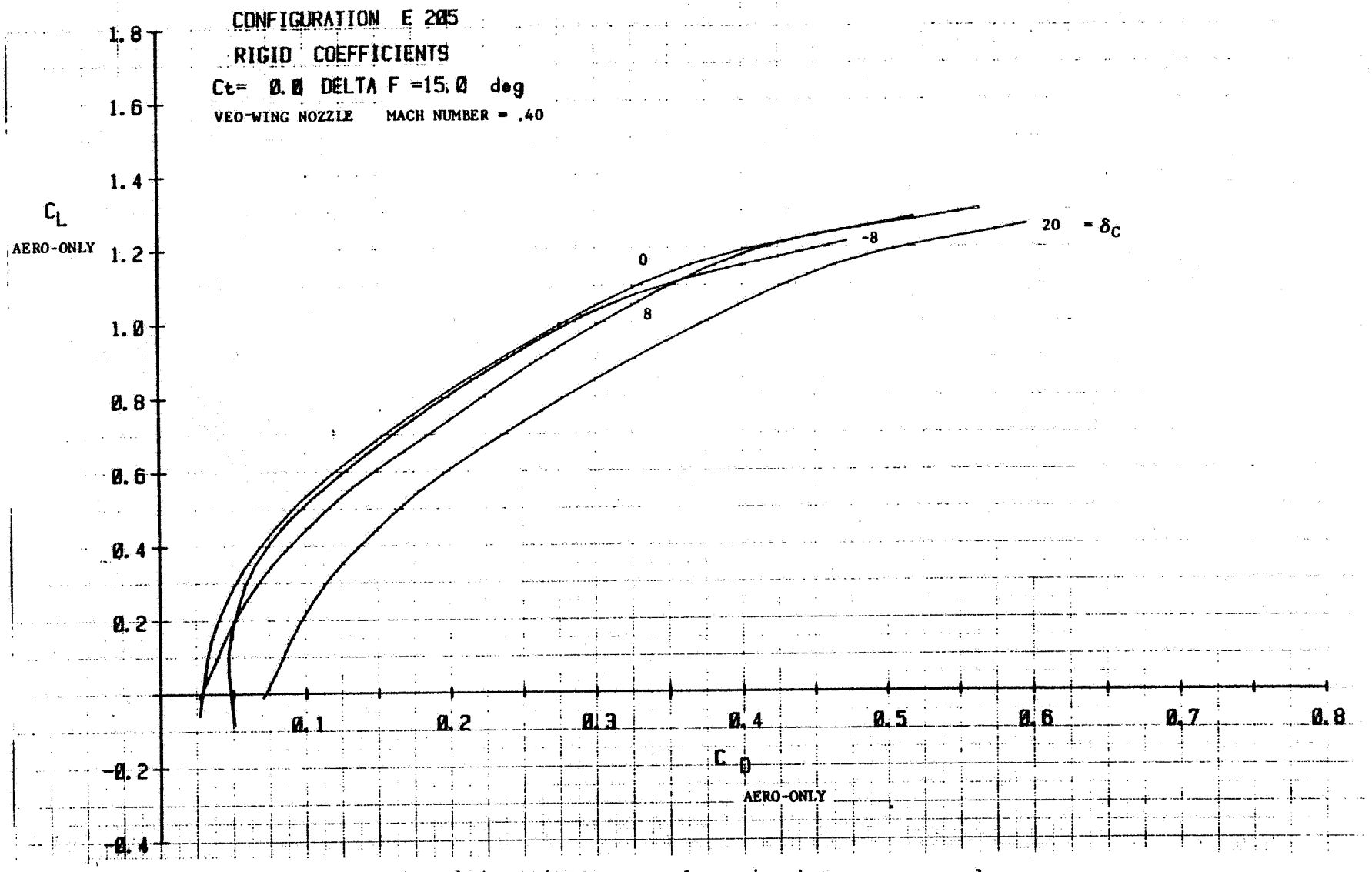

Figure 4-5b. (con't) V/STOL aerodynamic data, aero-only coefficients power off, δ_F = 15°, Mach = .4

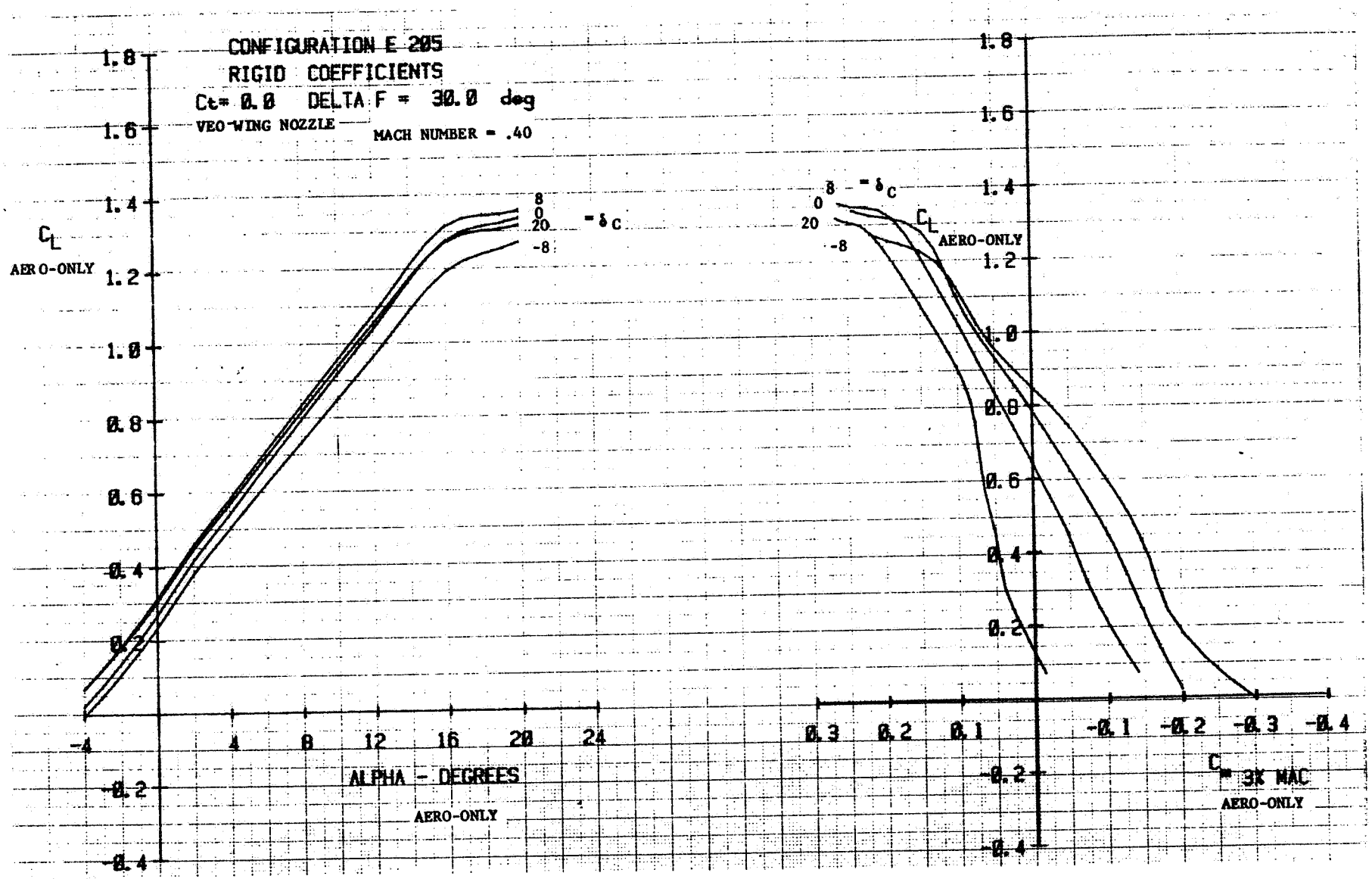

Figure 4-5c. V/STOL aerodynamic data, aero-only coefficients power off, $\delta_F = 30^o$, Mach = .4

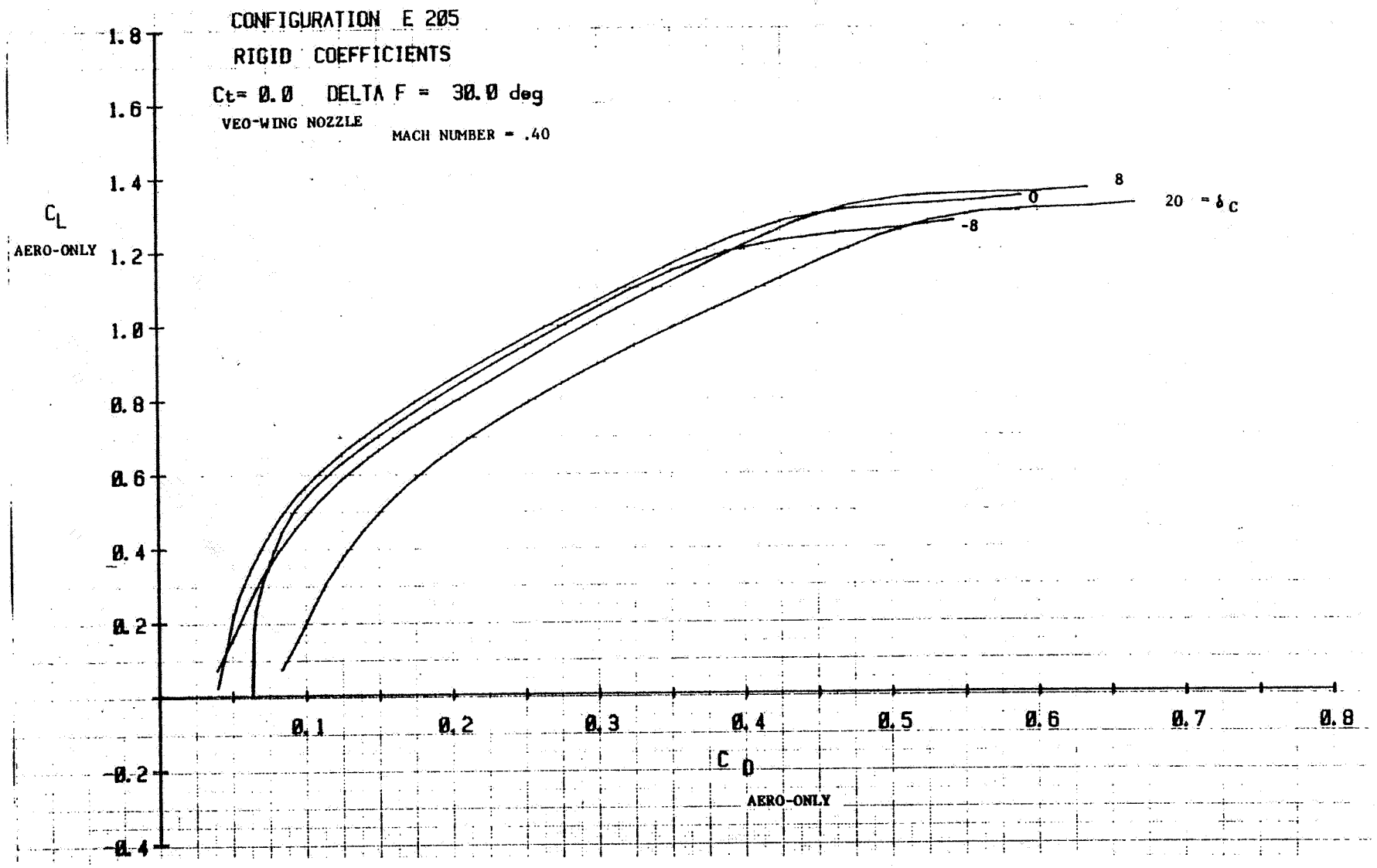

Figure 4-5c. (con't) V/STOL aerodynamic data, aero-only coefficients power off, $\delta_F = 30^o$, Mach = .4

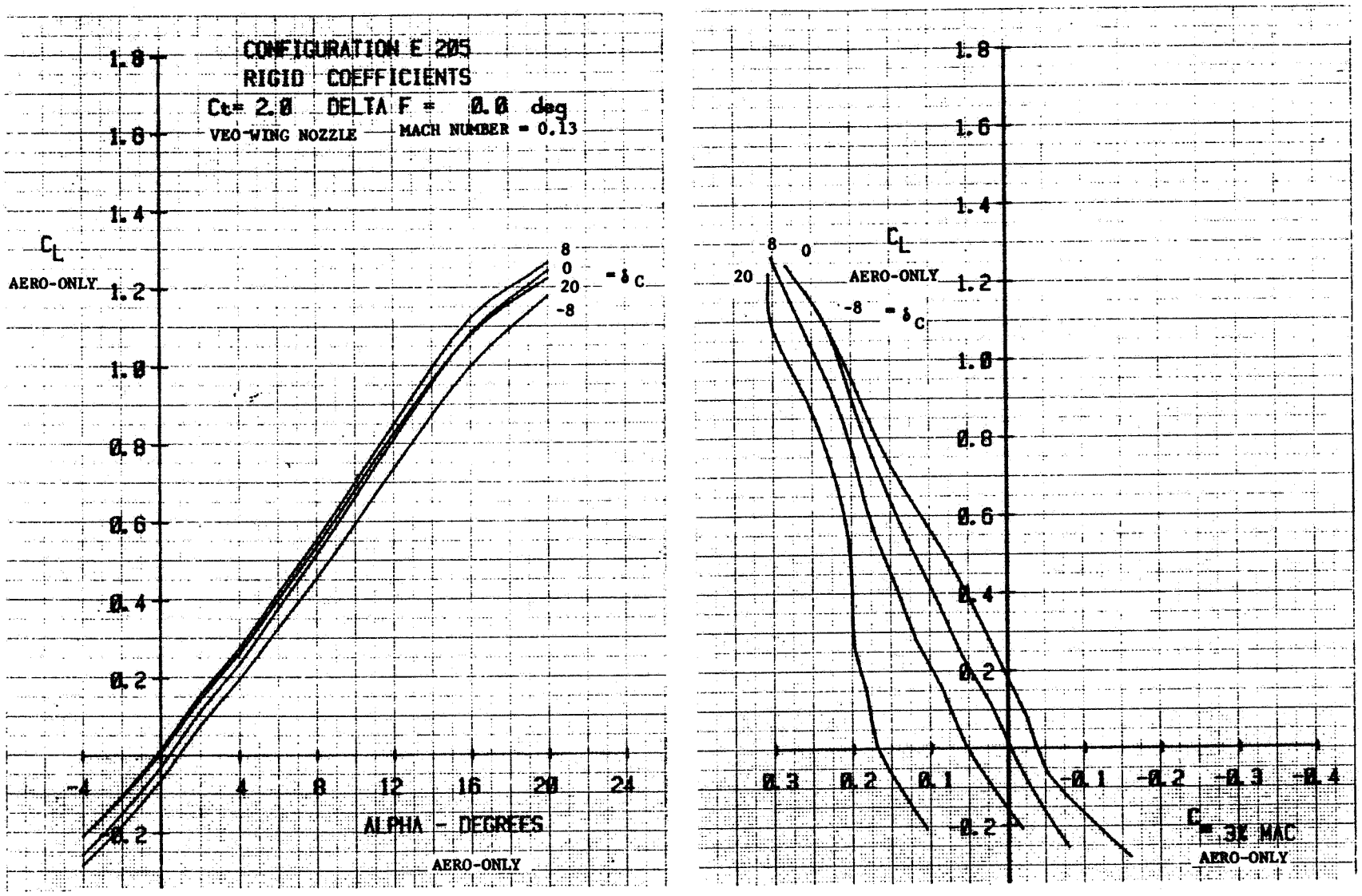

Figure 4-5d. V/STOL aerodynamics data, aero-only coefficients, C_T(total) = 2.0, C_T(VEO-wing nozzle) = 2.0, C_T(ejector) = 0, δ_F = 0°, Mach = .13

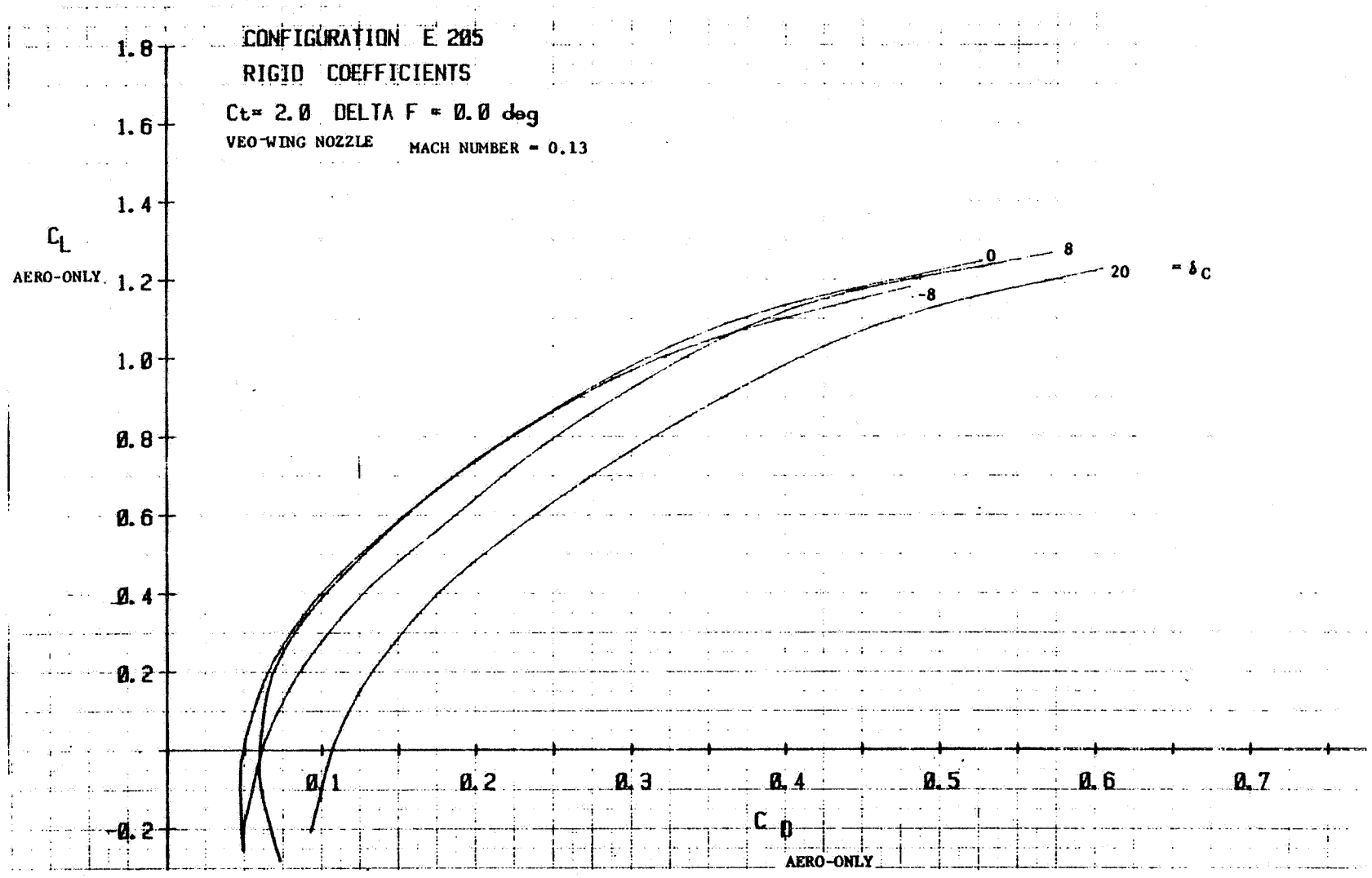

Figure 4-5d. (con't) V/STOL aerodynamics data, aero-only coefficients, C_T(total) = 2.0, C_T(VEO-wing nozzle) = 2.0, C_T(ejector) = 0, $\delta_F = 0^o$, Mach = .13

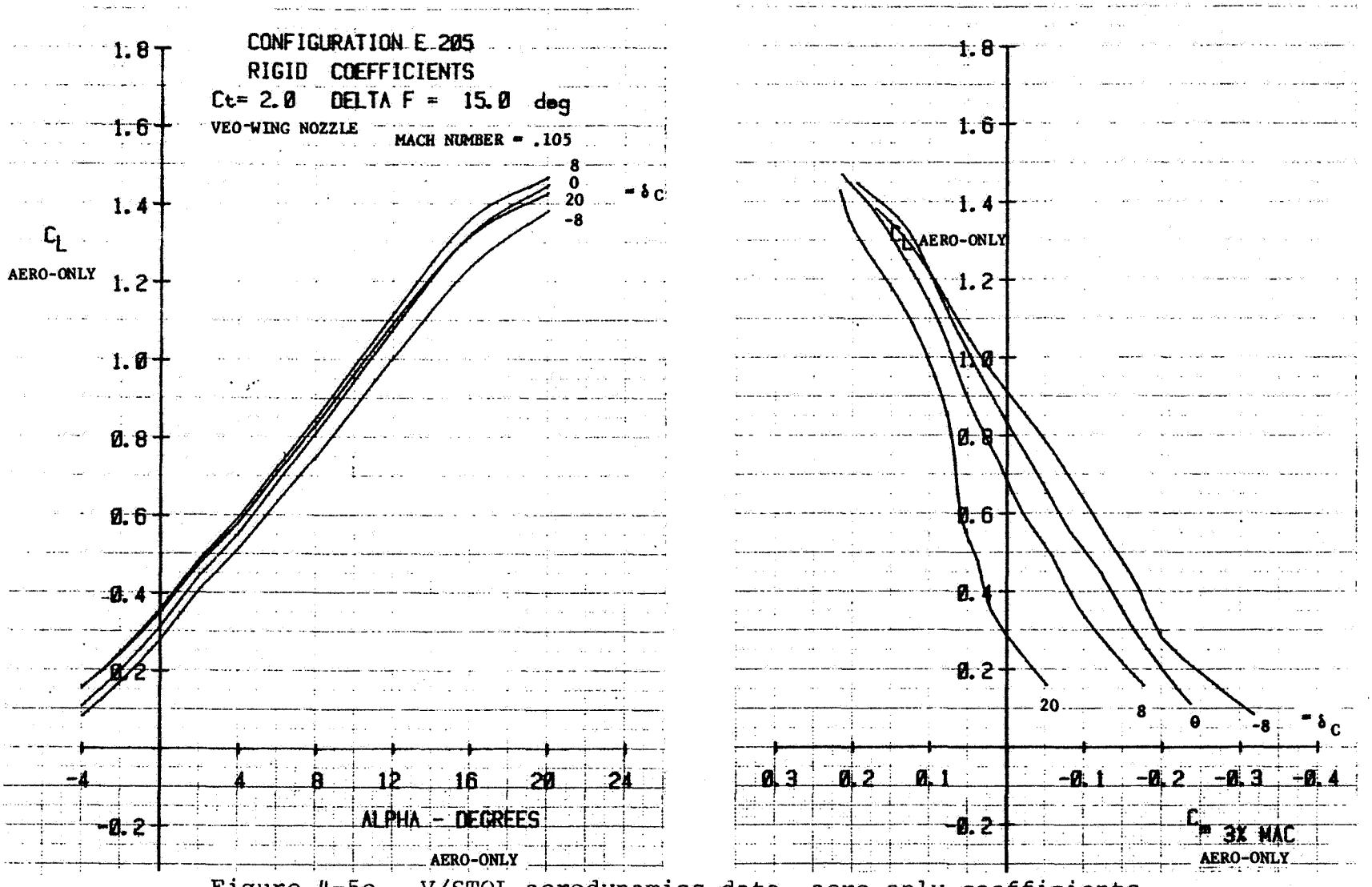

Figure 4-5e. V/STOL aerodynamics data, aero-only coefficients, C_T(total) = 2.0, C_T(VEO-wing nozzle) = 2.0, C_T(ejector) = 0, δ_F = 15°, Mach = .105

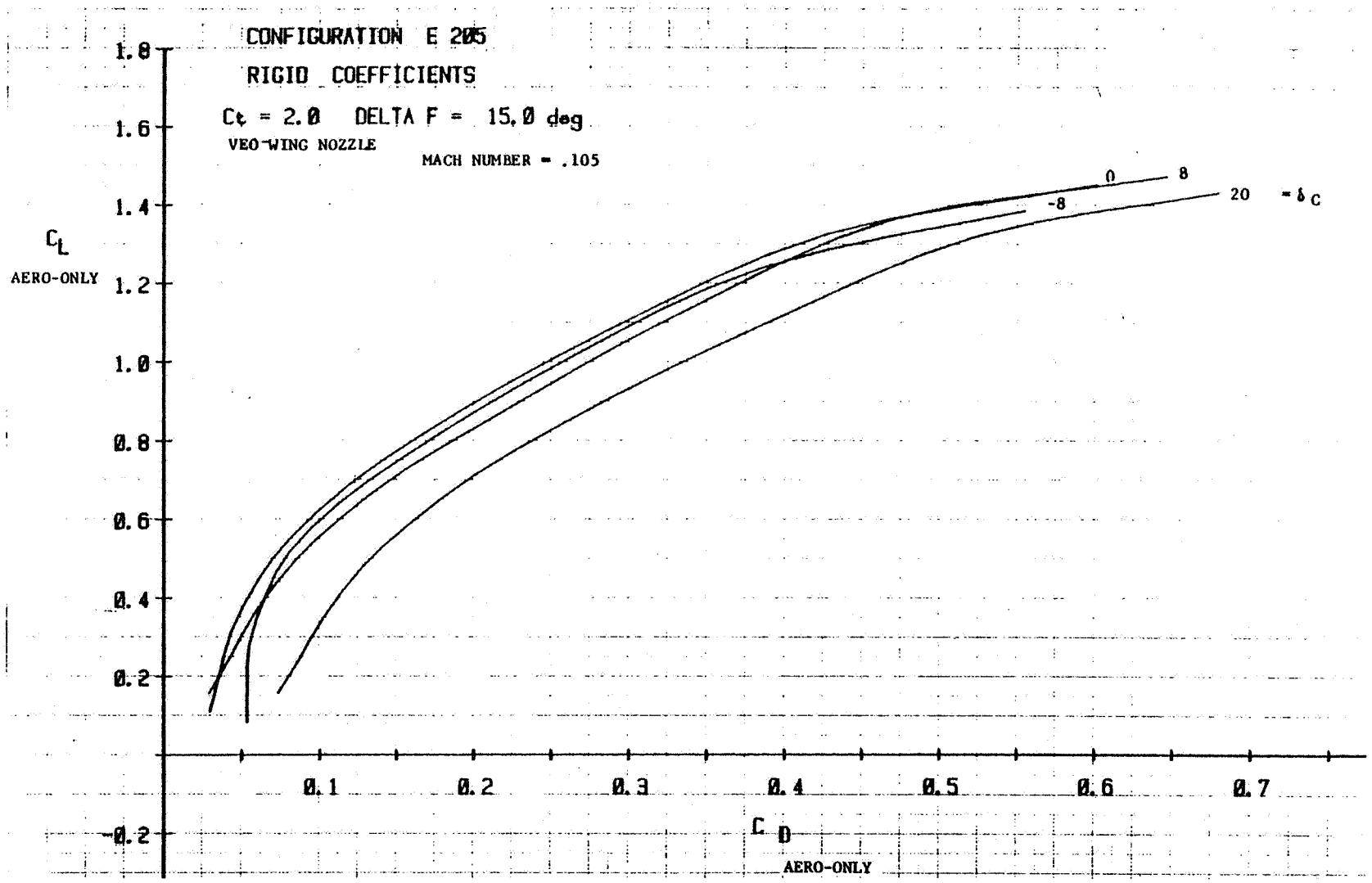

Figure 4.5e (con't) V/STOL aerodynamics data, aero-only coefficients, C_T(total) = 2.0, C_T(VEO-wing nozzle) = 2.0, C_T(ejector) = 0, δ_F = 15°, Mach = .105

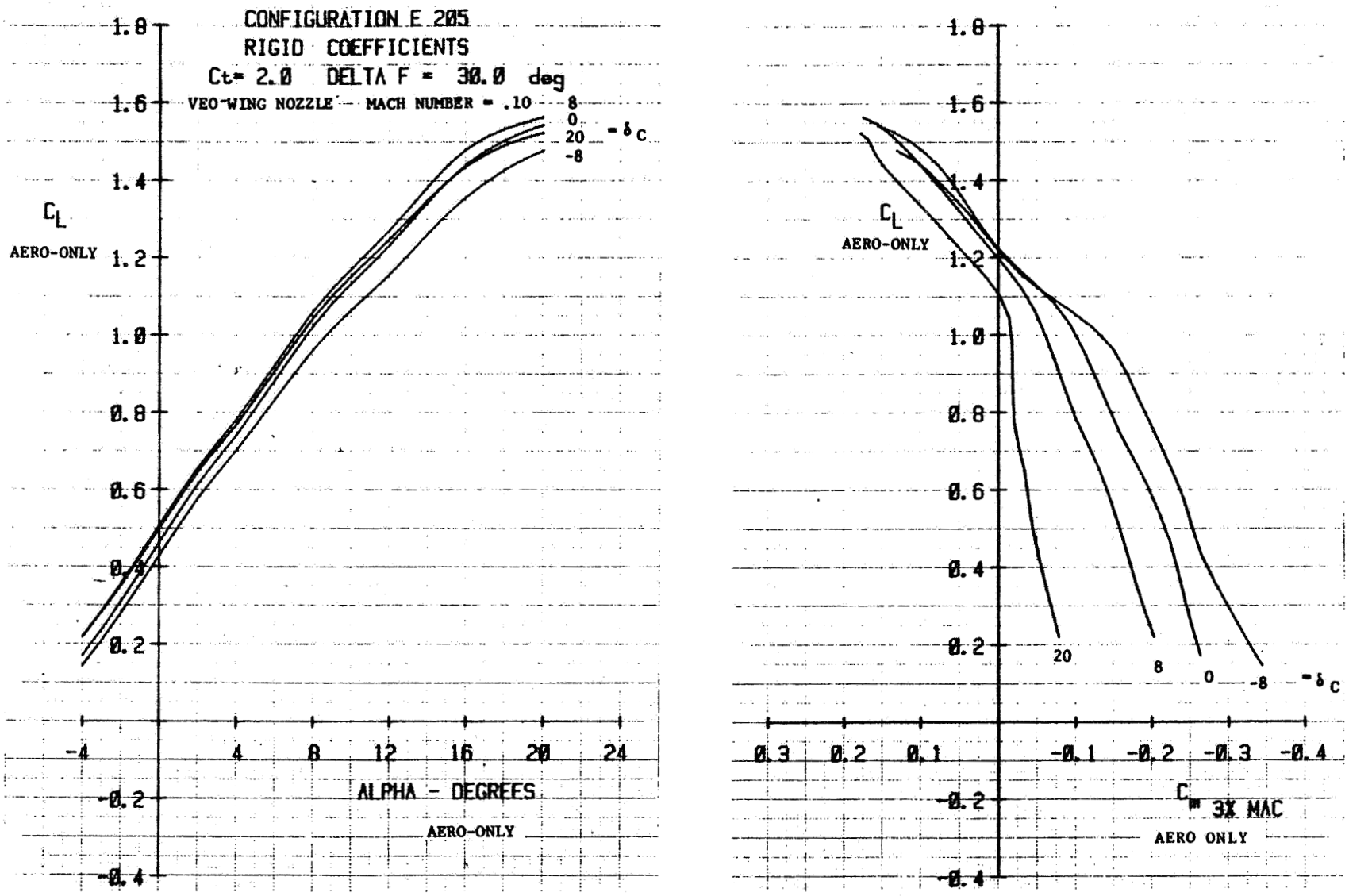

Figure 4-5f. V/STOL aerodynamics data, aero-only coefficients, C_T(total) = 2.0, C_T(VEO-wing nozzle) = 2.0, C_T(ejector) = 0, δ_F = 30°, Mach = .10

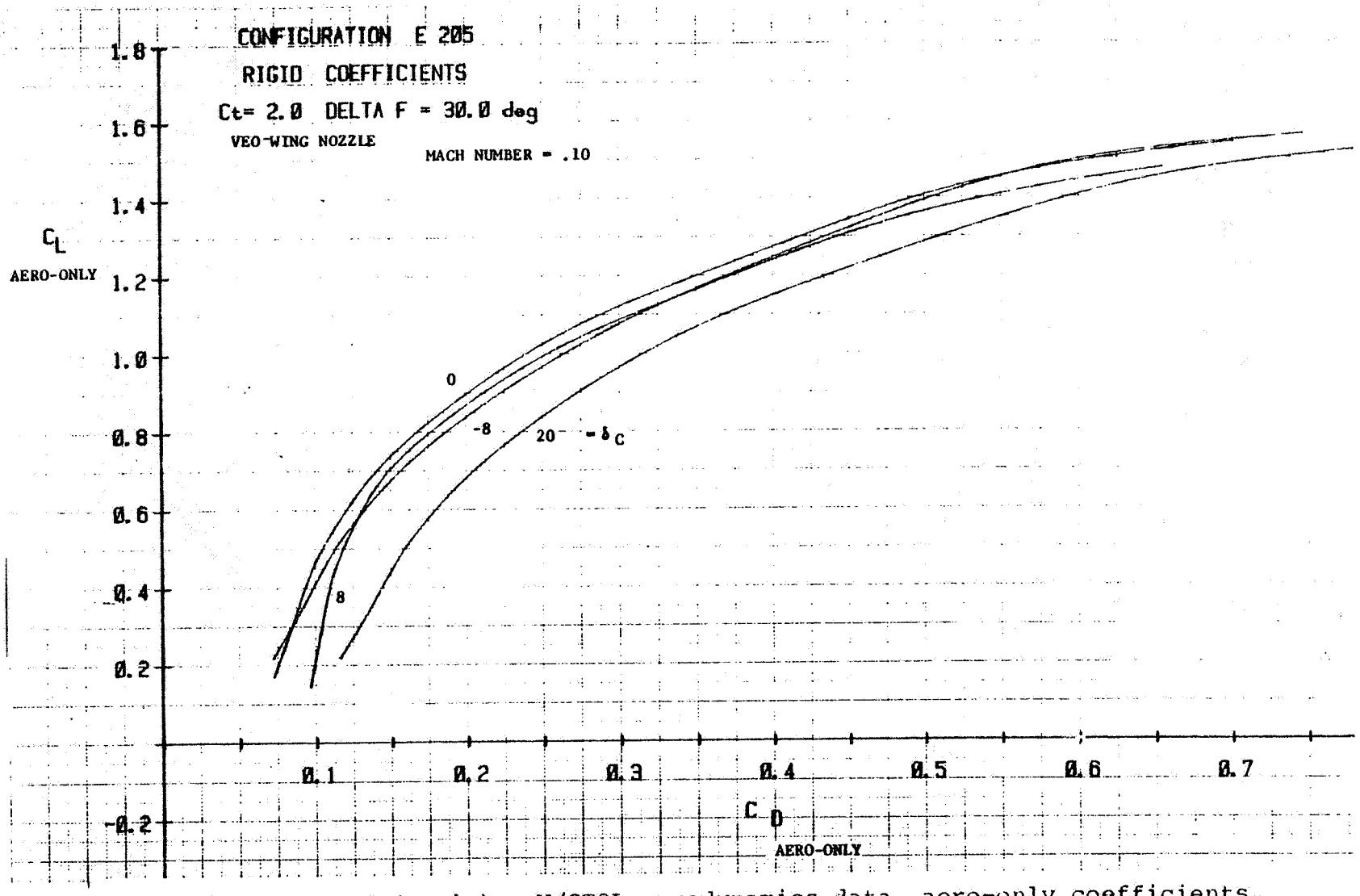

Figure 4-5f (con't) V/STOL aerodynamics data, aero-only coefficients, C_T(total) = 2.0, C_T(VEO-wing nozzle) = 2.0, C_T(ejector) = 0, δ_F = 30°, Mach = .10

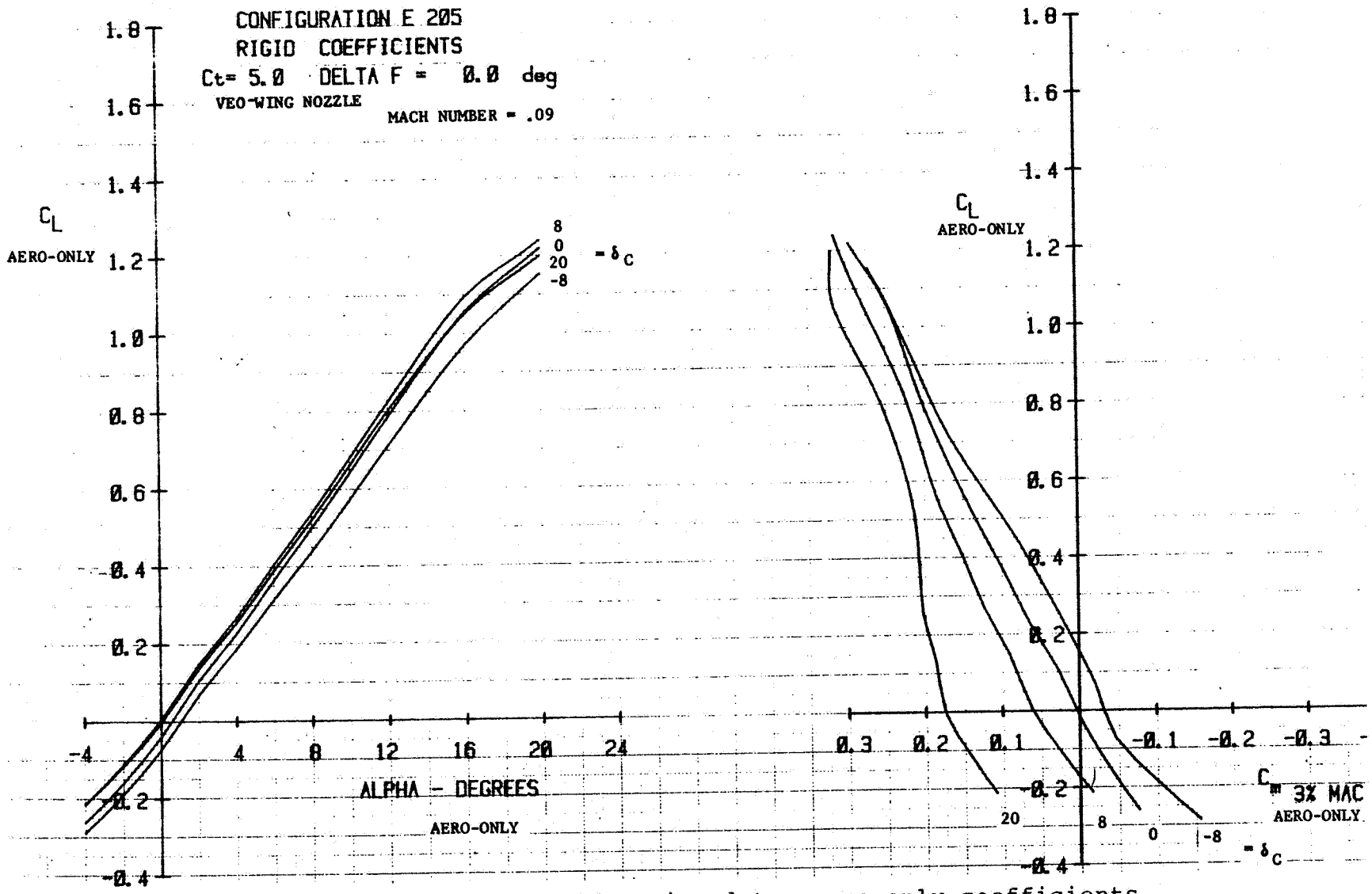

Figure 4-5g. V/STOL aerodynamics data, aero-only coefficients, C_T(total) = 5.0, C_T(VEO-wing nozzle) = 5.0, C_T(ejector) = 0, $\delta_F = 0^o$, Mach = .09

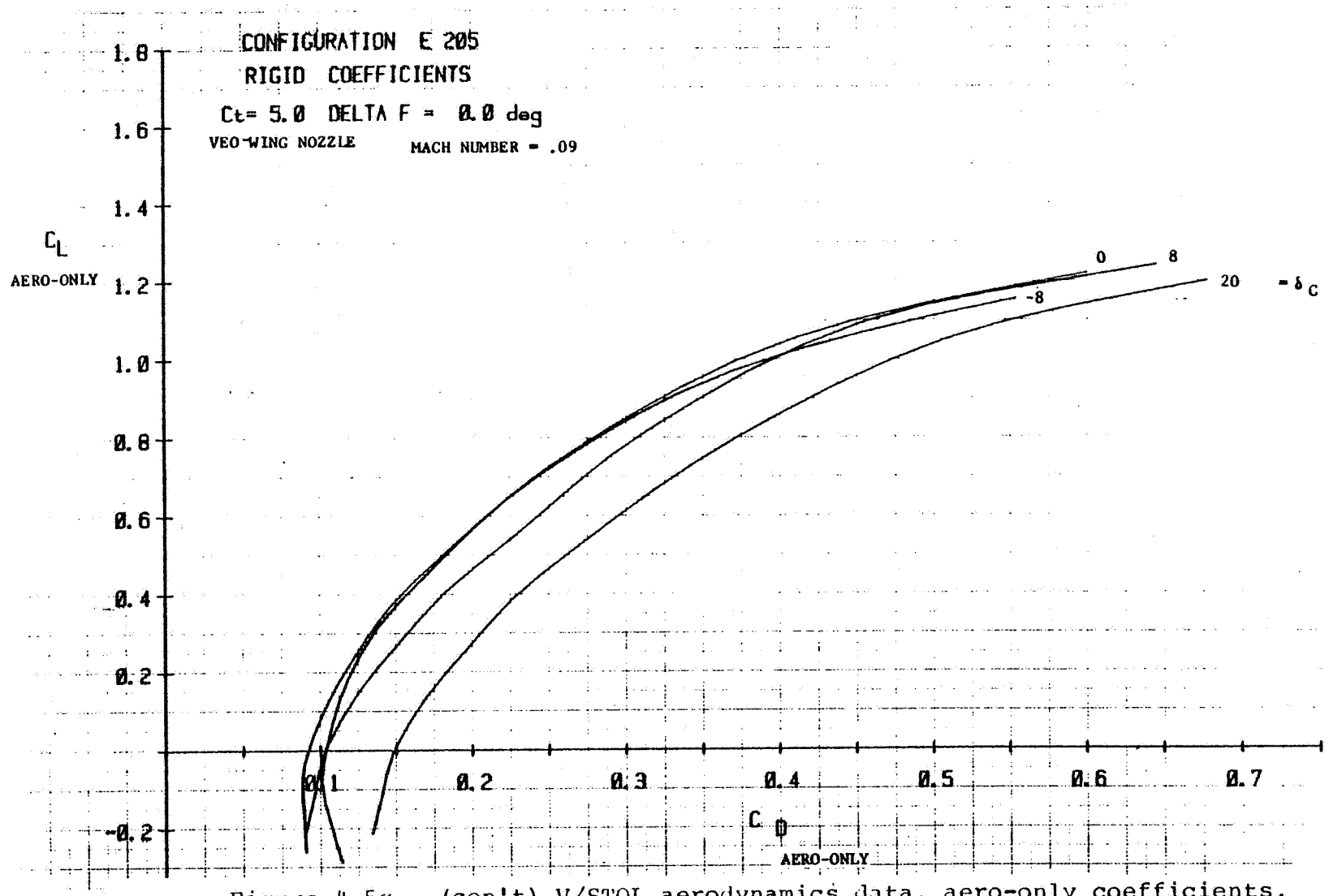

Figure 4-5g. (con't) V/STOL aerodynamics data, aero-only coefficients, C_T(total) = 5.0, C_T(VEO-wing nozzle) = 5.0, C_T(ejector) = 0, δ_F = 0°, Mach = .09

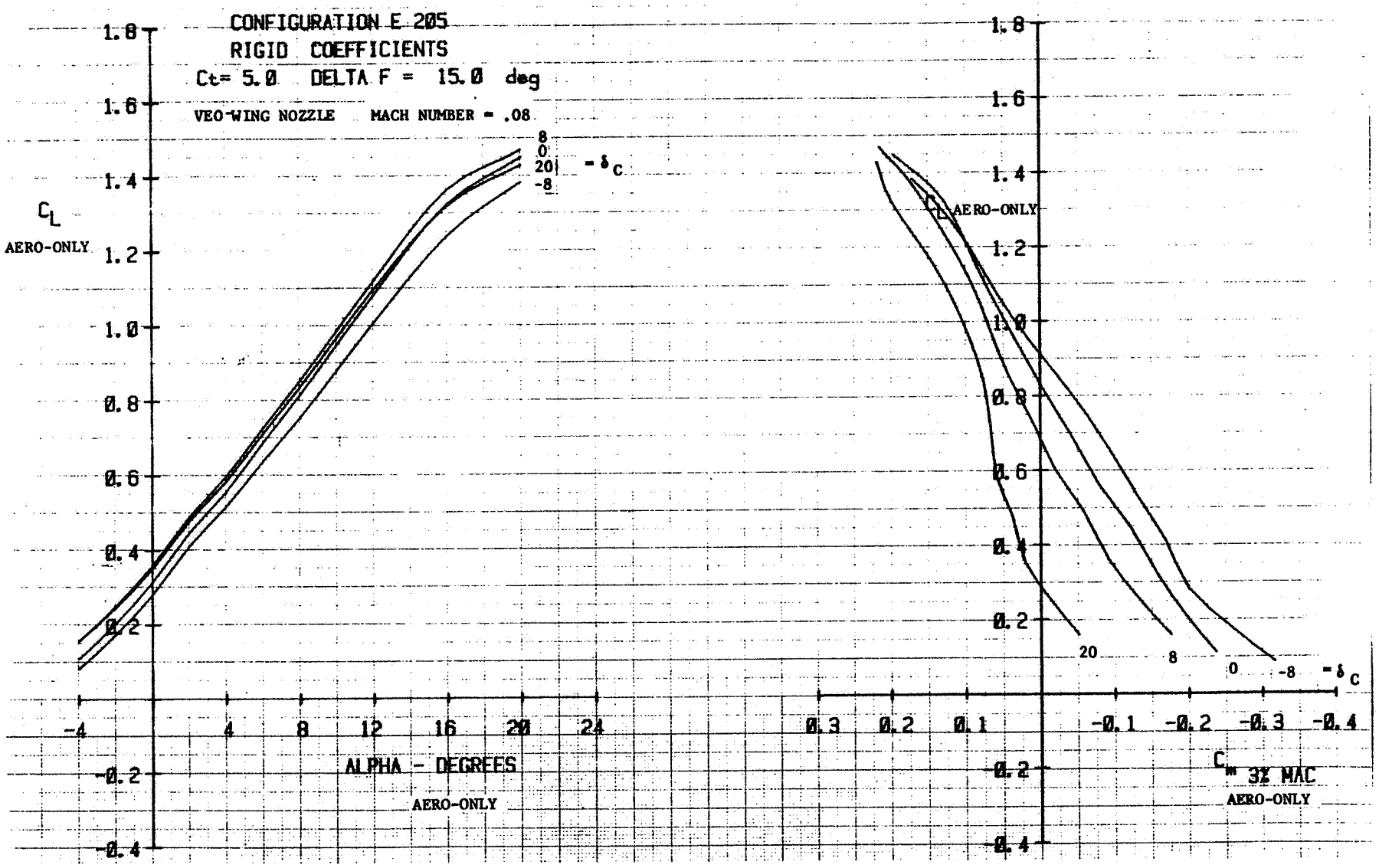

Figure 4-5h. V/STOL aerodynamics data, aero-only coefficients, C_T(total) = 5.0, C_T(VEO-wing nozzle) = 5.0, C_T(ejector) = 0, δ_F = 15°, Mach = .08

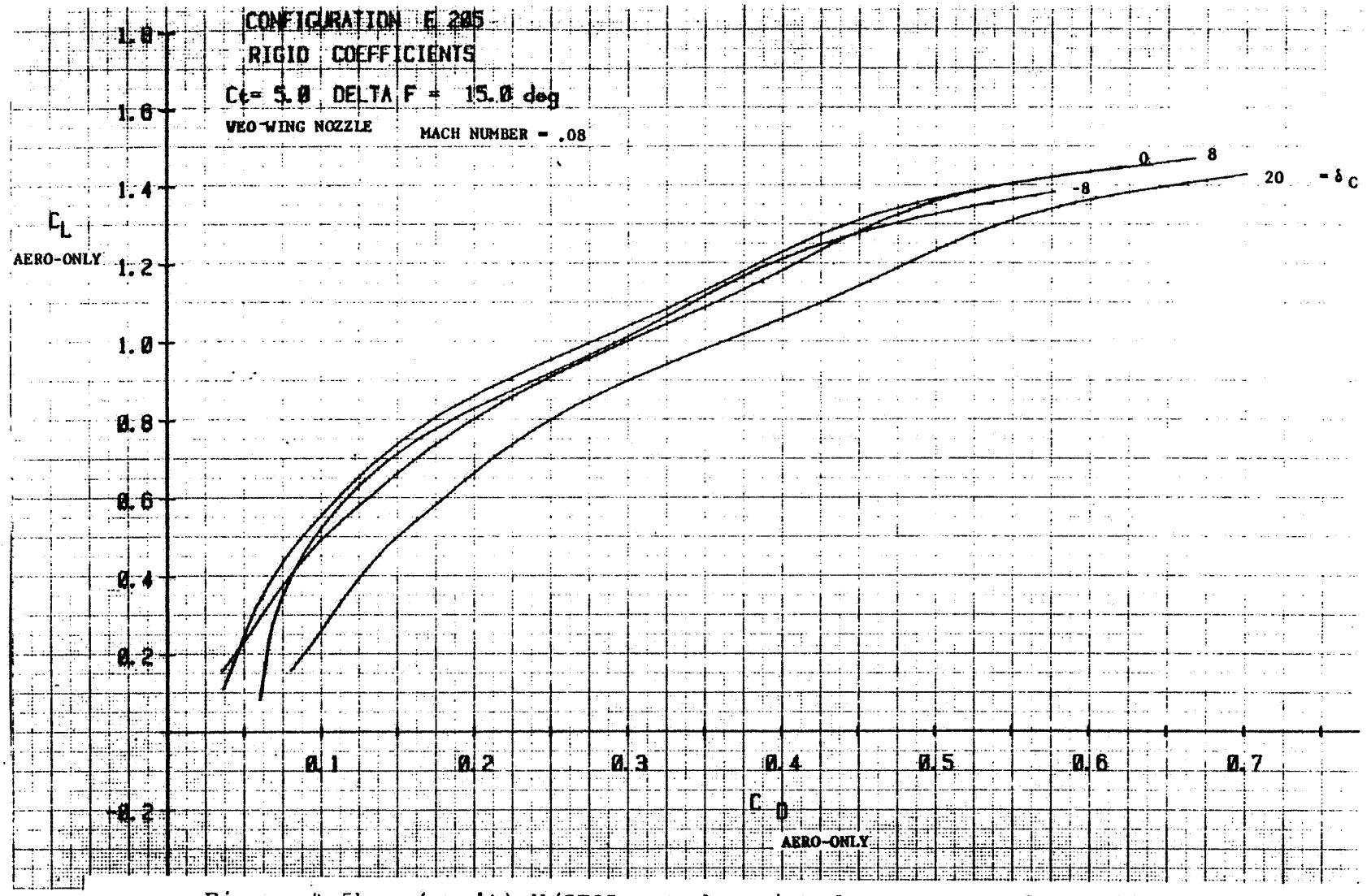

Figure 4-5h. (con't) V/STOL aerodynamics data, aero-only coefficients, C_T(total) = 5.0, C_T(VEO-wing nozzle) = 5.0, C_T(ejector) = 0, δ_F = 15°, Mach = .08

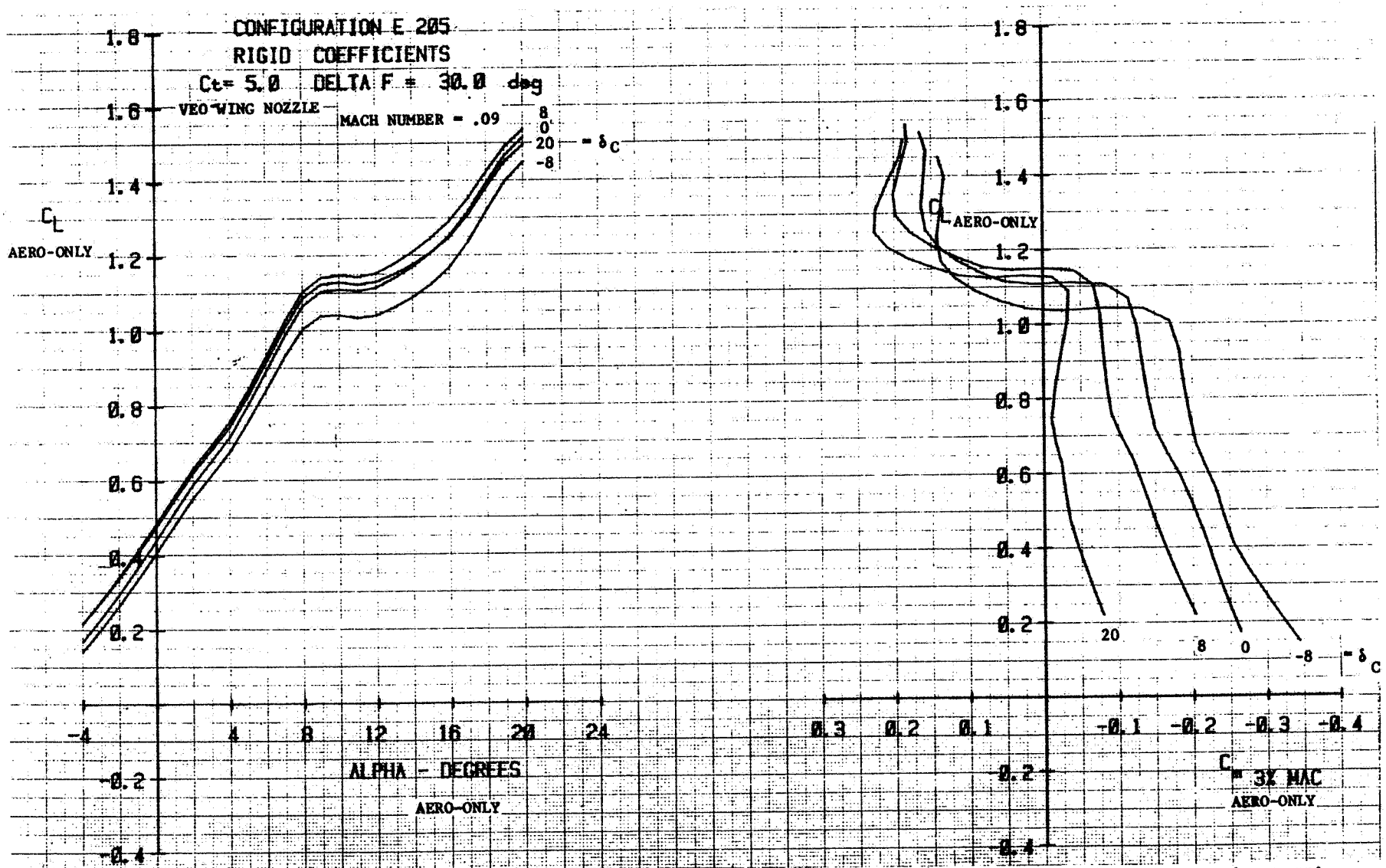

Figure 4-5 i. V/STOL Aerodynamic data, aero-only coefficients, C_T(total)=5.0, C_T(VEO-Wing nozzle)=5.0, C_T(ejector)=0, δ_F=30°, mach=.09

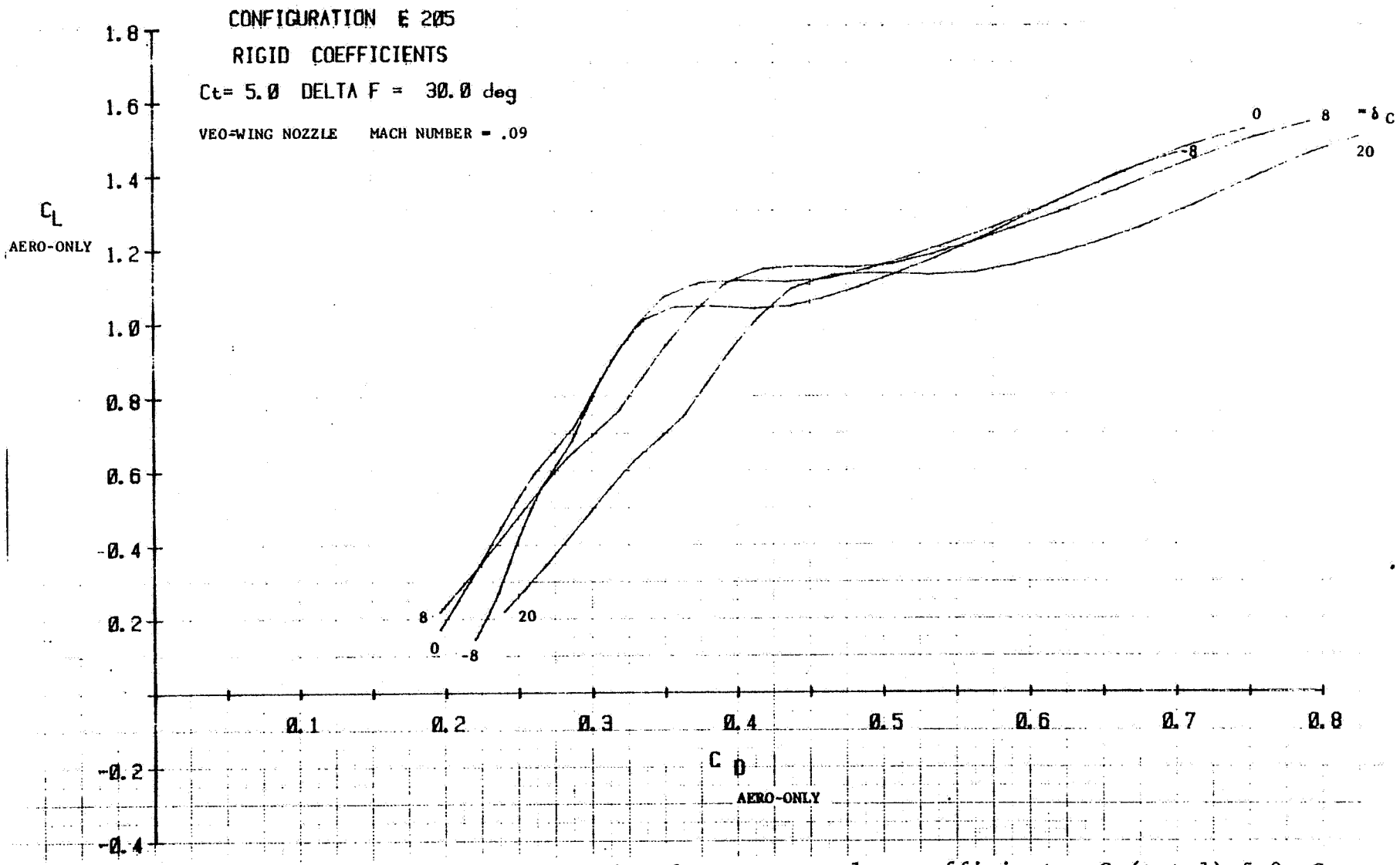

Figure 4-5 i. (cont.) V/STOL Aerodynamic data, aero-only coefficients, C_T(total)=5.0, C_T (VEO-Wing nozzle)=5.0, C_T(ejector)= 0, δ_F=30°, mach=.09

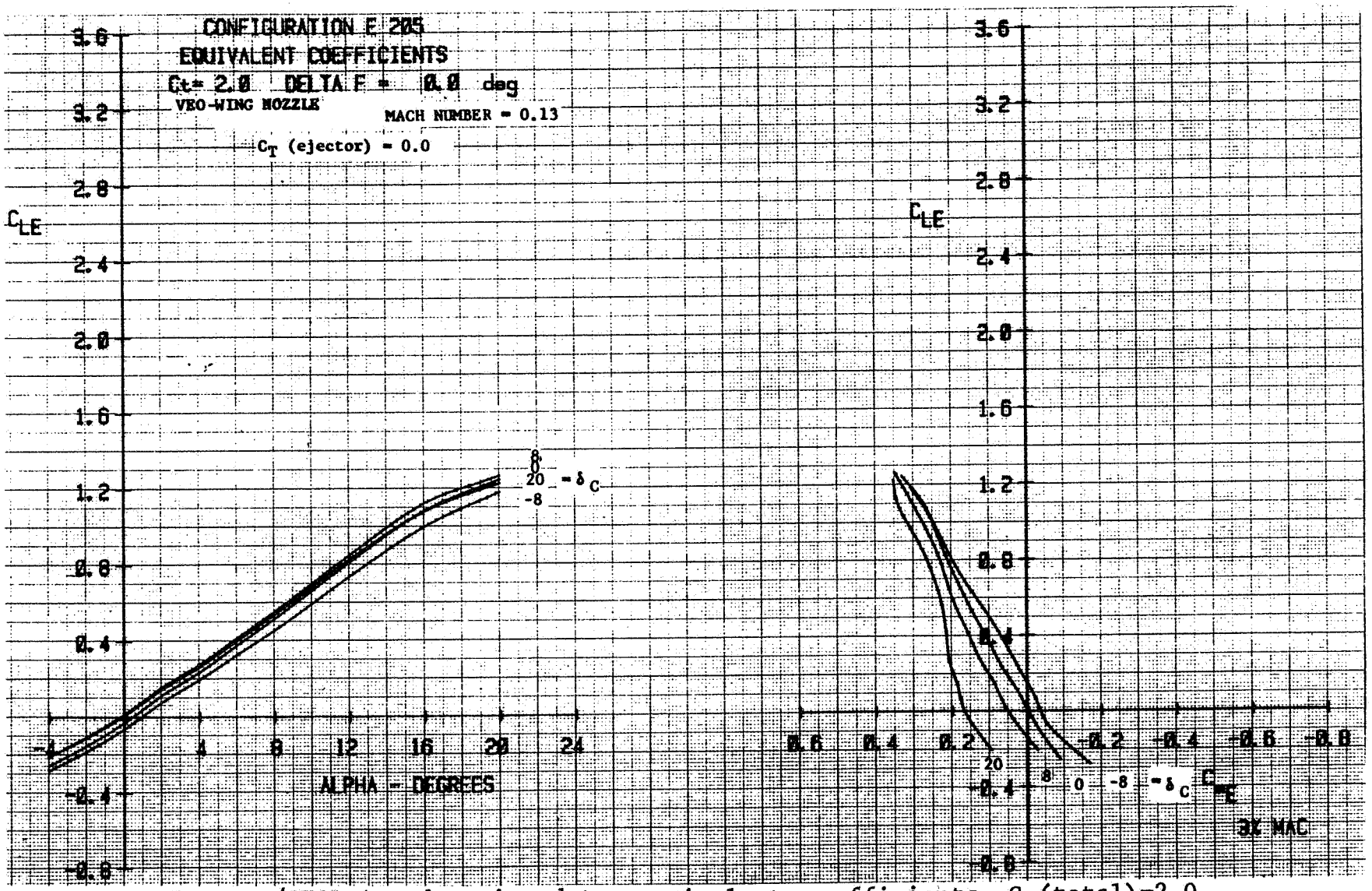

Figure 4-6 a. V/STOL Aerodynamic data, equivalent coefficients, C_T(total)=2.0, C_T(VEO-Wing nozzle)=2.0, C_T(ejector)=0, δ_F=0°, mach=.13

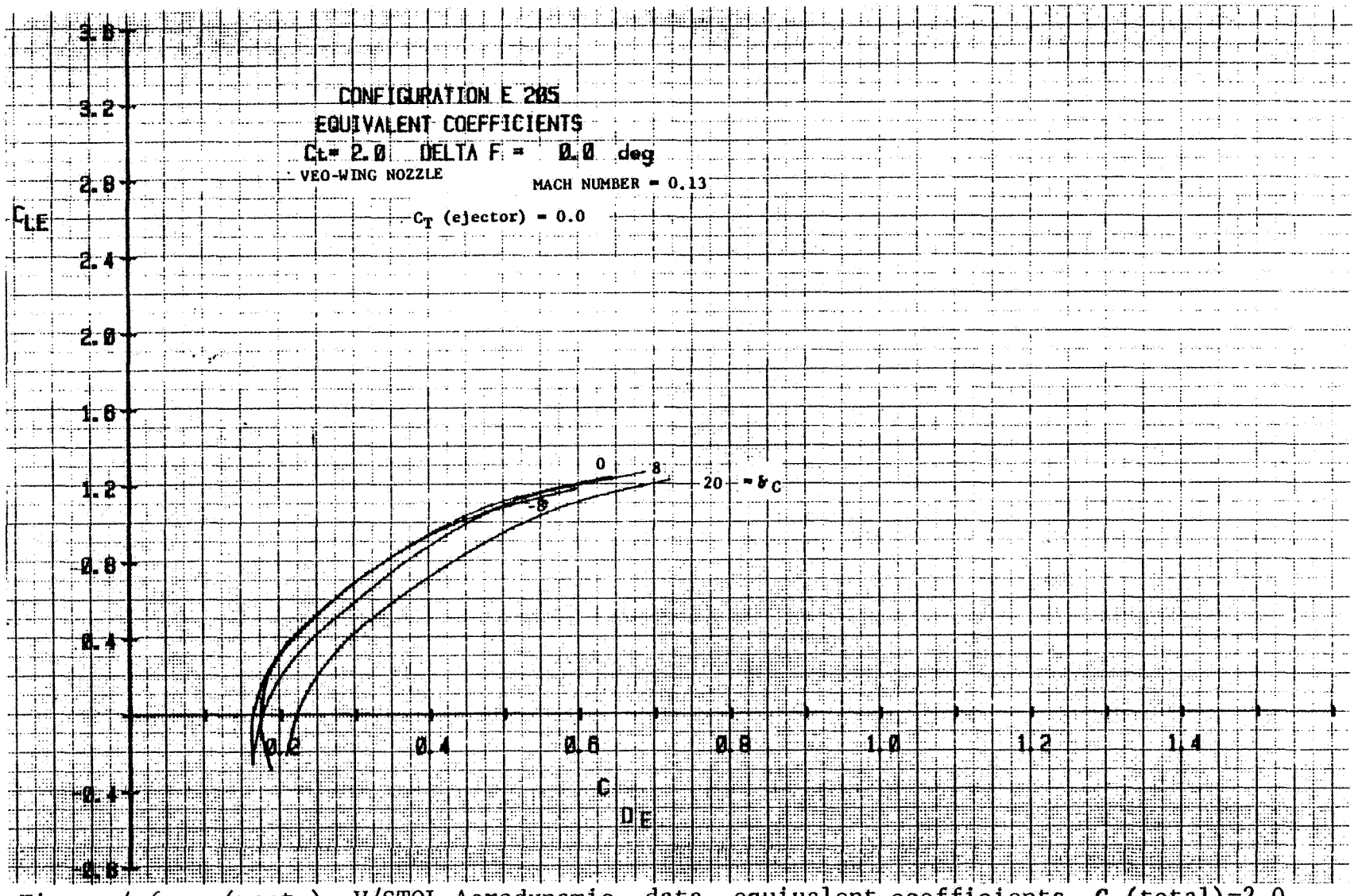

Figure 4-6 a. (cont.) V/STOL Aerodynamic data, equivalent coefficients, C_T(total)=2.0, C_T(VEO- Wing nozzle)=2.0, C_T(ejector)=0, $\delta_F=0^o$, mach=.13

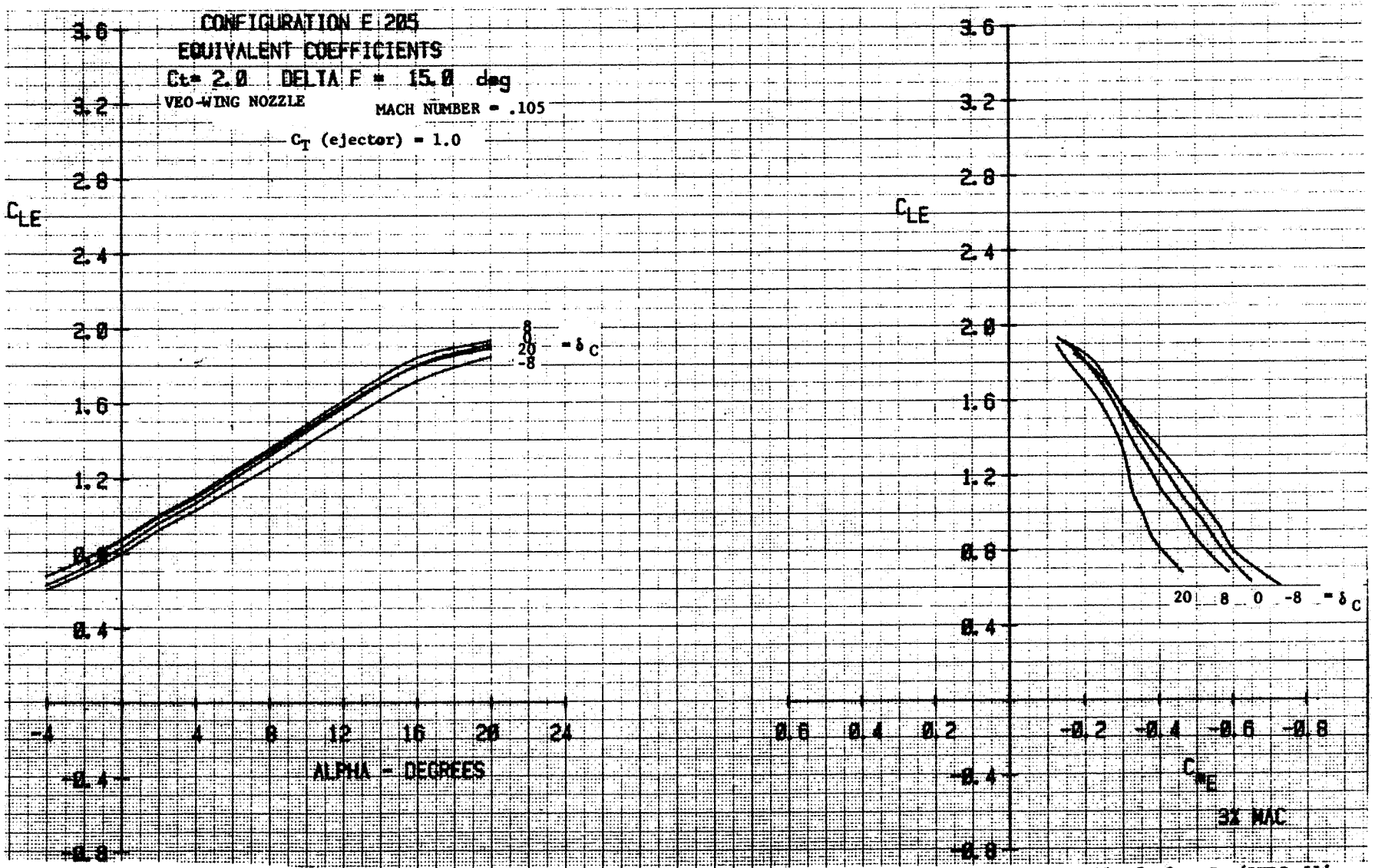

Figure 4-6 b. V/STOL Aerodynamic data, equivalent coefficients, C_T(total)=3.0, C_T(VEO-Wing nozzle)=2.0, C_T(ejector)=1.0, δ_F=15°, mach=.105

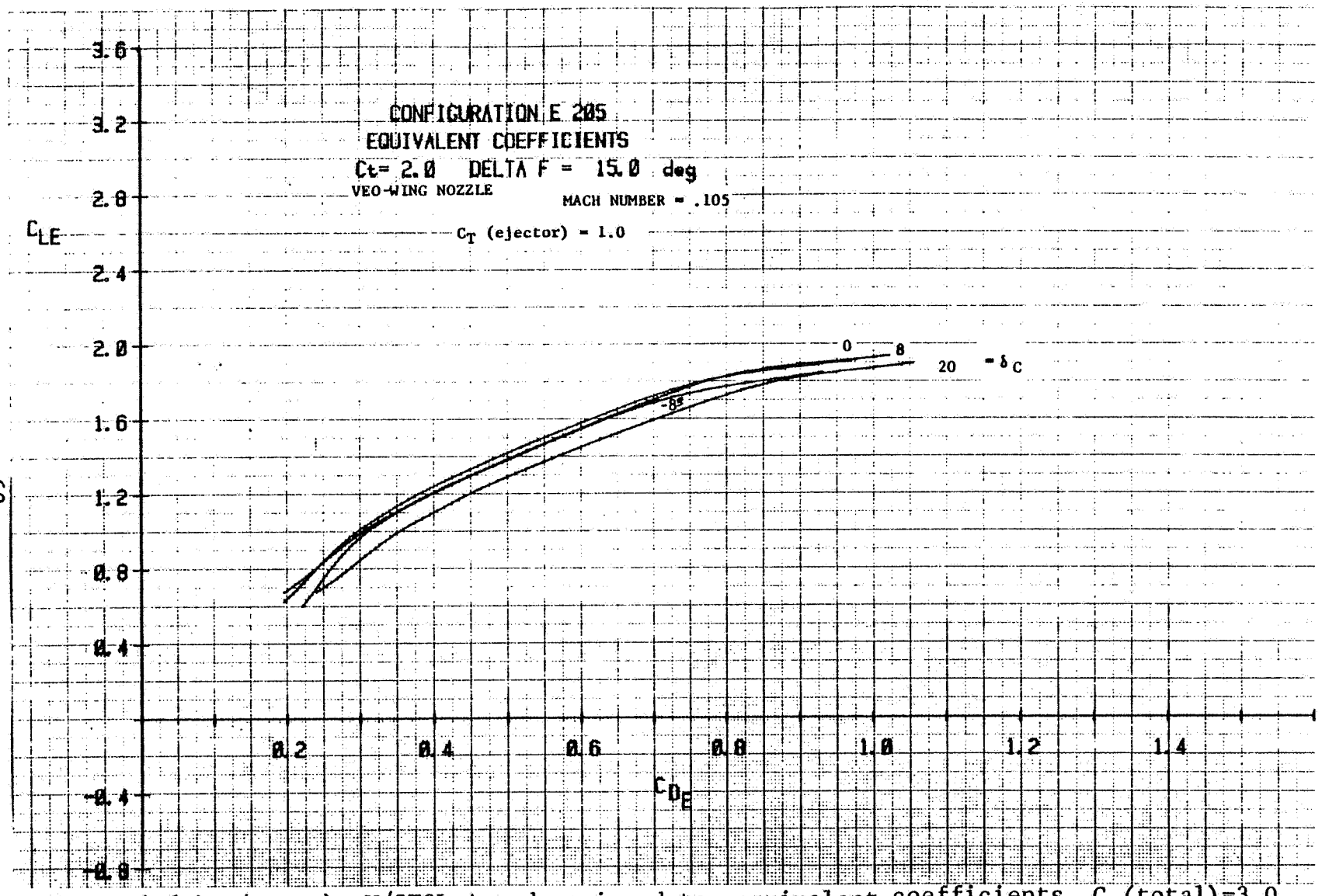

Figure 4-6 b. (cont.) V/STOL Aerodynamic data, equivalent coefficients, C_T(total)=3.0, C_T(VEO- Wing nozzle)=2.0, C_T(ejector)=1.0, δ_F=15°, mach=.105

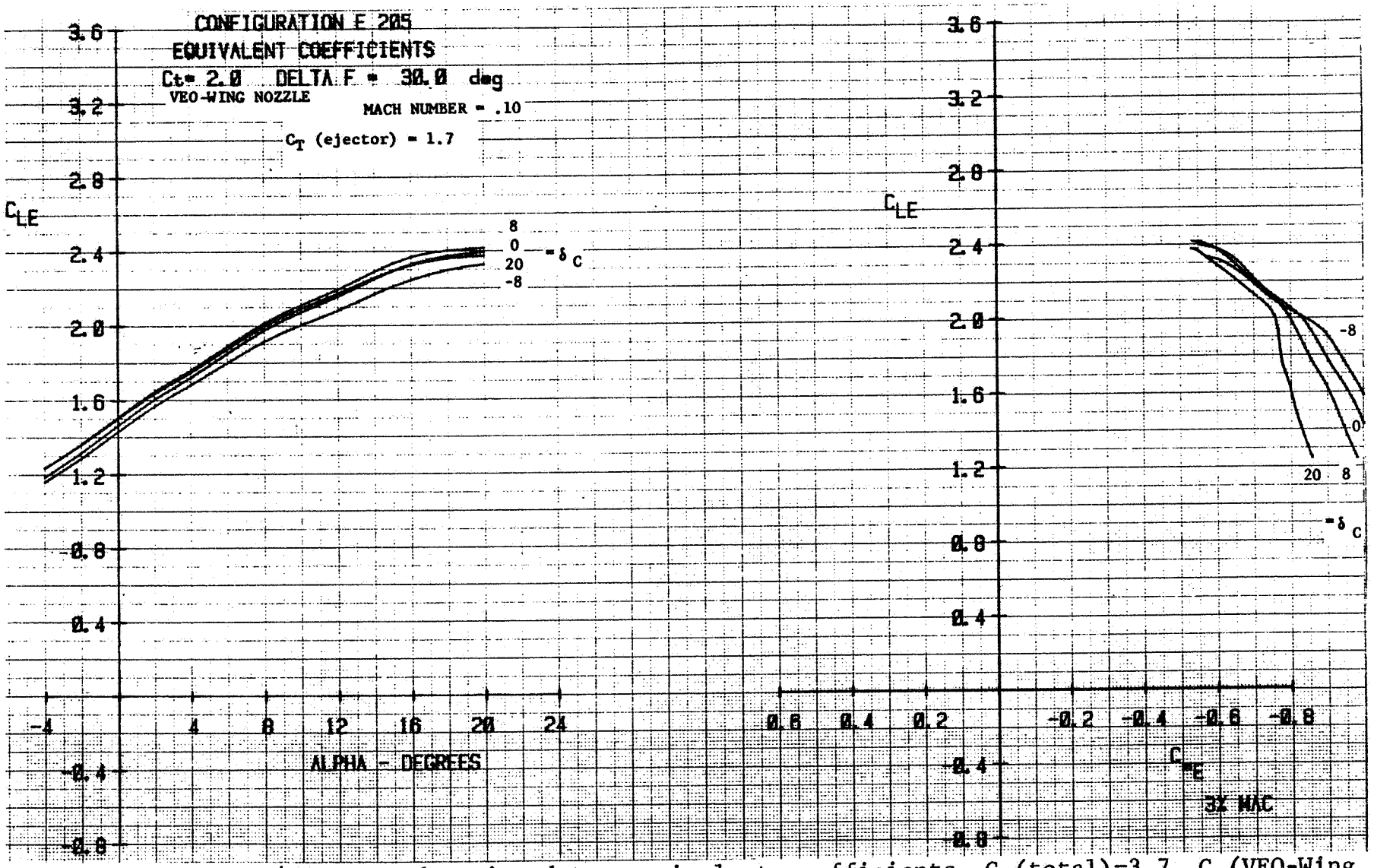

Figure 4-6 c. V/STOL Aerodynamic data, equivalent coefficients, C_T(total)=3.7, C_T(VEO-Wing nozzle)= 2.0, C_T(ejector)=1.7, δ_F=30°, Mach=.1

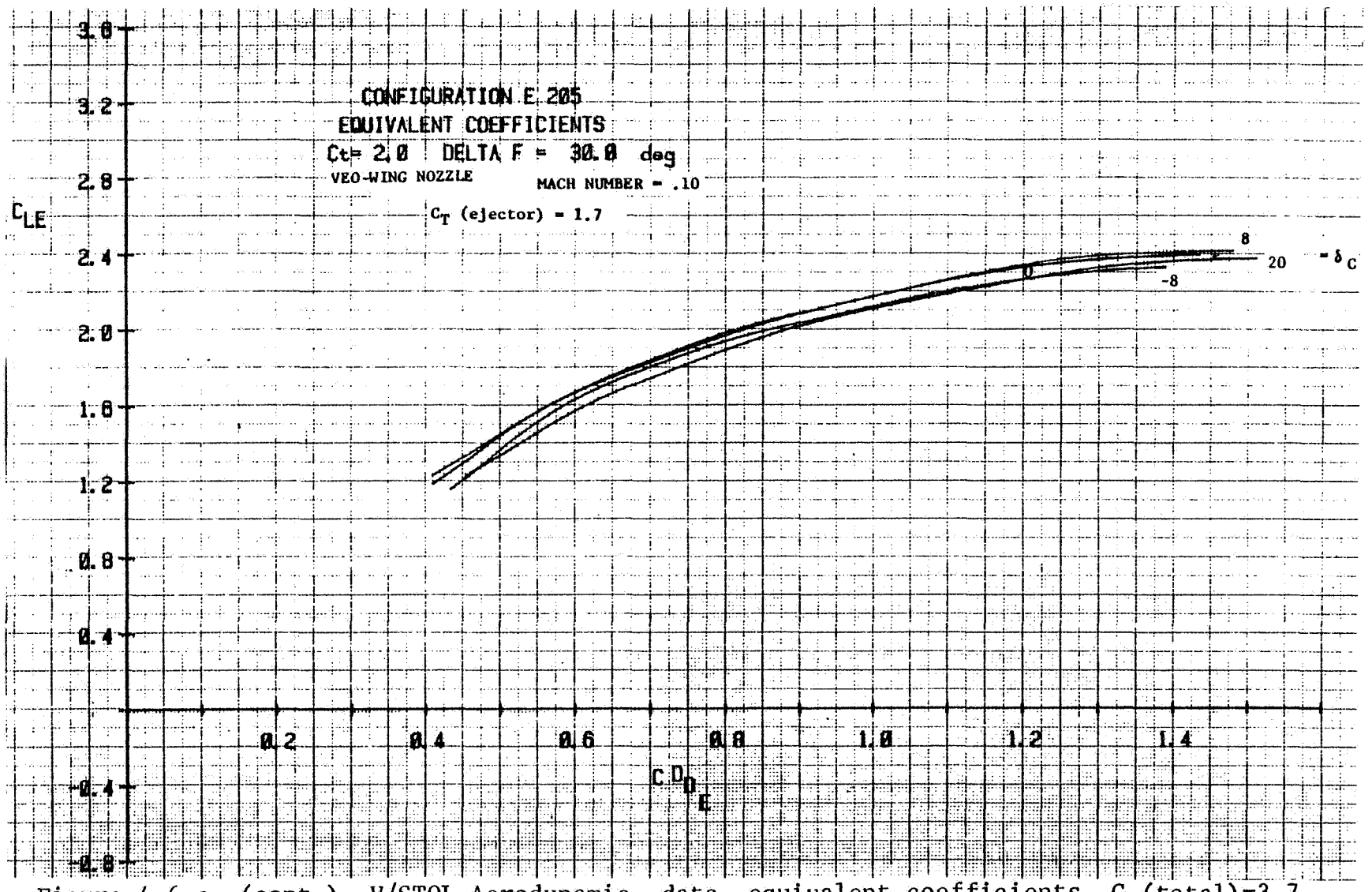

Figure 4-6 c. (cont.) V/STOL Aerodynamic data, equivalent coefficients, C_T(total)=3.7, C_T(VEO- Wing nozzle)=2.0, C_T(ejector)=1.7, δ_F=30°, Mach=.1

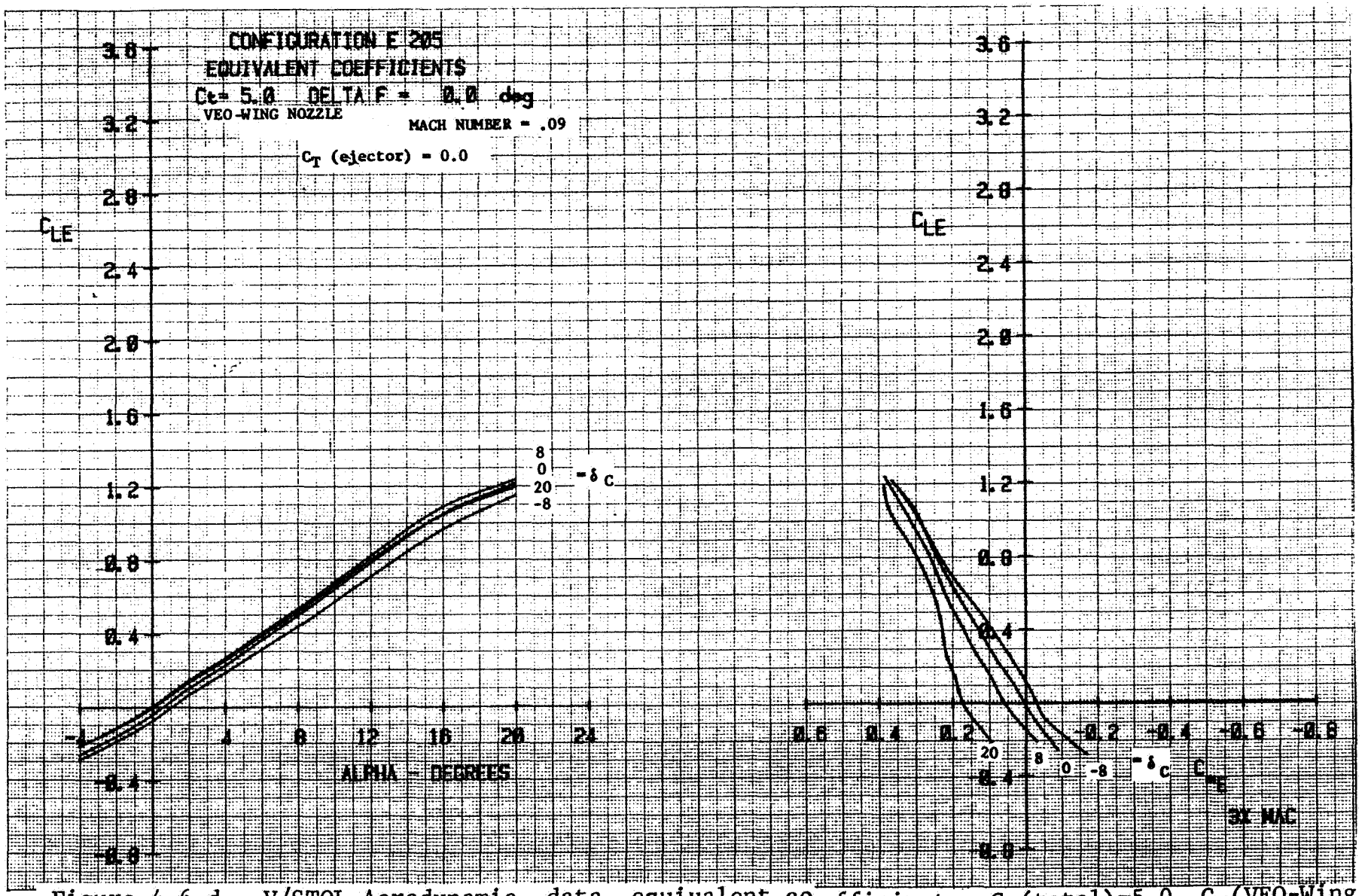

Figure 4-6 d. V/STOL Aerodynamic data, equivalent coefficients, C_T(total)=5.0, C_T(VEO-Wing nozzle)=5.0, C_T(ejector)=0, $\delta_F=0^o$, Mach=.09

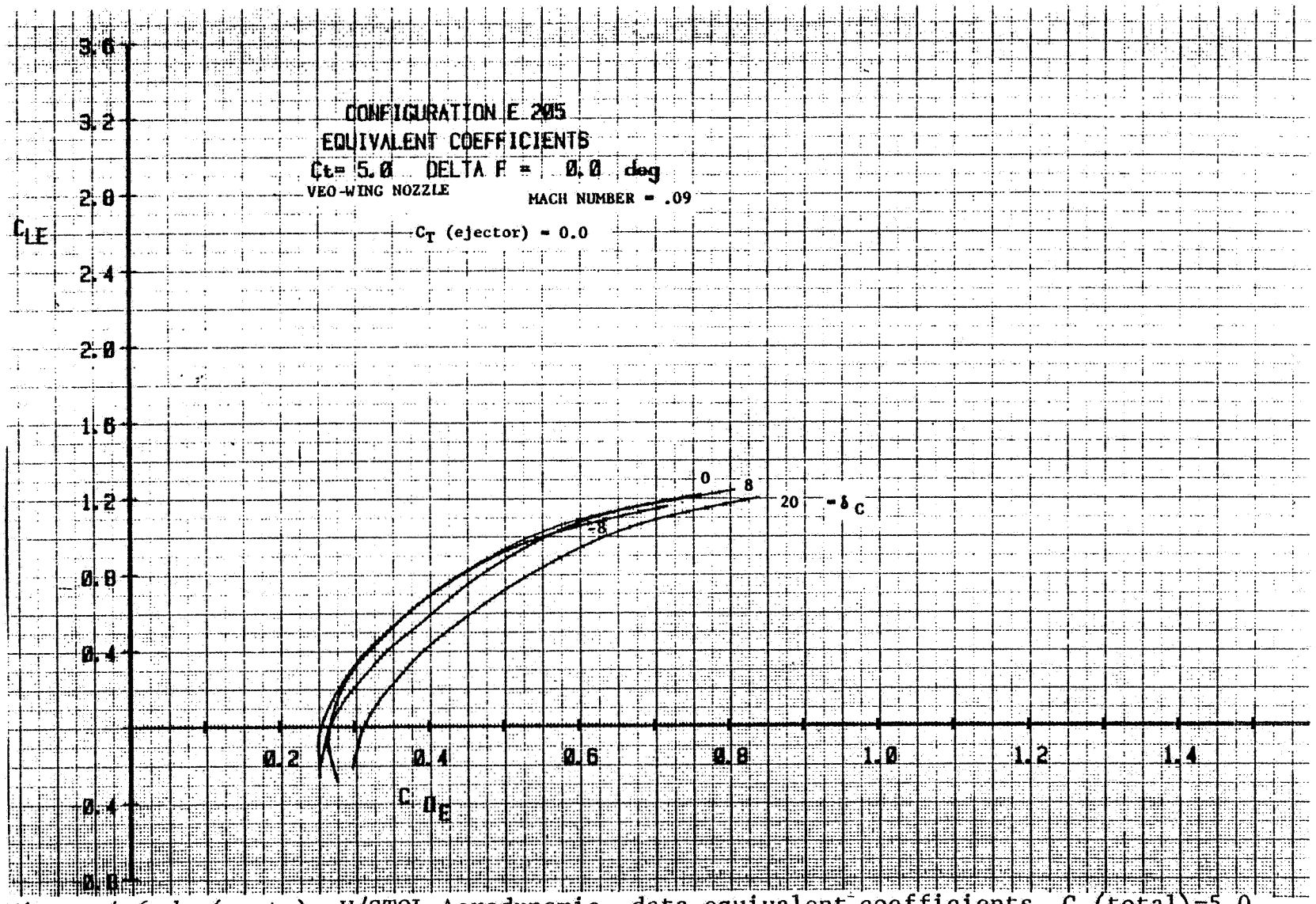

Figure 4-6 d. (cont.) V/STOL Aerodynamic data equivalent coefficients, C_T(total)=5.0, C_T(VEO-Wing nozzle)=5.0, C_T(ejector)=0, $\delta_F=0^o$, Mach=.09

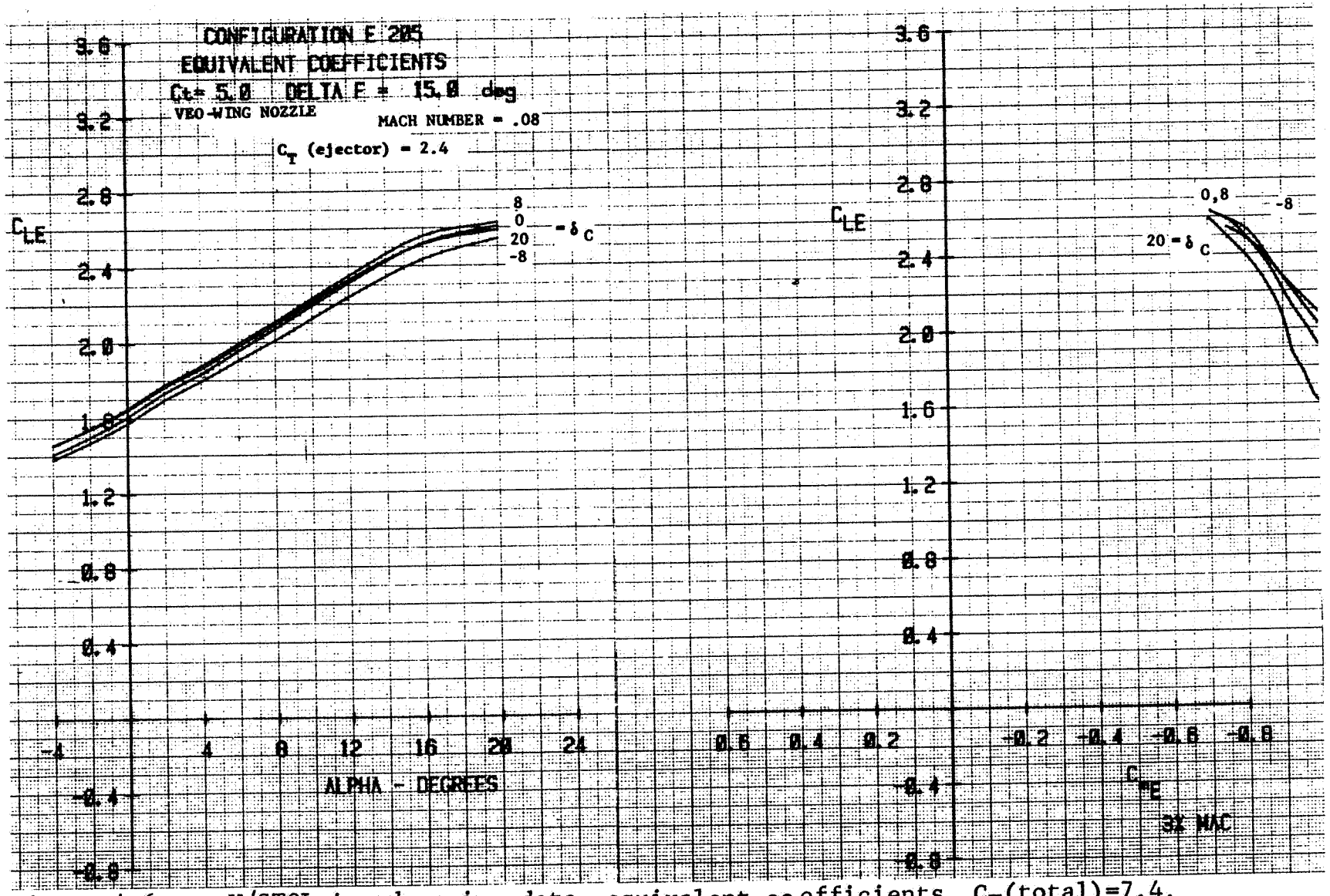

Figure 4-6 e. V/STOL Aerodynamic data, equivalent coefficients, C_T(total)=7.4, C_T(VEO-Wing nozzle)=5.0, C_T(ejector)=2.4, δ_F=15°, Mach=.08

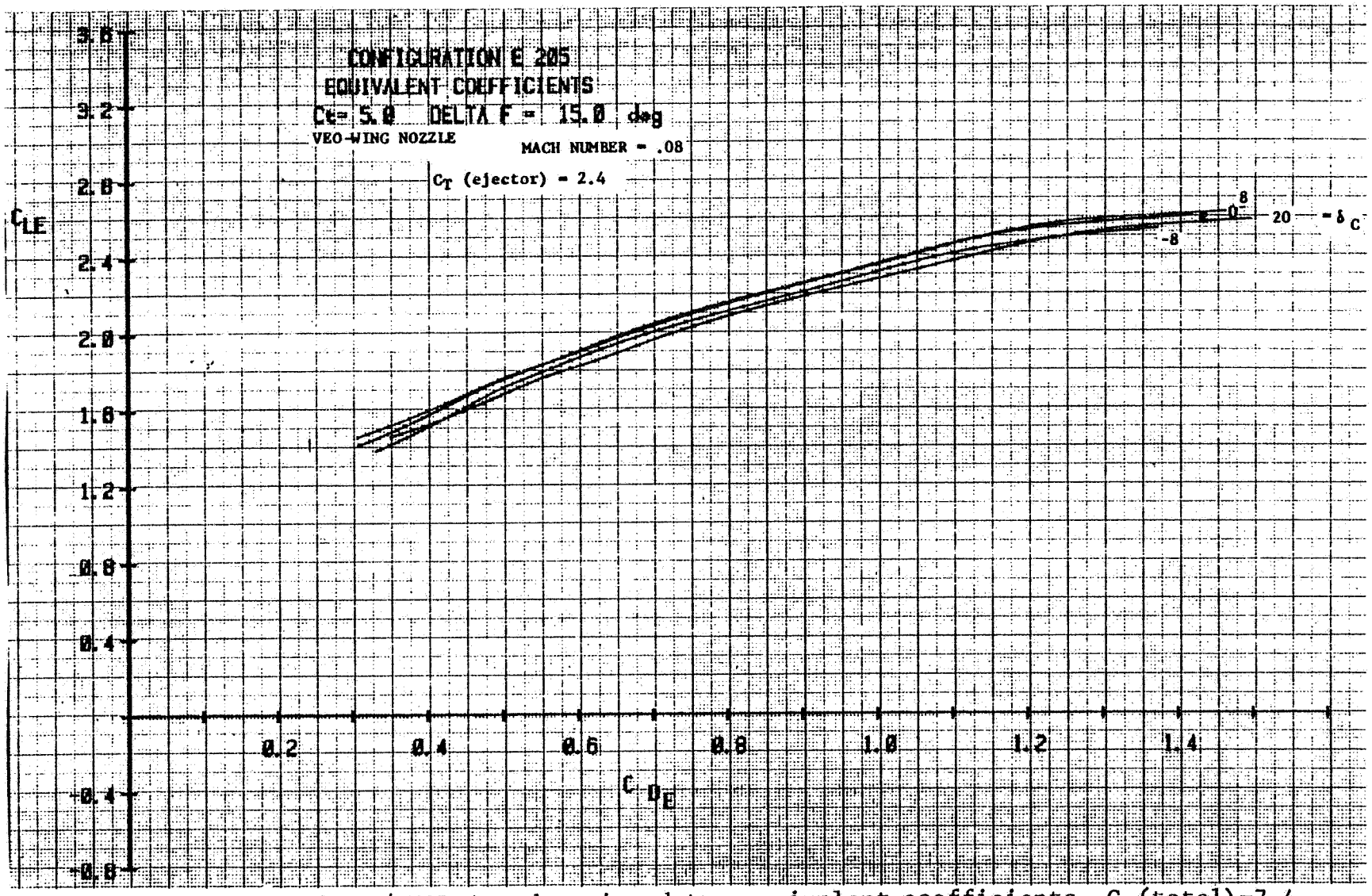

Figure 4-6 e. (cont.) V/STOL Aerodynamic data, equivalent coefficients, C_T(total)=7.4, C_T(VEO-Wing nozzle)=5.0, C_T(ejector)=2.4, δ_F=15°, Mach=.08

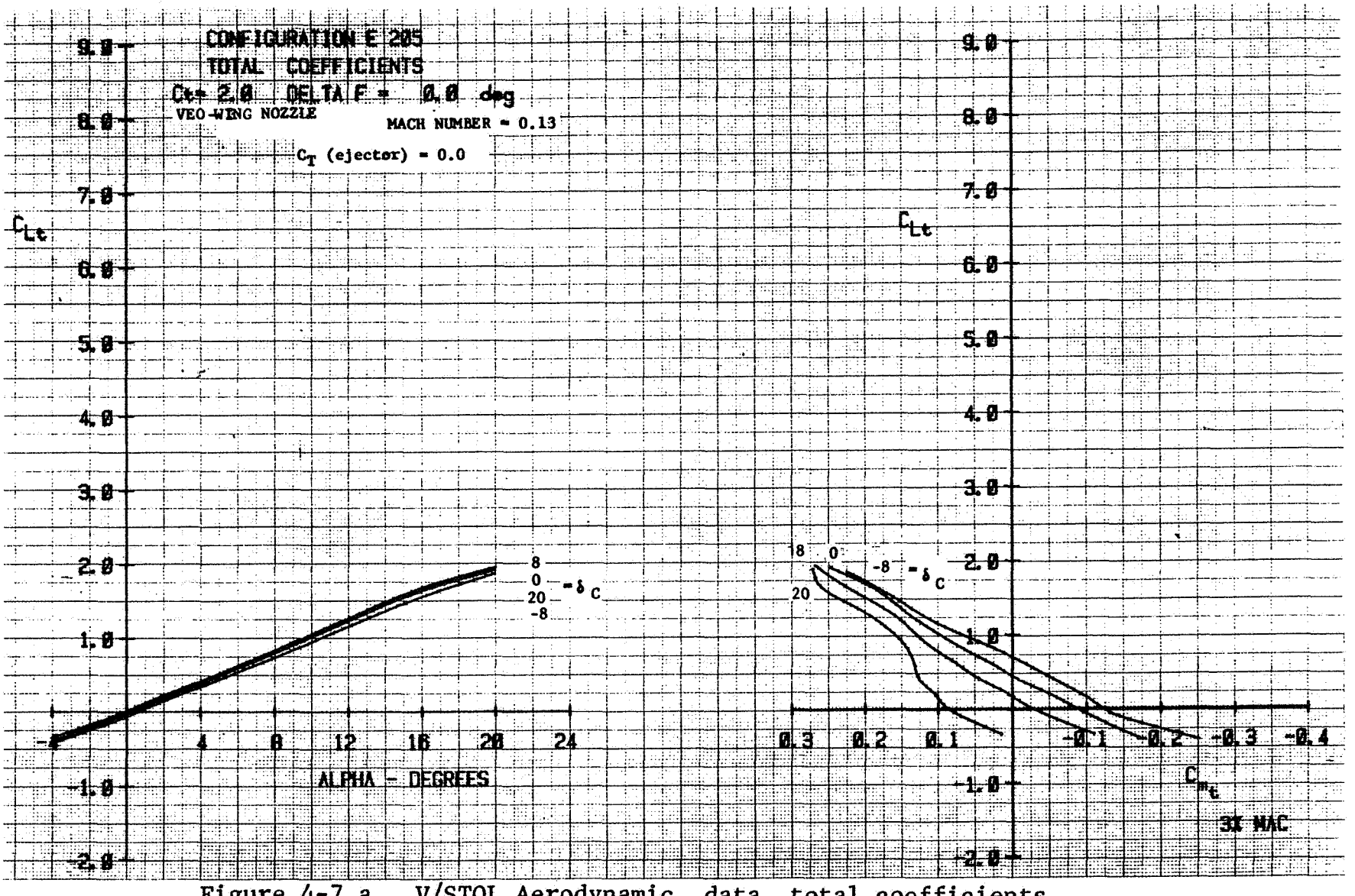

Figure 4-7 a. V/STOL Aerodynamic data, total coefficients, C_T(total)=2.0, C_T(VEO-Wing nozzle)=2.0, C_T (ejector)=0, δ_F=0°, Mach =.13

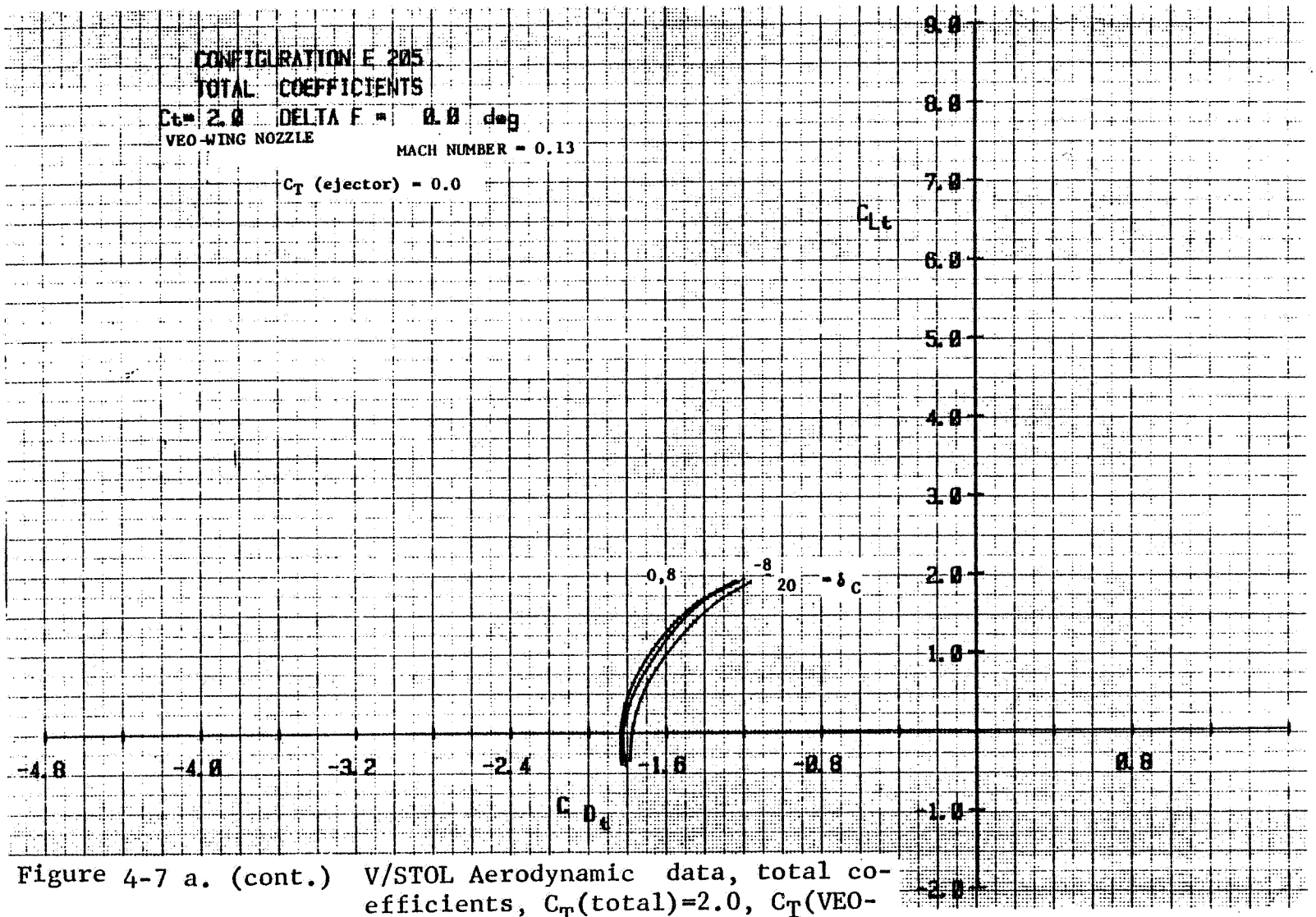

Figure 4-7 a. (cont.) V/STOL Aerodynamic data, total coefficients, C_T(total)=2.0, C_T(VEO-Wing nozzle)=2.0, C_T(ejector)=0, δ_F=0°, Mach=.13

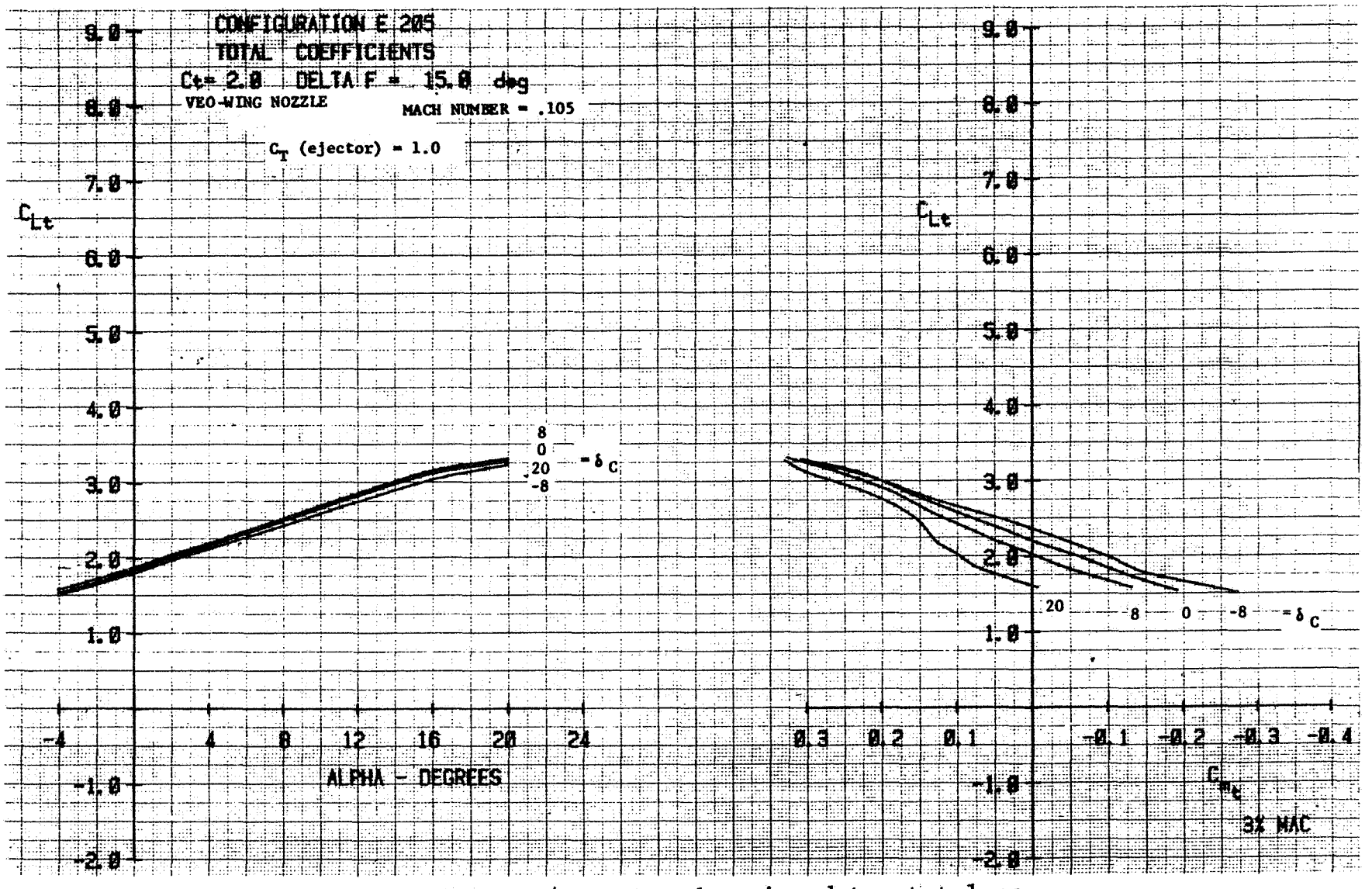

Figure 4-7 b. V/STOL Aerodynamics data, total coefficients, C_T(total)=3.0, C_T(VEO-Wing nozzle)=2.0, C_T(ejector)=1.0, δ_F=15°, Mach=.105

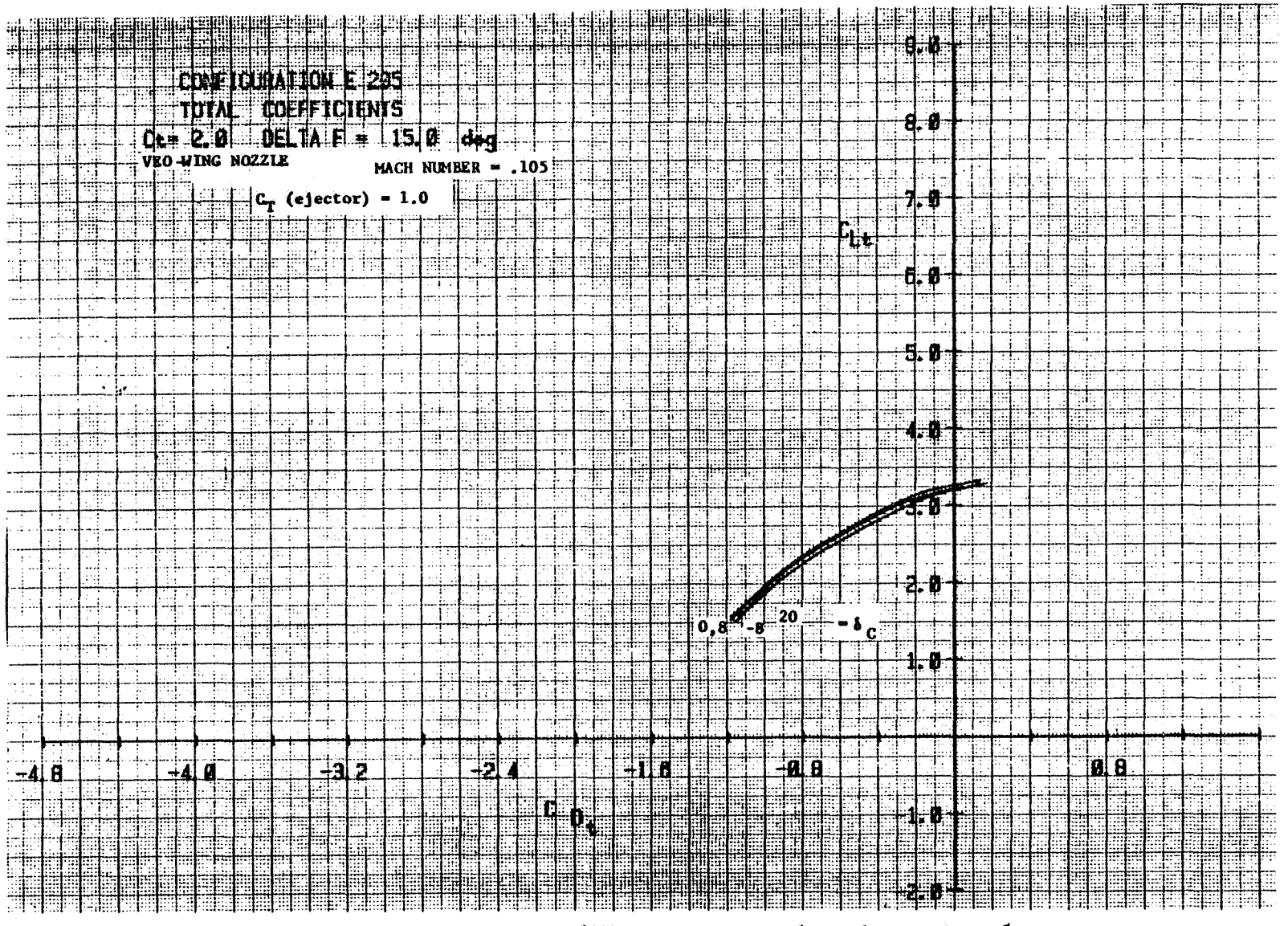

Figure 4-7 b. (cont.) V/STOL Aerodynamic data, total coefficients, C_T(total)=3.0, C_T(VEO-Wing nozzle)=2.0, C_T(ejector)=1.0, δ_F=15°, Mach=.105

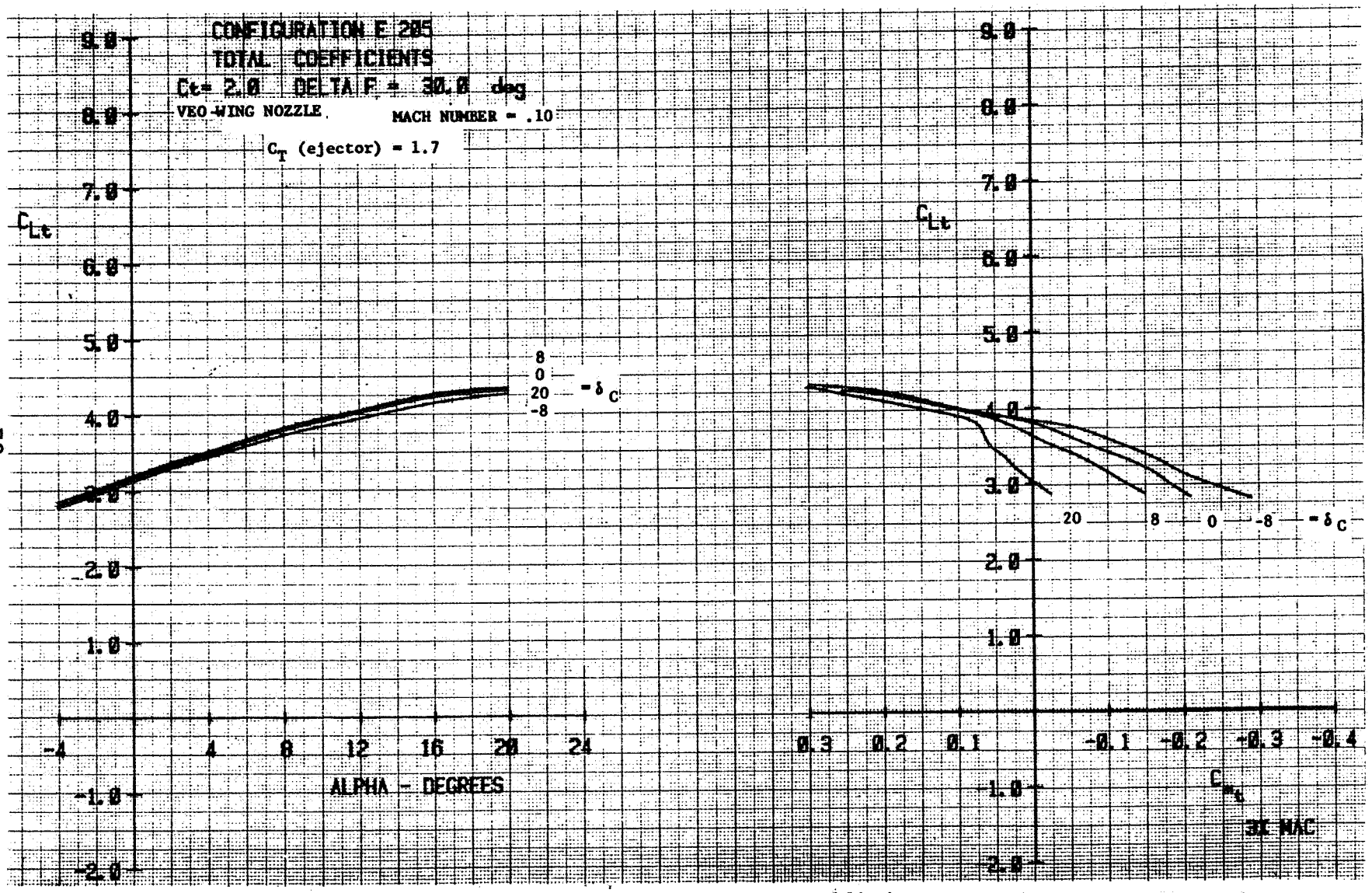

Figure 4-7 c. V/STOL Aerodynamic data, total coefficients, C_T(total)=3.7, C_T(VEO-Wing nozzle)=2.0, C_T(ejector)=1.7, $\delta_F=30^o$, Mach=.10

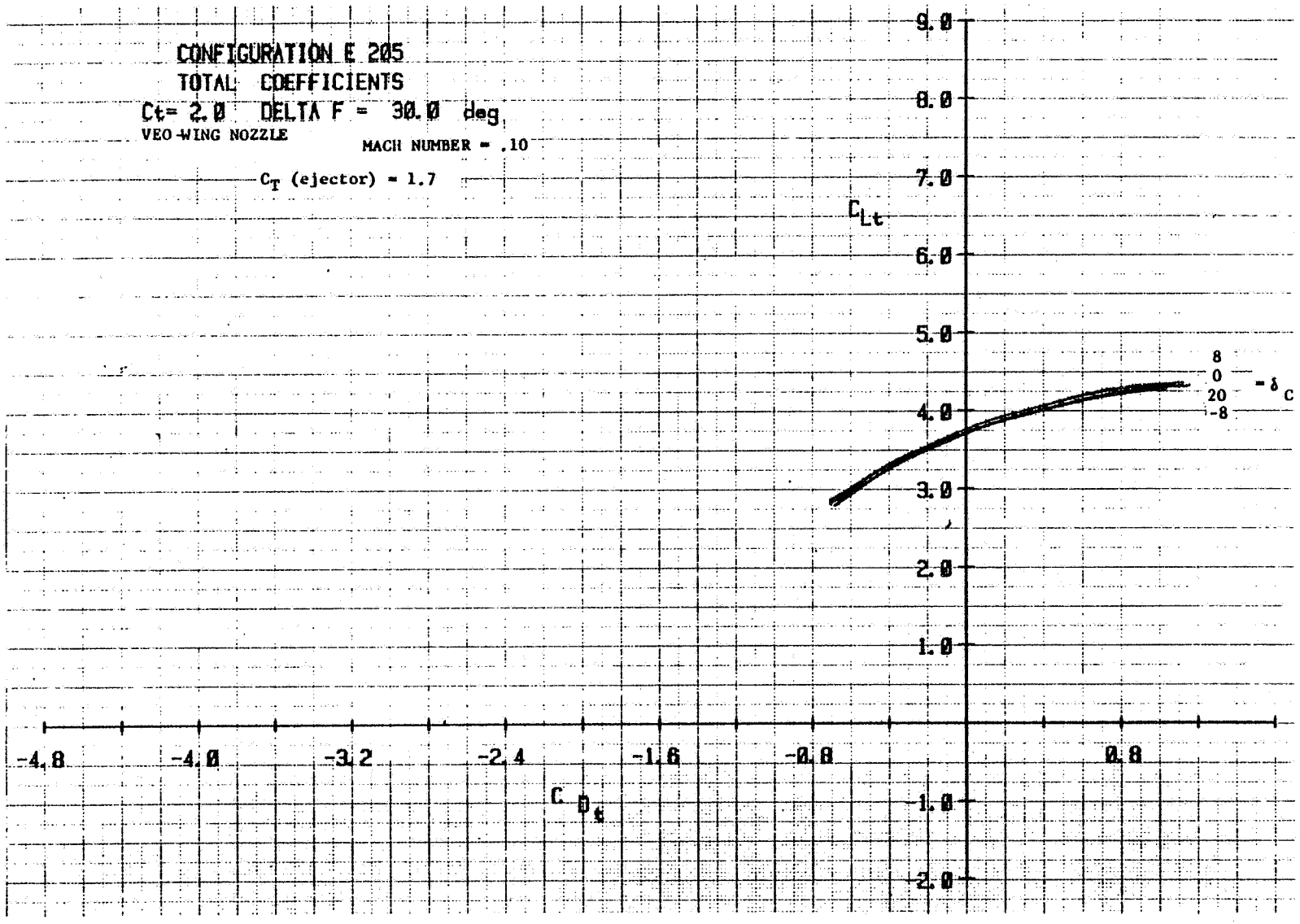

Figure 4-7 c. (cont.) V/STOL Aerodynamics data, total coefficients, C_T(total)=3.7, C_T(VEO-Wing nozzle)=2.0, C_T(ejector)=1.7, δ_F=30°, Mach=.1

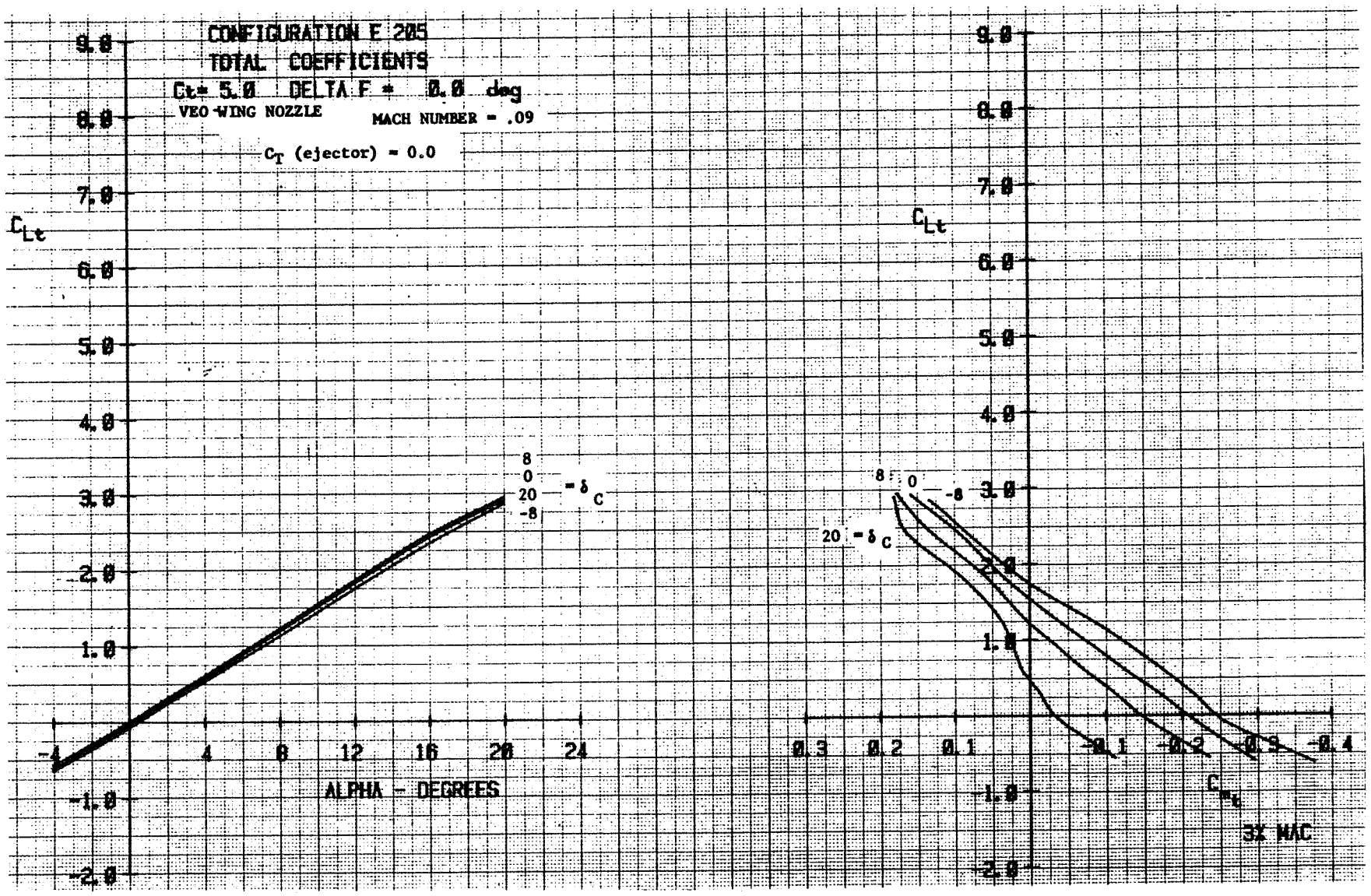

Figure 4-7 d. V/STOL Aerodynamics data, total coefficients, C_T(total)=5.0, C_T(VEO-Wing nozzle)=5.0, C_T (ejector)=0, δ_F=0°, Mach=.09

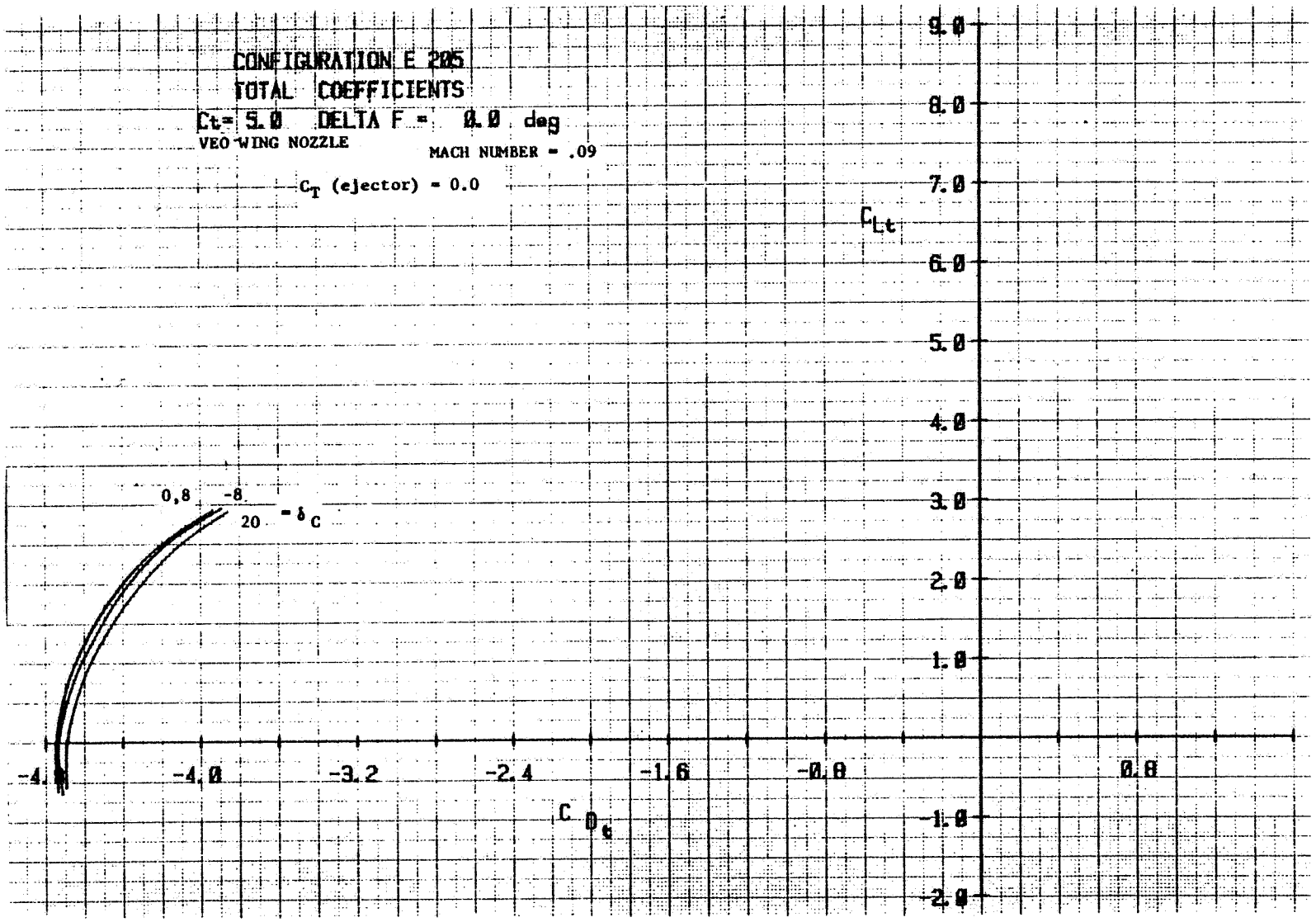

Figure 4-7 d. (cont.) V/STOL Aerodynamic data, total coefficients, C_T(total)=5.0, C_T(VEO-Wing nozzle)=5.0, C_T(ejector)=0, $\delta_F=0^o$, Mach= .09

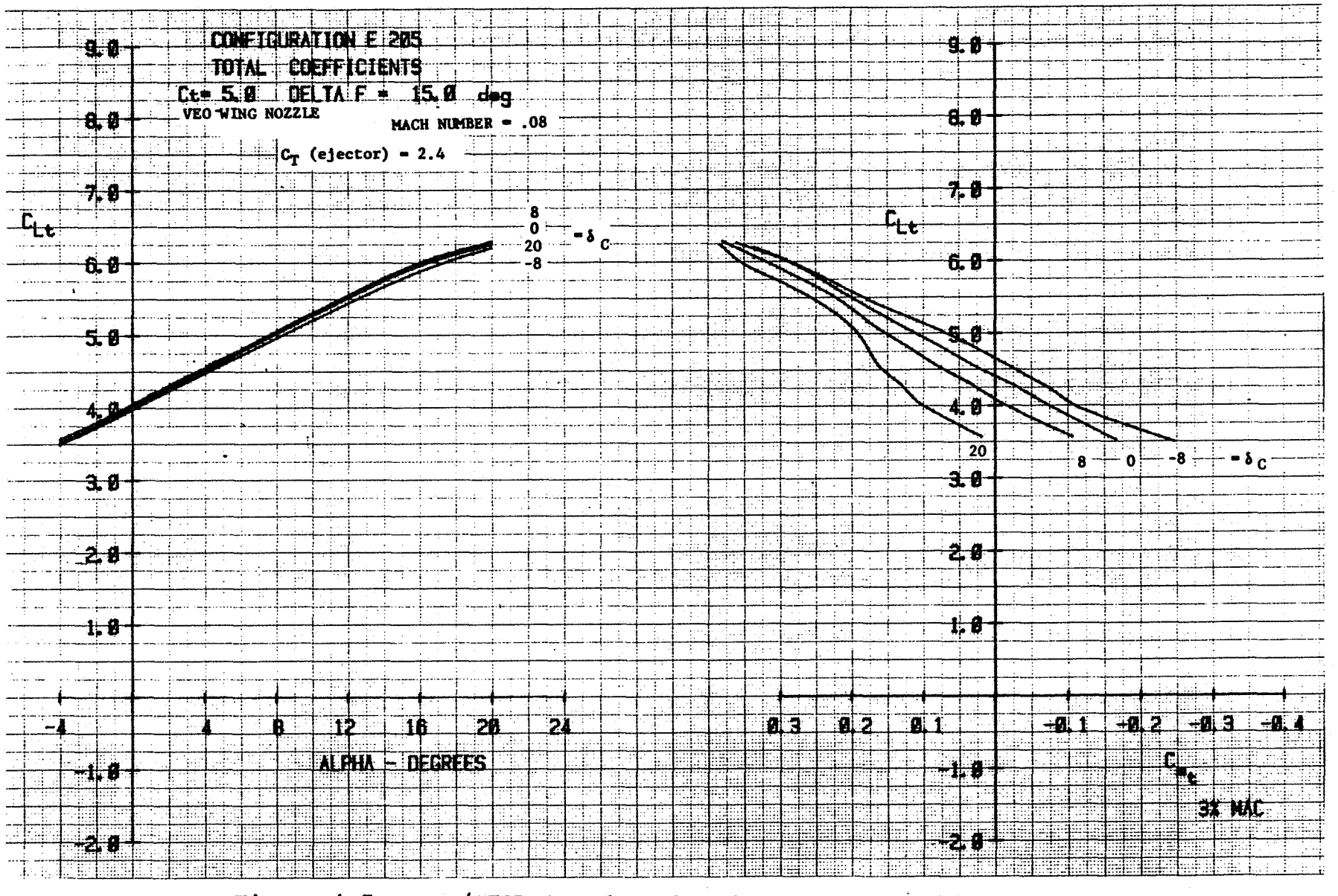

Figure 4-7 e. V/STOL Aerodynamic data, total coefficients, C_T(total)=7.4, C_T(VEO-Wing nozzle)=5.0 C_T (ejector)=2.4, δ_F=15°, Mach=.09

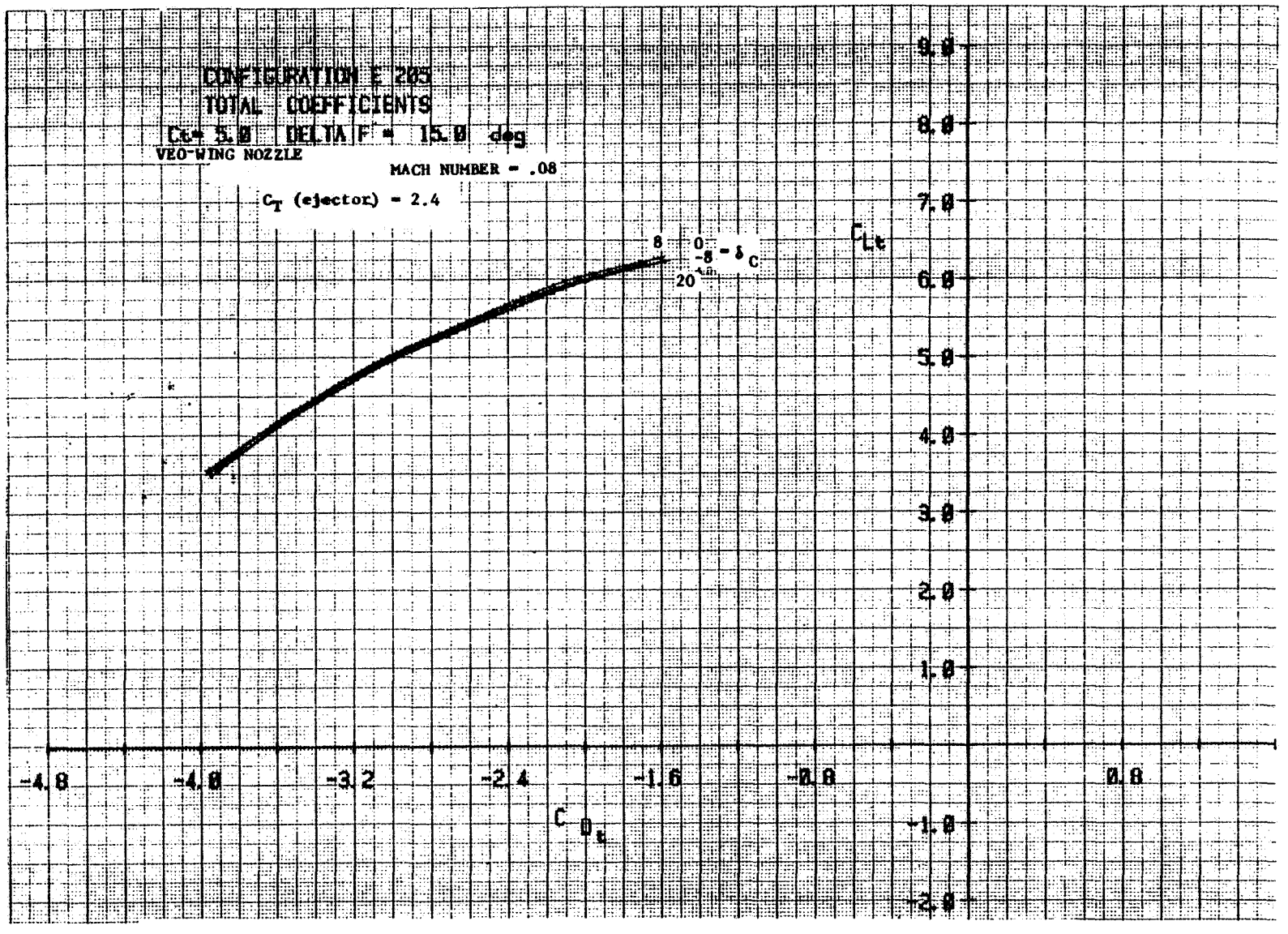

Figure 4-7 e. (cont.) V/STOL Aerodynamic data, total coefficients, C_T(total)=7.4, C_T(VEO-Wing nozzle)=5.0, C_T(ejector)=2.4, δ_F=15°, Mach=.09

Figure 4-8 provides an example of how a STOL/VTOL trimmed lift curve is developed using a combination of canard deflection at low α's and ejector thrust at higher α's. The trim process has been internally performed in the performance analysis as that required to achieve a given maneuver; there are vast numbers of combinations of trim possibilities. The optimum must be dictated by the performance; therefore, only one example is presented here for illustration of the trim scheme.

The cruise/maneuver (transonic) areo data estimates for airplane mission and maneuver sizing required an alternate approach from the STOL/VTOL data estimates. The limited existing data base prevented the development of aerodynamic estimates for variations in all of the desired parameter combinations (canard deflection, VEO-Wing nozzle deflection, flaperon deflection, C_T, and Mach number). Out of necessity an alternate approach was sought, which led directly to representative estimates of the trimmed cruise/maneuver drag polars without developing the untrimmed data as follows. Figure 4-9 schematically illustrates how a set of equivelent trimmed, optimum-span-efficiency (e) envelopes (vs C_{L_E} and Mach number) were developed from the powered VEO-Wing nozzle only for trim with a zero-degree canard deflection, maximum negative static margin = -18% at M = .2, and c.g. = +.03c (like Configuration E205).

For a given Mach No., VEO-Wing nozzle C_T, and with canard undeflected, the equivalent wing span efficiency is derived and plotted as a function VEO-Wing nozzle deflection, δ_{TE} and equivalent lift coefficient. The δ_{TE} required to trim (with undeflected canard) at various angles of attack and equivalent lift coefficient is determined from the equivalent lift and pitching-moment curves and allows the determination of the optimum trimmed span efficiency envelope as a function of equivalent lift coefficient.

However, since the estimated static margin for $\delta c = 0^o$ is more unstable than allowable for the E205 configuration (as explained in Subsection 4.1.3), the flight control computer schedules the canard with Mach no. and angle of attack to achieve the desired stability level. Therefore, a reoptimization of the canard/VEO-wing-nozzle deflections would be required at each Mach no. and blowing-momentum-coefficient combination to achieve the maximum obtainable e-envelopes. Since the existing data base is inadequate for developing these max-obtainable e-envelopes, the e-envelopes using the VEO-Wing nozzle only for trim (Figure 4-10) will be used in this study. Although these e's are not necessarily the optimum achievable with the canard/VEO-Wing nozzle trim, they are considered representative of what can be achieved with canard/nozzle deflection combinations given enough experimental data.

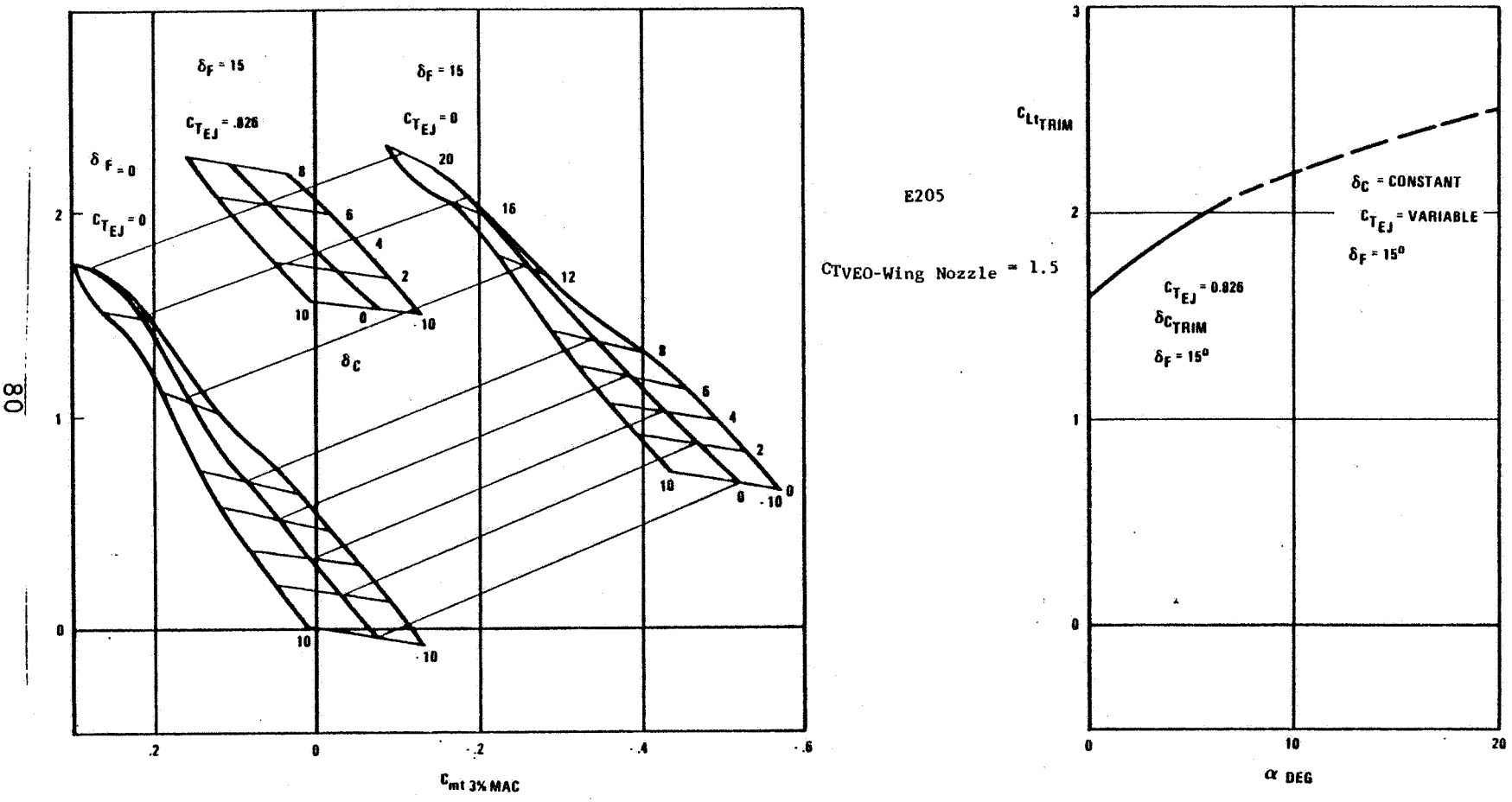

Figure 4-8 VSTOL Trimmed Lift Curve, Aerodynamic Plus Ejector Trim

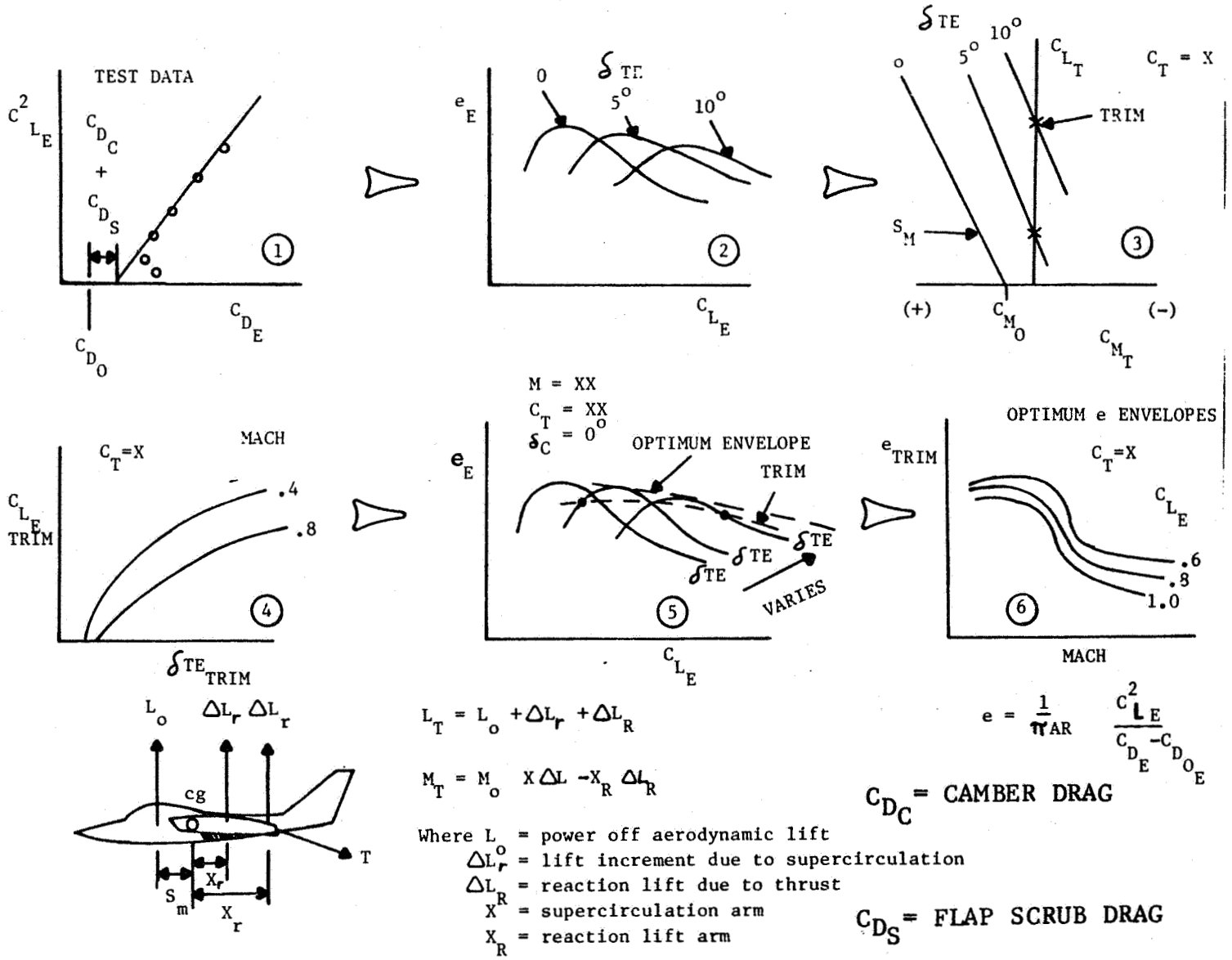

Figure 4-9 VEO-Wing Trim Method for Maneuver

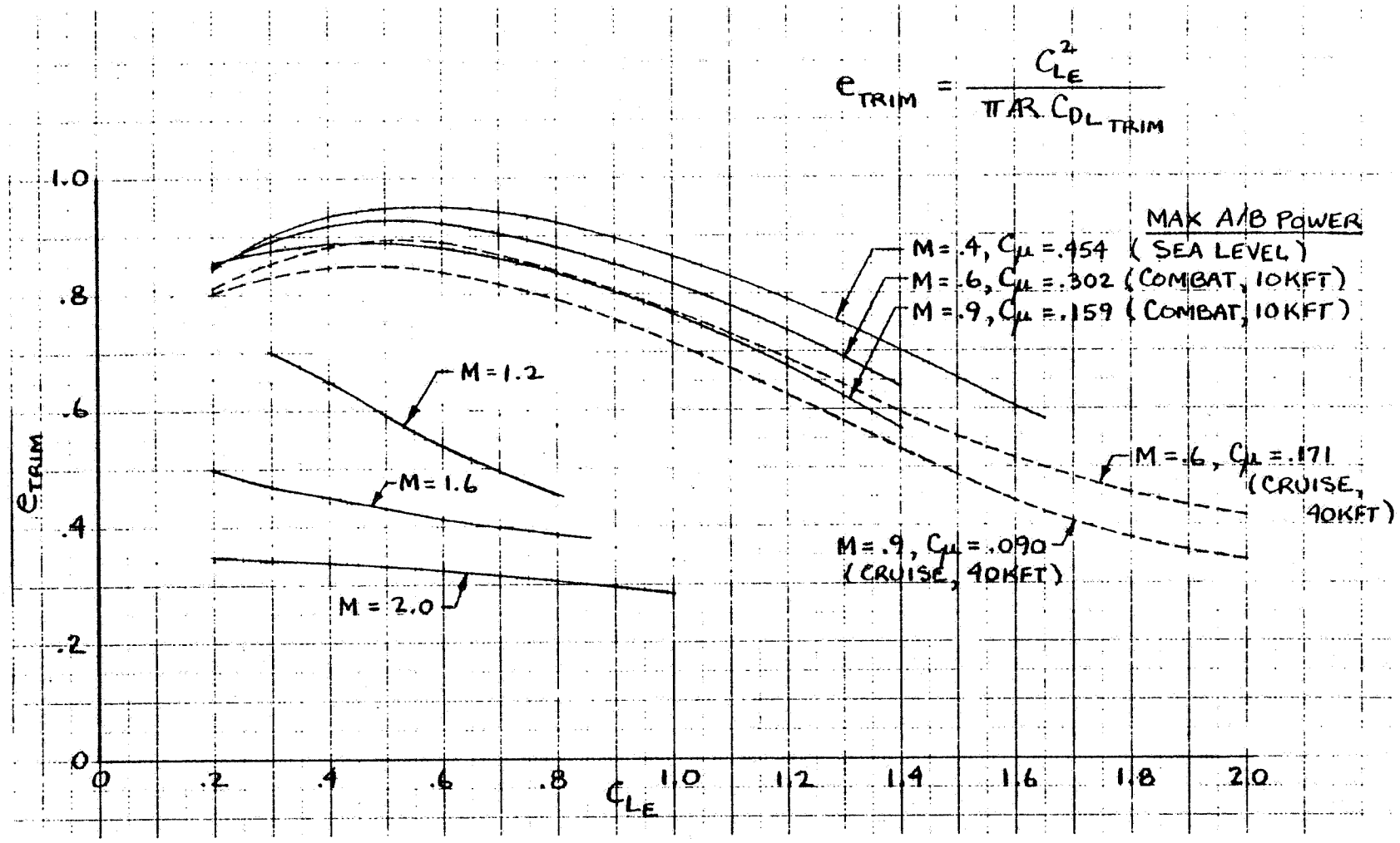

Figure 4-10 E205 Trimmed Span Efficiency

The C_L at $C_{D_{min}}$ is a fallout of the way the e's are derived; these e's are used directly with the estimated minimum drags (Subsection 4.1.1) to produce the resulting cruise/maneuver equivalent trimmed drag polars shown in Figure 4-11. (The minimum-drag trim penalty was negligible based on the powered model data).

This approach does not afford the development and visibility of the untrimmed lift, drag, and pitching moment curves directly because this would require enough experimental data to determine the canard/VEO-Wing nozzle deflection schedule with angle of attack, Mach no., and C_T (or C_μ). There is a real need to obtain this experimental data base and develop the canard/VEO-Wing nozzle schedules required to achieve these e-envelopes. The airplane sizing sensitivities of TOGW to variations in cruise/maneuver-optimum-envelope-trimmed e's are presented in Section 7 and highlight the need for resolving this aerodynamic uncertainty.

Estimated supersonic (M = 1.2 and 1.6) lift drag, and pitching moment curves were developed for the E205 configuration by correcting the unpowered VEO-Wing fighter model data (zero degrees VEO-Wing nozzle deflection) of Reference 4 for changes in C_{m_o}, canard arm, and reference areas. These data are presented in Figures 4-12 and 4-13 along with the trimmed lift curves and drag polars which are developed from these data.

4.1.3 Stability Analysis

Estimates of the E205 configuration aerodynamic-center travel with Mach no. have been made by use of the Carmichael Procedure (Reference 9) and the Datcom method (Reference 10). Figure 4-14 presents a General Dynamics a.c.-prediction-accuracy correlation for the Carmichael procedure for various configurations, including the VEO-Wing fighter model of Reference 4. The correction vs Mach no. indicated for the VEO-Wing fighter model was applied to the Carmichael predictions for the E205 configuration (a similar configuration) to produce the corrected Carmichael estimates, shown in Figure 4-15, for a zero-degree canard deflection and with canard off. The Datcom estimate for canard at a zero-degree deflection for M = .4 is also shown for reference and shows a significant disparity between the prediction methods.

It is very difficult to predict the E205 a.c. with either of these existing methods because of the unusual aspects of the configuration, the wide, flat body with separated nacelles,

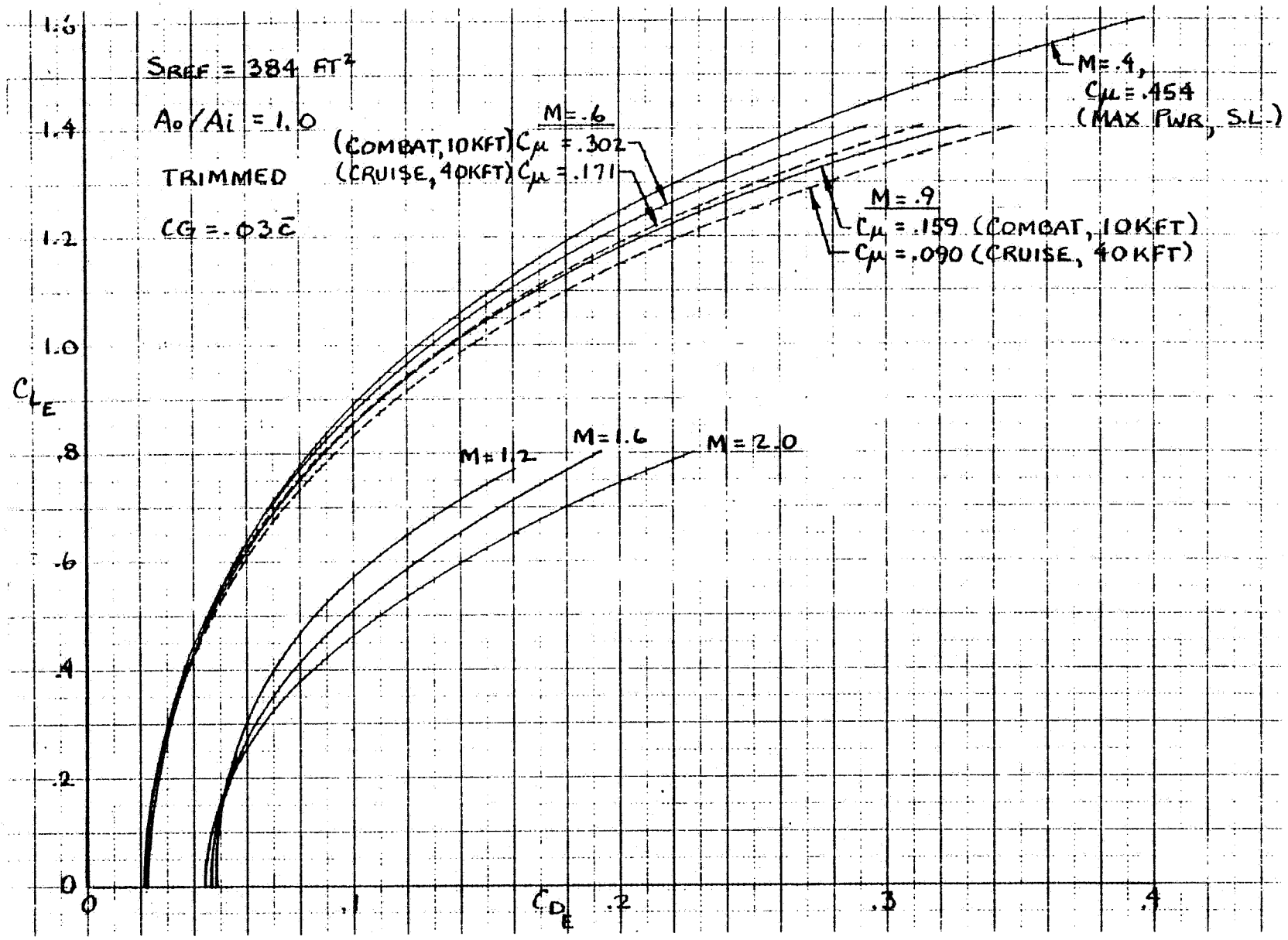

Figure 4-11 E205 Trimmed Cruise/Maneuver Drag Polars

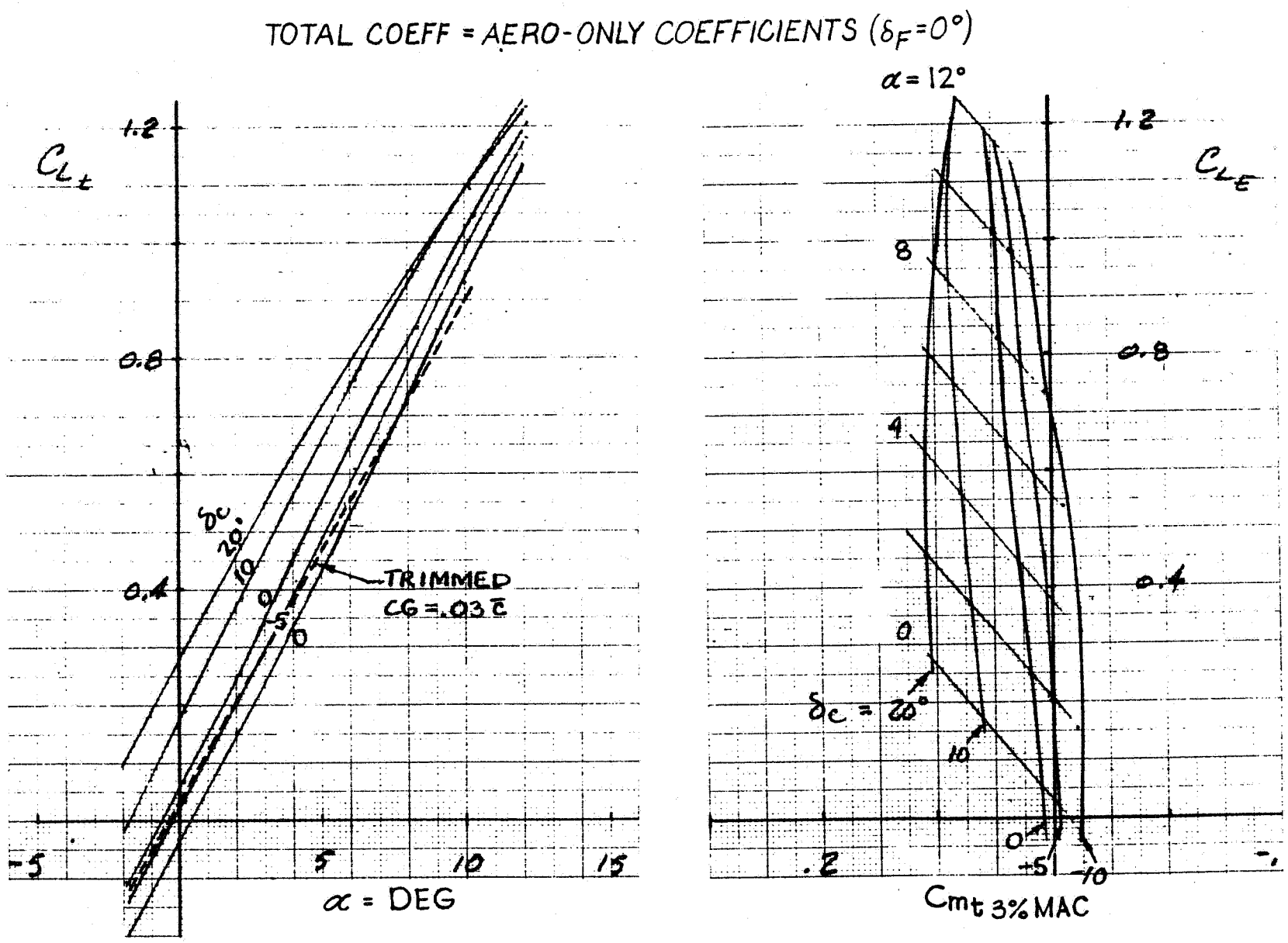

Figure 4-12a E205 Lift and Pitching Moment Curves at M=1.2 with Canard Deflection

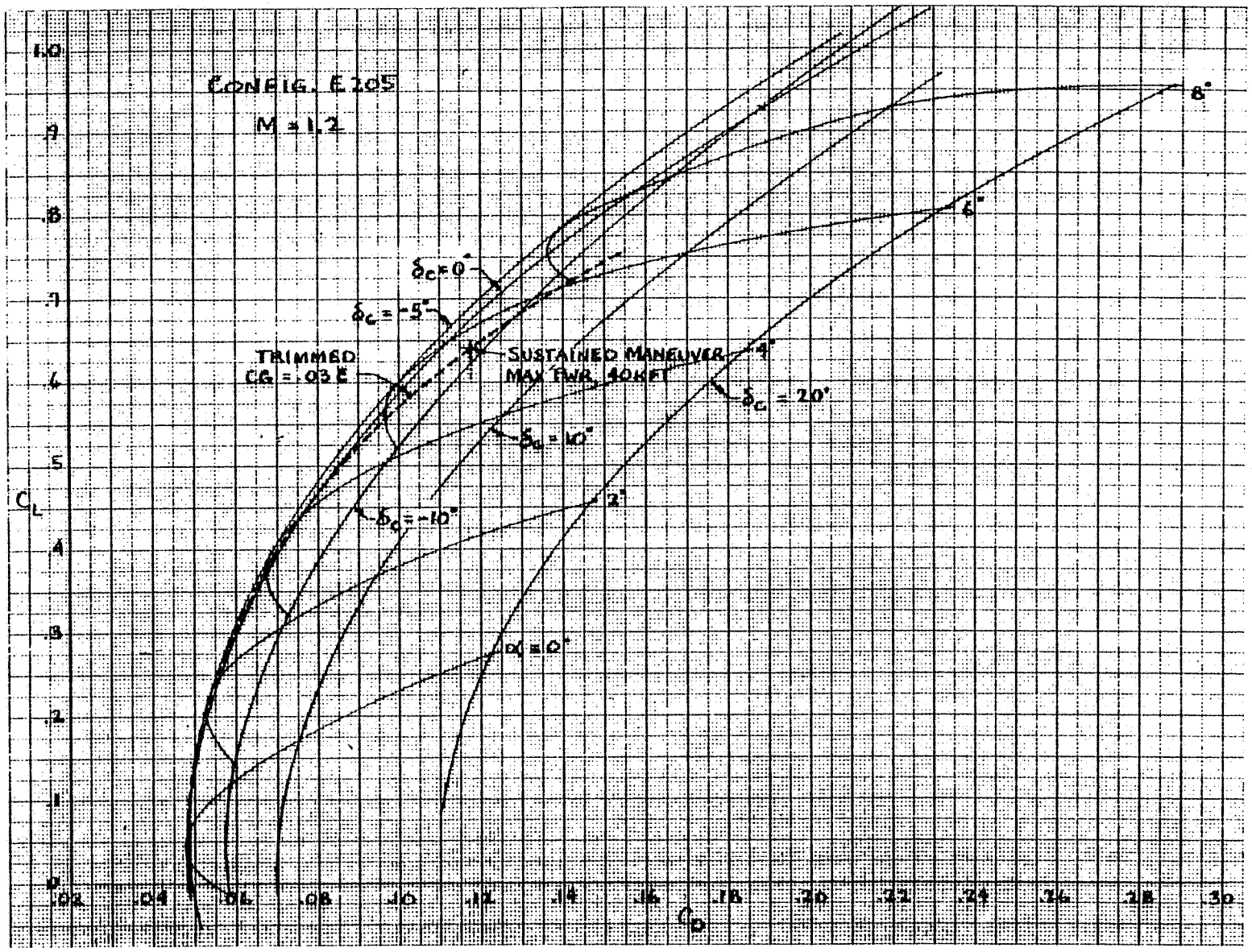

Figure 4-12b E205 Drag Polars at M=1.2 with Canard Deflection

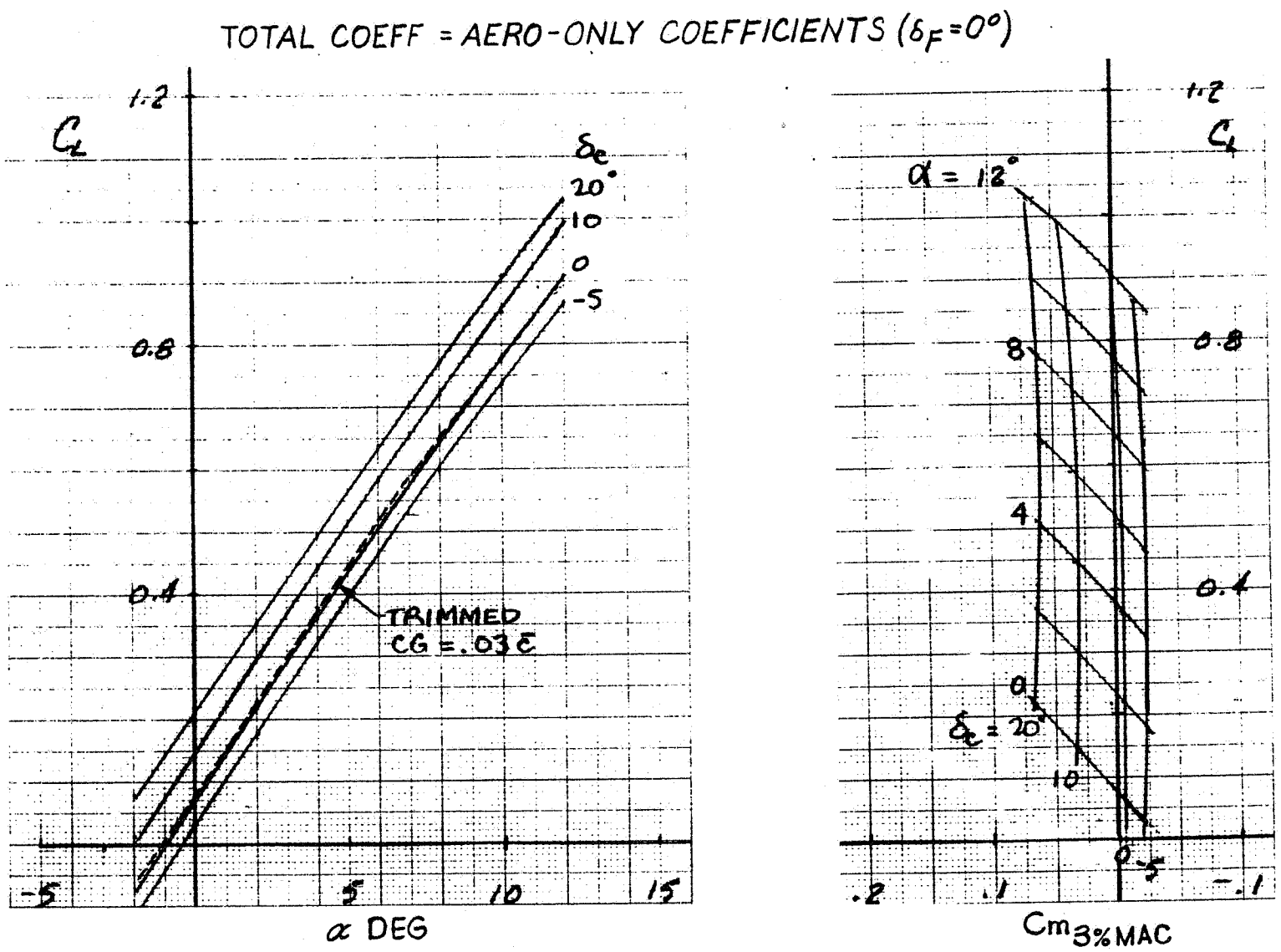

Figure 4-13a E205 Lift and Pitching Moment Curves at M=1.6 with Canard Deflection

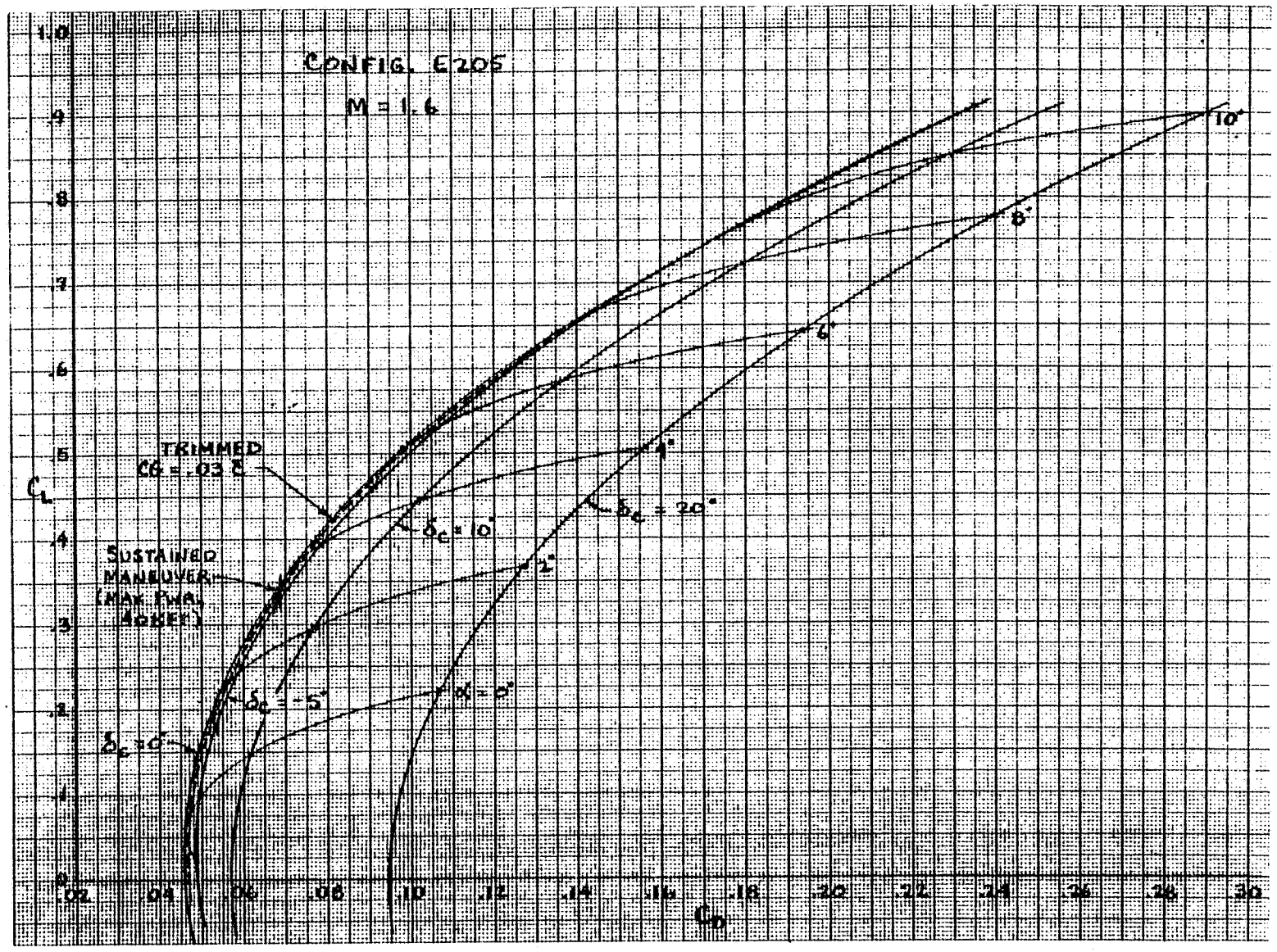

Figure 4-13b E205 Drag Polars at M=1.6 with Canard Deflection

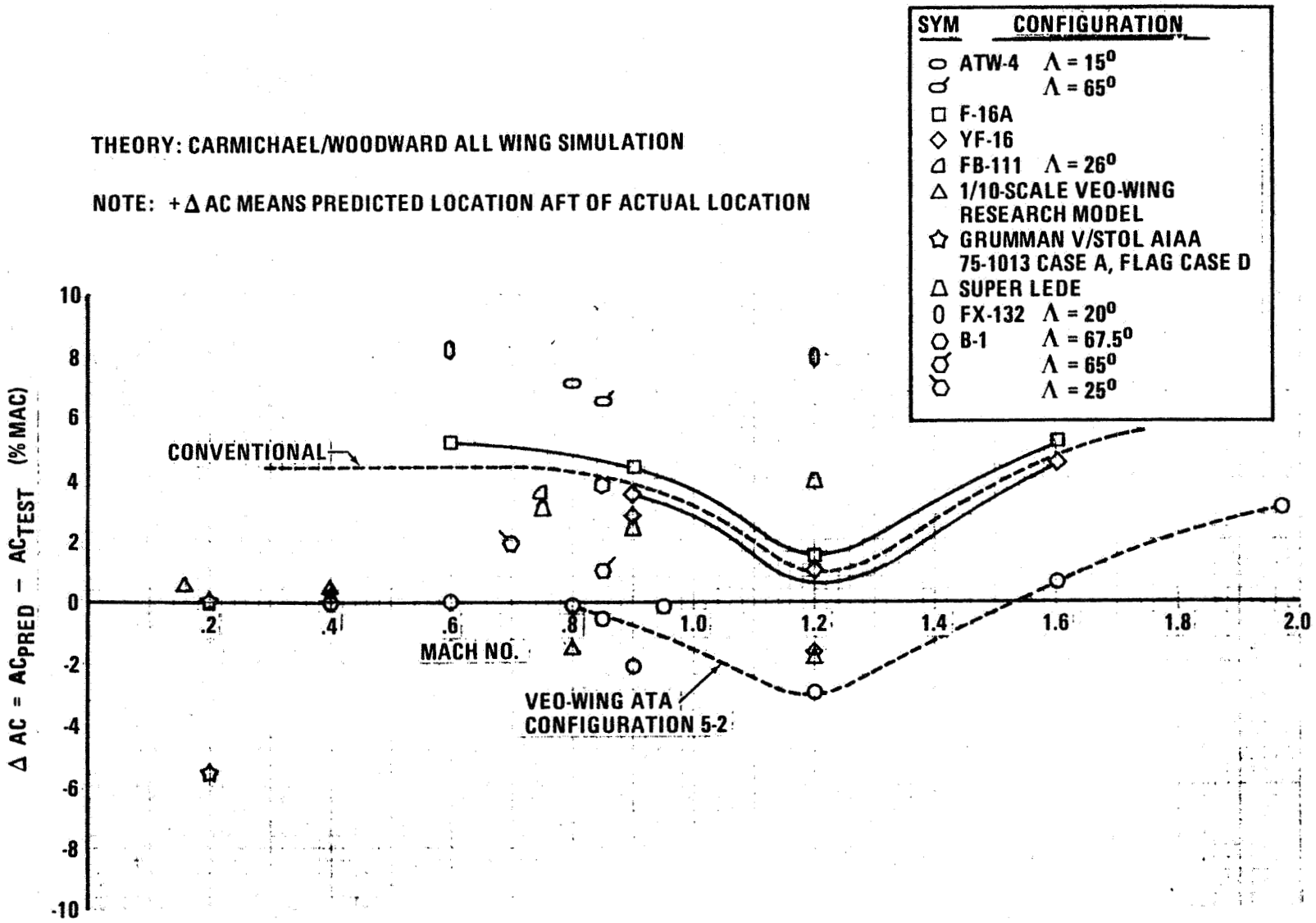

Figure 4-14 Aerodynamic Center Test/Theory Correlation

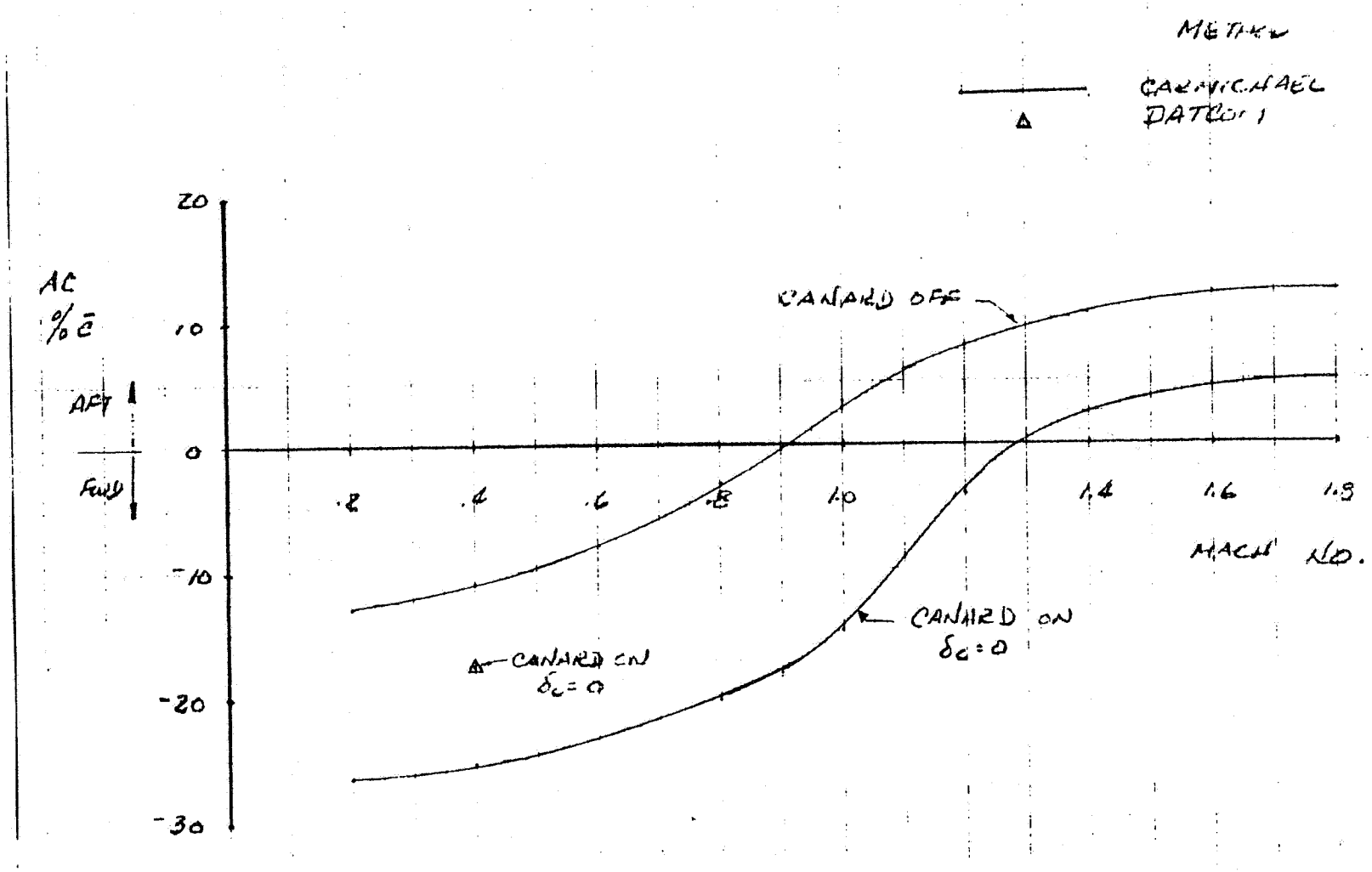

Figure 4-15 E205 Predicted Aerodynamic Center

the relatively blunt forward strake, etc. The methods do not lend themselves to this type of configuration. The configuration is being driven hard by the predicted instability levels. This is a major aerodynamic uncertainty that must be resolved with an experimental test program. The methods above predict the a.c. in the linear attached flow (low α) regions only; as non-linear effects are experienced at high α's, the a.c.-variation prediction methods are less reliable and experimental data must be used as a guide. So many aspects of the design (especially $C_{L_{max}}$) are dependent on these high-α stability characteristics; a wind tunnel program must be conducted to develop and tune the E205 configuration with any confidence.

The E205 configuration is longitudinally statically unstable to achieve the VEO-Wing nozzle benefits. The predicted instability levels are greater than can be presently tolerated. The maximum-allowable instability dictated by control system limitations is approximately 15-18% MAC. Therefore, the Flight Control System (FCS) will be used to augment the stability to the required level of frequency and damping. As part of this augmentation the flight control computer will be used to schedule the canard as a function of Mach number and angle of attack to achieve the desired level of static longitudinal stability.

4.1.4 High Lift Characteristics

$C_{L_{max}}$. The usual criteria for establishing trimmed $C_{L_{max}}$ are (1) the longitudinal wing stall characterisitcs, (2) the lateral-directional deterioration due to angle of attack, (3) structural load limitation, and (4) buffet onset. None of the data currently available or predictable indicates a wing stall or very serious directional deterioration. One of the difficulties in defining $C_{L_{max}}$ for the wide-bodied E205 shape is that although the wing operates and stalls normally, the lift generated by the body masks the stall, so that maximum lift is delayed to very high angles of attack ($\alpha > 30^{o}$).

Conventional powered aircraft trimmed $C_{L_{max}}$ is a function of α, M, δ_C, δ_{T_E} and $C_{T_{VEO\text{-}nozzle}}$. For a VSTOL airplane where forward-located thrusters are used for trim at low speeds, the low-speed trimmed $C_{L_{max}}$ is a function also of C_T for the Forward Thruster Ejector .

Therefore, for the VSTOL flight regime (Table 4-1) trimmed $C_{L_{max}}$ was determined by maximum negative canard deflection and an ejector thrust level for trim that provides an acceptable usable angle-of-attack range. For the supersonic regime, trimmed $C_{L_{max}}$ was determined by maximum negative canard deflection with a zero-degree nozzle deflection. For the cruise/maneuver regime (transonic) an estimated fairing was made between the VSTOL and supersonic regimes. These estimates are unclear owing to the undetermined canard/VEO-Wing nozzle deflection schedules required.

Figure 4-16 summarizes the estimated trimmed $C_{L_{max}}$ vs Mach number variation, which has served as $C_{L_{max}}$ for analysis in this study until test data can be obtained to determine the stall characteristics of the configuration. Both the aero-only and total coefficient (direct thrust effects included) are presented.

Buffet Characteristics. Because the E205 aircraft is intended to accomplish the roles of interceptor and attack aircraft, it is necessary to consider the buffet characteristics in the configuration development as important as the other handling qualities or the performance.

Angle-of-attack estimates for buffet onset rather than C_L buffet onset are presented for the E205 configuration because of the difficulties described previously in estimating trimmed $C_{L_{max}}$ and C_L vs Mach no. With the needed experimental data base to develop these lift coefficient trends, it will be possible to relate the estimated angle-of-attack for buffet onset to C_L buffet onset.

Some clues to the buffet characteristics of the E205 configuration have been obtained from analysis of the axial force data of the VEO-Wing fighter configuration force model (from test TF512 conducted at the AEDC PWT 4T transonic wind tunnel facility, Figure 3-3, Reference 4) by use of the methods of Reference 11. The wind tunnel model was not specifically instrumented to obtain buffet data in the initial tests for economic reasons. Future configuration development models should include specific instrumentation to determine the buffeting response characteristics of both the wing and the canard. Because these surfaces are thin plate-like structures, both tip accelerometers and bending strain gages are necessary to obtain buffet data adequate to estimate the buffet intensity

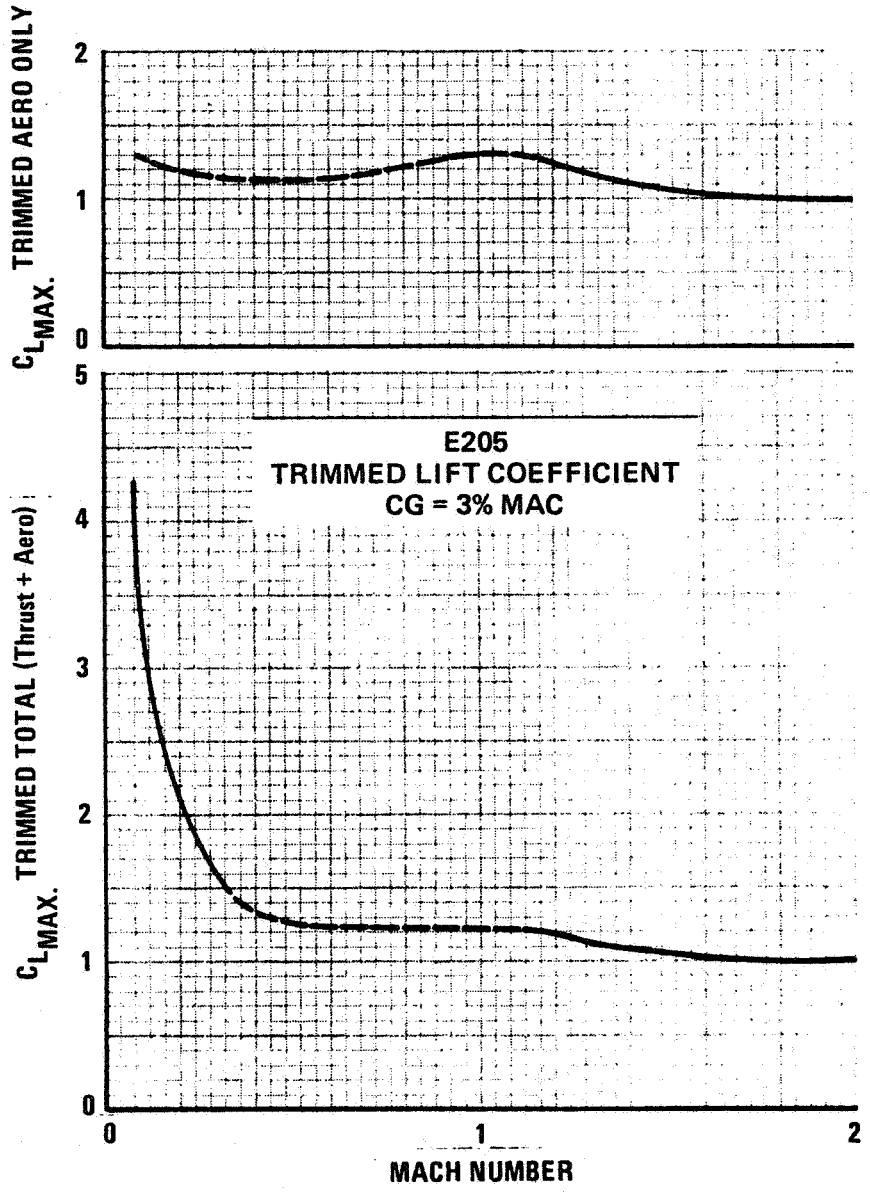

Figure 4-16 E205 Trimmed $C_{L_{max}}$ vs. Mach No.

and onset characteristics for the full-scale aircraft. Figure 4-17 presents variations of estimated buffet-onset angles of attack for several test configurations that are indicative of what would be expected for the E205 configuration. The upper plot illustrates the effects of adding the canards at several surface deflections. The variation for canard off is similar to data obtained on early versions of the lightweight fighter configuration development models that did not have maneuver strakes (Reference 12). The addition of the canard at a zero-degree deflection produces a positive increment in α_{BO} except in the "bucket" region at Mach 0.90. This result is consistent with experiences from configuration development wind tunnel tests of Convair Model 200 (Reference 13). A significant increase in α_{BO} is obtained for +10 degrees of canard deflection.

The lower plot presents the effects of a few combinations of leading-edge and trailing edge flap combinations which were tested. These results are consistent with out experience with leading and trailing edge flaps in both wind tunnel (Reference 14) and flight tests (Reference 15) of the YF-16 Lightweight Fighter prototypes. While the E205 configuration does not have a wing leading-edge flap, more definitive buffet testing may show that significant benefits in terms of reduced buffet intensities can be achieved if a leading-edge flap is used.

The effects of thrust deflection and spanwise blowing on the buffet characteristics are as yet unknown. It is anticipated on the basis of previous experience with transonic jet flap tests (Reference 16) and conceptual spanwise blowing tests (Reference 17) that the effects will be favorable.

4.1.5 Control Schemes and Effectiveness

Hover. The locations and uses of the thrusting devices employed for hover control are schematically shown in Figure 4-18. During hover, the E205 configuration achieves pitch control and heave by modulating the ejector primaries, achieves roll control by jet reaction in the wing tips (thrust up and down), and achieves yaw by differentially deflecting the ejector flaps. Heave is coordinated with all three axes controls. Table 4-3 demonstrates the control rates achievable for the sized configuration in and out of ground effect.

TABLE 4-3 E205 CONTROL ACCELERATION IN AND OUT OF GROUND EFFECT ~ RAD/SEC^2

	IGE	OGE (N_Z=1.05)
ROLL	.96	1.22
PITCH	.28	1.06
YAW	.40	.64

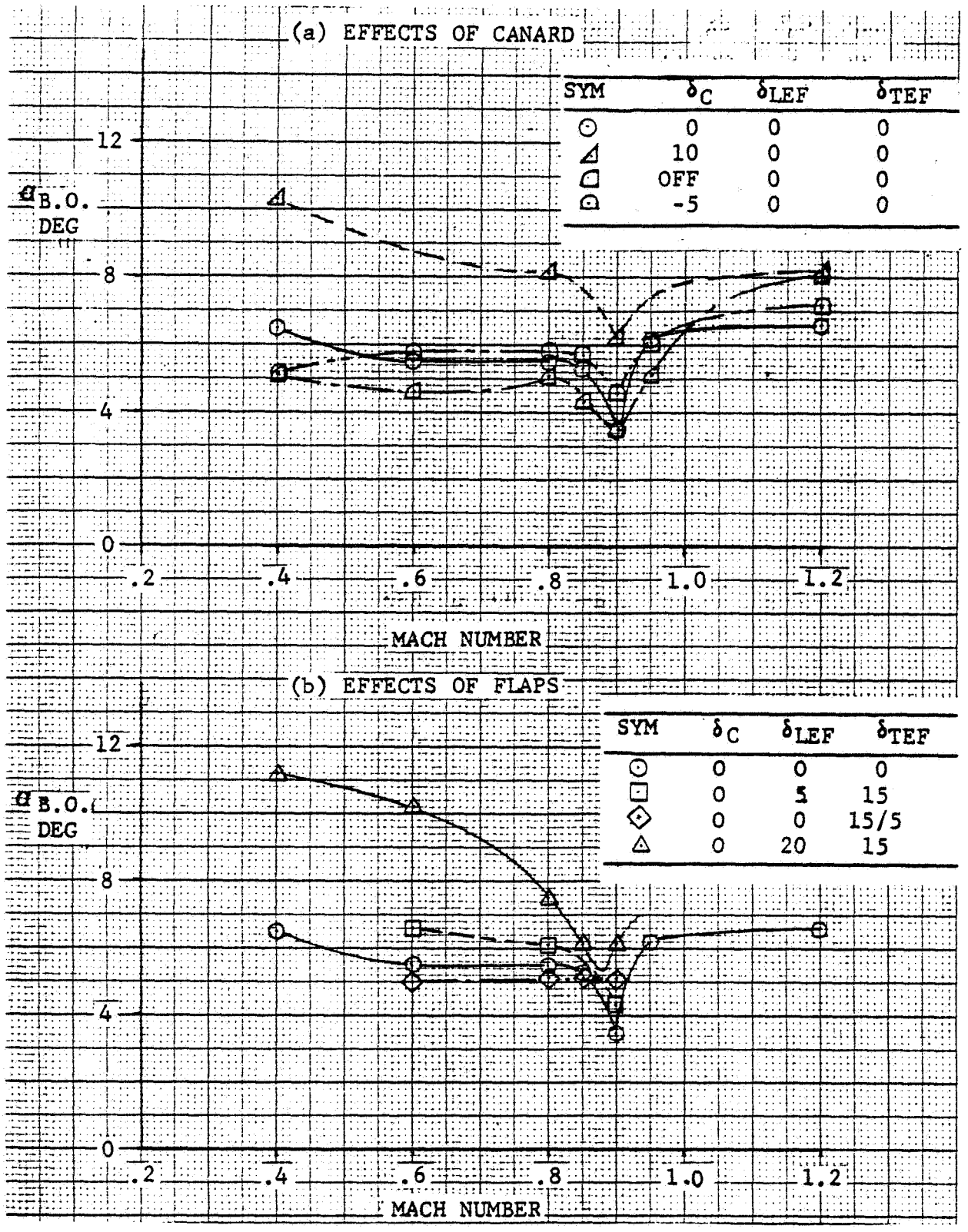

Figure 4-17 E205 Buffet-Onset Angle of Attack

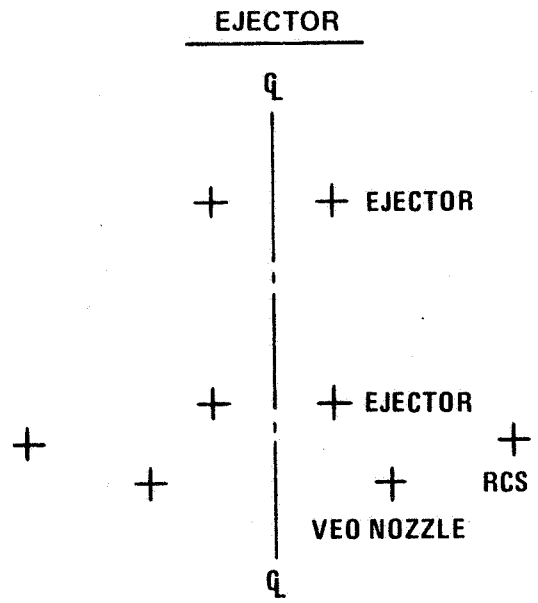

ROLL: RCS (Up and Down)

PITCH: MODULATE EJECTOR THRUST

YAW: VECTOR EJECTOR FLAPS
OR ASYMMETRIC PRIMARIES

TRANSITION: DIVERT EJECTOR AIR SUPPLY
TO OPENING VEO NOZZLES
(For T.O.)

Figure 4-18 E205 Hover-Control Thrusting Devices

VTO Transition. Transition is accomplished by diverting the excess thrust required to hover out of ground effect from the ejectors to the vectorable VEO-Wing nozzles. To achieve the VEO-Wing benefits for up and away flight, the c.g. is held at +3% MAC. The reaction control is capable of firing fore or aft (as well as up and down) to provide yaw control at very low speeds.

STOL. For STOL operations the hover controls are blended with the aerodynamic controls (the canard, elevons, and all-moving vertical tail) to provide control about the pitch roll and yaw axes.

The reaction controls are fired fore and aft or up and down as required to provide yaw and roll control at very low speeds or high angles of attack to augment the aerodynamic controls.

Up and Away. During conventional flight, control about the three axes is provided with canards, elevons, and the VEO-Wing nozzle for pitch; flaperons for roll; and the vertical tail and flaperon for yaw. The reaction controls are also available for augmenting the aerodynamic controls to extend the lateral-directional control capabilities at high angles of attack.

Control Effectiveness. The reader is referred to the lift, drag, and pitching moment curves presented in Subsection 4.1.2 for the longitudinal control effectiveness afforded by the canards, flaperons, VEO-Wing nozzles, and ejectors.

4.2 Lateral Directional Aerodynamics

Sideslip Characteristics. The static lateral-directional characteristics for Configuration E205 are presented in Figures 4-19a through 4-19e. These are based on the prediction methods of DATCOM. It should be noted that the wide forward fuselage fairing and nacelles contribute to the uncertainties in predicting the static lateral-directional instability and the effects on sidewash. The variation of the directional characteristics is largely dependent on this unorthodox fore-body loading, which is not easily predicted by standard methods. The dihedral effect, which is dependent on C_L, will be greatly effected by the induced supercirculation lift. The lateral characteristics are also affected by the canard and canard

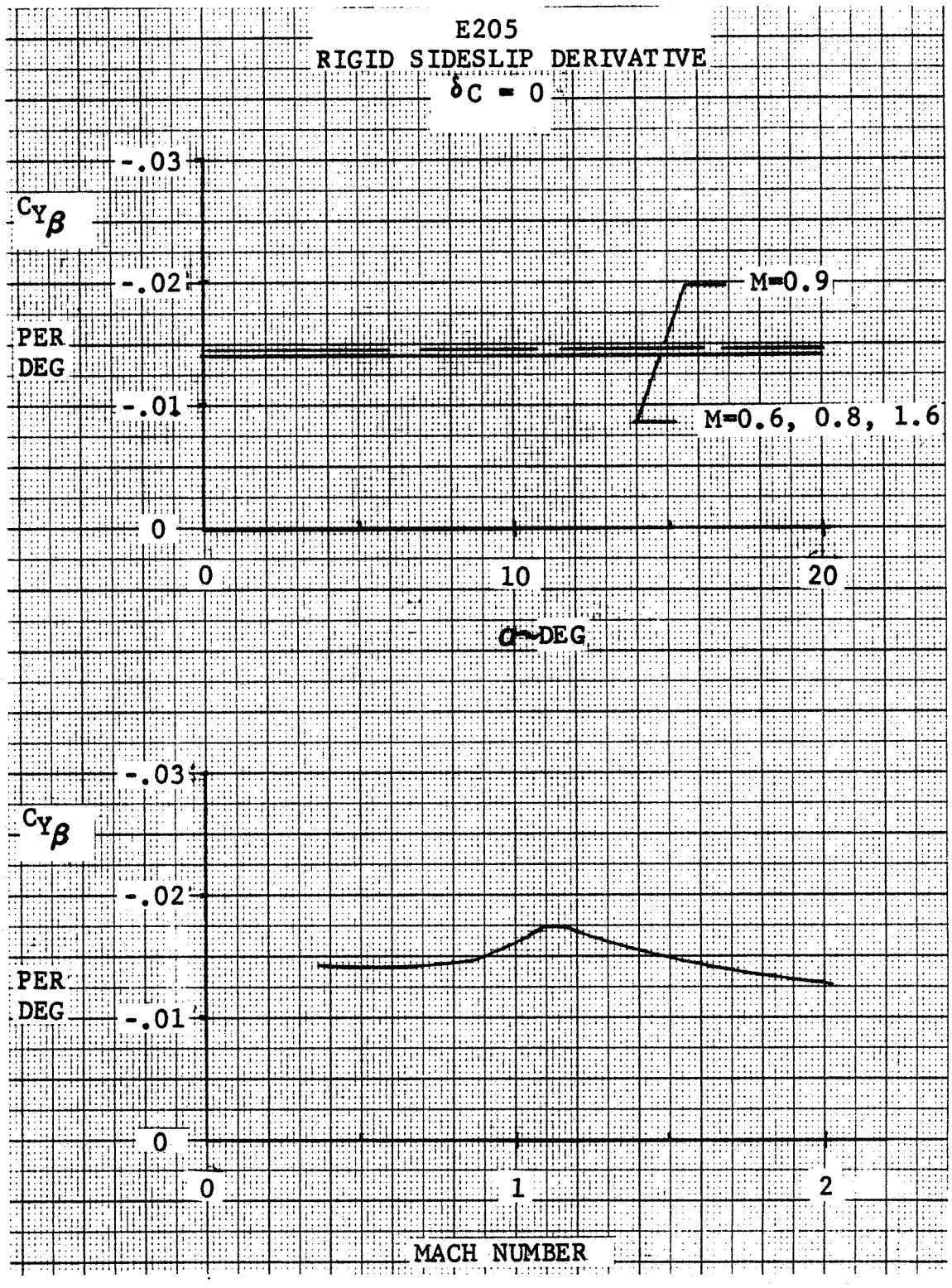

Figure 4-19 E205 Lateral-Directional Characteristics

a. C_{y_β} vs. α and Mach No.

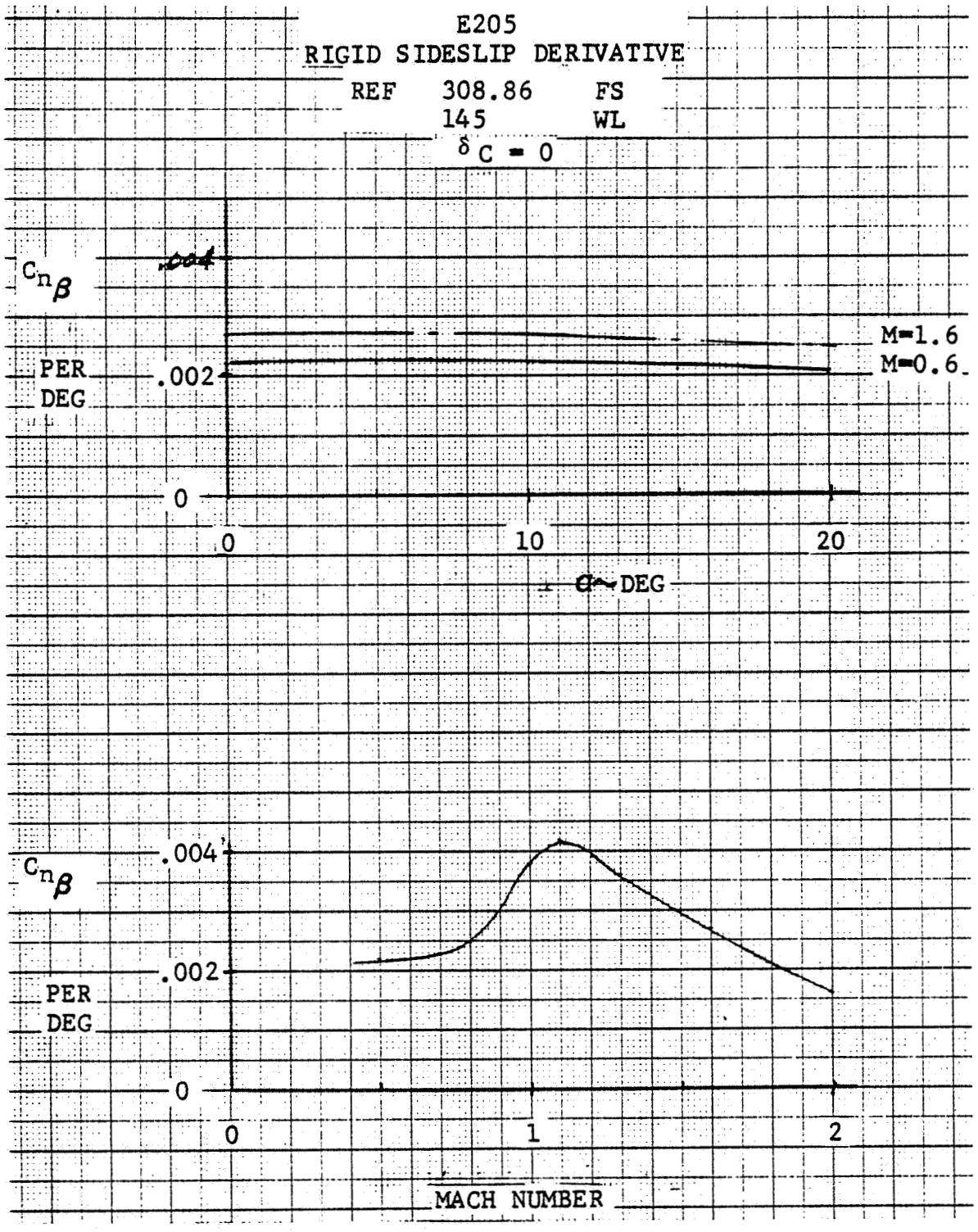

Figure 4-19 cont'd

b. C_{n_β} vs. α and Mach No.

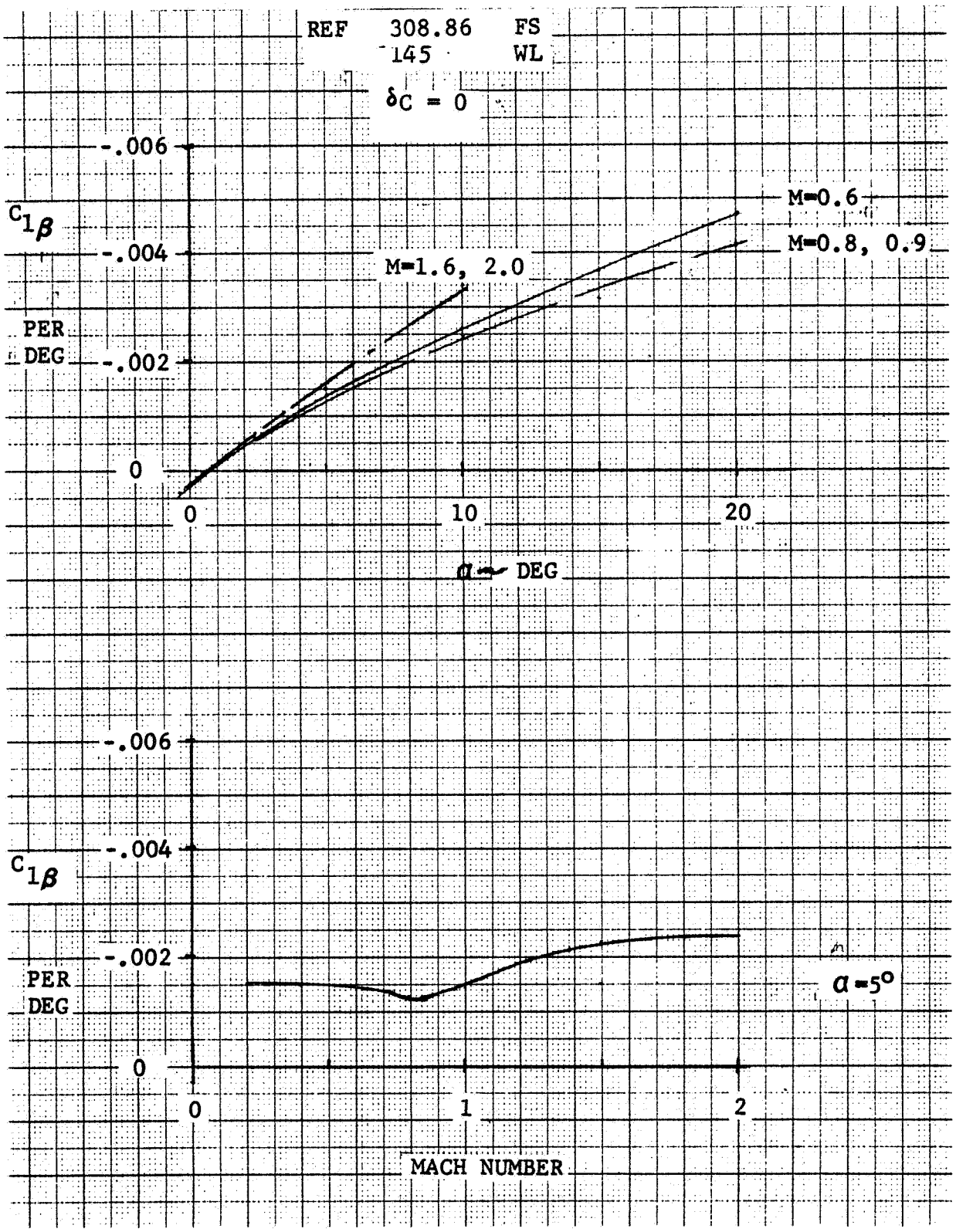

Figure 4-19 cont'd

c. C_{l_β} vs. α and Mach No.

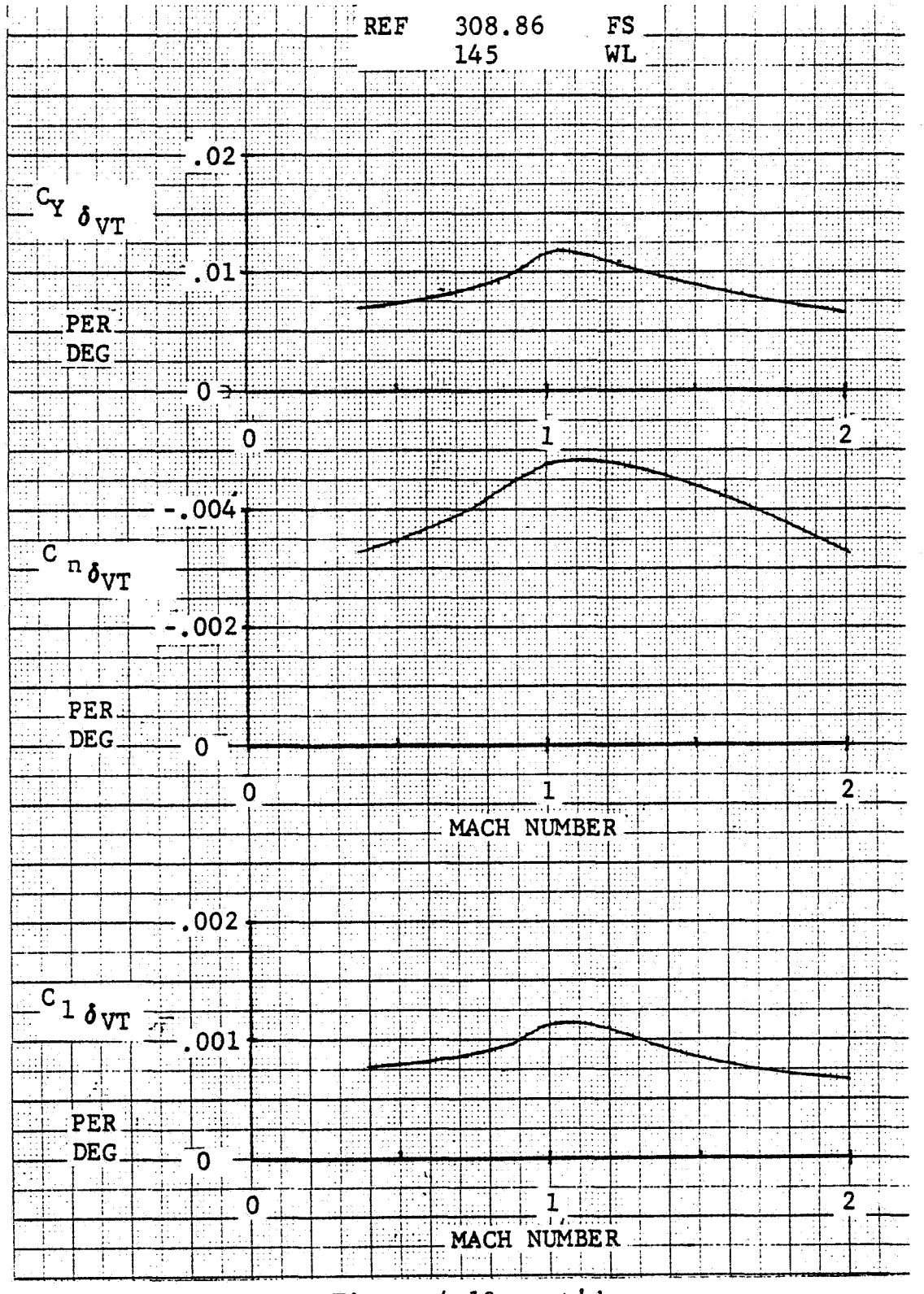

Figure 4-19 cont'd
d. Vertical Tail Effectiveness

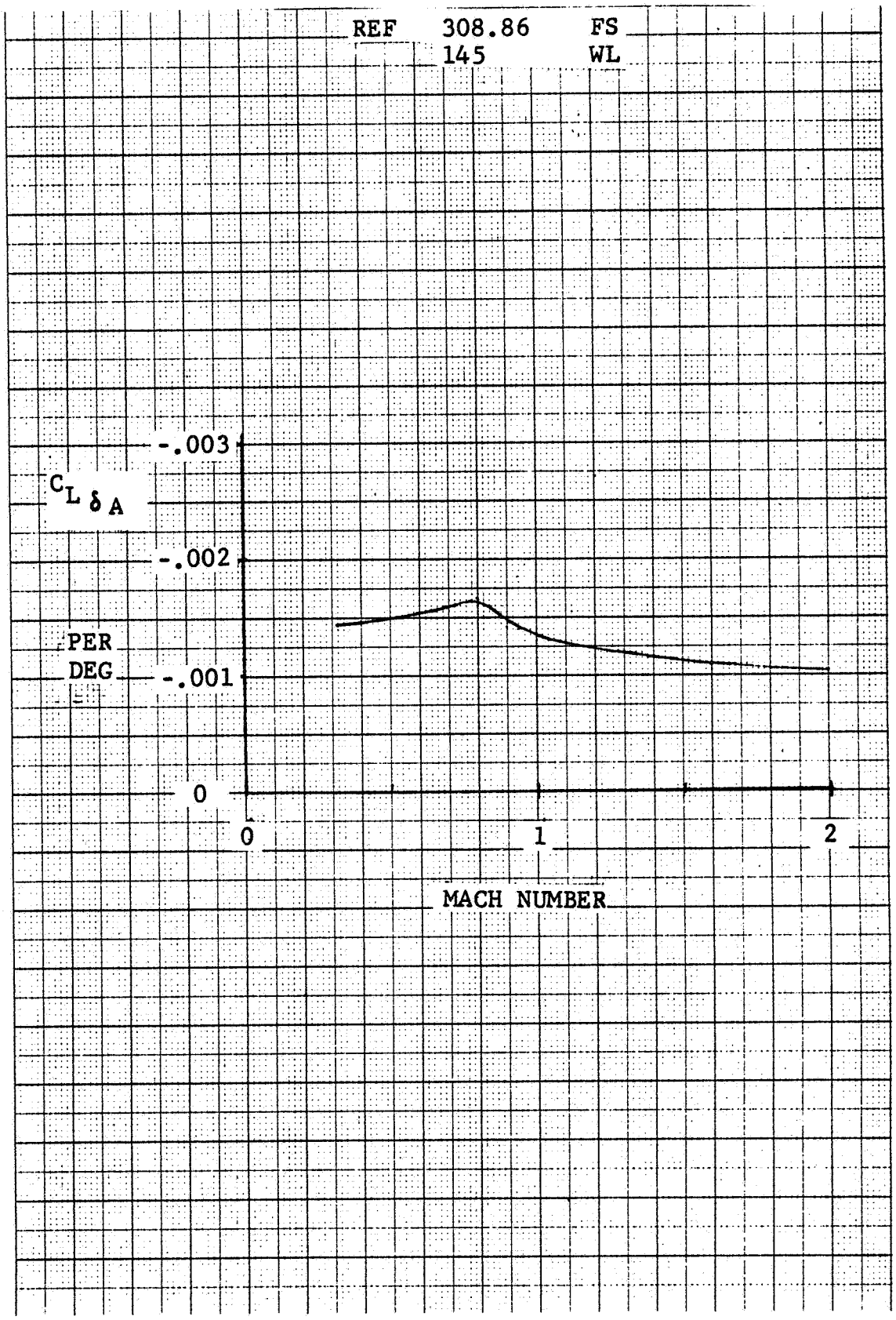

Figure 4-19 cont'd
e. Aileron Effectiveness

deflections and must be accounted for during a properly constructed wind tunnel test program. Data presented in these figures has been predicted for a zero-canard-deflection case.

Control Effectiveness. Directional control for Configuration E205 is obtained with an all-movable vertical tail. Control effectiveness of this surface is presented in Figure 4-19d. Standard DATCOM methods for these predictions were used.

Lateral control for configuration E205 is obtained with ailerons located from immediately outboard of the VEO-Wing nozzle to approximately 85% semi-span. The predicted values of roll-control effectiveness are presented in Figure 4-19e.

The augmentation in roll moment due to the VEO-Wing has not been included because of lack of available data. This is an area where a test program can be constructed to advantage. Side force and yaw moments due to aileron deflection were not predicted. The yawing moment is caused by the pressure gradient against the side of the fuselage. There is not enough experimental data available for correlation to any reliable prediction method.

4.3 Propulsion Induced Effects

Accurate estimates of the propulsion-induced effects on the aerodynamic characteristics are critical for any meaningful VSTOL design and sizing study. However, suitable analytical methods for predicting the propulsion-induced effects on the aerodynamics in VTOL or STOL modes are not available. An extensive ground-effects data base has been developed at General Dynamics through in-house contractual experimental programs (References 18, 19 and 20) and supplemented by available literature. The propulsion-induced effects on the aerodynamic characteristics of the E205 configuration were estimated by use of this empirical approach.

4.3.1 Induced Aerodynamics

The variation of the in-ground-effect (IGE), zero wind, critical attitude, propulsion-induced normal-force, and pitching-moment coefficients (C_{N_I} and C_{M_I}) with H/D_E (height of ejector flap trailing edges above ground/equivalent thrust diameter) for the E205 hover configuration are shown in

Figure 4-20; the induced-rolling moment variation (not shown) was also considered in the hover analysis. The propulsion-induced forces and moments are due to the induced flowfields in the airframe resulting in suckdown and fountains plus a back-pressure effect on the ejector, which causes an ejector augmentation ratio (ϕ) loss (or total airplane vertical thrust loss). The development of the effective ejector thrust augmentation in ground effect (including estimated suckdown and fountain effects on the airframe) from laboratory jet-diffuser-ejector test data is as follows:

GENERAL DYNAMICS PROPRIETARY INFORMATION

See Volume II

Ground-effects model testing of the E205 configuration has been conducted at General Dynamics very recently. Preliminary indications are that the estimated suckdown and fountain effects are in fair agreement with the test data. There are still large uncertainties associated with the back-pressure augmentation loss for the ejector operating near the ground. As discussed in Section 5.2, ejector model tests at General Dynamics have shown back-pressure increments comparable to that used above. Figure 4-21 shows the variation of ϕ available with ground height.

The effects of forward speed on these induced forces and moments and back-pressure effects are unknown. The variation of these effects with height above ground is assumed the same at zero (hover, into transition) and forward speeds (STOL analysis). These uncertainties must be experimentally resolved.

GENERAL DYNAMICS PROPRIETARY INFORMATION

See Volume II

Figure 4-20 E205 Propulsion-Induced Normal Force and Pitching Moment in Ground Effect

GENERAL DYNAMICS PROPRIETARY INFORMATION

See Volume II

Figure 4-21 Variation of E205 Ejector Augmentation Ratio

4.3.2 Reingestion Losses

The propulsion-induced flowfields that affect the aerodynamics of the airplane can also affect the engine performance by causing ingestion of the deflected lift system (ejector) exhaust gases by the engine inlet. The relatively low temperatures of the ejector exhaust gasses plus the blow-in doors located on the upper surface of the engine inlet (to capture required engine air from above rather in the hotter induced flowfield below) should help to minimize the reingestion and subsequent thrust loss. Therefore, no reingestion thrust losses were assumed for engine sizing in this study. An experimental test program would be required to confirm the validity of this assumption.

4.3.3 Footprints

Efflux velocities, total pressures, and temperatures for an E205-type ejector configuration are shown below. Ejector efflux exit conditions are provided in Table 4-4. The maximum temperature reflected back upon the aircraft surfaces is 60°F above ambient. This temperature occurs at the most critical condition, which is hover power at wheel height. The thermal ground footprint at this condition is shown in Figure 4-22; a plot of maximum velocities along the ground is given in Figure 4-23; and deck pressure is shown in Figure 4-24. Noise patterns have not been established.

TABLE 4-4 EJECTOR EFFLUX EXIT CONDITIONS

V_{Exit}	260 fps
T_{Exit}	230°F
$T_{O_{Exit}}$	232°F
$P_{T_{Exit}}$	15.75 psia

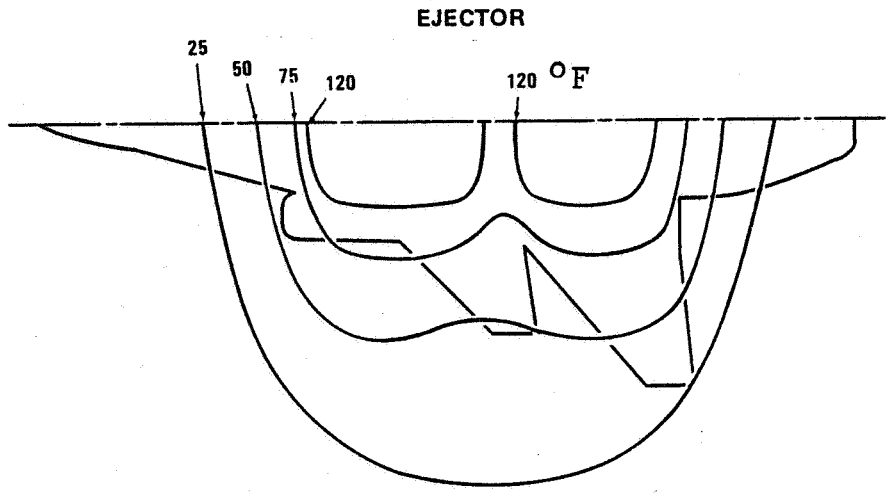

Figure 4-22 Ground Temperature Footprints

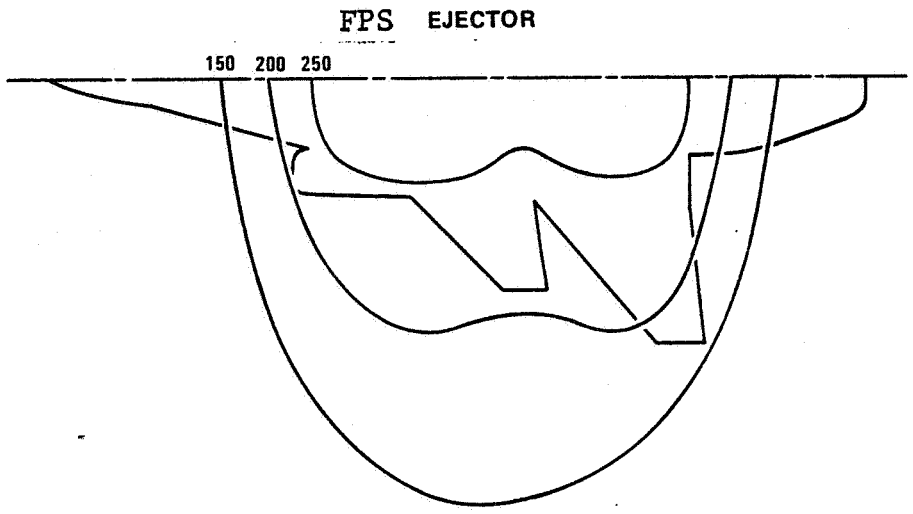

Figure 4-23 Ground Velocity Footprints

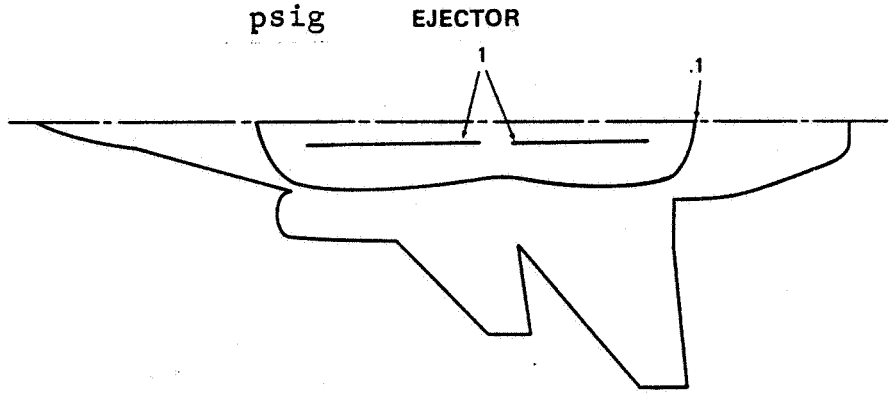

Figure 4-24 Deck Pressure Footprints

5. PROPULSION CHARACTERISTICS

The inlet, engine, exhaust-system-design and ejector characteristics and analyses are described in the following subsections.

5.1 System Description

The inlet design for the baseline aircraft configuration is an axisymmetric, open-nose, normal-shock design that provides best performance at subsonic and transonic speeds at lowest cost and complexity. The inlet location and the straight, short inlet duct provide high-quality air (high-pressure recovery, low distortion, low turbulence) to the engine at all flight conditions, including maneuvers.

The inlet design is complicated by conflicting requirements for high-pressure recovery and the demand for maximum airflow during VSTOL operations and for reduced airflow during supersonic cruise operation. Therefore, auxiliary inlets to augment primary inlet airflow for VSTOL operation and to minimize inlet size for reduced inlet spillage drag at supersonic speeds (e.g., blow-in doors) were incorporated.

The ejector lift system is powered by a Pratt & Whitney Aircraft advanced technology parametric engine having a 0.352 bypass ratio, a 25:1 pressure ratio, and a 2800°F turbine inlet temperature (.352-25-2800 parametric engine). This engine was selected from the Pratt & Whitney Parametric Fixed Turbine Geometry Afterburning Turbofan Engine Study data. The 0.352 bypass ratio was chosen on the basis of ejector requirements for a high primary pressure ratio. The engine is a twin-spool, fixed-geometry-turbine, mixed-flow, augmented turbofan. Maximum Mach number flight conditions were used to define the engine structural requirements, which are reflected in engine weights. The performance data for this engine are representative of hardware representative of the 1985-1990 time period.

Figure 5-1 shows typical operating modes of the two-dimensional wedge/convergent-divergent VEO-Wing nozzle used with the Pratt & Whitney .352-25-2800 engines. The relationship between the geometric nozzle deflection, δ_{TE}, and the jet-turning angle, θ_j, used for this nozzle is defined in Figure 5-2.

GENERAL DYNAMICS PROPRIETARY INFORMATION

See Volume II

Figure 5-1 Typical Operating Modes of Two Dimensional Wedge/CD Nozzle

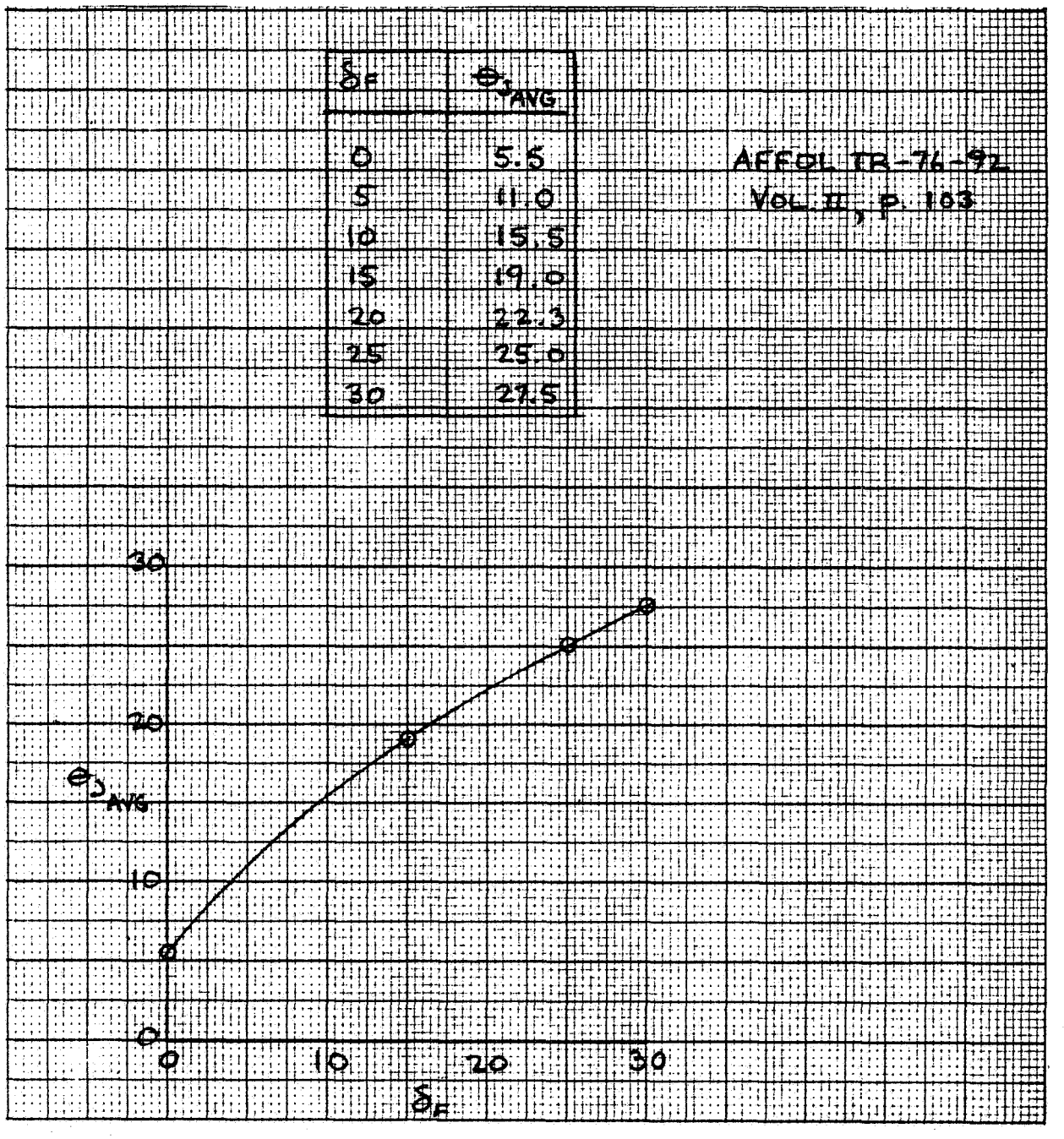

Figure 5-2 Jet Turning Angle vs. Geometric Nozzle Deflection for VEO-Wing Two-Dimensional Wedge/CD Nozzle

Recent developments (References 2, 21, and 22) have demonstrated the feasibility of using compact, high-performance ejectors to provide thrust for vertical takeoff and landing. Approximately 84% of the engine intermediate-power exhaust gas (mixed fan and turbine discharge) is required for ejector operation out of ground effect. This airflow is ducted to the ejector primary and wall nozzles, as shown in Figure 2-2. The main nozzle flow is blocked, and the remaining 16% of exhaust gas flow is used for the reaction control system and for acceleration from hover to normal flight conditions, and vice versa. Sea level static, tropical day design conditions for the ejectors are

- Installed ejector thrust (OGE)(tropical day)=42,965 Lb.
- Installed thrust augmentation ratio (OGE) = 1.98
- Engine intermediate power installed exhaust flow conditions (per engine) = 155 lbm/sec
- Exhaust gas total pressure and temperature = 54 psia and 1915°R.

5.2 System Performance

For assurance of correct airplane performance evaluation, a propulsion-aerodynamics bookkeeping procedure was defined. The inlet baseline condition is an inlet capture-area ratio of 1.0. The nozzle baseline condition is a long, constant-area rectangular-cross-section cylinder bounded by the cowl hinge line and flap hinge line (as shown in Figure 5-3) and the nozzle side plate. Pressure drag on the nozzle surfaces aft of the cowl hinge point is included in the propulsion deck. These baseline conditions are applicable to horizontal flight only and do not apply during VTOL operation. External inlet and nozzle drag during VTOL and transition operation are assumed to be negligible. This bookkeeping procedure accounts for inlet and nozzle drag forces that are a function of engine power setting by placing them in the installed-propulsion-system performance data. When the inlet stream tube (A_o) is less than inlet area (A_i), an inlet spillage drag force is included in installed net thrust. Nozzle drag forces are included in installed net thrust at all operating conditions. Drag associated with the trailing-edge flap is always included in the aerodynamic data.

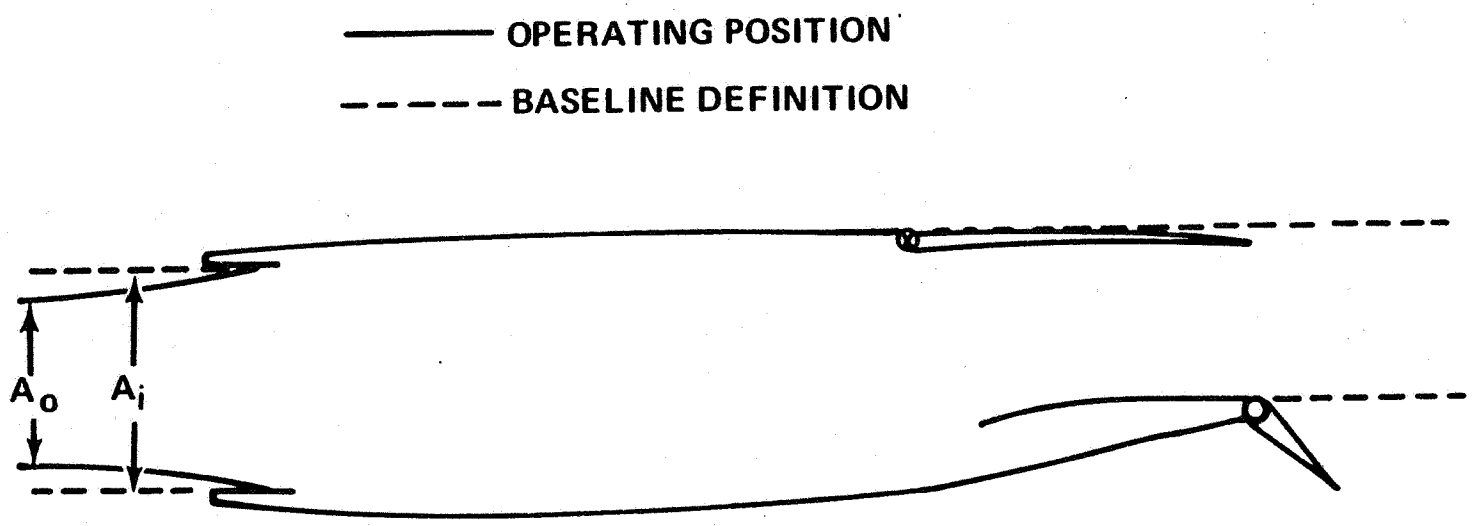

5-3 Baseline Inlet and Nozzle Definition

Installed net thrust, specific fuel consumption, and airflow data were generated from engine data supplied by the engine manufacturer and modified by General Dynamics so appropriate installation losses would be taken into account. These data conform to the bookkeeping procedure described above. Installed propulsion system performance data generated for representative maneuver flight conditions are presented for the Pratt & Whitney .352-25-2800 engines in Table 5-1. These performance data are corrected for the installation losses discussed in Section 5.3. Takeoff thrust and fuel flow data are also presented in this table.

5.3 Installation Losses

Inlet performance characteristics used for computing installed engine performance, i.e., compressor-face total pressure recovery, inlet spillage drag, and other installation losses such as inlet boundary-layer-bleed drag have been determined. Inlet-performance data for the inlet are shown in Figures 5-4 and 5-5 . Inlet spillage drag, defined as inlet additive drag plus cowl lip suction, is based on experimental data of similar inlet types.

Installed propulsion system performance also includes corrections for compressor bleed-air and engine horsepower extractions. The .352-25-2800 parametric engine performance data were corrected for engine bleed and horsepower extraction by reducing net thrust 3 percent.

The Pratt & Whitney engine data are based on an axisymmetric nozzle. An estimated loss in thrust coefficient required to correct for the installation of the VEO-Wing wedge/convergent-divergent nozzle of .01 is included in the installed performance data.

A technique for predicting nozzle afterbody drag has been developed by General Dynamics (References 23 through 24). In this method, experimental data are correlated via general, nondimensional parameters so that the resulting prediction technique can be applied to wide ranges of internal/external geometry and exhaust-plume conditions. Specifically, afterbody drag is predicted by superimposing interference effects due to plume shape and plume entrainment on geometry-dependent drag levels. Drag values predicted by this technique agree well with NASA test data in sample comparisons. The method is now also applicable to two-dimensional nozzles.

Table 5-1 PRATT & WHITNEY 0.352-25-2800 PARAMETRIC ENGINE INSTALLED PERFORMANCE DATA - 100% SCALE ENGINE

GENERAL DYNAMICS PROPRIETARY INFORMATION

100% SCALE $\left(\frac{w\sqrt{\theta}}{\delta}\right)_{DESIGN}$ = 267 lb/sec

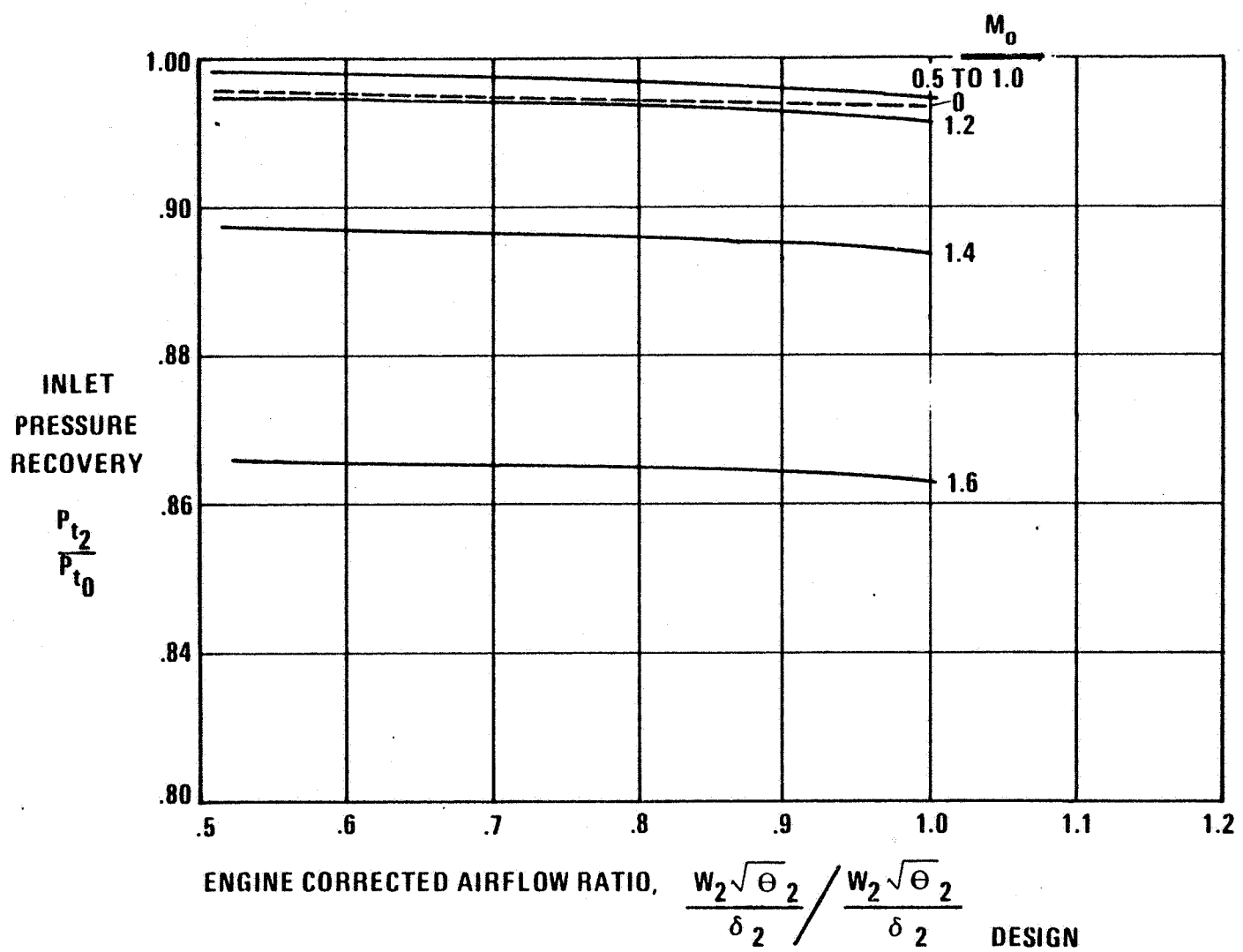

5-4 Estimated Inlet Pressure Recovery

o 100% SCALE A_i = 945 sq. in.

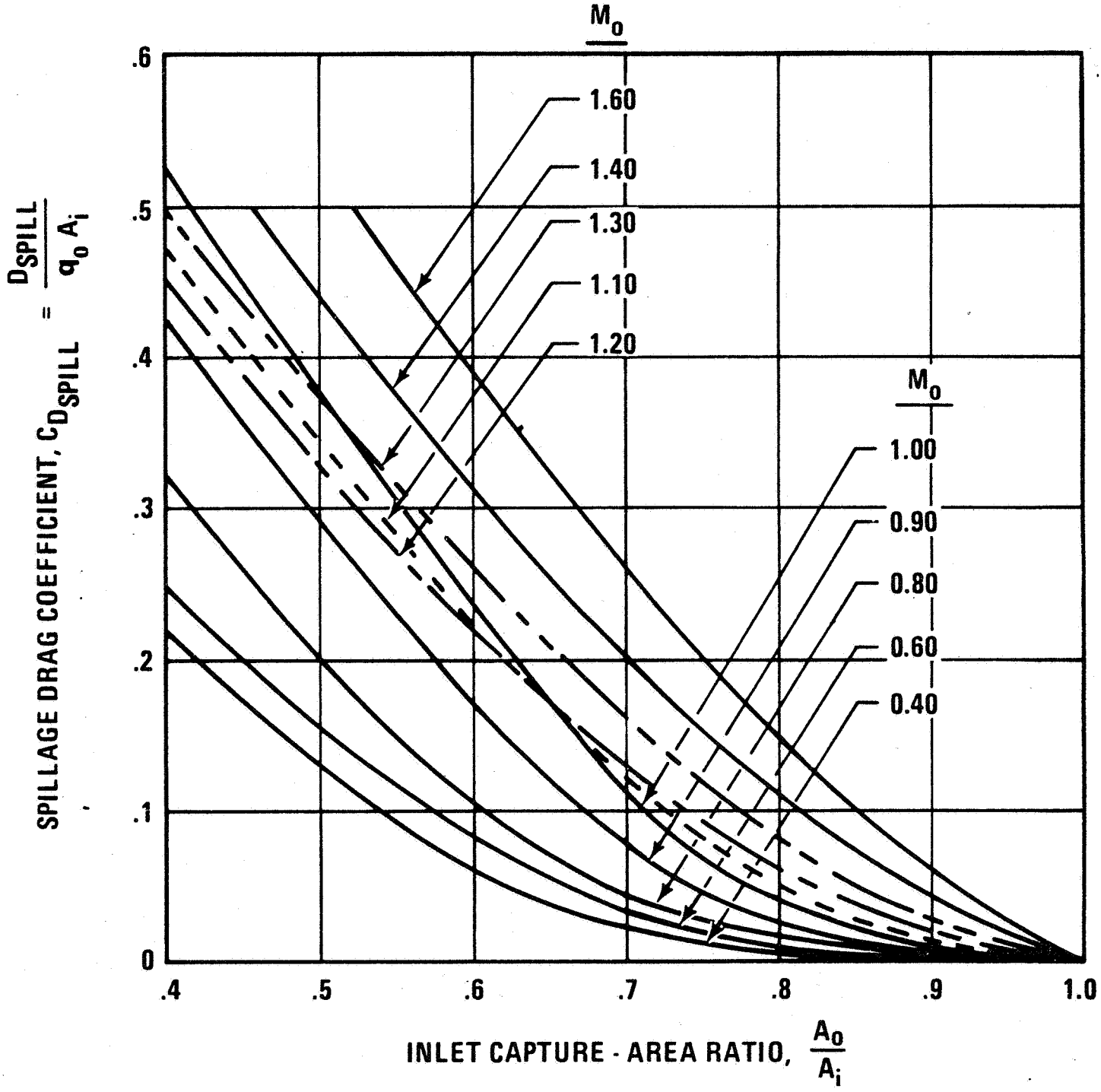

5-5 Estimated Inlet Spillage Drag Coefficient

Experimental measurements of the nozzle pressure drag on a VEO-Wing conceptual model are shown in Figure 5-6. These data (taken from Reference 25) represent a typical dry-power nozzle position. Additional two-dimensional nozzle afterbody drag data have been developed during the General Dynamics/ AFFDL studies of Advanced Tactical Fighters (ATF), Reference 26. These data and analytical methods were used to develop the external nozzle boattail drag increments for the study aircraft. The estimated external drag increments for the full-scale engine used in this study is shown in Figure 5-7.

The ejector concept and its performance employed in this study is discussed in detail in Section 5.4. Ejector performance degradation can be caused by (1) aircraft installation effects, (2) external stream effects during transition from hover to normal flight conditions, and (3) pressure losses due to the exhaust-gas duct/control system between the engine and ejector. Uninstalled ejector losses are a part of the overall ejector performance defined in terms of the thrust augmentation of a given isolated (without the presence of surrounding aircraft structure) ejector geometry, with specified primary and diffuser nozzle pressure ratios.

The presence of aircraft structure near the ejector alters the secondary flow entering and the mixed flow exiting the ejector. This effect may either degrade or enhance the thrust augmentation, depending on the nature of the change in pressure distribution around the ejector and surrounding structure. Because of the complex nature of the flow field around the installed ejector, its performance must currently be measured experimentally. The in-house experimental ejector program and the large-scale VEO-Wing model tests being planned by NASA/Ames will provide data to address these problems (Section 5.4). However, because these data were not available, no installation losses (or enhancements) were included in the concept evaluation.

Degradation in ejector performance caused by the influence of the external stream must also be measured experimentally.

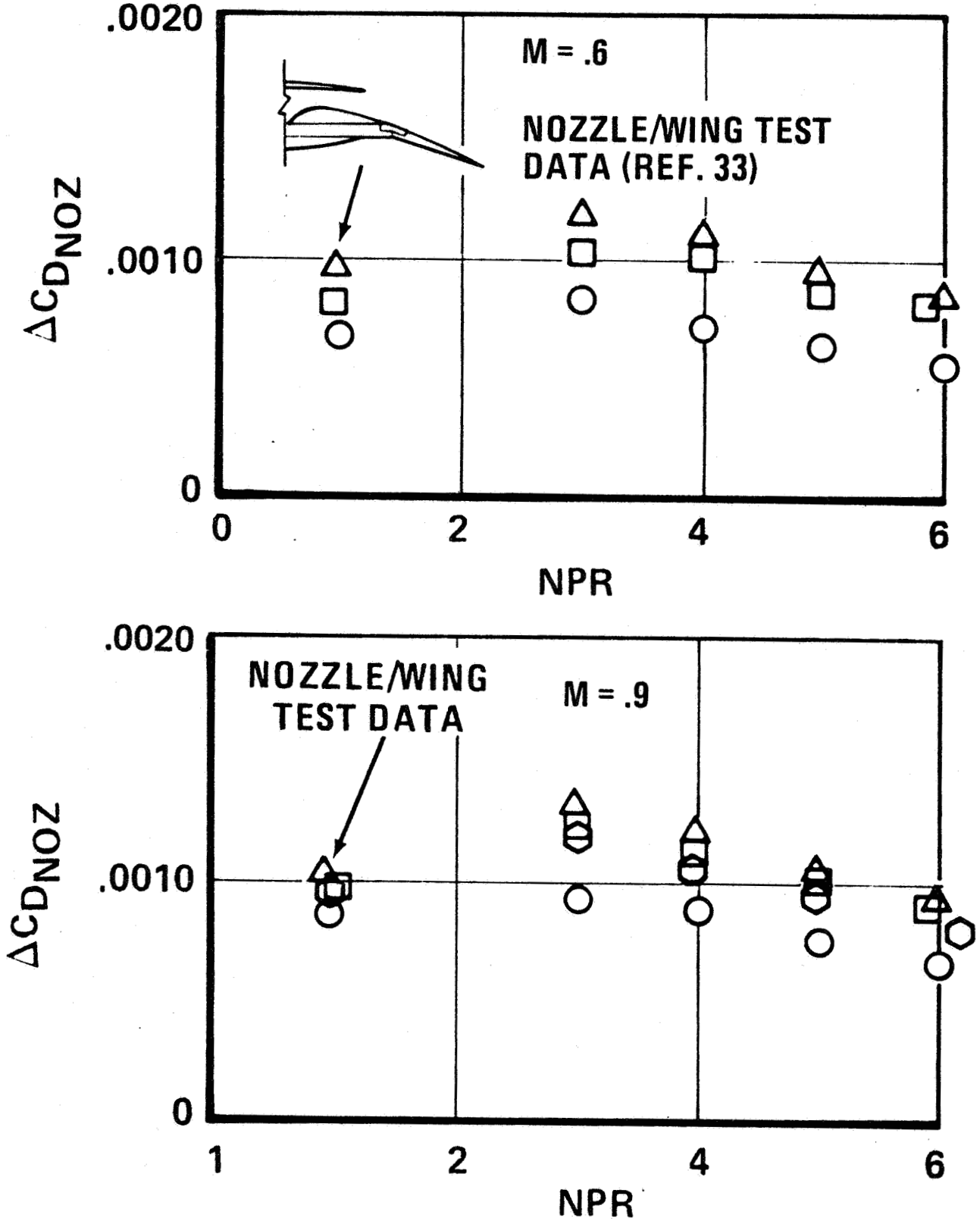

5-6 Measured Nozzle Pressure Drag on VEO-Wing Conceptual Model

- 100% SCALE ENGINE
- P&WA 0.352-25-2800 ENGINE
- DRAG PER ENGINE
- EXIT AREA = 496 sq. in
- REF AREA = 1944 sq. in.

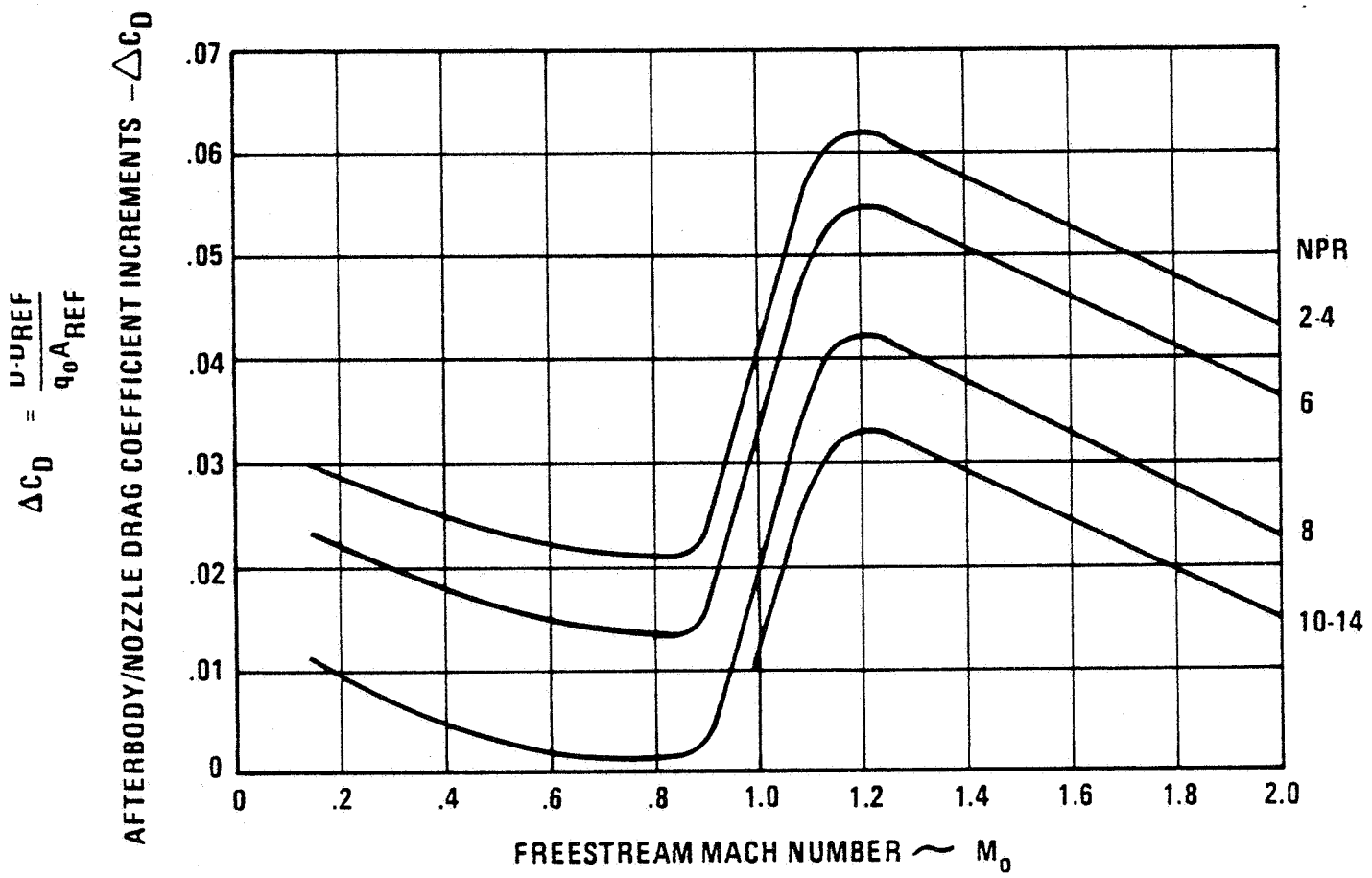

5-7 External Nozzle Boattail Drag Increments

5.4 Jet-Diffuser Ejector

The four jet-diffuser ejector bays, totaling 33.33 ft in length, generate the VTOL motive force and enhance the STOL performance of the E205 configuration. During VTOL the diverted hot gas flow from each engine feeds the primary and diffuser nozzles of the two adjacent ejectors. The primary nozzle areas are variable and provide differential lift (for pitch control during STOL or VTOL). This pitch control is accomplished by proper alteration of the primary nozzle area in each bay. The primary nozzles and diffuser flaps are retractable for conventional flight. Yaw control during VTOL is accomplished by vectoring the lower ejector flaps.

Concept. The jet diffuser ejector design incorporated in this configuration (see ejector cross-section and 3-view drawing, Figure 5-8 and Figure 2-2), is based on application of the research reported in Reference 2. The following excerpt from this report provides an introduction to the jet diffuser ejector concept.

> The thrust augmenting capability of an ejector depends, to a large extent upon its effective diffusion area ratio and upon the degree of completion of the momentum transfer from its primary energized fluid to the induced flow prior to recompression on the flow to ambient pressure. Both of the above require large distances in the flow direction, if conventional design configurations are utilized. Wide angle diffusers can obviously achieve reduction in the length of the diffuser for a given area ratio and without sacrifice in ejector performance if separation can be avoided.
>
> Injection of the primary fluid into a curved, low speed flow can accelerate the transfer of momentum.

The jet diffuser ejector is designed to achieve both of these goals by reducing the required diffusion and mixing lengths. This is accomplished by creating the entrainment flow with airflow out of the detached primary nozzles (located above the ejector inlet) and by preventing separation on the wide angle diffuser walls with a boundary-layer-control nozzle.

Ejector Performance and Aircraft Installation. The laboratory Alperin Jet Diffuser Ejector (AJDE) augmentation ratio (ϕ) performance of Reference 2 is plotted in Figure 5-9 as a

GENERAL DYNAMICS PROPRIETARY INFORMATION

See Volume II

Figure 5-8 Diffuser Ejector Design

GENERAL DYNAMICS PROPRIETARY INFORMATION

See Volume II

Figure 5-9 ADJE Performance and Pitching Scheme for E205

function of total nozzle-area to throat-area ratio (A_2/A_o) and for full-scale ejector lengths of 80, 100, and 120 inches. The Thrust Augmentor Wing results showed that for $A_2/A_o < 16$, $\emptyset$ decreased radically; there was concern that this might prove to be the case with the Alperin type ejectors, therefore $A_2/A_o = 16$ was selected as a design point to achieve the narrowest airplane (i.e. minimize airplane width to reduce frontal area for drag and roll inertial requirements for hover plus drive to a higher fineness ratio airplane for supersonic drag). The desire to keep the ejectors as small as possible also drove the engine selection to the low bypass ratio engine (.352) to achieve the highest nozzle pressure ratio (3.0) delivered to the ejector to minimize ejector size. Five-percent duct lossess were assumed from the engine to the ejectors for ejector/engine sizing purposes.

The $\emptyset = 1.9$ at $A_2/A_o = 16$ is the selected baseline point for ejector sizing in this study. Corrections to this $\emptyset$ for temperature, scale, and back-pressure effects were shown in Section 4. The temperature corrections have been derived from a General Dynamics unpublished correlation of experimental results including data from Greathouse (NASA), Ohio State University, the Lockheed Hummingbird and NAPC Data. The scale effects were derived from Reference 27.

With the nominal setting of $A_2/A_o = 16$ the ejector produces a laboratory $\emptyset$ of 1.9. By varying the primary nozzle area with the mechanism shown in Figure 5-10, the thrust can be varied up or down to produce changes in ejector thrust. With the four-ejector bay arrangement on the E205 configuration, this primary nozzle control concept can be used to produce a pitching moment couple with no loss in lift (i.e. no heave motion with moment control). This allows the engine to be sized for the average rather than maximum control loading with pitching moment control produced by ejector primary variation.

The primary ejector nozzles are capable of exit area A_o variation in order to modulate their thrusts for control and transition purposes (Figure 5-9). Lowering the nozzle area of a given ejector (and simultaneously raising the area of another ejector or the VEO-Wing nozzle in order to maintain constant engine airflow) lowers the primary mass flow and the isentropic thrust of that ejector. At the same time, $\emptyset$ is raised (Figure 5-9) but the effect of the primary mass flow change predominates so that ejector thrust, given by the equation

$$T = \dot{m} V_j \emptyset$$

GENERAL DYNAMICS PROPRIETARY INFORMATION

See Volume II

Figure 5-10 Variable Area Primary Ejector Nozzles

is lowered. While A_0 of an ejector can be varied to zero area without any problem, it cannot be raised indescriminantly. The ducts for the ejectors were designed for a maximum Mach number of .3 at $A_2/A_0 = 16$; raising A_0 will cause a corresponding rise in the Mach number and increased duct losses. For control purposes, a maximum change of A_0 of + 15% was allowed in order to present unacceptable duct losses.

It may also be possible to obtain yaw control by varying the nozzle primaries on opposite sides of the ejector to asymmetrically load the ejector walls; this would produce a net force that could be used for yaw control. The yaw control scheme, however, has been analyzed as ejector-flap vectoring.

The location and lengths of the ejector bays were determined by the hover control requirements in ground effect. The effects of back-pressure on ejector performance were derived from General Dynamics test experience as explained below. The variation of $\emptyset$ with height above ground used for the E205 design is shown in Figure 4-21.

The peak primary gas flow temperature in the ejectors is approximately 1450°F. This is beyond the capability of ordinary stainless steels (creep resistance is negligible at these temperatures); hence, the distribution ducts and primary and diffuser nozzles must be made of a heat-resistant alloy (inconel, Rene, etc.) producing a very high ejector system weight of 3298 lb.

As seen above, a very high laboratory augmentation has been demonstrated for a model of the AJDE concept. One of the key goals of the E205 configuration is a practical installation and integration of this ejector concept into the VEO-Wing concept aircraft without compromising the laboratory ejector performance levels.

To this end, the ejector-bay packaging scheme, illustrated in Figure 5-11, was developed; the stowed and deployed positions are shown. Not shown are the fuselage and nacelle doors, which must open to allow the primary nozzle to deploy and then close behind them to provide a reasonable ejector entrance. A great deal of mechanism, actuators, and linkages are required to make this packaging concept work, but this is considered a reasonable compromise to minimize strake depth and frontal area.

GENERAL DYNAMICS PROPRIETARY INFORMATION

See Volume II

Figure 5-11 Packaging Scheme for Jet-Diffuser Ejector

GENERAL DYNAMICS PROPRIETARY INFORMATION

See Volume II

5.5 Reaction Controls

Engine exhaust air is taken through a portion in the flap of the collector area (just ahead of the entrance to VEO-Wing nozzle, F.S. 350-375) at a temperature of 1915°R and a pressure of 54 psi and is ducted to the reaction control nozzles located near the wing tips. The ducts are formed by the upper

GENERAL DYNAMICS PROPRIETARY INFORMATION

See Volume 2

Figure 5-12 General Dynamics Ejector Model Details

and lower wing-skin surfaces and use up much of the wing volume that would normally be available for fuel. The reaction controls provide up, down, fore, or aft thrusting by lining a high-speed rotating valve up with holes in an upper and lower surface fairing. Convergent nozzle efficiencies have been used to estimate the thrust since thrust modulation will be accomplished by modulating the throat area of each nozzle port. The reaction control system has been sized by the roll requirement for hover in ground effect for the E205 configuration to provide 1240 lb of thrust per side. The reaction control system thrust required (total, 2 sides) as a function of airplane VTOGW has been estimated by scaling inertias as a function of VTOGW; the results for the ejector aircraft family are shown in Figure 5-13. For STOL and VTOL transition and high-α maneuvering, these reaction controls can also be used to enhance both the longitudinal and lateral-directional characteristics of the airplane. Their usefulness should also be explored for combat maneuvering.

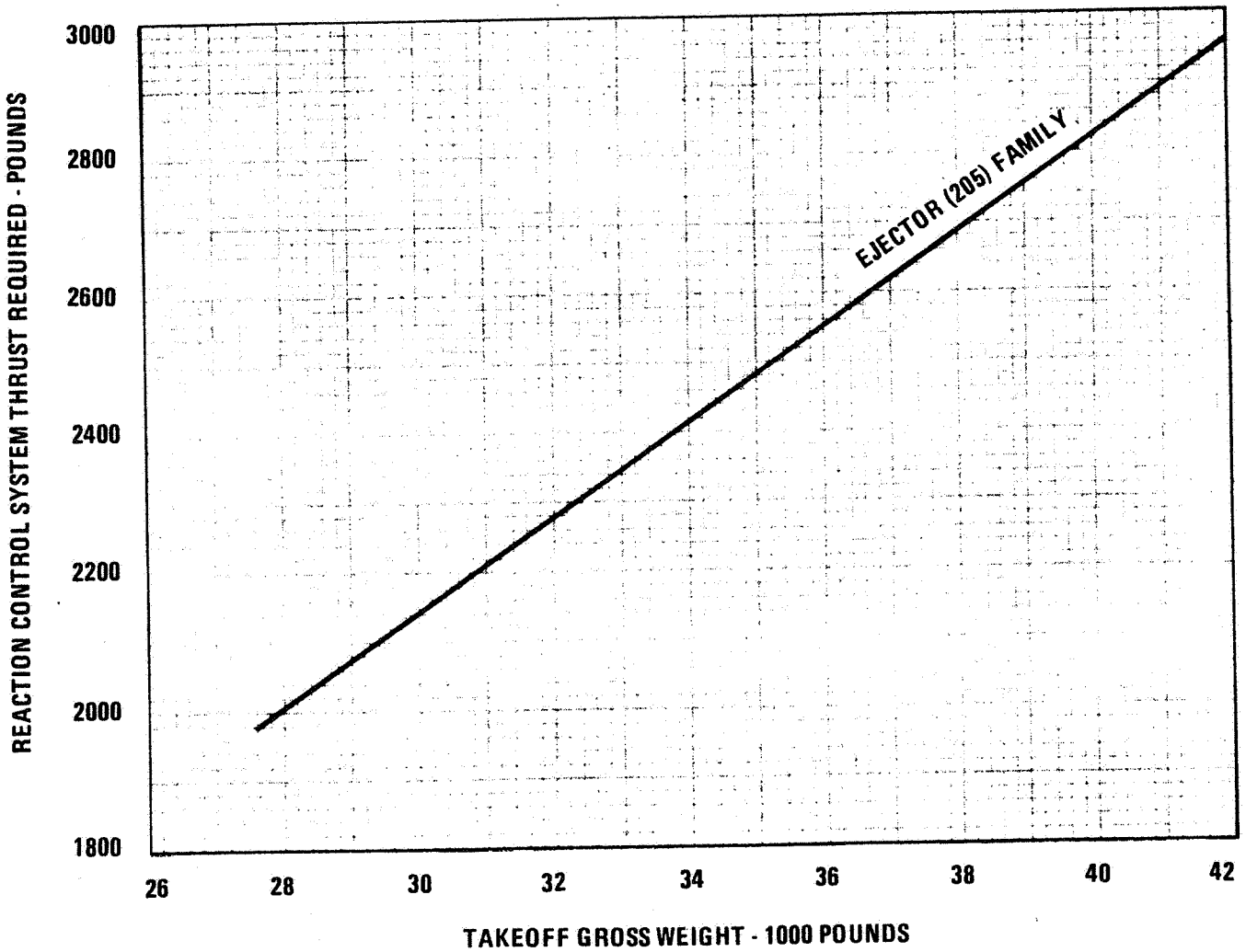

5-13 Reaction Control System Thrust Requirements for Variations in VTOGW

6. AIRCRAFT DESIGN

6.1 Mass Properties

The mass properties of the E205 design are predicated on the achievement of reasonable technology improvements consistent with IOC dates in the 1990's, as discussed in the foregoing design description. The weight values were obtained by use of proven empirical equations that utilize rational parameters and coefficients calibrated to existing known systems. Where new concepts were encountered (such as the jet diffuser ejectors), more reliance on design studies and stress analysis was practiced. Power plant weights and scaling equations were obtained from the engine manufacturers.

The mass properties of the point design when configured for the DLI mission vertical takeoff are summarized in Table 6-1. A weight breakdown of the vehicles is given in Table 6-2, following MIL-STD-1374. Breakdowns by construction material are shown in Table 6-3.

Weight sensitivity derivatives were obtained for the principal driving parameters, which were found to be (1) fuel fraction, (2) free-air vertical-thrust-to-weight ratio required for VTO, (3) fixed weight of required items, and (4) thrust augmentation ratio for the ejectors. The sensitivity study was conducted by varying each of the above parameters by an arbitrary amount and observing the change in gross weight after iterating to maintain the other ratio values. For example, when an arbitrary dry-weight increment of 1000 pounds was added to the requirement, the result was a larger lift propulsion system to maintain vertical-thrust-to-weight (900 lb), a larger airframe to maintain constant density and propulsion subsystems (1073 lb), and more fuel to maintain fuel fraction (1327 lb) for a total increment of 4300 pounds. In the case of the weight derivative for varying fuel, the increment introduced was a percentage fuel rather than a fixed amount. Thus the result is roughly representative of a percentage change in SFC, L/D, or range. In the case of the derivative for varying free-air thrust-to-weight ratio, the incremental change was likewise introduced as a percentage so as to reflect gross-weight sensitivity to a change in suckdown or thrust loss in the presence of the ground. These and other sensitivity factors are presented in Table 6-4. The derivatives shown were obtained

TABLE 6-1 E205 MASS PROPERTIES SUMMARY

	WEIGHT (Pounds)	CENTER OF GRAVITY % MAC	F.S.	W.L.	INERTIA (SLUG - FT^2) ROLL	PITCH	YAW
Operating Weight Empty + DLI Payload	24,550	-11.9	287.65	98.45	24,459	63,051	84,326
Zero Fuel Weight + Fuel	25,466	-11.8	287.75	97.64	27,497	65,093	88,944
VTO Gross Weight	34,987	3.0	308.87	98.13	30,637	104,463	131,429

Table 6-2 E205 Weight Statement

SHORT GROUP WEIGHT STATEMENT DATE

	MODEL	E205				
1.	WING	3,482				
2.	~~ROTOR~~ CANARD	708				
3.	TAIL - VERTICAL	354				
4.	BODY	3,850				
5.	ALIGHTING GEAR	1,210				
6.	ENGINE SECTION	1,723				
7.	PROPULSION					
8.	ENGINE INSTALLATION	3,797				
9.	ACCESS. GR. BOXES & DRIVE	300				
10.	~~EXHAUST SYSTEM~~ EJECTORS	3,298				
11.	ENGINE ~~COOLING~~ NOZZLES	507				
12.	WATER INJECTION					
13.	ENGINE CONTROLS	50				
14.	STARTING SYSTEM	125				
15.	PROPELLER INSTAL					
16.	SMOKE ABATEMENT					
17.	LUBRICATION SYSTEM					
18.	FUEL SYSTEM	468				
19.	DRIVE SYSTEM					
20.	JET DRIVE					
21.	FLIGHT CONTROLS	880				
22.	AUX POWER PLANT					
23.	INSTRUMENTS	136				
24.	HYDRAULICS & PNEUMATICS	306				
25.	ELECTRICAL	391				
26.	AVIONICS	1,057				
27.	ARMAMENT	235				
28.	FURNISHINGS & EQUIPMENT	290				
29.	AIR CONDITIONING	230				
30.	ANTI-ICING					
31.	PHOTOGRAPHIC					
32.	LOAD & HANDLING	5				
33.	MANUFACTURING VARIATION					
34.	WEIGHT EMPTY	23,402				
35.	CREW (NO. 1)	180				
36.	PASSENGERS (NO.)					
37.	FUEL-UNUSABLE	99				
38.	FUEL-INTERNAL	9,521				
39.	FUEL-EXTERNAL					
40.	OIL	58				
41.	FUEL TANKS. AUX					
42.	BAGGAGE					
43.	CARGO. TROOPS					
44.	GUNS	286				
45.	AMMUNITION	500				
46.	EQUIPMENT (O_2, SURVIVAL KITS)	71				
47.	WEAPONS INSTALLATION	224				
48.	BOMBS					
49.	ROCKETS, MISSILES					
50.	(2) LCLM	160				
51.	(2) AMRAAM	486				
52.						
53.	PHOTOGRAPHIC					
54.	MISCELLANEOUS					
55.	USEFUL LOAD	11,585				
56.	GROSS WEIGHT	34,987				

Table 6-3 E205 Materials Breakdown

COMPONENT	G/E	ALUM	Ti	STEEL	OTHER	TOTAL	CONSTRUCTION TYPE
WING	536	411	1911	540	84	3482	I Ti MULTI-SPAR PLATE O G/E MULTI-SPAR PLATE
HORIZONTAL TAIL	-	-	-	-	-	-	-
VERTICAL TAIL	177	75	2	38	62	354	G/E ADH. BONDED FULL DEPTH CORE
CANARD	241	113	181	64	109	708	G/E ADH. BONDED FULL DEPTH CORE
FUSELAGE	974	1112	470	646	648	3850	FWD G/E PLATE FRAME AFT Ti/STL PLATE FRAME
LANDING GEAR	-	454	1	168	587	1210*	-
AIR INDUCTION	161	144	13	29	10	357	PLATE FRAME
ENGINE NACELLE	406	416	179	337	28	1366	FWD G/E PLATE FRAME AFT Ti/STL PLATE FRAME
EJECTOR SYSTEM	-	828	445	1817	208	3298	RENE' 41 DUCTS Al/Ti DOORS
TOTAL STRUCT.	2495	3553	3202	3639	1736	14625	
TOTAL STRUCT. (W/O LG)	2495	3099	3201	3471	1149	13415	
% (INCL LG)	17.1	24.3	21.9	24.8	11.9		
% (W/O LG)	18.6	23.1	23.9	25.8	8.6		

* INCLUDES LANDING GEAR ROLLING STOCK @ 427 LB.

TABLE 6-4
E205 WEIGHT SENSITIVITY DERIVATIVES

	E204
1. IF FUEL REQUIRED IS INCREASED 5%, VTOGW INCREASES	7.0%
2. IF DRY WEIGHT OR PAYLOAD REQUIRED INCREASES 1000 lb, VTOGW INCREASES	4300 lb
3. IF FREE AIR MAX A/B (S.L.S. UNINSTALLED) THRUST/WEIGHT REQUIRED INCREASES 10%, VTOGW INCREASES	15.7%
4. IF ENGINE THRUST/WEIGHT IMPROVES 10%, VTOGW DECREASES	4.5%
5. IF THRUST AUGMENTATION RATIO DECREASES BY 0.1, VTOGW INCREASES	+1995 lb

at the design points and are not constant throughout the range of appropriate values of the parameters.

6.2 Structural Design

The scope of this study does not allow detail structural analysis for the purpose of determining member sizes or exact selection of optimum structural concepts and material mixes.

The basic analyses techniques that were used in the structures material, and weights area are statistically based on some 50 in-service aircraft. These basic techniques are modified by factors (e.g., strength-density, E-density, etc.) and calibrated and compared to advanced material flight, test and study data (e.g., F-16 G/E empennage, F-16 G/E forward fuselage design, fabrication, and test data and data from other advanced material studies from throughout the aerospace industry).

This type of analysis, although proven accurate in many previous studies from an overall weight and parametric cost analysis standpoint, does not precisely define optimum structural concepts or optimum material mixes, even though the overall component (wing, tails, etc.) weight effects of basic material selection are included.

Since exact definition of detailed structural data has been precluded by the nature and scope of this study, structural concept selection and material usage data has been projected by design analogy from past hardware, test, and design studies.

The tentative selection of structural concept and percent material usage for each major structural component are shown in Table 6-3.

In the case of the wing outer panel (outboard of the engine nacelle), a graphite-epoxy multi-spar-plate structural concept has been selected. This selection is based on geometry and load similarities to a series of F-16 designs and other studies.

In the case of the canard and vertical tail, a graphite-epoxy, adhesive-bonded full-depth-core design has been selected. This concept has been selected based on F-16 and other design experience as being in the most efficient concept compatible with aerodynamic surfaces that are in general influenced to a large degree by aeroelastic considerations.

For the fuselage and inboard wing forward of the engine exhaust nozzle area a combination of graphite-epoxy, aluminum, and titanium-plate frame construction has been selected. The fuselage forward of the ejector cutouts will be graphite-epoxy-plate frame construction similar to F-16 forward fuselage test component. In the mid-fuselage/inboard-wing area, ejector cutouts (structural complexity) and engine cross-bleed ducts (environment) will dictate a mixture of largely titanium and aluminum with some limited applications of graphite-epoxy (e.g., specific bulkhead and longeron cap strips where environment permitted, etc.).

In the fuselage aft of the engine exhaust nozzle area, preliminary estimates have indicated in flight plume temperatures in the 300°F range and ground-run-up plume radiation temperatues in the 500°F range, thereby dictating, at least for the outer fuselage-skin panels, titanium or parasitic heat-shield-type structure. The internal structure will be a mixture of aluminum and titanium with a very limited (if any) application of graphite-epoxy.

The forward portion of the engine nacelle structure will be typical graphite-epoxy plate frame structure with some titanium and aluminum used at local load introduction points (e.g., canard pivot shaft).

The aft (hot) portion of the engine nacelles will be typical steel-titanium high-temperature structure.

The landing gear will be a typical mixture of aluminum, steel, and titanium with graphite brakes.

For the ejector nozzles and duct system the operating environment (estimated to be in the 1500°F range), part complexity, and dimensional control requirements are similar in nature to jet engines operating in the 1200° to 1800°F range.

Rene' 41 is nickel-based high-temperature alloy currently used in high-temperature (1200°F to 1800°F) turbine and afterburner parts. It has been used for the purpose of preliminary analysis.

The results of this preliminary analysis indicate distribution-ducts wall thickness in the minimum gage range (assumed to be .040). The distribution ducts represent a significant portion of the overall ejector weight and durability (service life)may dictate significant increases in duct wall thickness.

It should be noted that the weight (3298 lb) for the ejector ducts and nozzle system represents a significant weight penalty (approximately 9.5% of the takeoff gross weight) and represents one of the more significant structural technology risks associated with this overall concept.

6.3 Flight Control System

6.3.1 Conceptual Design

The Flight Control System for the VSTOL fighter aircraft will be divided into longitudinal and lateral-directional modes, although it is likely that in conventional flight some of the pitch elements will be required for the lateral and directional modes at larger angles of attack. The flight modes that require separate types of controller will be the V mode and the conventional flight. The STOL mode will blend the controllers of the two modes.

Longitudinal. In conventional flight the FCS will have the canard as its primary control element. Because the airframe with canard fixed at zero is too unstable, this canard will be scheduled as a function of Mach number and angle of attack to achieve the desired level of static longitudinal stability. The frequency and damping of the system will be obtained with pitch rate, angle of attack, and normal acceleration appropriately compensated and fedback. A schematic of this approach is shown in Figure 6-1.

For the V mode, the control elements are the VEO-Wing flaps and pitch reaction control system. These elements will be used to control the pitch trim, maneuvering, and disturbances through appropriately compensated networks of the feedback elements.

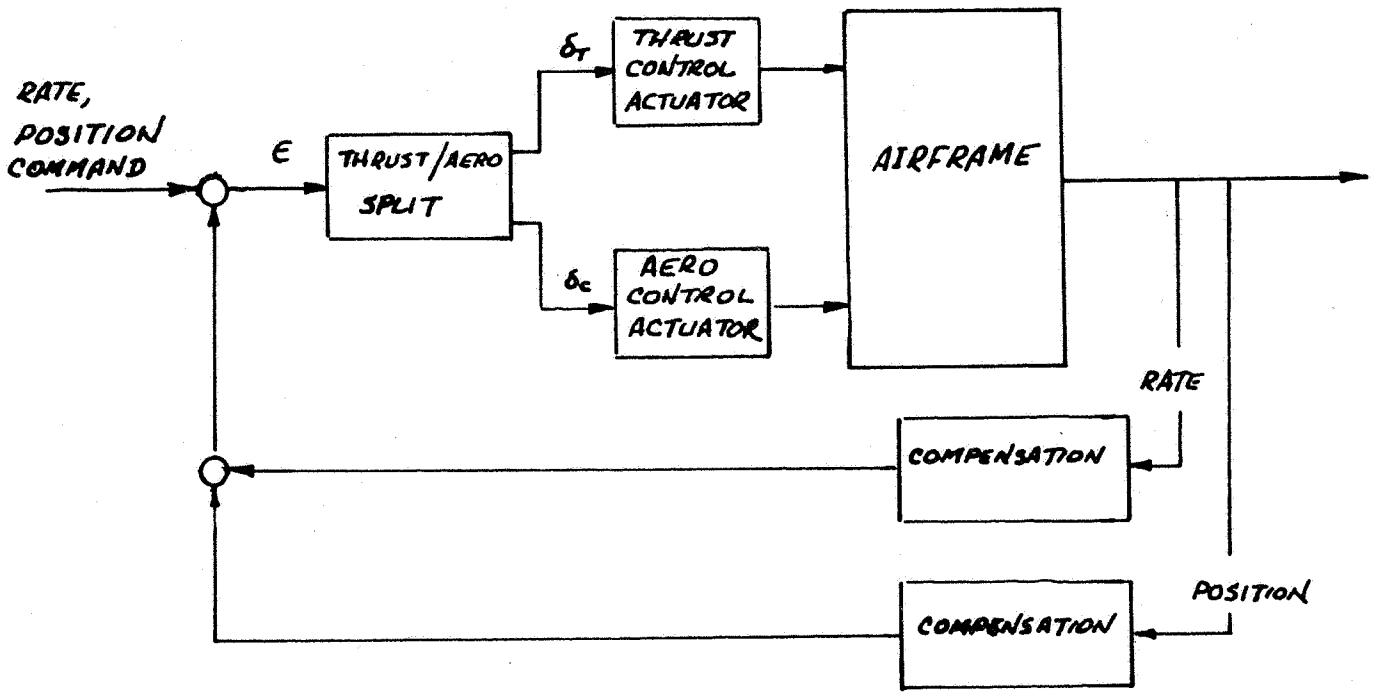

Figure 6-1 Functional Longitudinal Control Schematic

The STOL mode will be a blend of both control elements, with the reaction control being phased out with dynamic pressure while the canard is being phased in. This blending will occur during transition.

Lateral. In conventional flight the lateral control elements are the ailerons. Damping in roll maneuvers will be augmented with these elements. The VEO-Wing augmented lift makes these control elements very powerful in roll.

For operation in the V mode, the lateral control power is supplied by air bled from the engine and fed to a wing-tip-located reaction control system. This system is used at low dynamic pressures and will be phased out as the speed increases and the aileron becomes effective.

Damping in roll will be effected by appropriately compensated networks throughout all flight phases.

Directional. During conventional flight, an all-movable vertical tail provides the basic stability and control. The airplane is directionally statically stable, so the control element will be used as a damper and to adjust the frequency, when required, by feeding back yaw rate.

For V and STOL operations, the same networks will be used in conjunction with the ejector (or RALS) elements to provide the necessary damping and augmented frequency for satisfactory flying qualities.

6.3.2 Physical Design

Flight Control. The flight control system is a full fly-by-light (fiber optics) flight control system. Advanced electronic mechanization (digital, three channel) and control will be used to eliminate conventional mechanical linkages and control cables in all axes. The system is similar in concept to the F-16 fly-by-wire flight control system. Fiber-optics eliminates the possible electro-magnetic problems that can be experienced with wire systems; also, higher data rates are possible.

Alternative Flight Control. A higher-risk system exists similar to that described above except that no hydraulics will be used.

A high-voltage DC (HVDC) system will be used to perform flight control functions. The all-electric concept (power by wire) is an attractive alternative for this aircraft. Increased reliability (no hydraulic leakage, problems, etc.), lower life cycle costs, and the elimination of backup pneumatic emergency systems (redundant DC systems replace the emergency systems) are considerations that favor this approach. The HVDC system will also be used to provide a partial backup flight-control actuation system (a less-capable get-home type only). Samarium-cobalt DC actuators will be incorporated in the design. The selected gun requires electric power (gas operated), which also supports the no-hydraulic approach. There is concern that the actuators, motors, and other wing devices of a 270-V-DC system may not be developed for the 1990 time frame.

6.4 Crew Station and Excape System

An E205 aircraft cockpit configuration has been developed to provide an efficient one-man cockpit that is responsive to the functional and operational requirements of this type of air vehicle. Cockpit geometry and sizing have been established to accommodate the 3rd through 98th percentiles of the Navy pilot population (NAED ACEL 533). The "design eye" location and the seat geometry were selected to provide the pilot with maximum external visibility consistent with the aerodynamic lines, increased g-tolerance/comfort, and mobility during all flight modes.

Cockpit CRT-type displays/instruments and fly-by-fiber-optics (FBFO) primary and secondary controls are located and arranged for maximum efficiency and visual/tactile access during all normal and emergency flight modes and restraint conditions. All manually operated controls are located on either the right or left side of the cockpit, leaving the center area unobstructed for maximum display utilization. Adequate clearances permit rapid normal or emergency ingress/egress or safe escape throughout the subsonic flight envelope. The wide-angle head-up display (HUD) provides the primary display of flight control, nagivation, weapon delivery, energy management, and selected threat-situation information. Other CRT-type displays are located on each side of and below the HUD to provide the necessary radar/E-O sensor, mission data, aircraft subsystems status, and warning/caution/advisory displays. Solid-state FBFO primary controls are extremely responsive (higher data rates than MUX bus) and are essentially immune to the effects of

external high-energy pulses. Primary controls and high-priority manual functions are located for access within Zone 1 reach limits and leg lengths of the specified pilot population.

The cockpit is enclosed by a one-piece, clamshell, aft-hinged windshield/canopy (consisting of a polycarbonate transparency attached to a peripheral frame structure) that seals against fuselage longeron sills and by an aft bow-frame located just aft of the escape clearance envelope. The transparency will provide the desired resistance to bird strikes during subsonic operations. The windshield/canopy is easily jettisoned by the pilot or ground rescue personnel. Pyrotechnically initiated thrusters react against the forward portion of the canopy frame, rotating it up and aft until it unlocks from the aft hinges and is carried aft to provide clearance for emergency escape. The HUD combiner plane and the hard-panel glare shield provide adequate wind-blast protection during deck/ground-handling/taxi modes and during emergency flight operations after inadvertant canopy loss. The hard-panel glare shield may be easily unfastened and removed for easy access to the forward side of the instrument panel, etc.

A lightweight, rail-mounted, rocket ejection seat is installed at a 15-degree seat-back angle (SBA).

The escape system consists of the rocket ejection seat, jettisoned windshield/canopy, and an initiation and sequencing system. Normal escape system operation is initiated by the pilot pulling the "D-ring" on the seat and ejecting prior to water entry. Underwater escape (when canopy has not been jettisoned prior to water entry) is accomplished by manually cranking the canopy open after the internal/external pressures are equalized. A water-pressure sensor automatically activates a mild-detonating-cord (MDC), aft (fixed) canopy-fracturing system, which will admit water rapidly to equalize the pressures and permit the canopy to be quickly opened for underwater escape.

6.5 Subsystems

6.5.1 Avionics Subsystem

The avionics subsystem will be a lightweight integrated system configured primarily for intercept from combat air patrol and deck-launched intercept, staged from an air-capable ship. It will also provide targeting for a surface-launched air-targeted (SLAT) missile and be capable of air-to-surface attack. The functional capability of the avionics is essentially the same as that of the F-16, providing weapon control, navigation, communications, identification, electronic warfare, and subsystems monitoring and control. Weight and volume data projected to an IOC in 1995, shown in Table 6-5, are derived from the F-18 equipment by use of prediction techniques described in Reference 5 to project weights and volumes. This weight projection is shown in Figure 6-2 along with similar projections for F-14, E-2C, and S-3A type avionics suites. The predictions assume that the capabilities will remain the same. This assumption is contrary to tradition. In general, avionics weight has remained a percentage of aircraft total weight; greater functional density has simply allowed more capability to be incorporated at the same weight for a given airplane type. However, the challenge of the VSTOL requirements to minimize weight and improve operational availability in a limited basing environment demands that functional improvements be limited in favor of weight reduction. A great deal of mission flexibility, dynamic reconfiguration, and crew efficiency is realizable because the components that allow the flexibility in mode control, information handling, and data processing are shrinking so phenomenally in size that a great deal of processing hardware can become insignificant in overall weight (illustrated in Figure 6-3).

System flexibility will accommodate new weapons and requirements. Redundancy and multi-path mode configuration will enhance mission availability. Modular packaging with multiple standard modules at system, subsystem, and sensor levels will make it feasible to maintain the hardware with the minimal number of spares and logistics support that can be afforded on the variety of air-capable ships being considered for VSTOL airplanes. Maintenance at operational level will consist of replacement of weapon replaceable assemblies, fault-isolated by built-in test.

Table 6-5 Avionics Predictions for V/STOL B Projected to 1995

HARDWARE	CURRENT CAPABILITY		1995 PROJECTIONS		
	Wt (lb)	Vol (ft^3)		Wt (lb)	Vol (ft^3)
CNI					
UHF	18	.30			
SECURE VOICE	10	.12			
IFF (W/Coder)	18	.27	TIES		
DATA LINK	17	.15	JTIDS	90.0	1.5
TACAN	32	.61	GPS		
RADAR ALT	8	.10			
ADF	7	.30			
HEADING REF	3				
AIDS					
HUD	50	.98			
MFD	30	.74			
MMD	30	.60	IMPROVED		
ICS	18	----	AIDS	140.0	2.2
FUNCT GEN	28	.97			
HSI	14	.21			
ARMAMENT CONTROL	30	.75			
CARRIER LANDING	27	.33	NAVTOLAND	25.0	0.4
SENSORS					
RADAR	330	5.00	MODULAR RADAR	270.0	4.4
INERTIAL	38	.63	IISA	30.0	0.5
ECM					
ASPJ (Prov)	(190)	2.40		(150.0)	2.2
ALR	110	1.40	IEWS	145.0	2.3
DISPENSERS	35	.78			
BLANKER	7				
DATA PROCESSING	50	1.20	DISTRIBUTED	40.0	0.5
TOTAL	910	17.84		740.0	14.0

Initial Weight from Table	910	
Susceptible to Change (36%)	328	
Unsusceptible	582	lb
Projected 1990 IOC Weight of Susceptible Avionics	158	
Total	740	lb

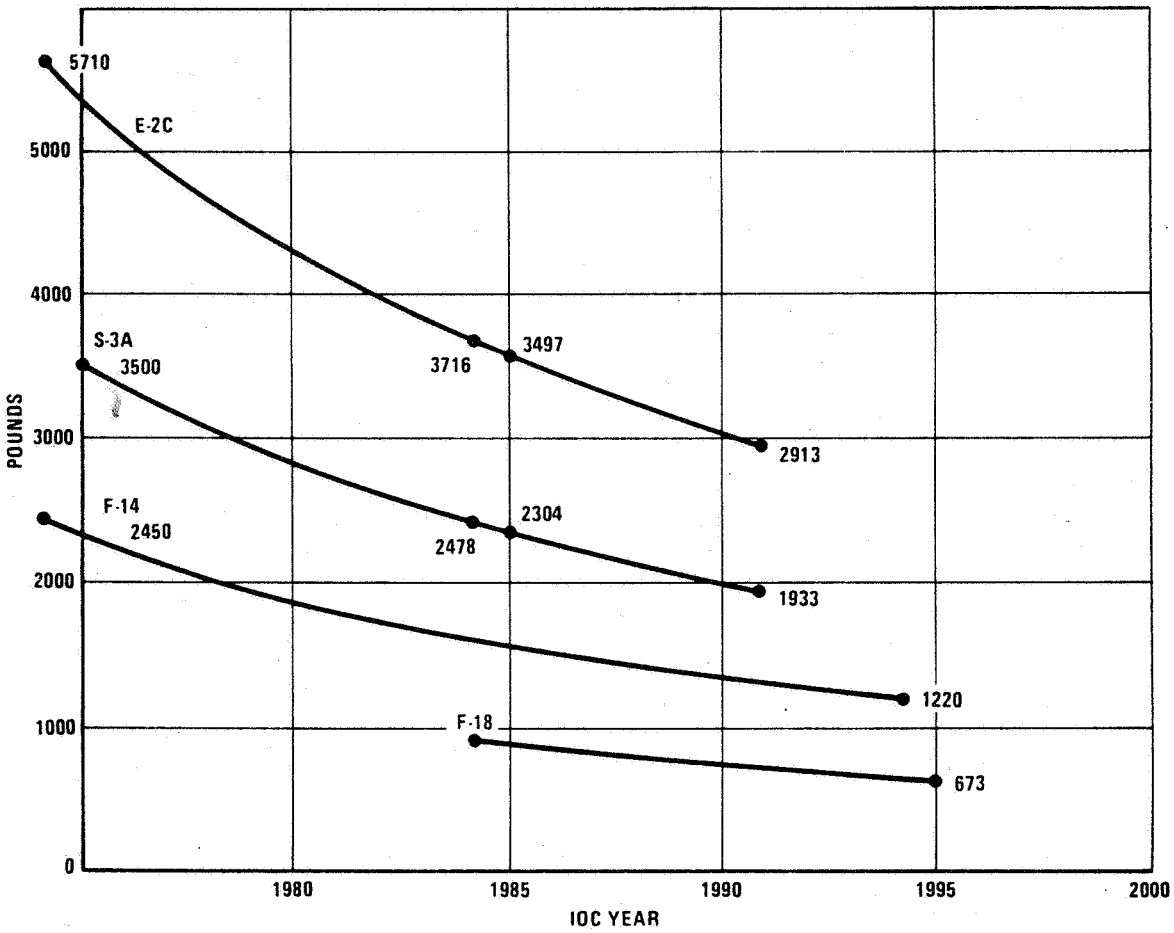

6-2 Avionic Weights Forecast

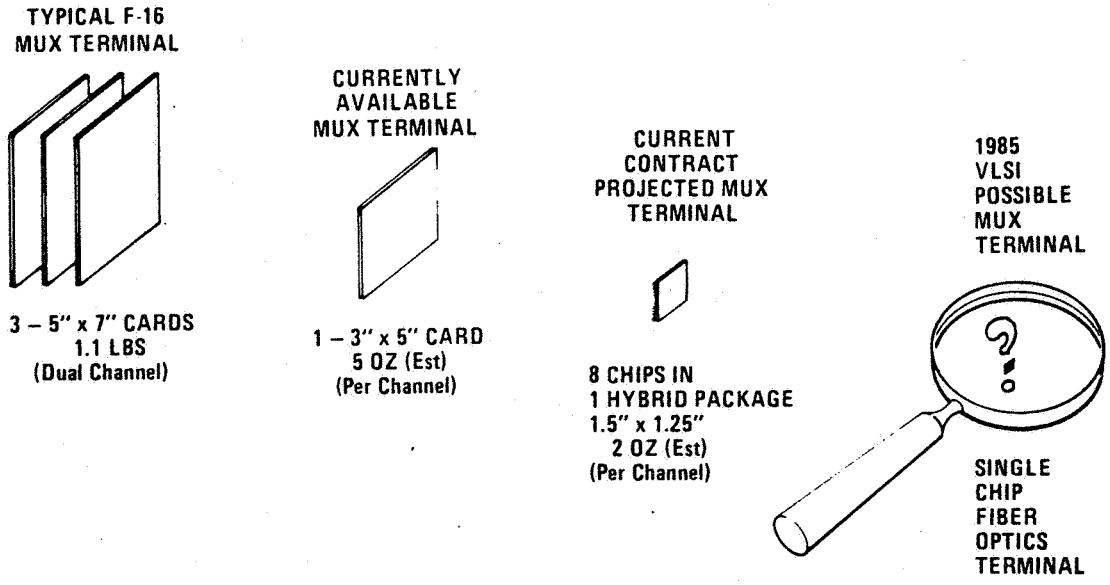

Figure 6-3 Digital Hardware Weight Reduction

The system will accommodate close-air combat weapons (SRAAMMs and gun), medium-range weapons (AMRAAMs and ATAAMs), and longer-range weapons (AIAAMs) as well as the complement of air-to-surface weapons.

The pilot will have clear visibility of combat status and efficient control of target acquisition, weapon selection, aiming delivery, and breakaway.

6.5.1.1 Architecture

The avionics subsystem will be integrated with the other aircraft subsystems as shown in Figure 6-4. Operational flight programs, communicating over MIL-STD multiplex buses, implement the integration, An advanced all-digital system architecture with standard microcomputer modules and tiers of multiplex buses at the airplane, system, and subsystem levels is shown in Figure 6-5. This architecture, being developed at General Dynamics' Fort Worth Division features, distributed microprocessors, solid-state memory, high-density mass memory, large-scale integrated (LSI) multiplex interface terminals, and fiber-optics multiplex buses.

Integration. Operational flight programs coordinate sensor and equipment data transfers over the data buses and schedule processing activities to implement the modes selected by the pilot. Processing instructions will be in Navy-developed high-order language. Use of such a high-order language (HOL) facilitates modular design and testing. Each functional requirement is mapped into one or more components for implementation through top-down structured programming methodology, resulting in a linear, modular program with readily identifiable hierarchical levels and single-entry and -exit points for each module.

Multiplexing. The system and subsystem elements communicate with each other over a high-data-rate, serial digital multiplex data bus, which provides flexibility and enhances fault tolerance by simplified, redundant paths and regulated error rates. The interface characteristics will be compatible with the MIL-STD requirements (Now MIL-STD 1553).

The multiplex bus will have dual signal-path redundancy and dual controllers. Each element can be commanded to transmit and receive data over either of two fiber-optics transmission lines of the bus.

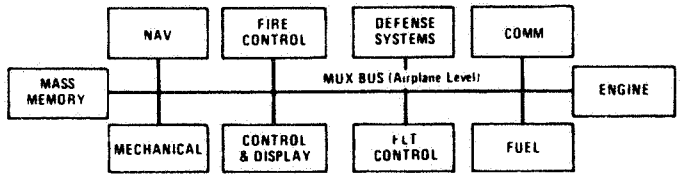

6-4 Subsystem Integration.

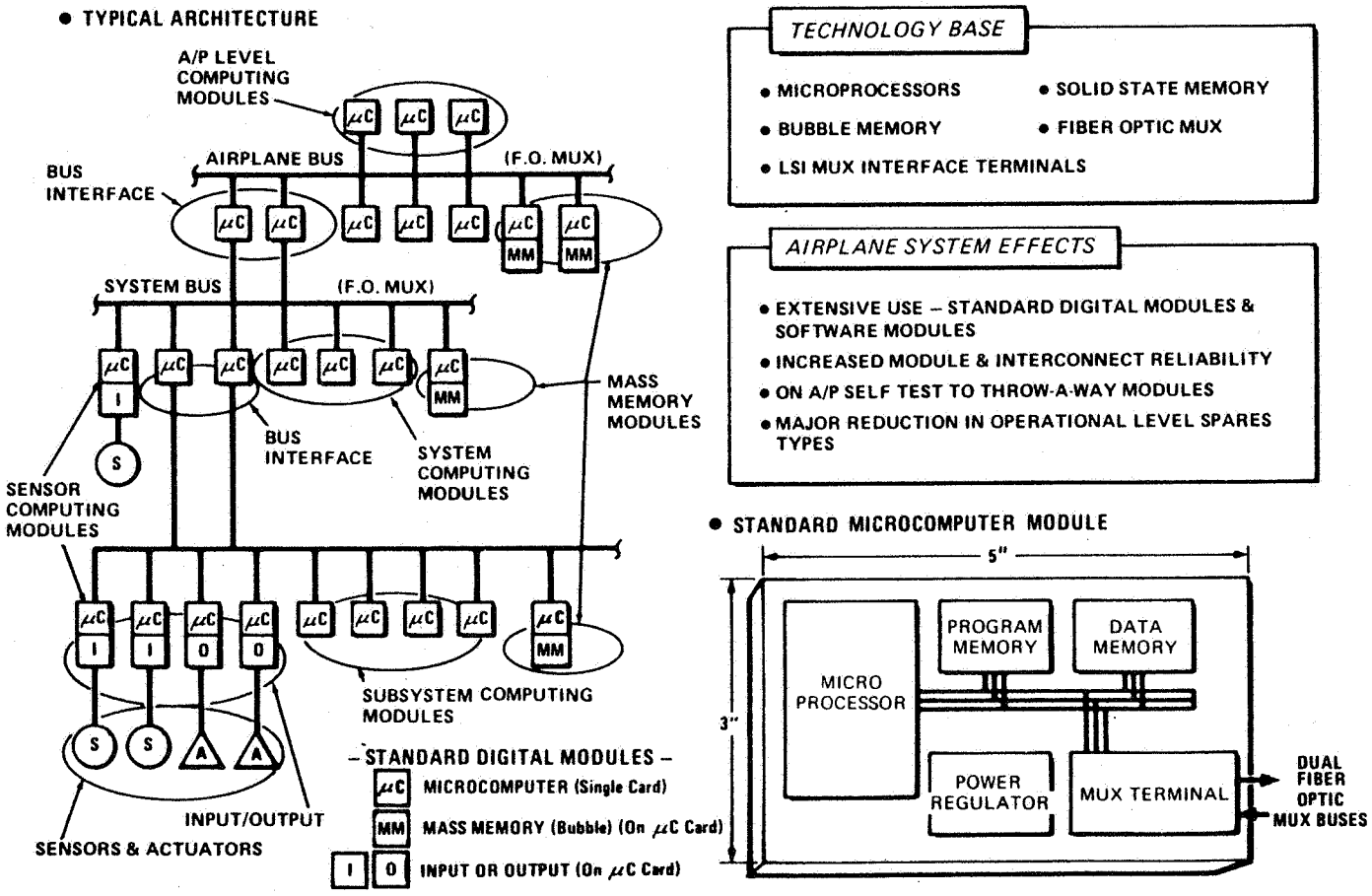

Figure 6-5 Advanced Digital System Architecture

System Test. Self-test and built-in-test functions will be mechanized to support both in-flight fault detection and system reconfiguration and ground-maintenance fault isolation to a weapon replaceable assembly (WRA). Self tests are characterized as automatic non-interfering performance testing in which either continuous or iterative monitoring techniques may be applied. Built-in tests interrupt normal operation and may require participation of maintenance personnel or the pilot for operation or interpretation of the test.

Test capability will be integrated into the computer programs. Fault information will be transferred over the buses and the processors, reprogrammed accordingly for corrective action and reconfiguration to allow mission completion at the highest level of capability available.

6.5.1.2 Functional Descriptions

The functions provided in the VSTOL fighter are equivalent to those of the F-18, projected to the 1995 IOC and accommodating the weapon, threats, and basing of that time period. They will include the following:

- Fire Control

  Radar sensing (target detection, ranging, angle measurement, and tracking)

  Inertial velocity, acceleration, position, and attitude measurement

  Head-up display of air combat and weapon delivery cues

  Display of mode, weapon, and sensor information

  Display of horizontal situation information -

    Navigation and target data in fighter version

    Moving map display and targets in attack version

  Sensor data processing and control

  Weapon firing and release computations

Air targeting computation for SLAT missile

Laser spot illumination and tracking

Integrated control of weapons, modes, and sensors

Interface with armament management

Software programs to implement fire control

o Navigation

Inertial velocity, acceleration, and attitude measurement (with provision for alignment and position updating)

Radio navigation (TACAN, ADF, ILS, Global Positioning)

Radar altitude and velocity measurement

Landing aid (ILS, ACLS, NAVTOLAND)

Precision course direction and steering

Backup heading and attitude reference

Integrated control of modes, sensor, and data sources

Navigational data processing and control

Navigational, steering, and alignment calculations

Position updating

Display of position, heading, and steering information

Display of moving map (attack missions)

Software programs to implement navigation and steering

- Communications

  Voice communications and relay (secure and clear)

  Data communications

  Landing aid communications

  Intercommunications and audio control

  Beacon communications for landing augmentation and precision ground control

  Integration of tactical information exchange (TIES)

- Identification

  Self identification (secure and non-secure) and reporting of status, position, speed, etc.

- Electronic Warfare

  Passive threat warning

  Threat data analysis and evaluation

  Internal active ECM control and transmission

  Passive ECM dispensing

  Interference blanking

  Integrated control of EW and ESM

  Software programs to implement threat analysis and evaluation

- Monitoring and Control

  Flight attitude, air data, altitude, velocity, and acceleration sensing and display

  Energy-management assessment and display

  Engine and engine control parameter sensing and display

Fuel-status and flow-sensing display

Weapon status, readiness, and mode control

System status monitoring, test, and reconfiguration control.

6.5.1.3 Packaging

Modular avionics packaging techniques will be used in the VSTOL fighter. Present concepts visualize equipment racks that are integral parts of the aircraft structure. Electrical connections will be kept to a minimum. Avioptics (fiber optics) techniques will be used where feasible and at as low a hierarchial level as possible (to avoid wires and connectors). A maximum of commonality in module types is a design goal to support standardization and multiple usage. This will result in greater operational availablity and lower cost (both initially and in total system life cost). Module cost will be held consistent with either throw-away or return-to-depot-for-repair costs. In either case, there will be no repair at operational level. Spares requirements will also be minimized, and the feasibility of making at least some critical modules available to the crew for replacement in flight will be investigated.

Some sensors may even be modularized. A solid-state modular radar may replace the present centralized transmitter/receiver and planar-array antenna now on the F-18. The radar would consist of low-power modules containing an antenna element, RF transmission, RF reception and conversion to IF signals. The IF signals would then be combined, detected, and converted to digital data. A high-speed digital signal data processor (such as fast Fourier transforms (FFT) and recursive doppler filters) would collect the digital data and process it for distribution on the multiplex buses. An integrated inertial sensor using a ring laser gyro can be a strapdown system, which lends itself to integrated airframe structural packaging.

A concept for packaging is shown in Figure 6-6. Electrical connection will be made to distribution buses, an integral part of the rack. Solid-state logic circuitry will control module power. Multiplexed signal input/output will be via fiber optics or wired mux terminal.

6.5.1.4 Environmental Control

Innovative concepts are needed for the avionics equipment environment control. Much of the weight now required in electronics packaging is due to the requirement to dissipate heat generated in the equipment and to protect it from vibration, dust, electromagnetic effects, humidity, etc. It would be highly desirable to utilize aircraft structure to act as housing, shield, heat control, and conduit for conductors and optical transmission paths. Technology studies are scheduled to develop lightweight environmental control systems. This technology development will be monitored and utilized. Also, the proper integration of the avionic packages and the airframe should minimize cooling requirements. Shielding problems associated with the operation of avionics in a composite structure environment are being studied extensively at General Dynamics in a contracted R&D program associated with the F-16. The program is scheduled to culminate in shielding and lightning protection specification requirements, validated by analysis and test.

Present concepts visualize that the avionics equipment racks will incorporate cooling and electrical services as an integral part of the rack. Each module will probably be shielded on its own and heat conduction provided to the rack integral heat sink. Either individual modules or the rack compartments will be sealed from the airplane ambient environment.

6.5.2 Vehicle Equipment and Power

Engine Installation. The engines are located in pods outboard of the ejector bays and are installed and removed axially from the rear on an integral rail. The nacelle also houses the main landing gear. The MLG wheel well is located in the lower aft portion of the nacelle but is isolated from the engine and from engine hot components. Nacelle features include:

1. An air-induction system consisting of a simple axisymmetric inlet duct with aerodynamically operated blow-in doors to ensure adequate air intake flow for takeoff, landing, and low-speed flight.

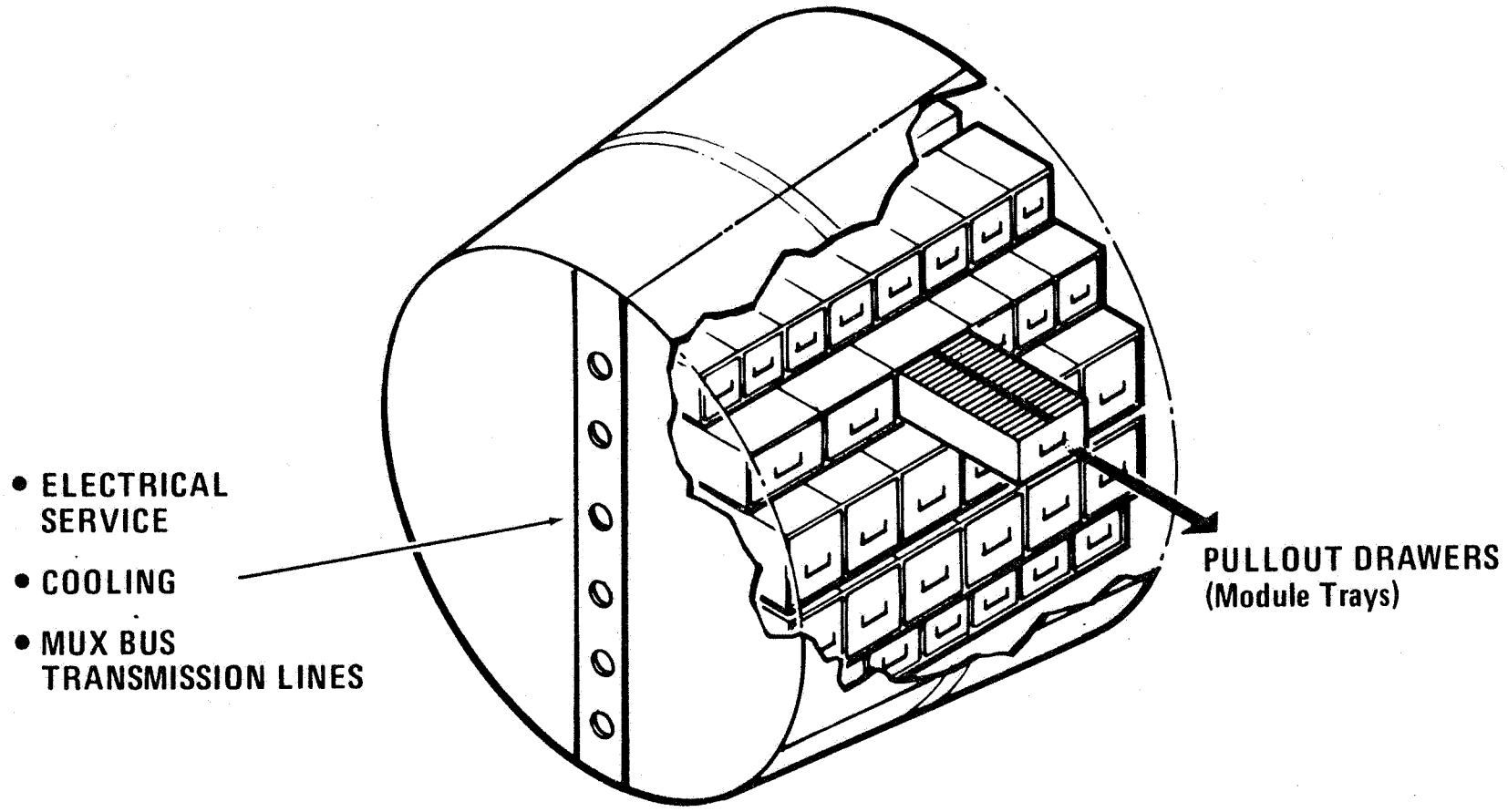

Figure 6-6 Avionics Packaging Concept

2. An anti-icing system with the inlet lips and blow-in-door lips heated with hot air from the ECS. The engine nose dome and inlet guide vanes are heated with engine bleed air. A vibrating-probe-type ice detector will be installed in one engine inlet to alert the pilot to icing conditions and to automatically activate the engine and inlet de-icing air flow, if so commanded.

3. Fire-protection provisions, including the time-tested fire-protection provisions of isolation (by vapor-tight firewall), ventilation (unidirectional - by fan bleed and RAM air), fire and over-heat detection (dual, continuous-loop, solid-state thermal detectors and radiation detectors), fire extinguishing (by use of Halon extinguishing agents), compartmented accessories and over-board drains (for fluid leakage), insulation (of hot bleed ducts to reduce ignition sources), and a precooler (for ECS air to reduce temperature prior to distribution to the ECS).

The engine is a conventional augmented turbufan that incorporates hot-gas diversion-duct outlets (for ejectors), a nozzle dam (to block off the nozzle flow when ejectors are operating), hot-gas valves (to control diversion flows), an augmentor (not used when the ejector and the reaction control system are operating), and a 2-dimensional convergent-divergent exhaust nozzle (which operates in conjunction with the wing flap to provide vectored thrust for pitch control during transition, STOL, and conventional flight).

To reduce life cycle costs and to facilitate remote operations, checkout and maintenance power will be obtained from a 1990-technology-level JP-air auxiliary power unit (APU). The APU will provide electrical power for starting the engines. Either a pneumatic (pressurized air start system - PASS) or a liquid-oxygen JP APU start system will be incorporated. Either approach will save weight relative to the conventional hydraulic accumulator approach; also, either will facilitate cold-weather starting as contrasted with battery systems.

Emergency power (hydraulic and electrical) will be obtained from the APU by use of an added oxygen JP combustor. Oxygen will be obtained from a breathing stripper system. The Emergency Power System will protect against a maneuver-caused two-engine deep-stall condition and/or accessory gearbox shaft failure or damage and will provide adequate time for crew escape if required. Also, this aircraft is powered by turbofan engines, which have poor windmilling characteristics, has a fiber-optics/hydraulic-type flight control system, and incorporates negative static margin in its design; both the latter require non-interrupted secondary power.

The above technical facts and the cost of the aircraft dictate that steps should be taken to reduce peace-time attrition and combat losses. Long-duration emergency power is required to permit aircraft recovery in the event of a dual AMADS damage.

A solid-propellent augmented ram-air turbine will be considered as an alternate emergency power system. This system utilizes a solid-propellant gas generator to provide rapid start-up of a ram-air turbine (RAT) and to assure sufficient power during marginal RAT aerodynamic conditions.

Electrical engine starting will be used. HVDC power from the APU will drive either the HVDC generator on each engine or a motor to provide the necessary N_2 rotation for start-up. HVDC ground cart power or cross-ship power (from the opposite operating engine) are alternate starting power sources. The alternative power-by-wire electrical system does not require AMADS. The generator is mounted directly on the engine with lubrication shared with the engine.

Secondary-Power Generation. In-flight electrical and hydraulic power will be obtained from a generator and pumps driven by a low-cost, remote airframe-mounted, accessory-drive (gearbox) system (AMADS). The main engines provide the shaft power for the gearboxes. Lightweight, fatigue-resistant, composite (graphite, etc.) gearbox housings, and possibly some composite gearing will be incorporated into the design. High-pressure bleed air for the ECS will be obtained in a conventional manner from the main engines.

Electrical. The electrical system will consist of a variable-speed constant-frequency (VSCF) generating system for the 400-Hz AC system and a high-voltage DC system (270 V). A reliable multiplex-type distribution system will be incorporated in the aircraft. It is assumed that by 1990 the VSCF system will be developed to the point where its reliability, weight, and cost will far surpass that of a constant speed drive (CSD)/generator system.

The high-voltage DC system will perform the non-flight-control functions presently performed by a utility hydraulic system. Increased reliability (no hydraulic-leakage, etc., problems) and elimination of backup pneumatic emergency systems (redundant DC systems replace emergency systems) are considerations that favor this approach. The high-voltage DC system will also be used to provide a partial backup flight-control-actuation system. Samarium-cobalt DC actuators and servo valves will be incorporated into the design. These high-strength magnetic actuators potentially can serve as the electro-hydraulic interface, thus eliminating the primary stage of the typical two-stage servo valves, or function directly as the electro-mechanical interface. Batteries will only be used to assure uninterrupted power to the fly-by-fiber-optics system.

Hydraulic. Two 4000-psi hydraulic systems dedicated to flight control are incorporated in the design. If higher-pressure hardware is developed by 1990, the obvious volume and weight reductions would be incorporated. However, it is felt at this time that the 4000-psi level is probably the best cost and technical blend for the projected aircraft. Also, it is assumed that a new non-flammable hydraulic fluid with acceptable cold-weather characteristics will be developed by 1990 and be available foruse with this aircraft. Pumps, valves, actuators, and other hardware components are typical of totay's units. Centrifugal, gear, etc., pumps, if developed into efficient units by the mid-90's, could be incorporated into the design. Reservoir-level sensing and/or fusing will be used to the level needed so detailed analysis shows significant survivability payoffs.

Environmental Control System. A conventional bootstrap air-cycle environmental control system will be used. The turbo-compressor will feature variable area, dual entry, and any other appropriate performance features that will be available in the time frame of this aircraft. Air recirculation, fuel heat transfer, and high-pressure water separation are probable system features. A programmable electronic control with diagnostic capability will be incorporated into the system design to increase capability, reduce life cycle cost, and improve reliability.

Oxygen Generation. An oxygen breathing system will be incorporated that will be a stripper-type (molecular sieve, etc.) or a chemical-type system. Oxygen will thus be obtained from ram air and stored in a high-pressure gaseous state. Logistic problems associated with replenishment, especially at dispersed bases, are reduced significantly.

Fuel System. Fuselage fuel tanks of bladder construction are located forward (aft of the crew compartment), center (between the engines, aft of gun), and aft (in the fuselage tail). Wing tanks of integral construction are located in each wing. Ample insulation will be provided on the side of the aft tank to protect against A/B radiation.

An open-vent system with ram-air pressurization will be used. Motive-flow fuel transfer and conventional capacitance-type fuel gaging will be utilized. A dry-bay fire extinguishing system utilizing a Halon fire-extinguishing agent will be used to ensure fire safety in the areas surrounding each fuel tank. All components will be of the latest-proven designs which are available in the aircraft time frame. JP5 fuel or equivalent will be used.

Fire Protection. The multiple combustors and the proximity of the fuel tanks makes an overall fire protection policy for the entire aircraft a necessity. In general, time-tested nacelle fire-protection features will be employed throughout the aircraft. Particular features are as follows:

1. Isolation of hot-gas ducting by separating it from aircraft structure by vapor-tight firewalls.

2. Isolation of fuel tanks located in the insulated bays.

3. Insulation of all hot surfaces with inert non-wicking material.

4. Ventilation of all areas containing flammable fluids with ram and fan air to prevent the accummulation of flammable concentration of vapors.

5. Detection of any hazardous conditions by means of heat-sensing or radiation-sensing detectors (as appropriate) in all critical areas.

6. Extinguishing of any fire by means of an aircraft fire-extinguishing system (using Halon agent as noted above).

7. Separation (to the maximum extent practical) of components and plumbing so that no flammable fluid shall be routed in the same compartment as a primary ignition source (hot-gas duct, engine, etc.).

8. Use of bleed-air precoolers at engine bleed parts to temper the air prior to transmission out of the nacelle area.

9. Elimination of flammable fluids by use of the alternative electrical system (all hydraulic fluids are removed from the aircraft).

Landing Gear and Brakes. The main landing gear is a conventional-post type retracting forward and slightly in board.The 28x9-14 tire is repositioned by a rotating collar (similar to that on the A-6 and F-14) to lie flat under the inlet duct. Stroke and structural strength are incorporated for vertical landing on a heaving deck. Carbon brakes and a simplified anti-skid system are incorporated for conventional landings.

The nose gear is installed off center to accommodate the gun. It incorporates a single 22x6.6-10 tire. It retracts aft to stow behind the crew compartment aft bulkhead. Full-power steering is provided for precise shipboard maneuvering.

7. AIRCRAFT PERFORMANCE

7.1 Aircraft Sizing

The E205 configuration was sized to meet the requirements presented in Section 3.2 by use of General Dynamics' Conceptual Design Synthesis Program (CDSP). The airplane was sized on the Deck Launch Intercept (DLI) Mission, defined in Figure 3-5, and carried a payload consisting of two LCLM missiles, two AMRAAM missiles, and a 30mm gun with 300 rounds of ammunition.

Selection of the sized design point was done by applying the hover and sustained-load-factor (6.2 g's at M.6/10kft) requirements specified in the statement of work. Figure 7-1 shows the takeoff gross weight and associated performance parameters for the matrix of airplanes generated for the sizing study. Each dependent variable was plotted versus wing area and engine size factor (ESF) (S.L.S. uninstalled MAX A/B thrust = 34500 lb at ESF = 1.0). The selection of the sized configuration was done by transferring onto the TOGW plot the required values for hover and sustained load factor. In addition, constraint lines for a 70 second acceleration from M.8 to 1.6 at 35000 ft and for a STO takeoff distance of 400 ft in 20 kts WOD were included to evaluate the sizing effects of these constraints.

A flight performance summary of the sized E205 aircraft is shown in Table 2-1. Table 7-1 summarizes the characteristics of the ejector airplanes sized to meet the following constraints:

1. Mission only
2. Mission + hover
3. Mission + hover + maneuver (E205 configuration)
4. Mission + hover + maneuver + STO (E205 configuration)
5. Mission + hover + maneuver + STO + acceleration

The maximum VTO gross weight (zero WOD) for the E205 configuration that meets the DLI mission, hover, and combat requirements is 34,987 lb. The maximum vertical landing weight will be about 5% less to provide a T/W takeoff weight improvement for landing on rocking and heaving ships in sea State 5 conditions.

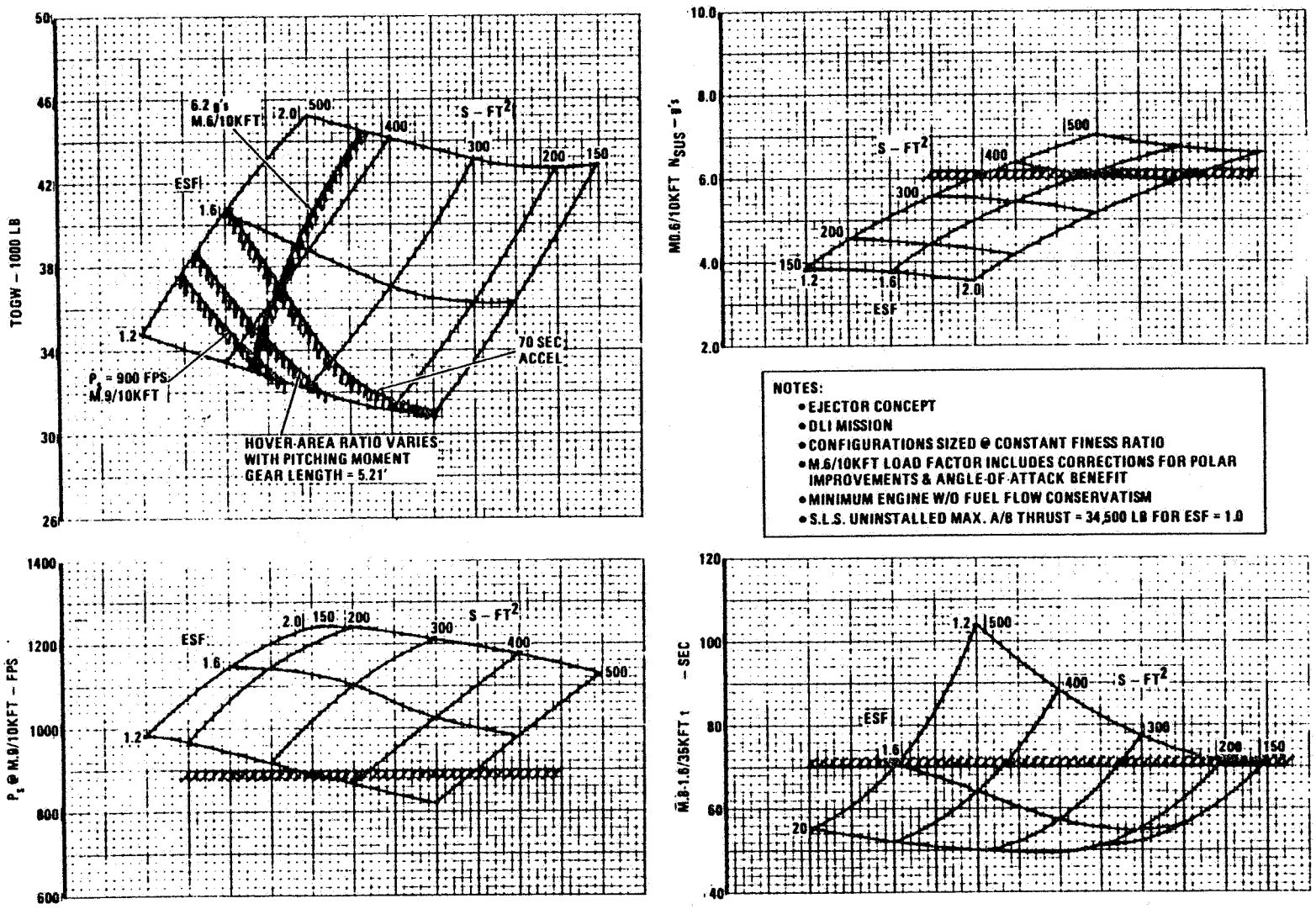

Figure 7-1 Aircraft/Engine Sizing Carpet, E205

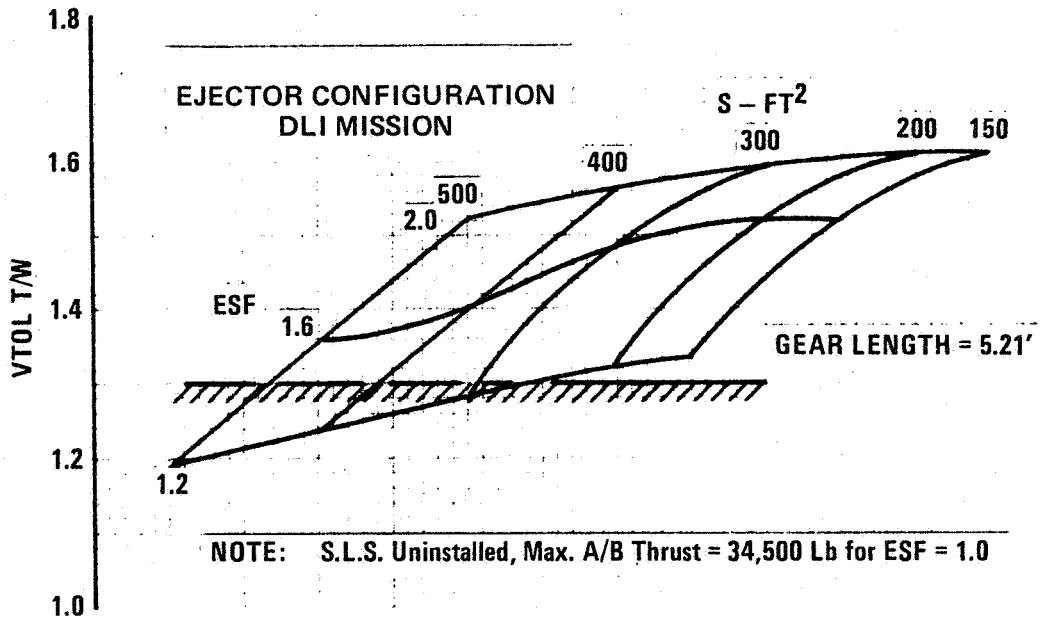

Figure 7-1 Aircraft/Engine Sizing Carpet, E205 (Cont'd)

TABLE 7-1

SIZED EJECTOR AIRPLANE CHARACTERISTICS

		MEETS MISSION (AS DRAWN)	MEETS MISSION & HOVER	MEETS MISSION & HOVER & MANEUVER
TOGW	lb(kg)	34360 (15583)	33724 (15294)	34987 (15867)
WING AREA	$ft^2 (m^2)$	337 (31.3)	337 (31.4)	384 (35.67)
ENGINE SCALE (2 ENGINES)		1.30	1.27	1.317
MISSION RADIUS (DLI)	n.mi(km)	150 (277.8)	150 (277.8)	150 (277.8)
FUEL REQUIRED	lb(kg)	9472 (4296)	9209 (4176)	9521 (4318)
FUEL FRACTION		.276	.273	.272
P_S (M.9/10kft/1g)	fps/mps	942 (287)	935 (285)	931 (284)
N_Z (M.6/10kft/P_S=0)	g	5.8	5.85	6.2
ACCEL TIME (M.8-1.6/35	sec	78	75.8	76.8

		MEETS MISSION HOVER MANEUVER & STO	MEETS MISSION HOVER MANEUVER STO ACCEL
TOGW	lb(kg)	34987 (15867)	37300 (16900)
WING AREA	$ft^2 (m^2)$	384 (35.67)	405 (123.4)
ENGINE SCALE (2 ENGINES)		1.317	1.48
MISSION RADIUS (DLI)	n.mi(km)	150 (277.8)	150 (277.8)
FUEL REQUIRED	lb(kg)	9521 (4318)	10200 (4626)
FUEL FRACTION		.272	.273
P_S (M.9/10kft/1g)	fps(mps)	931 (284)	980 (299)
N_Z (M.6/10kft/P_S=0)	g	6.2	6.2
ACCEL TIME (M.8-16/30kft)	sec	76.8	70

VTOL T/W = 1.22 (THRUST OUT OF EJECTORS)

7.2 Mission Performance

Presented in Table 7-2 is a breakdown of the performance of the E205 configuration on the DLI mission. As expected, most of the fuel is expended on the climb and high-speed-dash segments.

No alternate mission performance is presented in this document. However, a variety of alternate mission studies have been reported (Reference 1) for the E204 VEO-Wing ejector airplane described in Table 7-1 sized to meet only the hover and DLI mission constraints.

7.3 Combat (Maneuver) Performance

After selection of the sized configuration, a more extensive analysis of the combat (maneuver) performance was conducted by use of a General Dynamics procedure, the Mission Analysis and Performance System (MAPS). All of the combat performance was computed at 88% of VTOGW. Plots of P_s vs N_z at Mach = 0.5, 0.6, 0.9, 1.2, and 1.6 for 10,000, 20,000 and 30,000-ft altitudes at maximum afterburning thrust are shown in Figure 7-2. Figure 7-3 presents the maximum afterburning thrust flight envelope. The service ceiling for the E205 configuration is 62,000 feet at Mach = 1.1. Maximum speed for the E205 configuration is Mach = 1.83. Restrictions on high speed were imposed by the structure. Although they did not effect E205 configuration sizing a dynamic pressure limit of 2133 psf was assumed at the lower altitude along with a temperature cut-off constraint of 308°F, standard day. Low-speed flight was restricted to a nominal 3.5 maximum trimmed lift coefficient.

7.4 VTO Transition Studies

VTO transition studies conducted for the E205 configuration are summarized in Figures 7-4 through 7-6. The object of these studies was to demonstrate the <u>feasibility</u> of VTO transition for the sized configuration. Since the requirements for the transition are not well defined, it was felt that the feasibility of the transition could be demonstrated adequately by treating the aircraft as a point mass propelled along the desired flight path by a thrust vector (TVEC) resolved from the ejector and VEO-Wing nozzle thrusts through a resultant angle (θ_r), as shown in the sketch at the bottom of Figure 7-4. The analysis was further simplified by allowing the TVEC to be unconstrained by trim requirements during transition.

Table 7-2 Mission Segment Performance

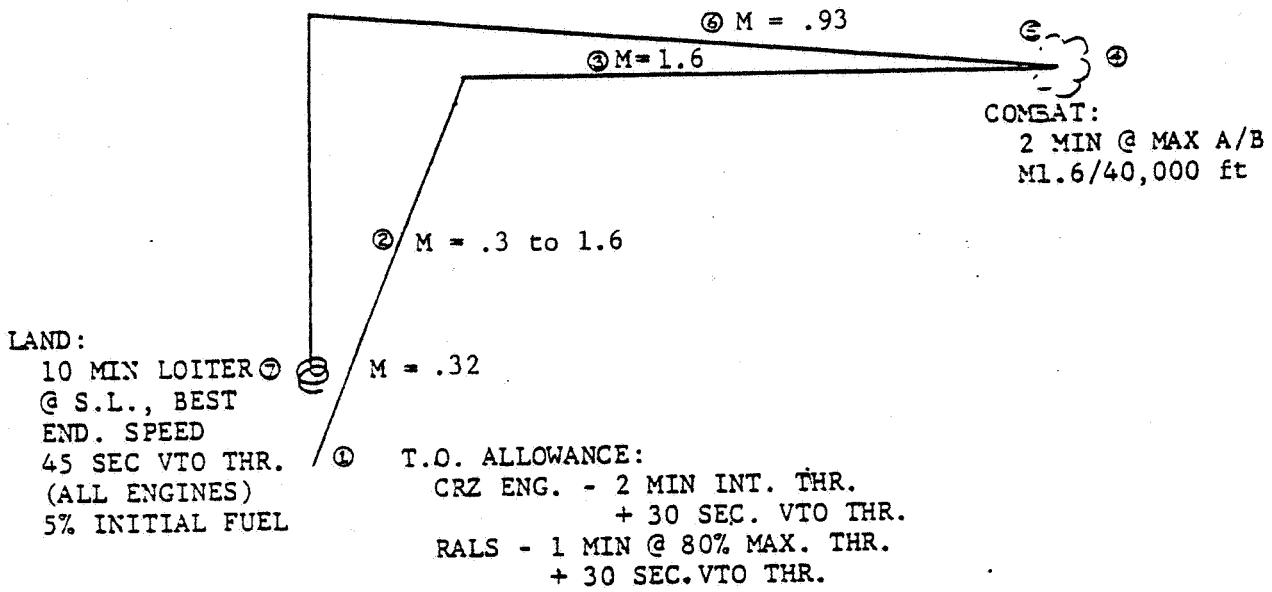

LOADING:
(2) LCLM
(2) AMRAAM
GUN + 300 RDS AMMO

	INITIAL CONDITIONS		INCREMENTS		
	ALT (ft)	WEIGHT (lb)	FUEL (lb)	DIST (n.mi)	TIME (min)
① WARM UP & T.O.	0	34987	1006	0	0
② CLIMB-MAX A/B PWR.	0	33981	2053	31	2.9
③ DASH-CONSTANT M,h	40000	31928	2912	119	7.8
④ COMBAT	40000	29016	1361	0	0.6
⑤ CLIMB TO CRUISE	40000	27655	95	7	0.6
⑥ CRUISE - OPT. M, h	46249	27560	813	143	16.1
⑦ LAND	0	26747	1281	0	10.0
TOTALS			9521	150	39.4

EJECTOR - DLI MISSION

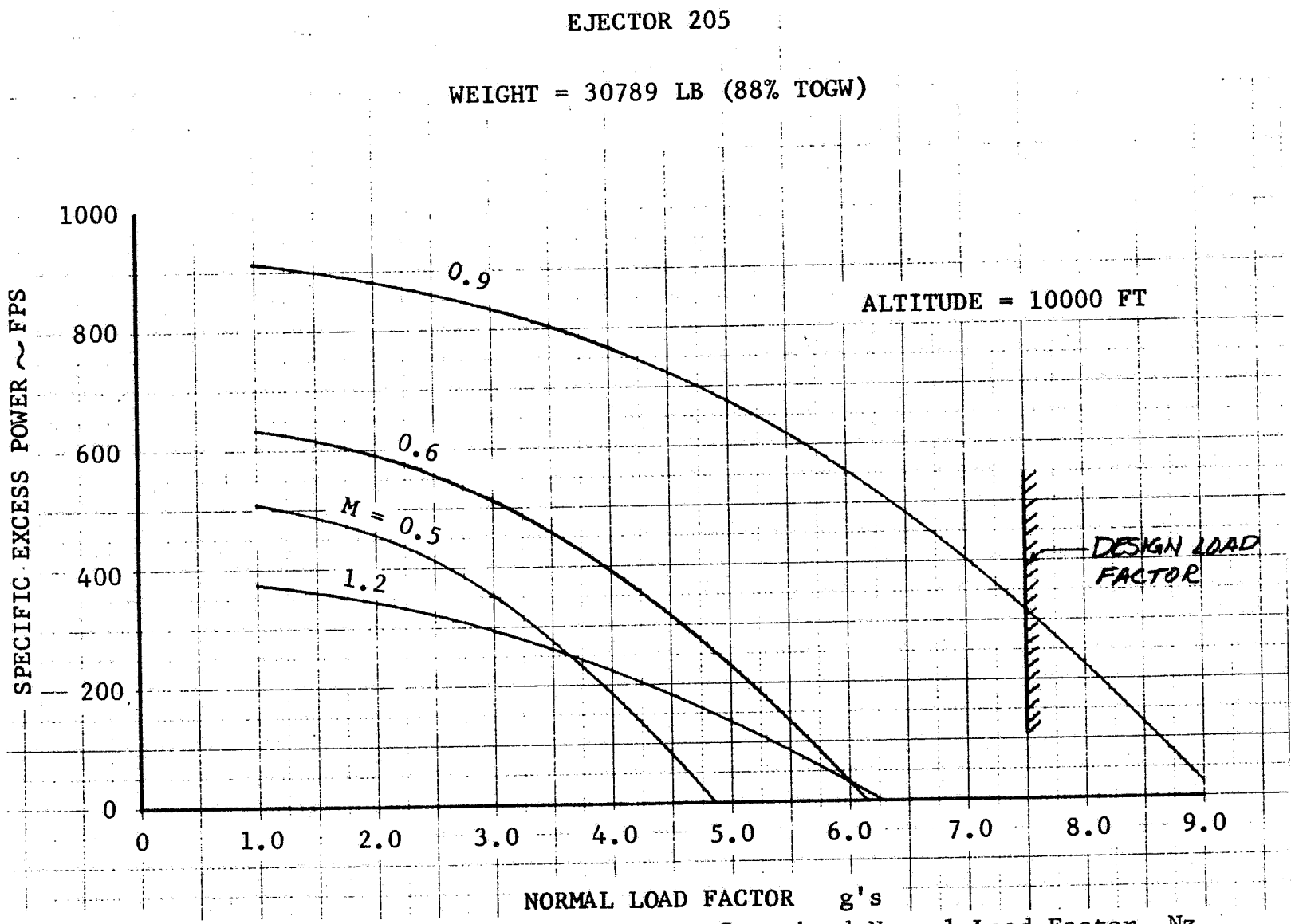

Figure 7-2a Specific Excess Power, Ps vs. Sustained Normal Load Factor Nz, ALTITUDE = 10,000 Ft.

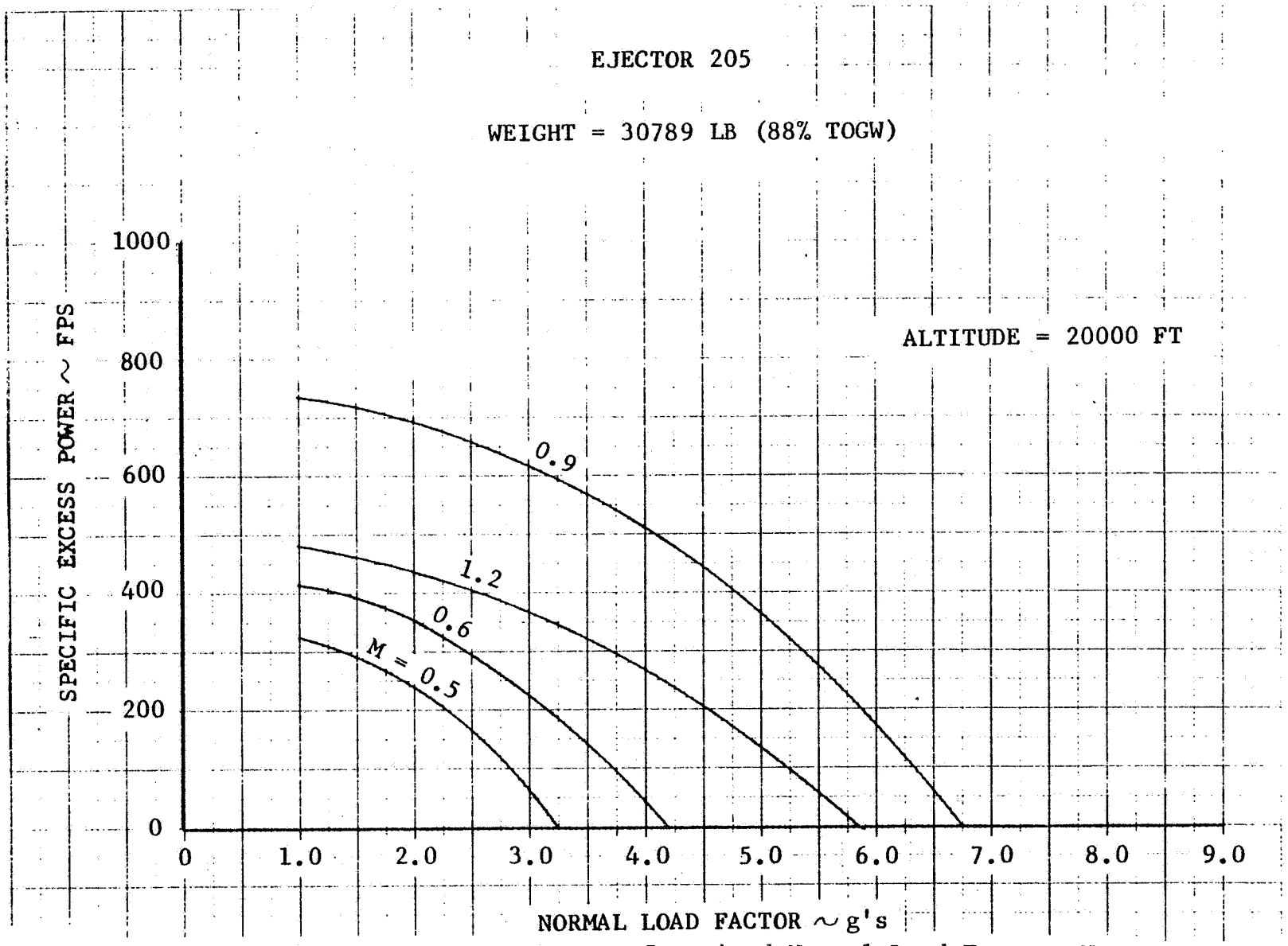

Figure 7-2b Specific Excess Power, Ps vs. Sustained Normal Load Factor Nz, ALTITUDE = 20,000 Ft

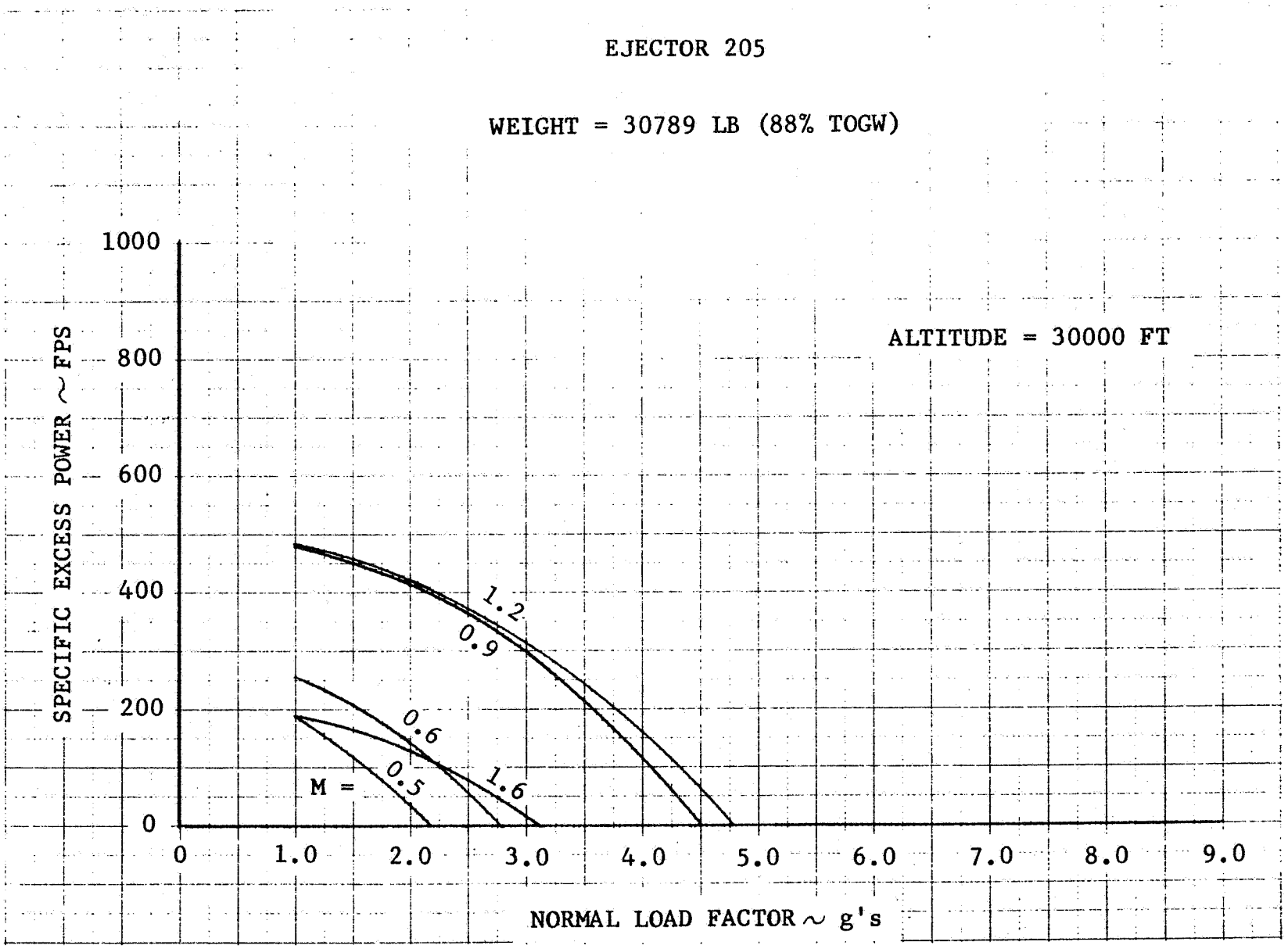

Figure 7-2c Specific Excess Power, Ps, vs. Sustained Normal Load Factor Nz, Altitude = 30,000 Ft

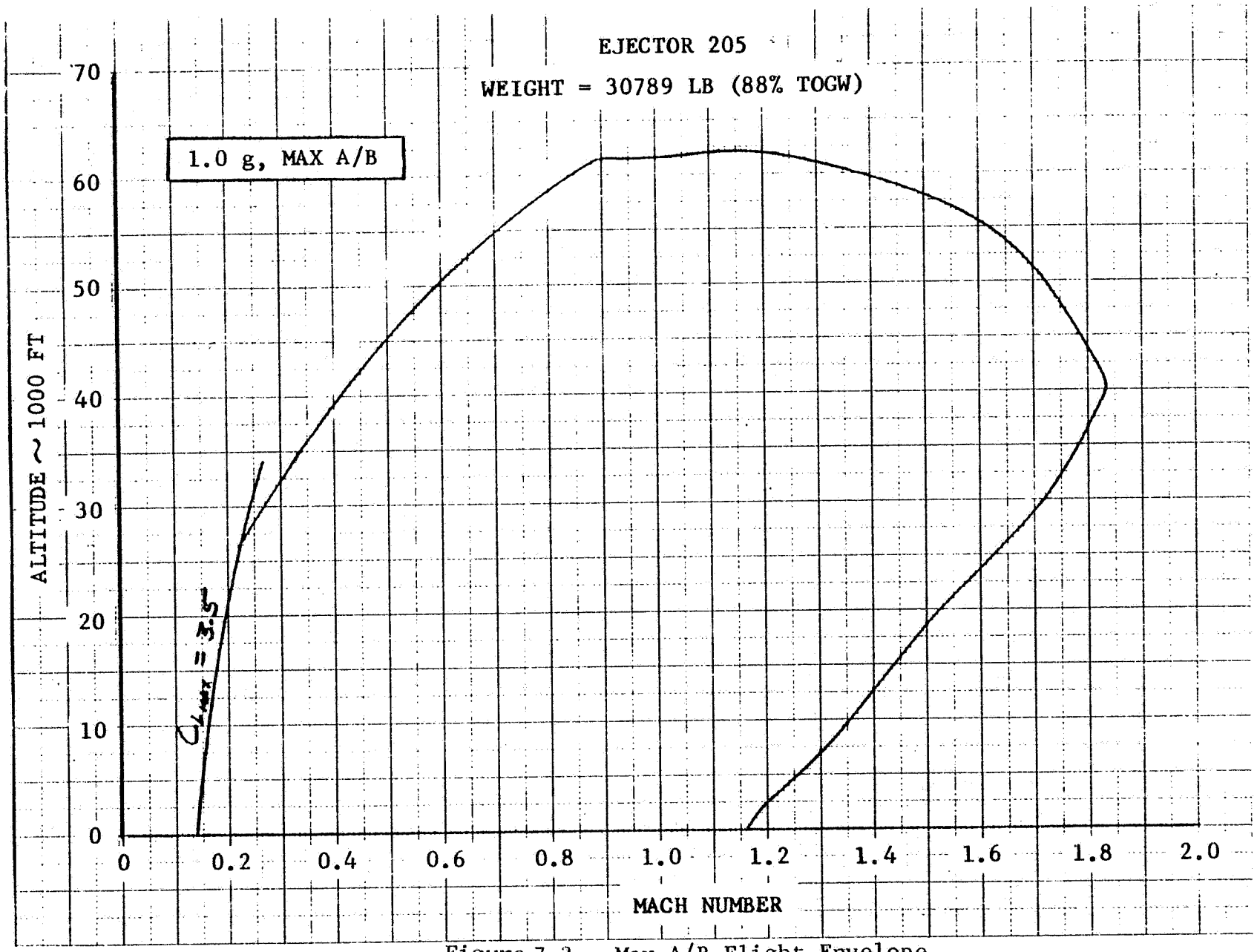

Figure 7-3 Max A/B Flight Envelope

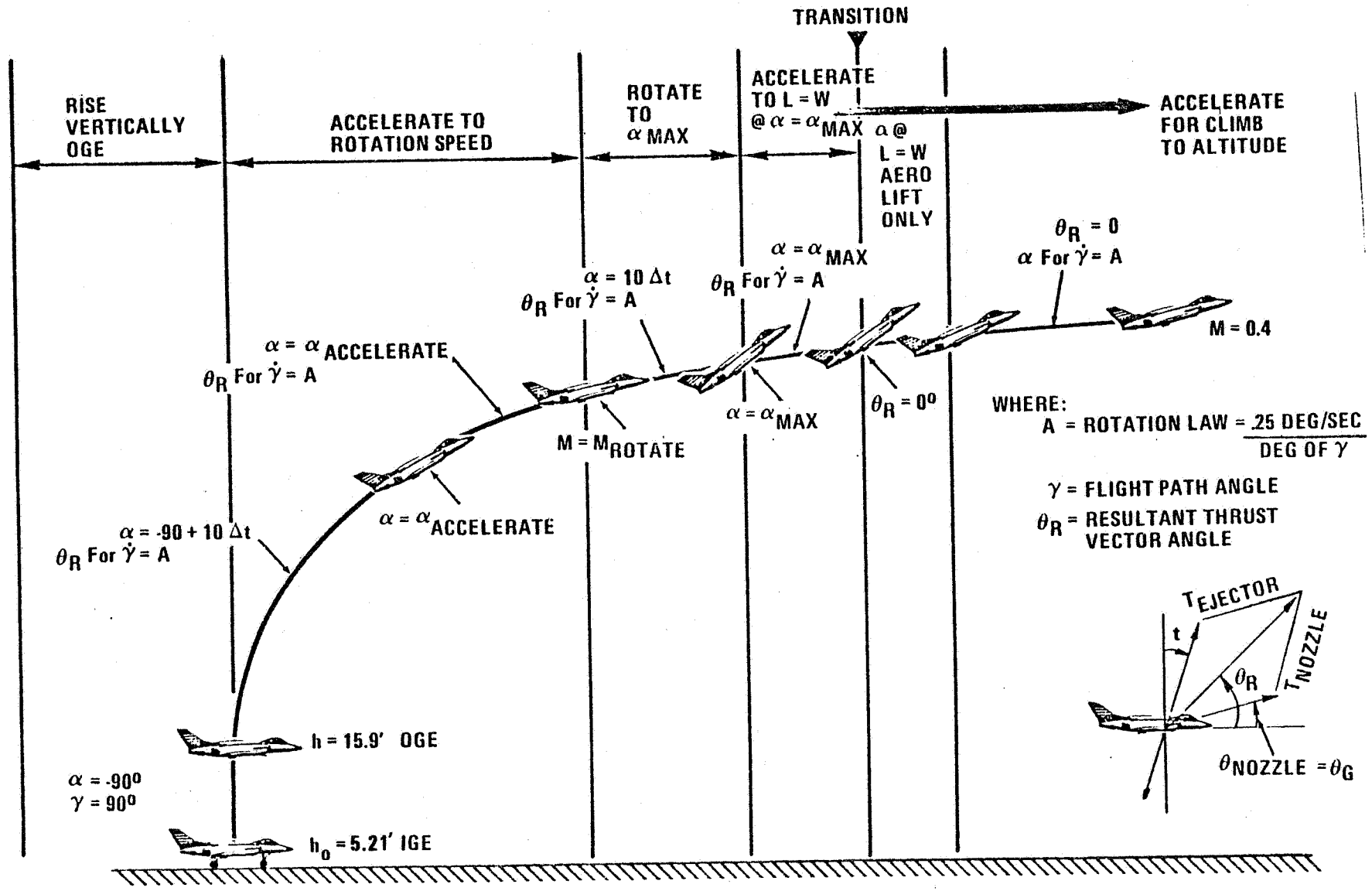

7-4 VTO Transition Flight Profile Segments

SCHEDULES OF ENGINE AIRFLOW SPLIT vs VEO NOZZLE DEFLECTION FOR MAX AXIAL THRUST

$$K_S = \frac{\text{ENGINE AIRFLOW TO EJECTORS}}{\text{ENGINE AIRFLOW TO VEO NOZZLES}}$$

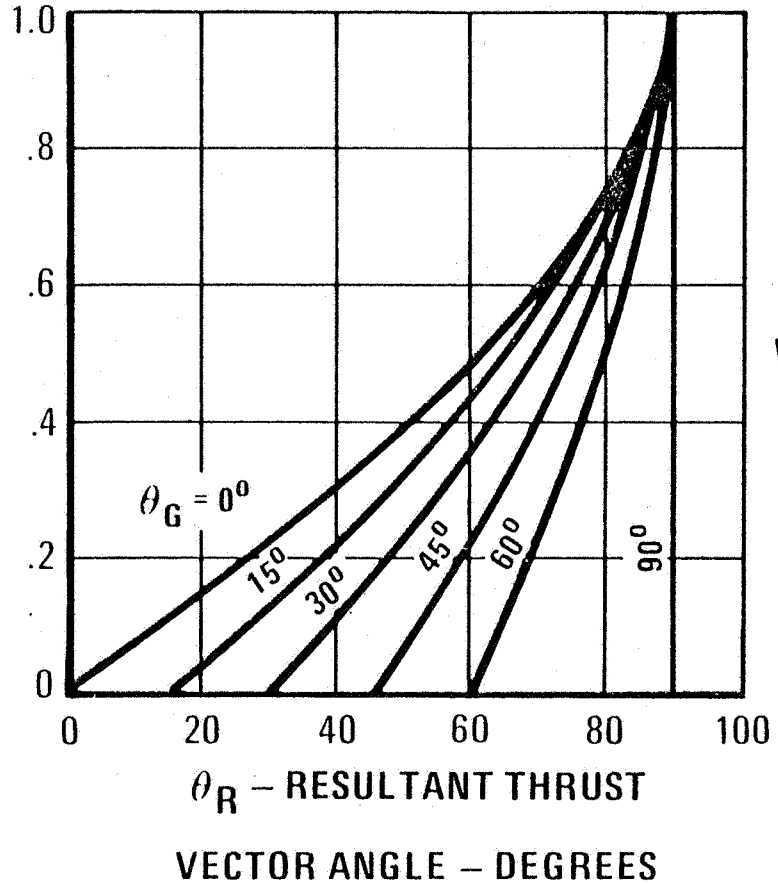

WHERE θ_G = VEO NOZZLE THRUST DEFLECTION ANGLE

$K = \left(\frac{\text{EAT}}{D_{RAM}} = \text{EJECTOR AXIAL THRUST}\right)_{EJECTOR}$

= 1.0 @ EAT = D_{RAM} EJECTOR

= 0 @ EAT = 0

7-5 Schedules of Engine Airflow Split vs. VEO Nozzle Deflection for Max Axial Thrust

$\theta_G = 30^o$, $M_{ROTATE} = .09$, $\alpha_{MAX} = 20^o$, EAT = 0, $\alpha_{ACCEL} = 0^o$

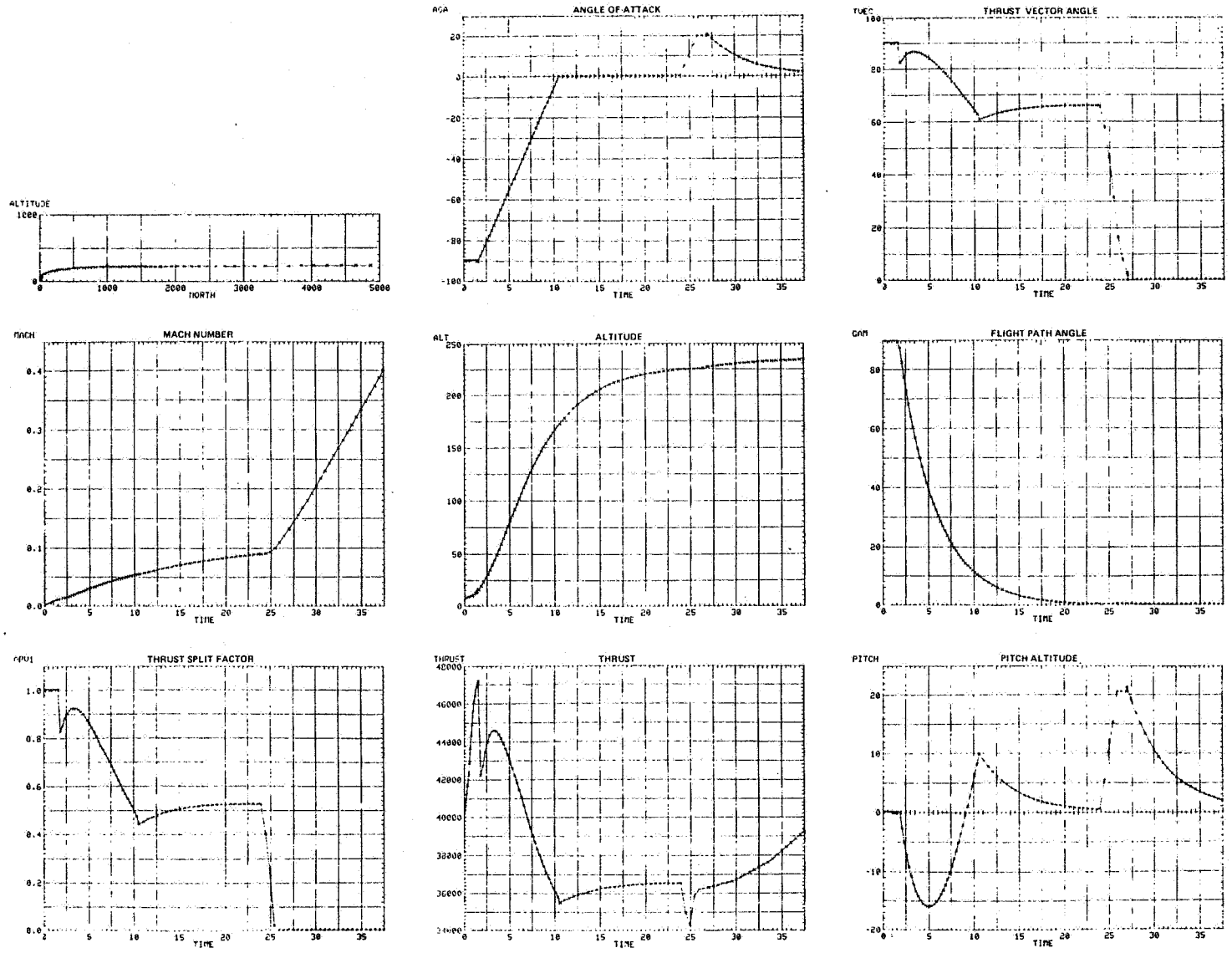

Figure 7-6 Ejector Configuration E205 VTO Transition Time Histories

A sketch of the transition flight profile divided into various segments is also shown in Figure 7-4. The initial VTO conditions are: VEO-Wing nozzles are closed and all engine thrust is to the ejectors with engine operating at intermediate powersetting; A warm-up fuel allowance of 100 lb is assumed. The airplane rises vertically until it is out of ground effect (H 16 ft.). Because of the excess thrust available from reduced control demands out of ground effect, engine air can be diverted to the VEO-Wing nozzles; the afterburner is then lit and the airplane accelerated to "rotation" speed along a prescribed flight path rotation law $\left(\frac{d\gamma}{dt} = \frac{.25 \text{ deg/sec}}{\text{deg of } \gamma} \right)$. The resultant thrust vector rotates to achieve this flight law. Schedules of the percentage of engine airflow that can be diverted from the ejector (K_s) to the VEO-Wing nozzles while maintaining maximum axial thrust (for minimum transition time) are presented in Figure 7-5 as a function of the maximum allowable VEO-Wing nozzle deflection (θ_G) and the resultant thrust vector angle θ_R. $\theta_{G_{max}}$ for E205 is 30°. The ejector thrust is not vectorable in the 90-degree position because of the concern that any turning vane devices for vectoring would back pressure the ejector and result in substantial Ø losses. At rotation speed, the airplane is rotated at a prescribed rate to an αmax to "get on the wing" as soon as possible. This attitude is held while the airplane continues to accelerate to the speed for aerodynamic lift to equal weight. Angle of attack can then be reduced and the resultant thrust vector angle brought to zero degree (since ejector thrust = 0, the condition is VEO-Wing nozzle deflection = 0°). Transition to complete wing-borne flight then occurs when the TVEC = 0°.

The effect of varying the profile parameters on transition time is shown in Table 7-3 for several airplane cases; the amount of ejector thrust converted to axial thrust (EAT) was assumed to be equal to 0 for all cases (i.e., the heavy ejector ram axial-force penalty defined in Subsection 4.1.1 was incurred whenever the ejector was operated with no benefit of thrust recovery).

The study airplane transitions in 27 seconds. The transition time is less sensitive to the aerodynamics than to the engine power setting as might be expected (viz., Cases 3 vs 5 and 1 vs 2 and 3 in Table 7-3). Figure 7-6 provides time histories of the important parameters in the transition of the study airplane (Case 3).

Table 7-3 Summary of VTO Transition Cases Studied

A/P SIZED TO MEET	AIRPLANE CHARACTERISTICS												
	CASE	S_w	ESF	VTOGW AT LIFT OFF in lb	POWER	ACCEL	M_{ROTATE}	α_{MAX}	K	θ_G	TRANSITION TIME--sec	TIME TO M = .4(sec)	FUEL EXPENDED
MISSION + HOVER	1	337	1.27	33624	MAX A/B	0.0	.09	20°	0	30°	18 SEC	28.5	518
MISSION + HOVER + COMBAT	2	384	1.317	34887	INT	-10.9	.095	20°	0	30°	58.2	74.5	454
MISSION + HOVER [1] + COMBAT	3	384	1.317	34889	MAX A/B	0.0	.09	20°	0	30°	27	37.5	704
MISSION + HOVER	4	337	1.27	33624	INT	-10.0	.09	20°	0	30°	∞		-
MISSION + HOVER [2] + COMBAT	5	384	1.317	34887	MAX	0.0	.09	20°	0	30°	39	48	897

where:

1. $K = \frac{\text{Ejector Thrust Converted to Axial Thrust (EAT)}}{\text{Ejector Ram Drag}}$

   $K = 0$ EAT = 0

   $K = 1$ EAT = Ejector Ram Drag

2. θ_G = Max Allowable VEO-Nozzle-Deflection During Transition

3. α_{max} = max rotation angle to achieve aerodynamic lift

4. α_{accel} = for acceleration segment

5. M_{rotate} = Mach number for rotation

[1] Sized airplane for this study

[2] Sized airplane for this study with double the drag and half the lift at constant α

Determination of absolute transition times requires more rigorous analysis of the transition paying attention to the trim requirements.

7.6 STOL Takeoff Performance

Analysis Method. Overload short-takeoff performance for the E205 configuration was calculated with a General Dynamics longitudinal three-degree-of-freedom, closed-loop control, digital computer routine, which simulates the takeoff by solving the dynamic equations of motion including landing-gear dynamic characteristics, aerodynamics, and control system dynamics with both aerodynamic and propulsive controls. The method allows the user to actually "fly" the airplane to investigate various takeoff techniques by selecting the control laws that are desired for each segment of the takeoff. As shown in Figure 7-7, the routine provides the option of selecting either position or rate command control laws; position command was selected for this study. The damping functions within the control system can be varied to achieve satisfactory flight characteristics. The method yields a time history of all elements of the takeoff including: velocity, time, distance, altitude, angle of attack, flight path angle, control surface, VEO-Wing nozzle deflection, movement, and thrust, ejector thrust, and rotation rate.

A dynamic analysis of the short takeoff problem is required because the times and distances required to achieve rotations are a large percentage of the total times and distances available for the takeoff. For example, the entire takeoff of 400 ft only requires about 5 seconds from brake release. The time for rotation is approximately 1 second and about 100 feet are covered during that rotation. Attention must be paid to the dynamics when the time to achieve the maneuvers becomes a significant percentage of the total time for the takeoff.

Takeoff Methods. Two free-deck takeoff methods were studied: (1) a conventional vectored-thrust takeoff that a VEO-Wing fighter could perform and (2) a VTO/VEO-Wing fighter takeoff, which makes use of the ejector lift system. This obviously affords a comparison of what the V-capability buys for STO operations.

The groundules for the short takeoff were as follows:

1. STO TOGW = VTOGW + 10,000 lb

   = 44,987 lb (off-loaded 476 lb of fuel)

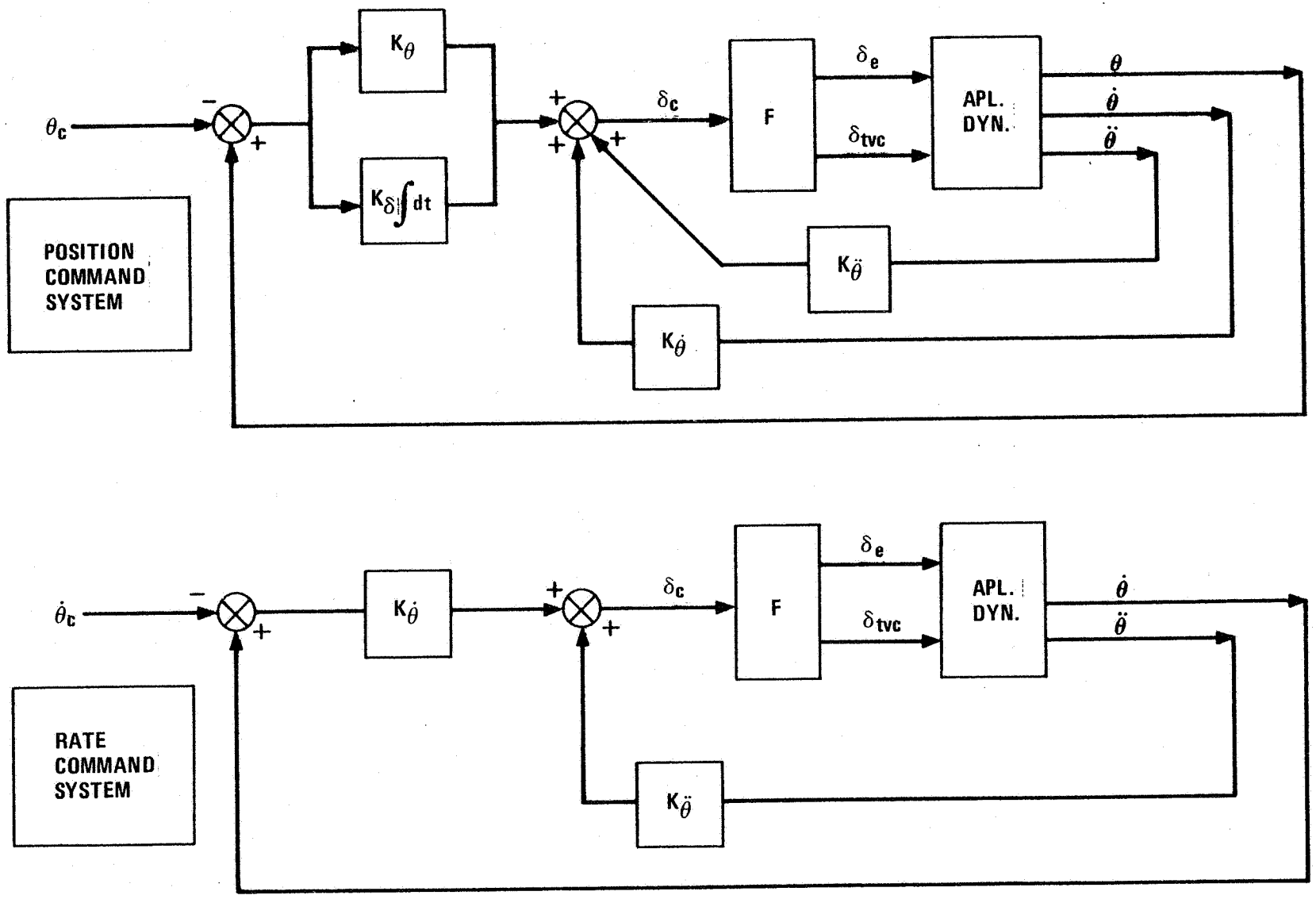

Figure 7-7 Control System Models for STOL Analysis

Store loading: Payload + Rack Weight = 10,476 lb
(See Figure 4-4 2 wing-tip-mounted LCLM missiles
4 guided advanced general-purpose bombs on wing pylons
2 370-gal fuel tanks on nacelle shoulder-mounted pylons

2. Wind over deck = +20 kt

3. Tropical day

4. Maximum allowable sink over the bow = 5 ft

5. Gear not retracted until takeoff is completed (achieve wing-borne flight). Although not specified, the takeoff distance goal for this type of aircraft should be 400 ft based on projected ship size.

The analysis method for both takeoff methods studied is divided into two segments, before and after lift off. The approach has been to assure a set of deck-edge lift-off conditions (α, θ , velocity) and concentrate on determining if the airplane can be "flown" through a successful transition to equilibrium flight. The before-lift-off segment has been studied to the extent that we are confident that we wil be able to achieve these lift-off conditions with additional study of control sequencing. It is very difficult to find the control sequencing that achieves both the desired angle-of-attack and pitch rate simultaneously. A study of multiple takeoff techniques was considered more instructive than determining the exact control sequencing before lift-off.

The required velocity at deck edge can be determined for a matrix of thrust/weight and wing loading combinations for either takeoff method as shown in Figure 7-8. The approximate deck-run velocity profiles are then calculated (Figure 7-9). (They are approximate because the exact control sequencing has not been determined to produce the lift-off conditions; however, enough work has been done to ensure that these are very close to the exact distances that go with the assumed lift off conditions).

The approximate deck run velocity profiles then yield the takeoff distances required for thrust/weight and wing-loading combinations.

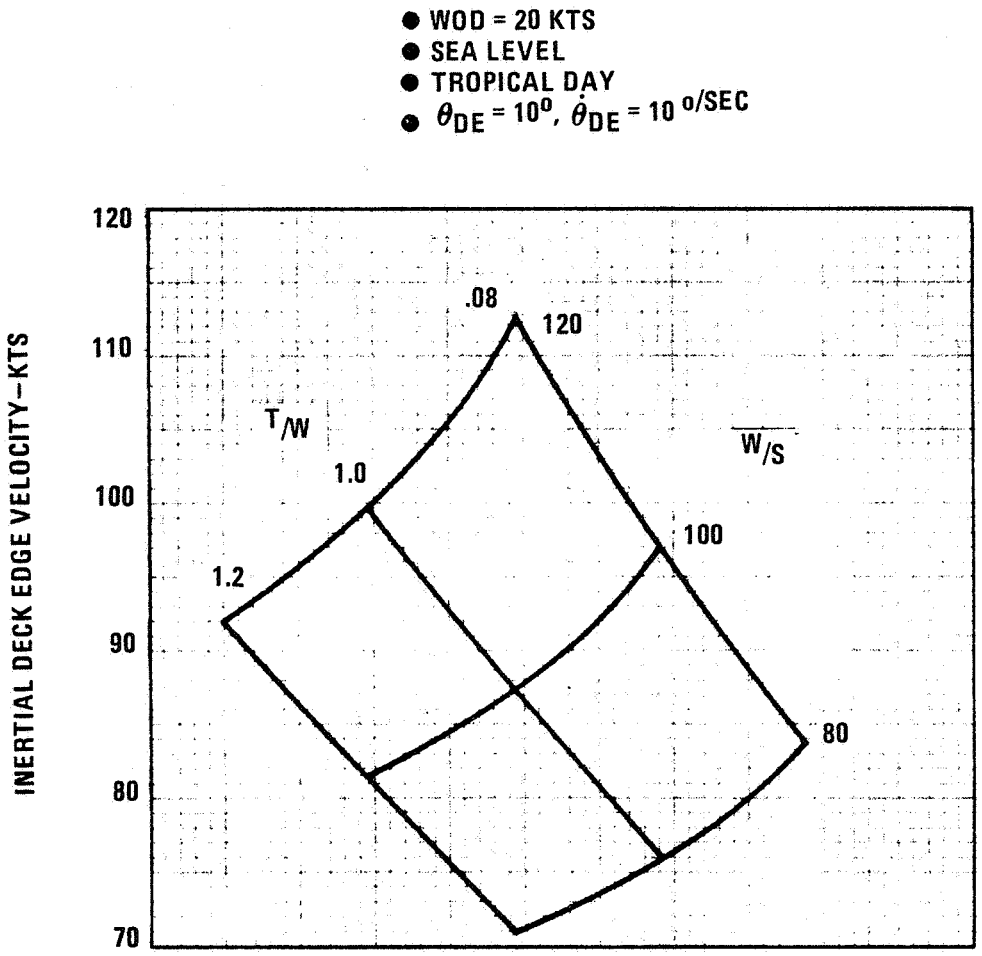

Figure 7-8 Deck Edge Relative (Inertial) Velocity Requirements for Desired Lift-Off Conditions

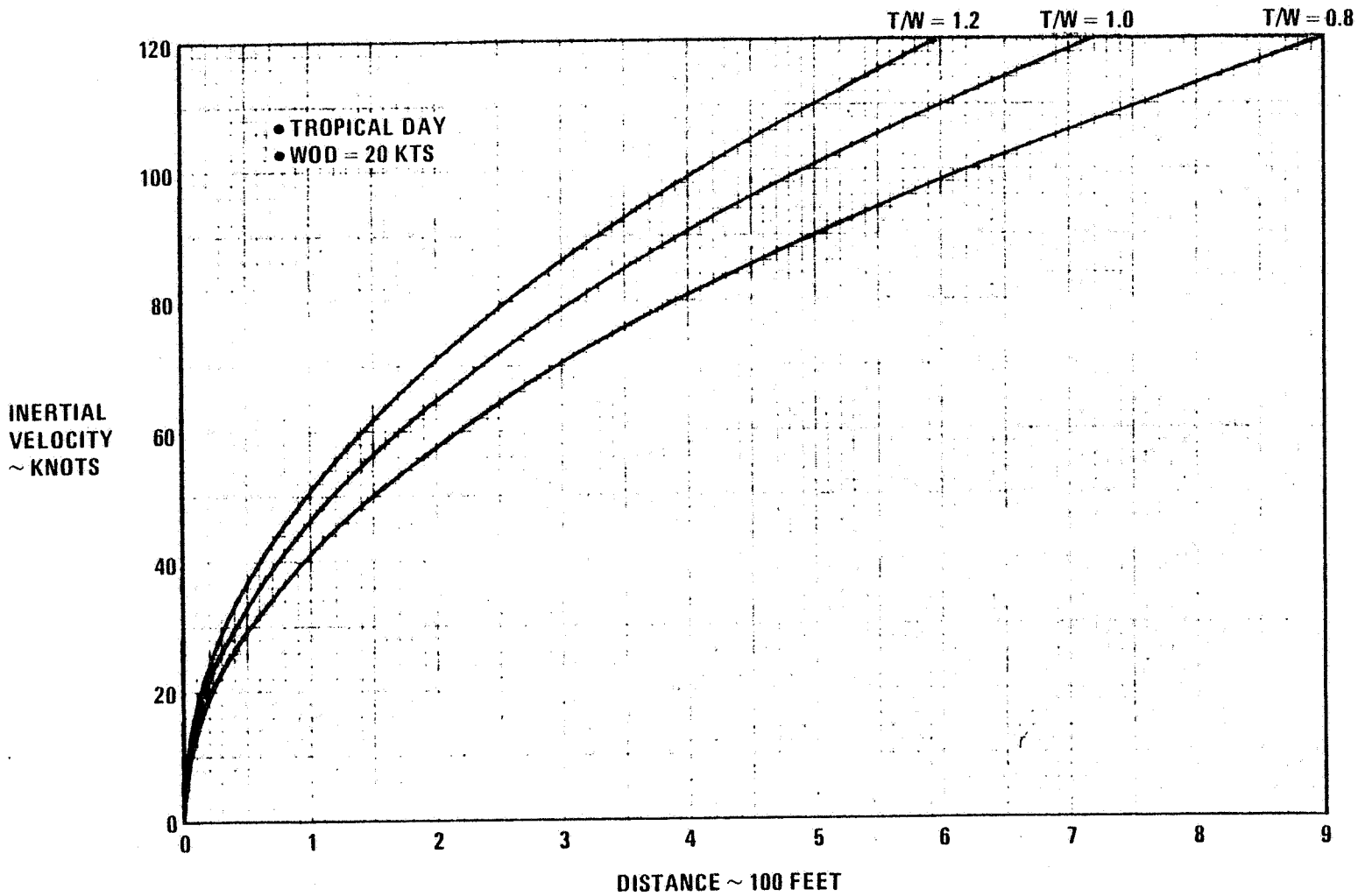

7-9 Approximate Deck Run Velocity Profiles Requirements for Desired Lift-Off Conditions

Conventional VEO-Wing Takeoff vs VTO/VEO-Wing Takeoff Description. Figure 7-10 compares the takeoff sequences for the conventional thrust-vectored and VTO takeoff methods. Maximum afterburning powersetting is maintained throughout the takeoffs. Both methods begin with the VEO-Wing nozzle at $\delta_{TE} = 0^o$ with the forward ejector deployed and pressurized (primaries closed). As the airplane accelerates to rotation speed the VEO-Wing nozzle starts moving down at 60°/sec for the "conventional" and stays at 0° for the "VTO." For the conventional method, at rotation speed the forward ejector is "pulsed" for .4 second to initiate nosewheel rotation. The canard is also driven to maximum incidence to aid the rotation while the VEO-Wing nozzle continues to be driven down to maximum deflection (30°). This nozzle deflection arrests the increasing rotation rate caused by the airplane instability to the desired lift-off $\dot{\theta}$, 10 deg/sec at $\alpha = 10^o$; the canard has also been driven to negative incidence to help arrest the rotation rate. The initiation of rotation does not have to be produced by an ejector firing. It could be done by any means that imparts a nose-up rotation, such as releasing a compressed nosewheel gear oleo on conventional catapult takeoffs. For this reason we say this takeoff technique could be accomplished by a non-VTO or "Conventional" VEO-Wing aircraft.

For the VTO takeoff at rotation speed, the forward ejectors are activated with the primaries set to produce a maximum nose-up moment to initiate rotation. Simultaneously the VEO-Wing nozzles are deflected at 60°/sec to begin arresting rotation. The ejector continues to provide nose-up moment and lift while the VEO-Wing nozzle reaches $\delta_{TE} = 17.5^o$ ($\dot{\theta}g = 22.5^o$) and the desired rotation conditions above are achieved. (The assumed lift-off conditions are based on takeoff experience and have not been optimized in this study). After lift-off, the conventional takeoff method employs the canard and VEO-Wing nozzle for trim while climbing out to an altitude suitable for stabilized flight. The VTO method employs the forward ejector and VEO-Wing nozzle for trim after lift-off. The canard deflection is fixed at zero degree for simplicity of analysis. All engine air is diverted to provide ejector lift and trim control after lift-off except that which is required out of the VEO-Wing nozzles to maintain a minimum longitudinal acceleration of .065g (which is a standard carrier suitability requirement for NAVY aircraft). Maximum angle of attack allowed during takeoff was constrained to 20°, which is well below power on $C_{L_{max}}$ for this configuration.

COMPARISON OF TAKE OFF METHODS STUDIED

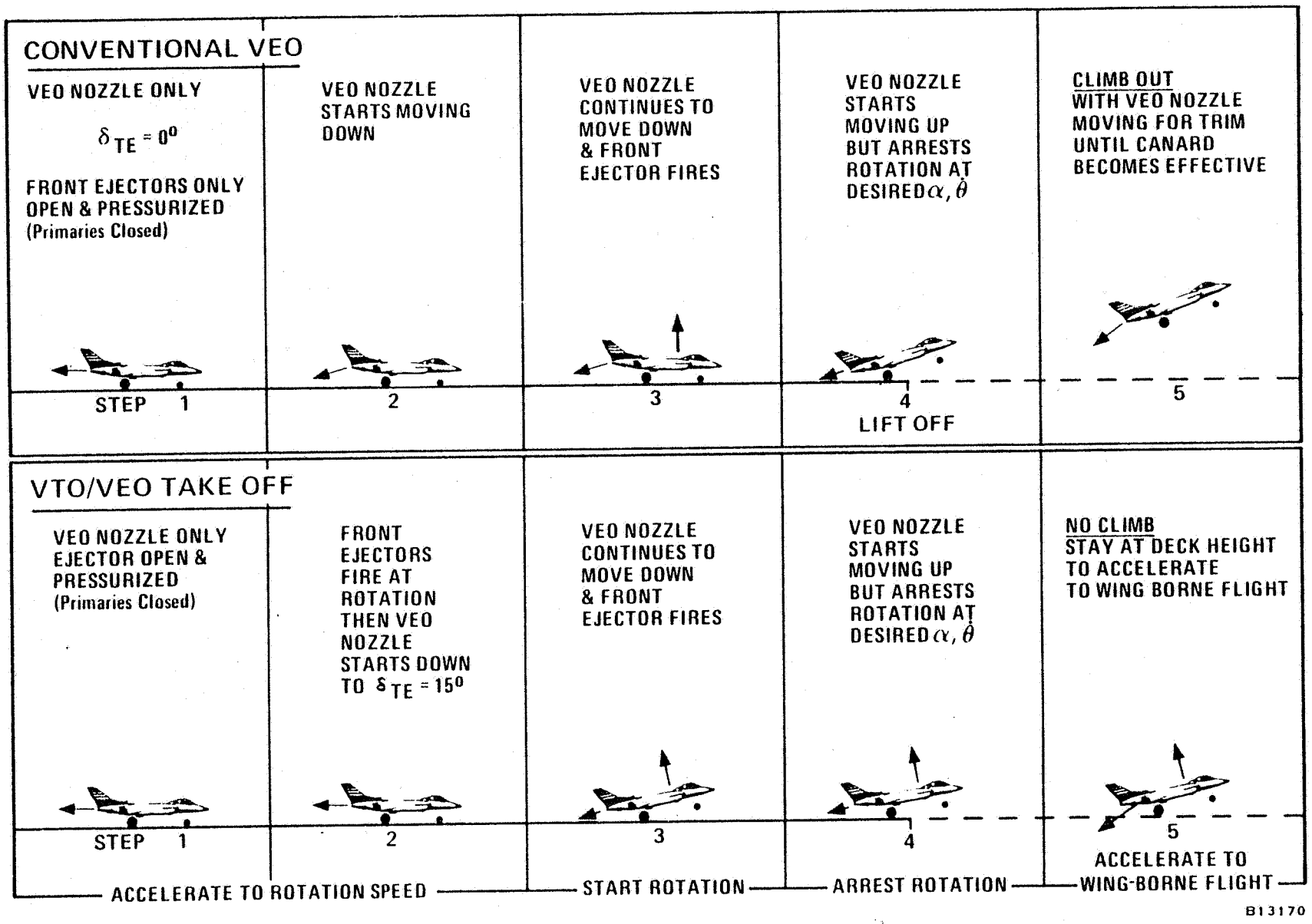

7-10 Comparison of (STO) Takeoff Methods Studied

Results. Takeoff distance as a function of thrust/weight and wing loading for conventional method and VTO takeoff methods is presented in Figure 7-11 and 7-12, respectively. The conventional-method takeoff distance for E205 is 760 ft with a 5-ft sink over the bow, while the VTO method allows lift-off in only 400 ft with zero sink over the bow. This means the airplane sized to do the mission + hover + maneuver requirements can also accomplish the STOL goals. The V-capability of the E205 configuration clearly provides a STOL advantage over the airplane designed for STOL (at the same horizontal thrust/weight and wing loading).

Figure 7-12 also illustrates that if an additional trim device were available to provide nose-up moment without increased drag or loss in axial thrust (i.e., more ejector moment couple), a substantial additional take-off distance savings could be achieved.

Figure 7-13 demonstrates that after lift-off there is a very narrow corridor of vectored-thrust incidence (nozzle deflection) and airspeed to accelerate to wing-borne flight; there is also, however, some excess acceleration capability above the required minimum that can be traded for altitude to climb-out. A more detailed time history for the vertical takeoff method after lift-off has not been developed, but the excess acceleration capability looks very plausible.

Time histories after lift-off for the conventional takeoff methods are presented in Figure 7-14. Canard and VEO-Wing nozzle deflections, aircraft pitch attitude, angle of attack, pitch rate and inertial velocities versus time are shown. The flight trajectory is shown in Figure 7-15.

The forward ejectors and VEO-Wing nozzles very effectively complement each other by allowing large lifts to be produced while balancing moments for trim; i.e. the ejector nose-up moment allows the VEO-Wing nozzle to be deflected to produce the large supercirculation increments (and nose-down moments) at a trimmed condition and at very low speeds, where aerodynamic surfaces like canards are ineffective. The big disadvantage of using the ejector in this manner is the tremendous ejector-ram-drag penalty experienced when the ejector is activated at forward speeds. Since we are assuming no thrust recovery, this ram drag severely hampers acceleration after lift-off. If a means of achieving ejector thrust recovery could be employed without back-pressuring the ejectors, tremendous gains in STO and VTO transition performance could be achieved.

FREE DECK TAKEOFF

- SEA LEVEL
- TROPICAL DAY
- NO EJECTOR OPERATION IN FLIGHT

∴ 5 FEET SINK OVER THE BOW

- WOD = 20 KTS.
- $\theta_{DECK\ EDGE} = 10°$
- $\dot{\theta}_{DECK\ EDGE} = 10°/SEC$
- $\alpha_{MAX} \leq 20°$

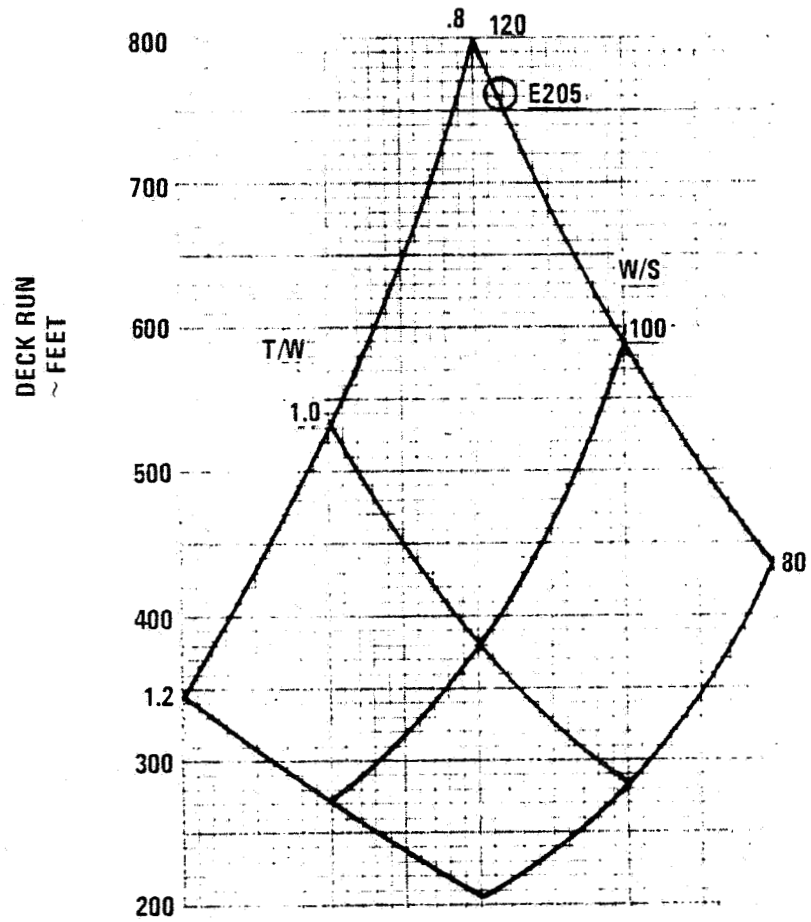

PITCH ATTITUDE
CLOSED LOOP CONTROL
GAINS
$K_\theta = 1.5$ $K_{\dot{\theta}} = .4$

Figure 7-11 E205 Deck Run Requirements for Conventional VEO STOL Takeoff Method

E205 DECK RUN REQUIRED FOR VTO/VEO STOL TAKEOFF METHOD

OVERLOAD TAKEOFF CONFIGURATION

- QUASI STEADY STATE LEVEL FLIGHT (EJECTOR AUGMENTATION OF LIFT AS REQUIRED
- SEA LEVEL
- TROPICAL DAY
- $\gamma = 0$
- $\alpha = 15°$
- a/g $\geq .065$

WOD = 20 KTS
$\delta_c = 0$

— — θ_J = MAXIMUM = 27.5°

——— θ_J VARIED AS REQUIRED FOR TRIM WITH FORWARD EJECTORS

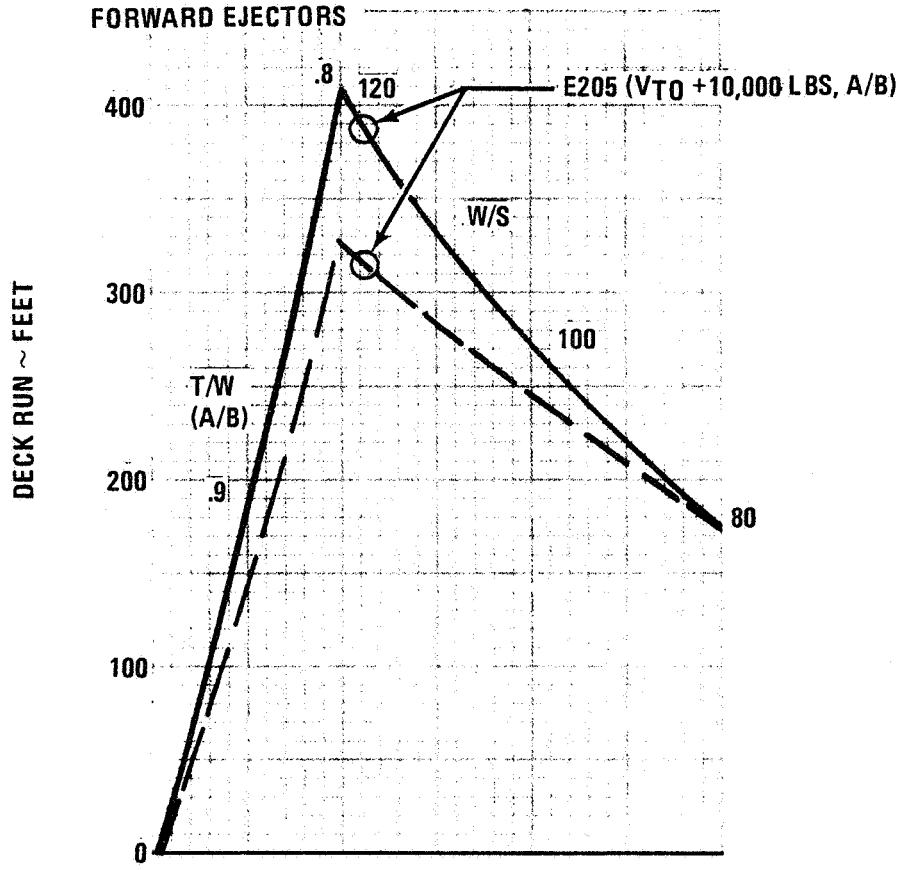

Figure 7-12 E205 Deck Run Requirements for VTO/CEO-Wing STOL Takeoff Method

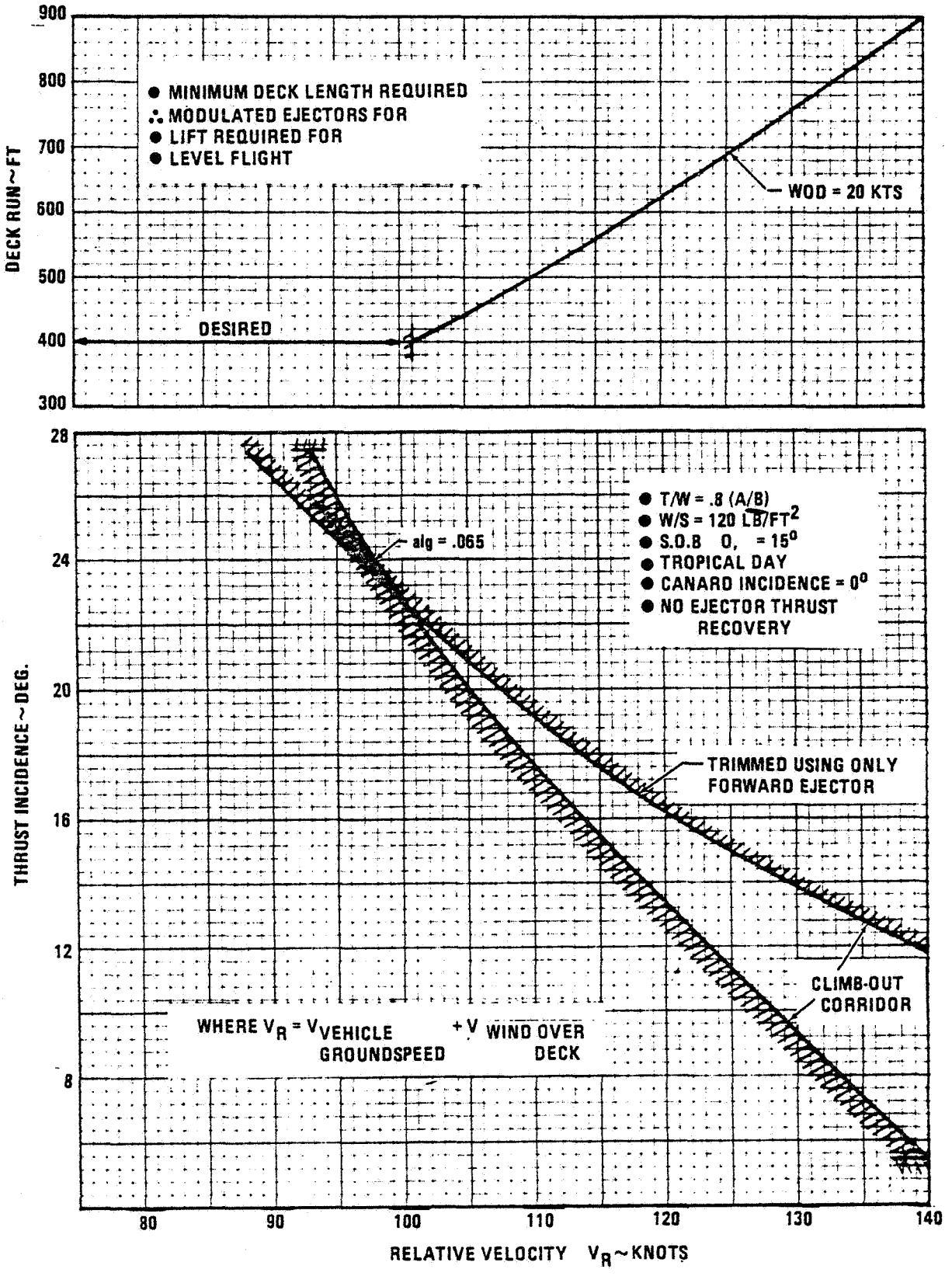

7-13 Climb Out Corridor for VTO/VEO-Wing STO Takeoff Method

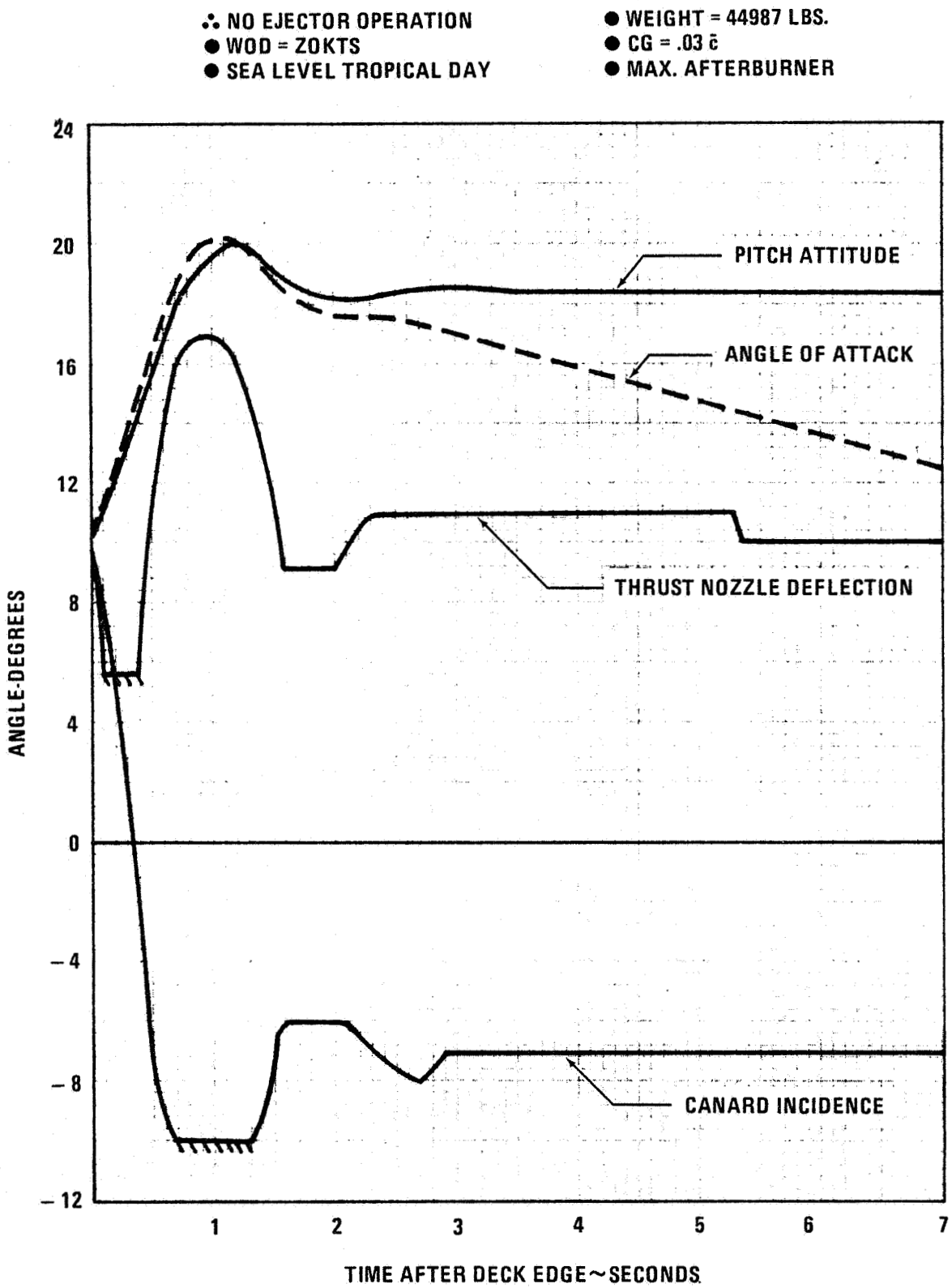

7-14 After-Deck-Edge STO Time History for Conventional VEO-Wing Takeoff Method

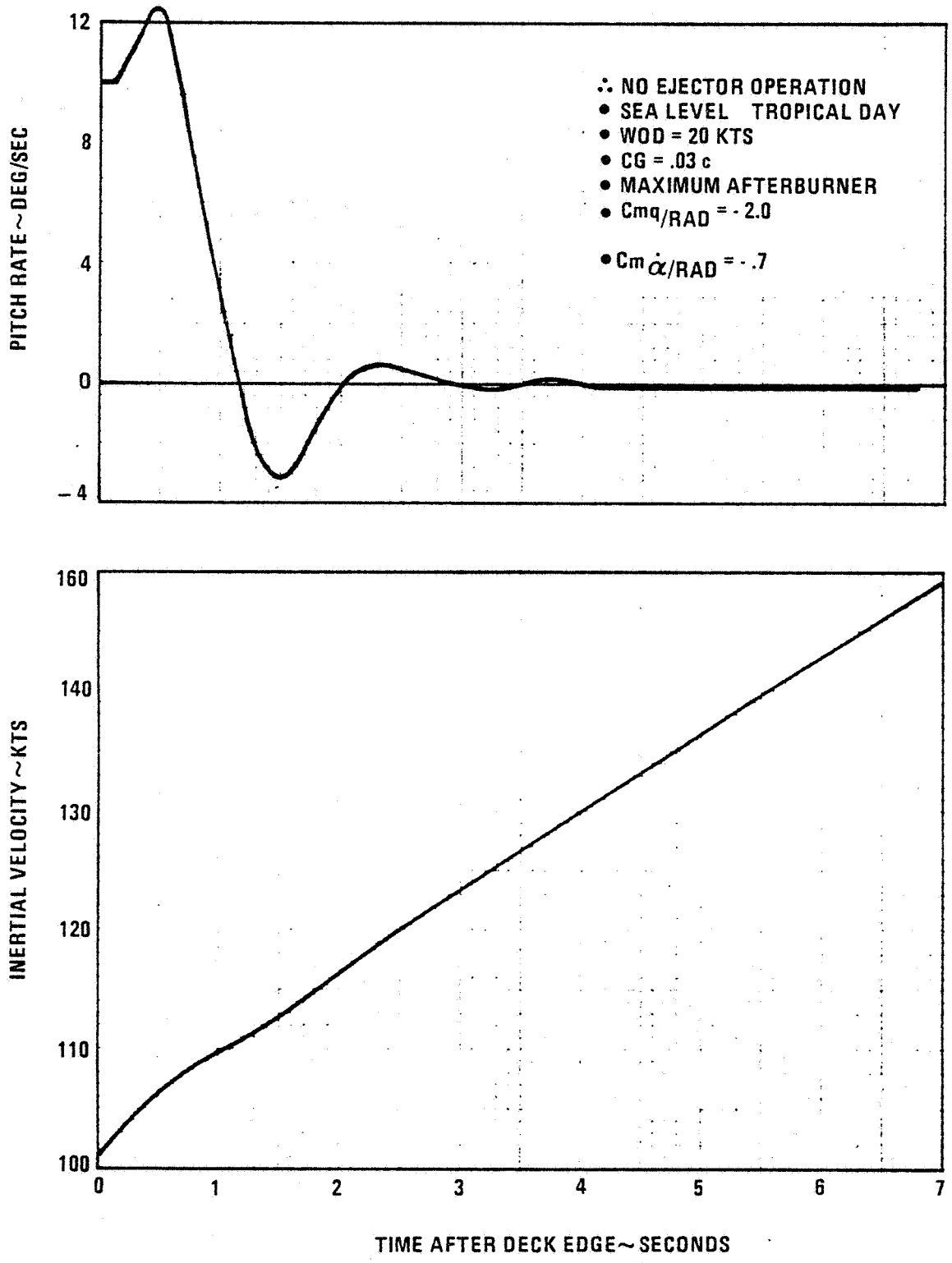

7-14 After-Deck-Edge STO Time History for Conventional VEO-Wing Takeoff Method (Cont'd)

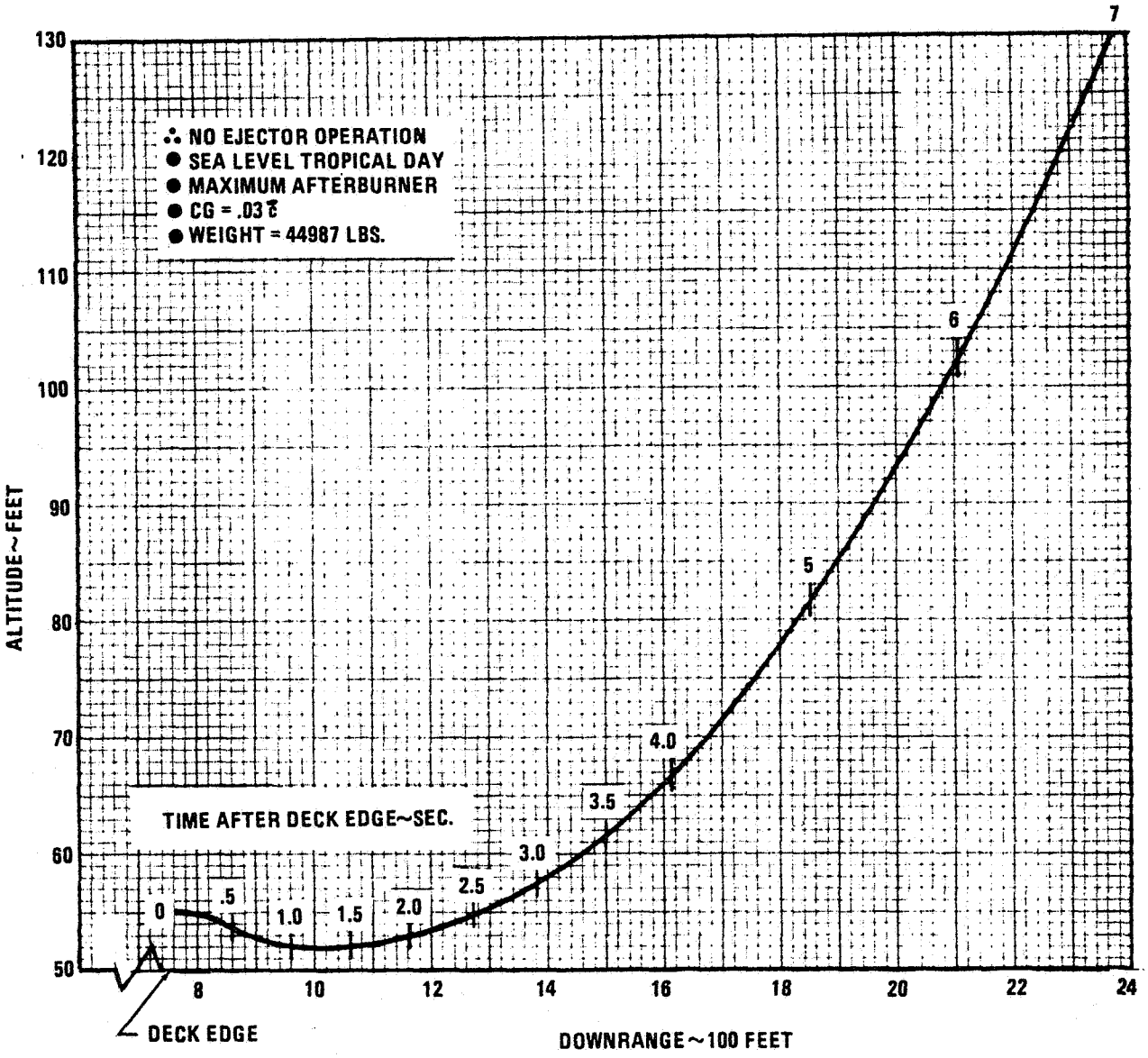

7-15 Flight Trajectory After Lift-Off for Conventional VEO Takeoff Method

Nevertheless, a corridor for climb-out has been demonstrated and the results look very promising.

7.6 Single Engine Recovery

The twin-engine ejector aircraft can be recovered in the event of a single-engine failure if a conventional-field landing can be made. The minimum single-engine-out lateral control speed as a function of engine power setting afforded by the all-moving vertical tail and reaction control system is shown in Figure 7-16. If failure occurs during ship-based operation, the aircraft must be refueled to a shore base. If an engine is lost during hover or low-speed transition, the running engine will be shut down to maintain aircraft attitude for pilot ejection.

7.7 Design Sensitivities and Tradeoffs

Sensitivity of aircraft VTO gross weight required to accomplish the DLI mission has been determined as a function of several perturbations. The sensitivities are presented as follows:

<u>Figure</u>

<u>Aircraft Sizing</u>

7-1	Carpet plots showing effects of wing size and engine-scale variations on TOGW, turn rate, P_s, and acceleration time. The second page of each figure translates the data into uninstalled thrust/weight (sea-level static Max A/B uninstalled).
7-17	Carpet plots with 5% increased fuel flow. The basic aircraft design was sized using engine data representative of a minimum engine without 5% fuel flow conservatism - which also is about the same as an average engine with 5% conservatism. Fuel reserves of 5% are included in all cases. The influence of excessive conservatism is reflected in these sizing charts and summarized in the SFC-effects graphs below.

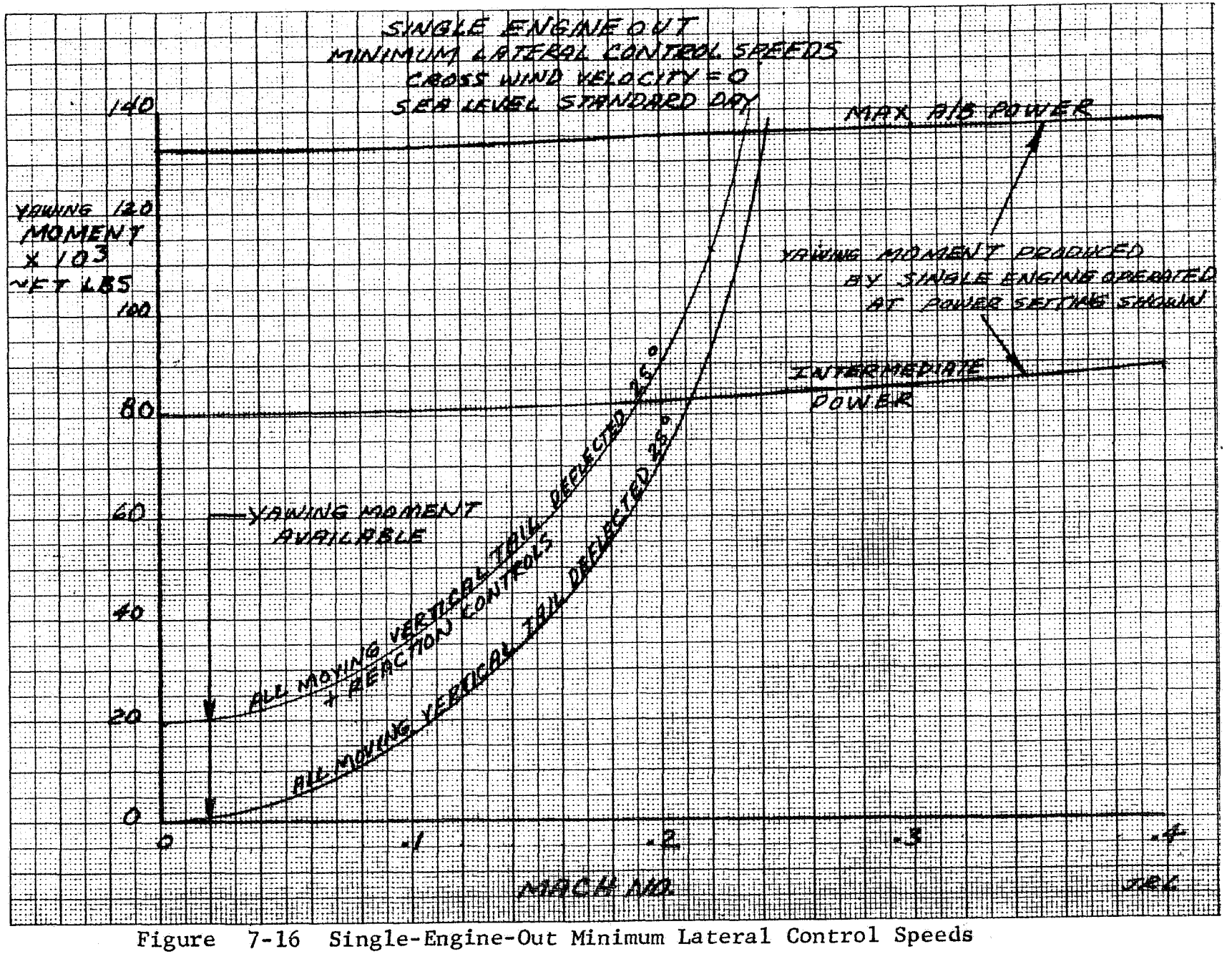

Figure 7-16 Single-Engine-Out Minimum Lateral Control Speeds

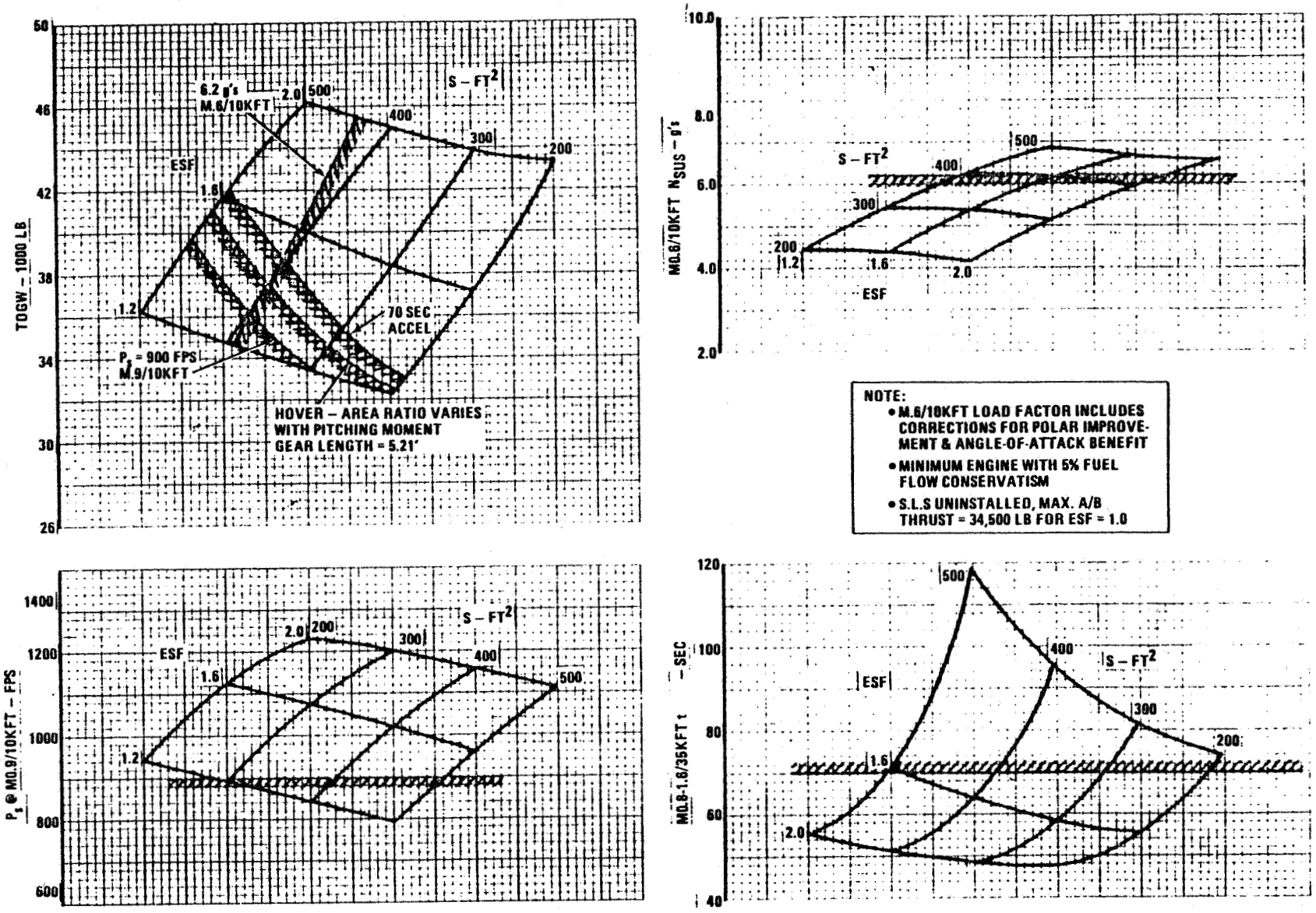

Figure 7-17 Sizing Carpet with 5% Increased Fuel Flow

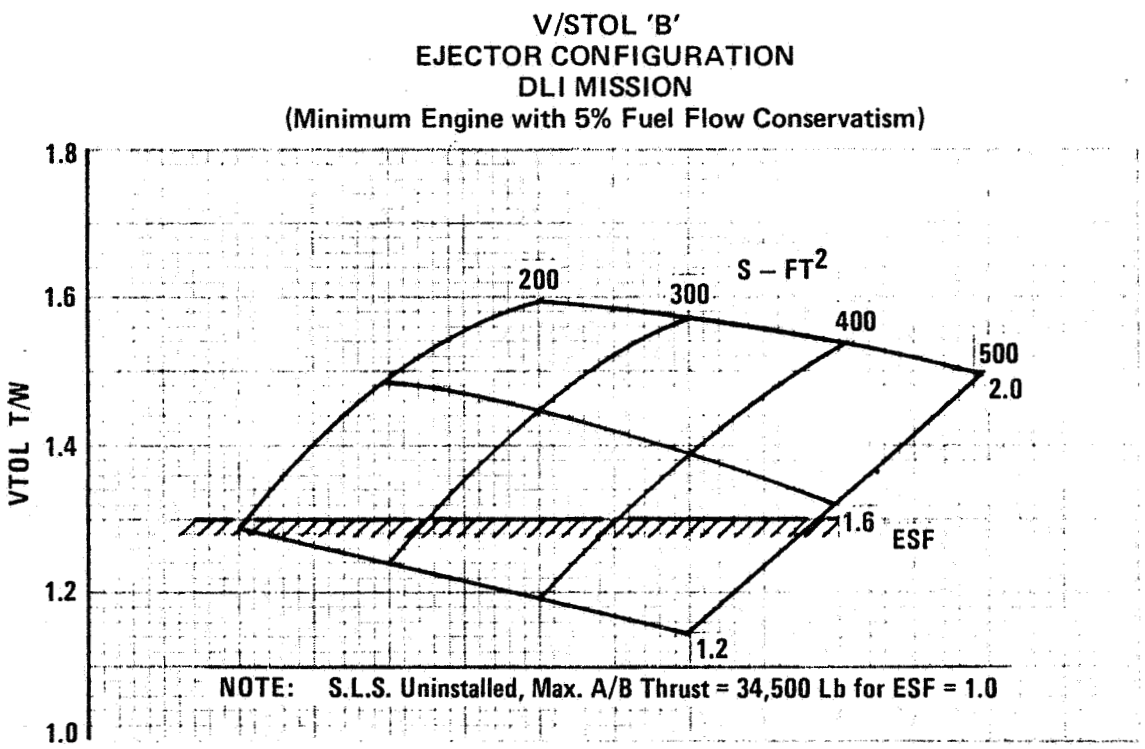

Figure 7-17 Sizing Carpet with 5% Increased Fuel Flow (Cont'd)

Aircraft Sizing

7-18 Landing-gear-length sensitivity. The back-pressure effects on the ejector change significantly with height above ground and has a pronounced effect on sizing.

Technology Levels

Perturbations of technology states of the art are shown in terms of TOGW required along with the associated wing area and engine thrust rating (SLS, horizontal A/B, uninstalled).

7-19 SFC sensitivity.

7-20 Engine thrust-to-weight-ratio sensitivity.

7-21 Minimum drag sensitivity.

7-22 Trim drag sensitivity.

7-23 Span efficiency (e) sensitivity.

Flight & Mission Capabilities

7-24 DLI-mission-radius sensitivity.

7-25 Specific excess power sensitivity, P_s at Mach 0.9, 10,000 ft.

7-26 Sustained load factor sensitivity, N_Z at Mach 0.6, 10,000 ft.

7-27 Acceleration time sensitivity, time from Mach 0.8 to 1.6, 35,000 ft.

Airplane Thrust/Weight

7-28 Sensitivities to max A/B, S.L. static, uninstalled thrust/weight required for hover in ground effect.

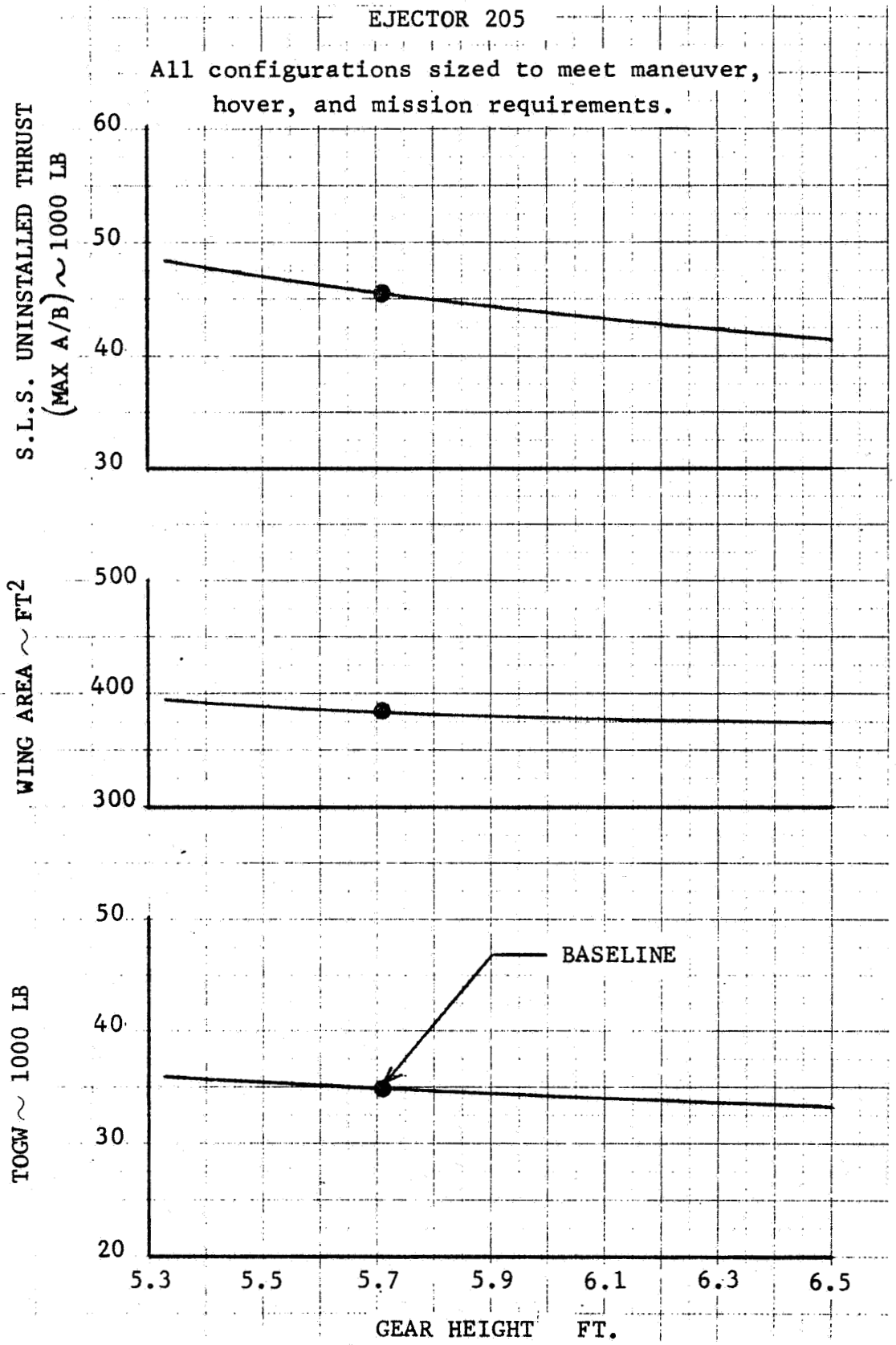

Figure 7-18 Landing Gear Length Sensitivity

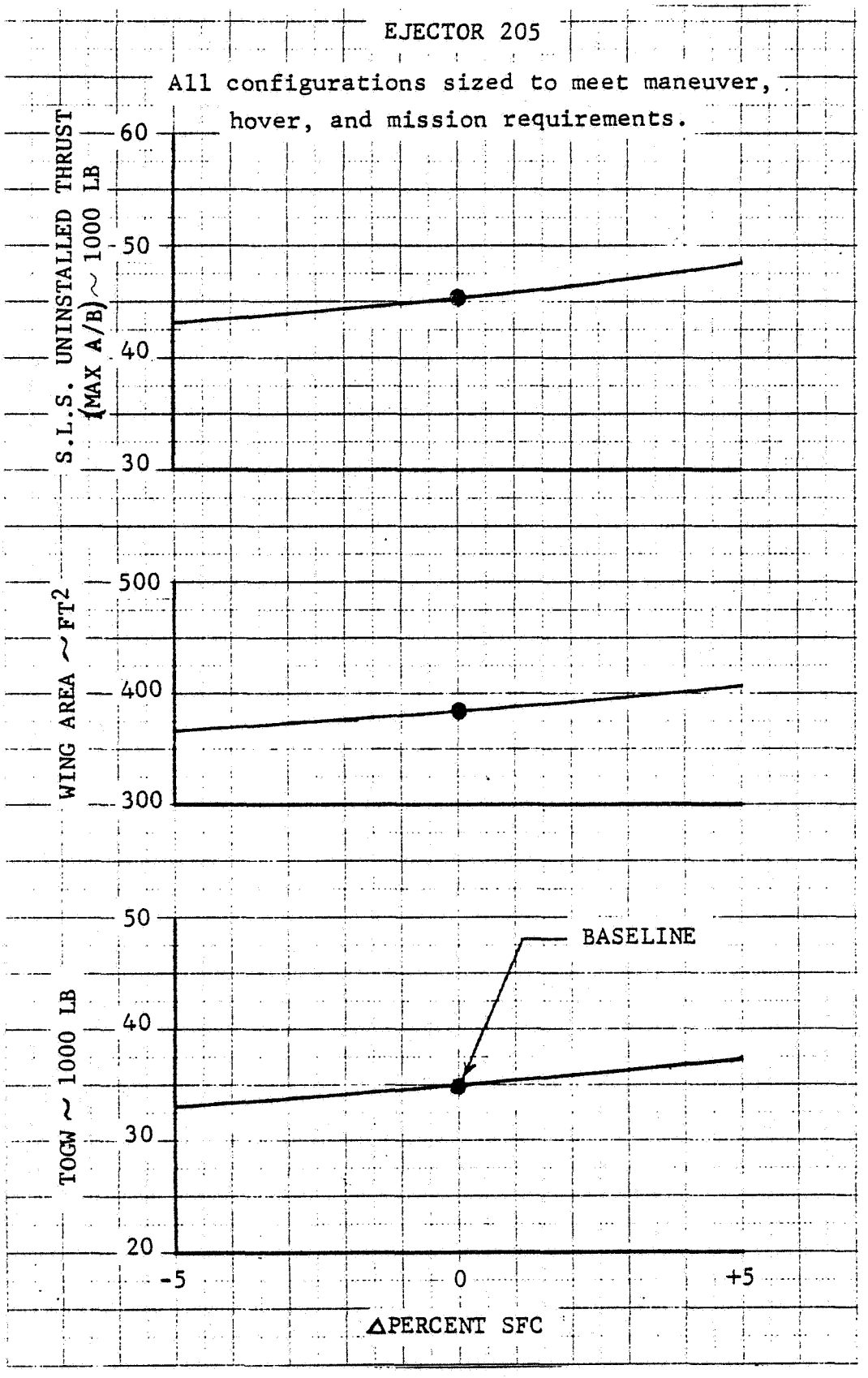

Figure 7-19 SFC Sensitivity

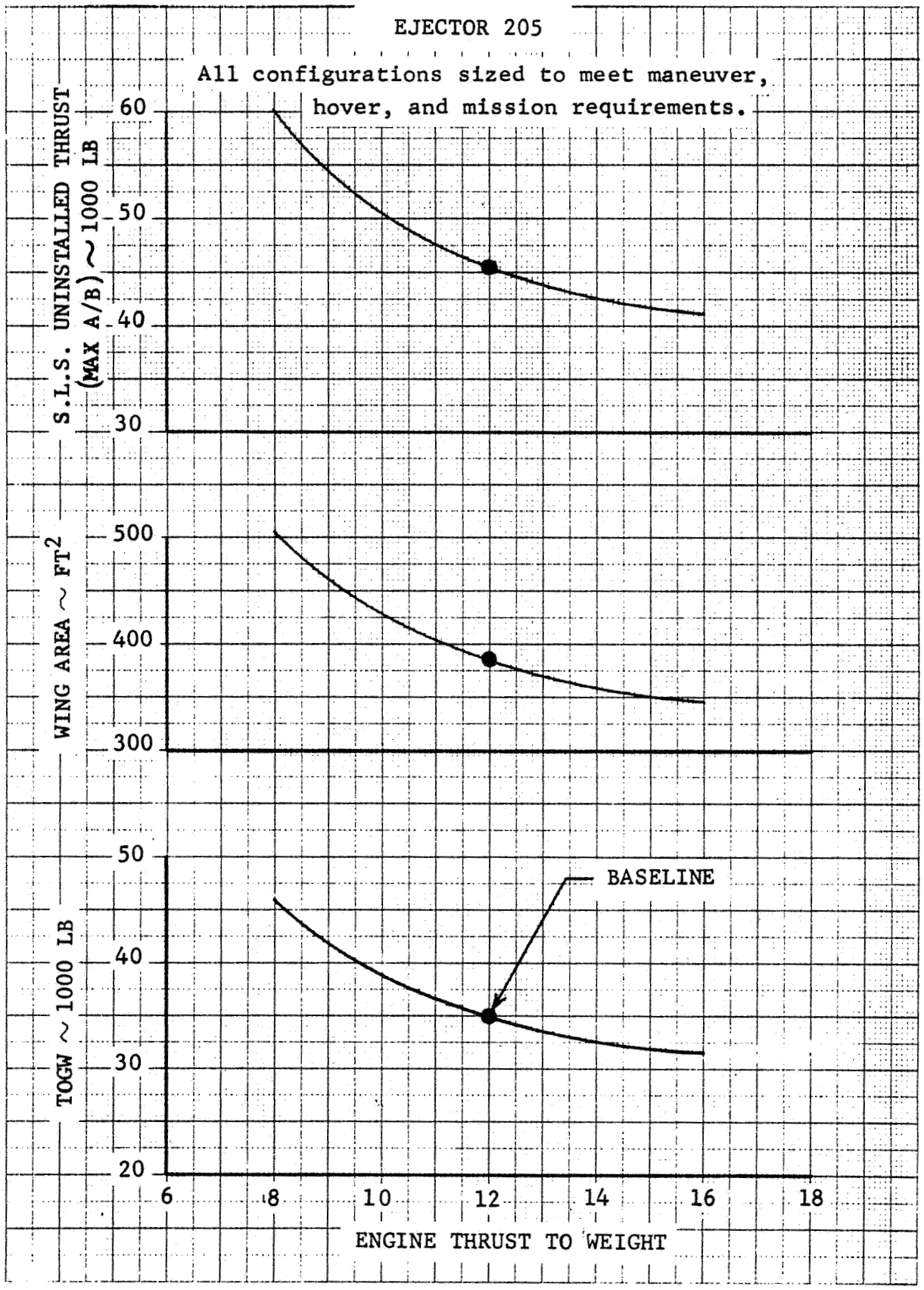

Figure 7-20 Engine Thrust-to-Weight Ratio Sensitivity

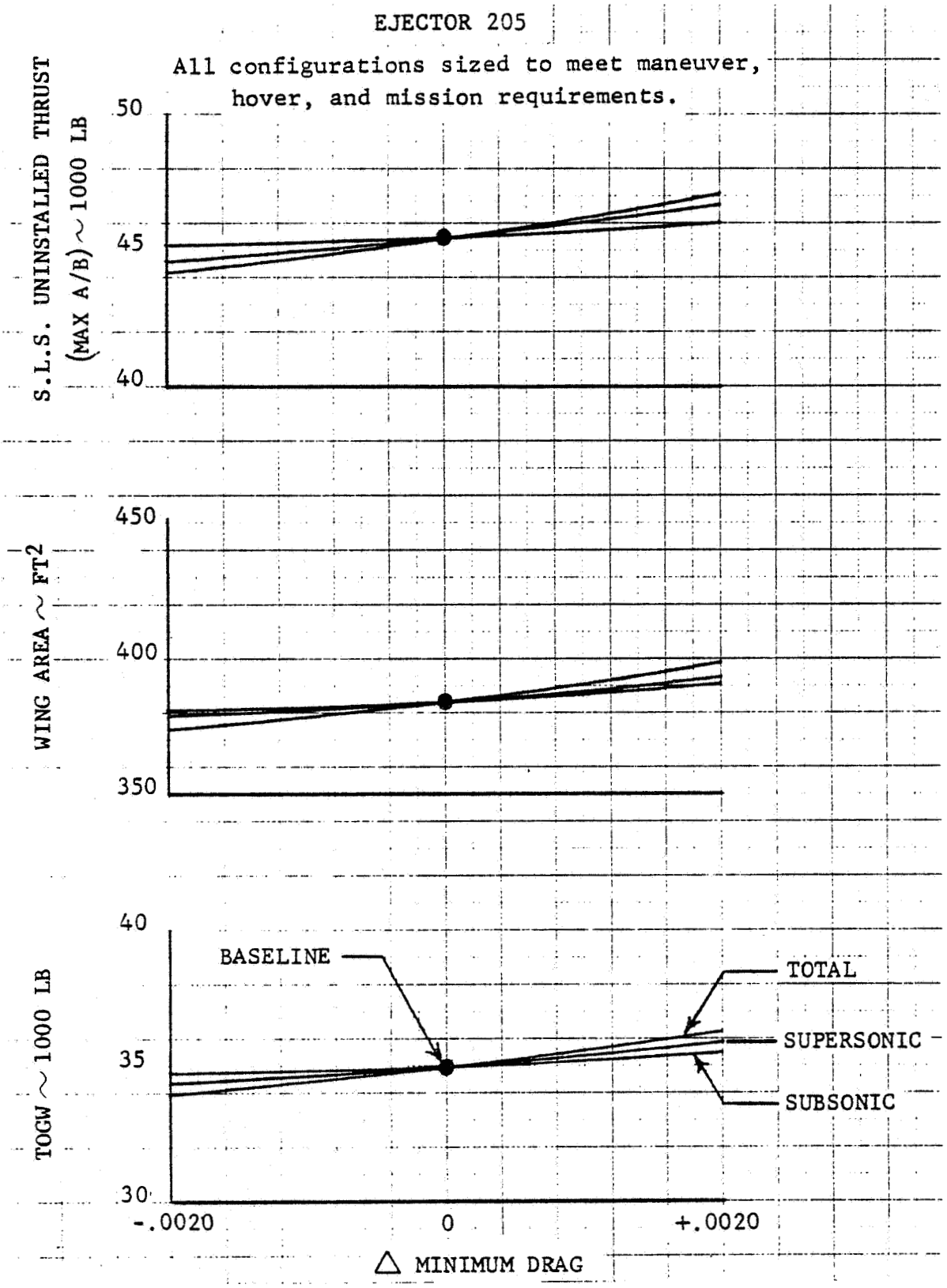

Figure 7-21 Minimum Drag Sensitivity

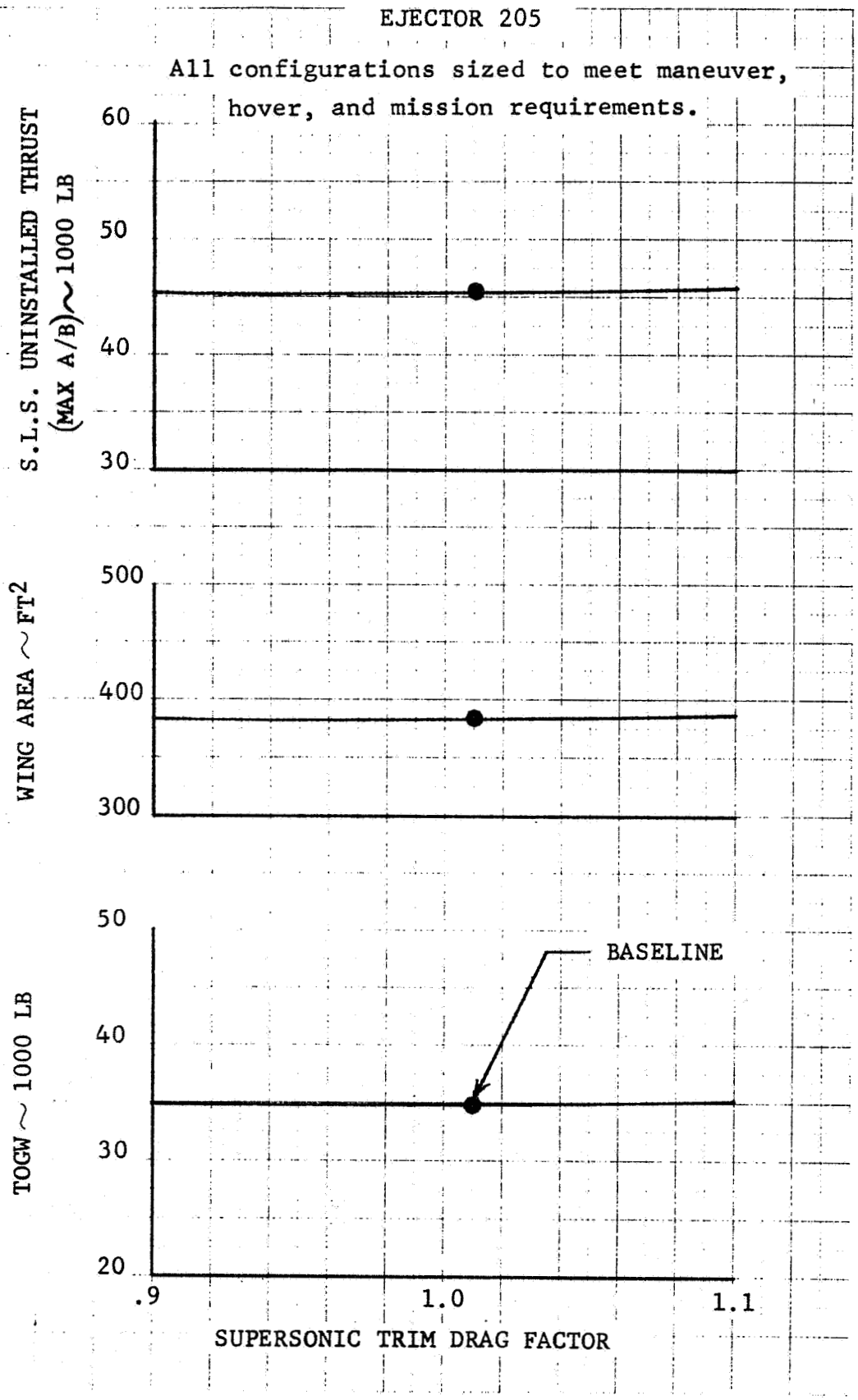

Figure 7-22 Trim Drag Sensitivity

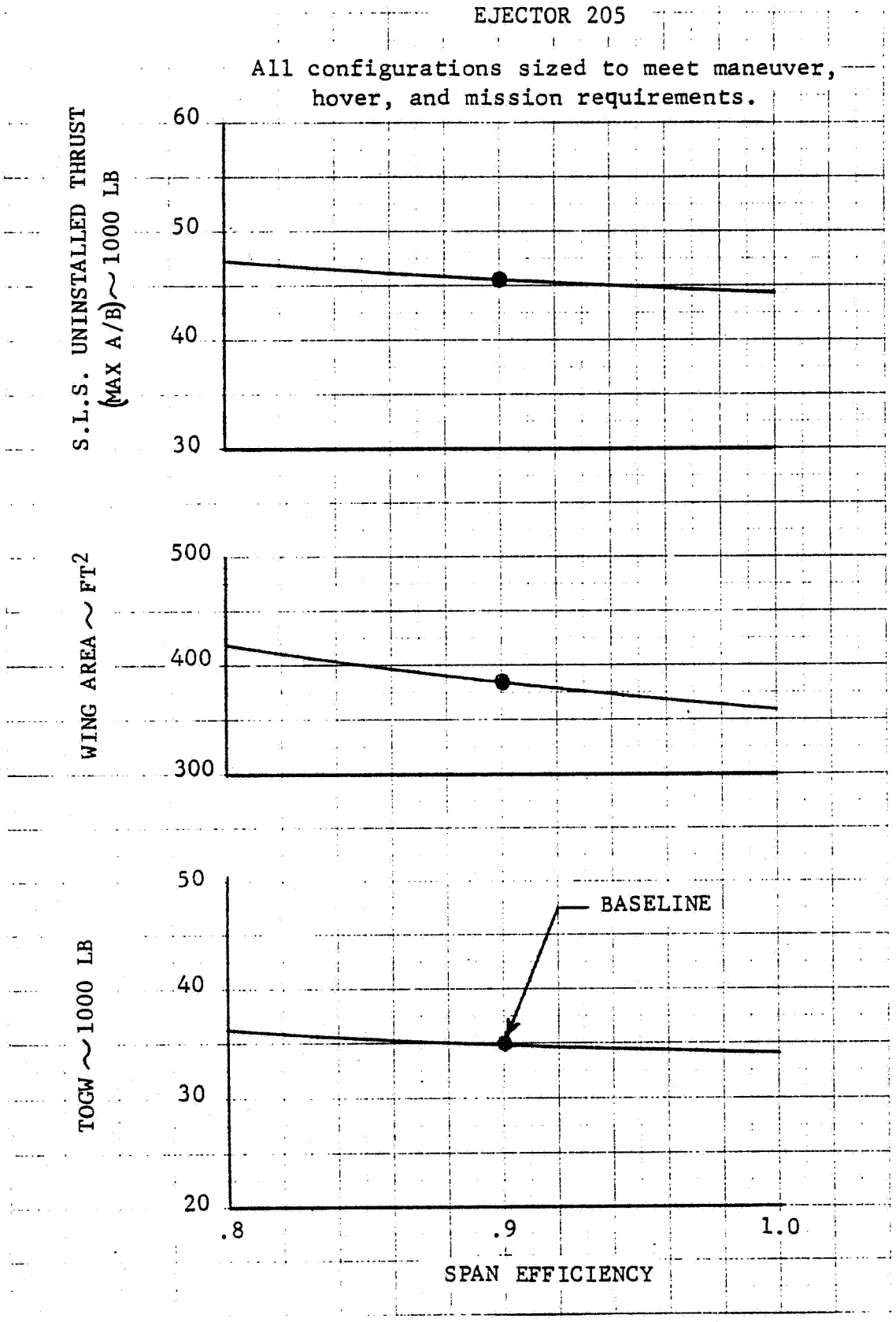

Figure 7-23 Span Efficiency (e) Sensitivity

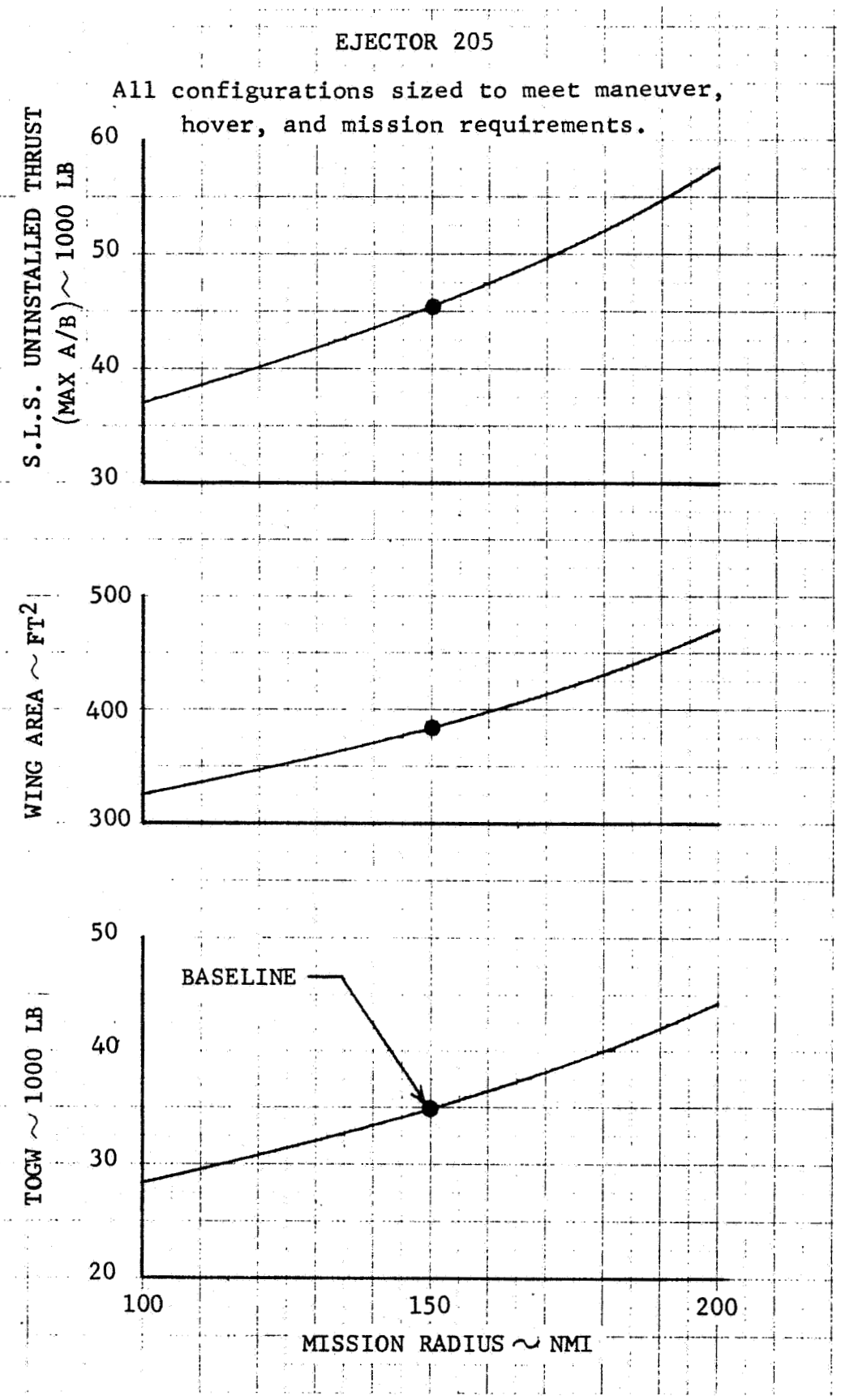

Figure 7-24 DLI Mission Radius Sensitivity

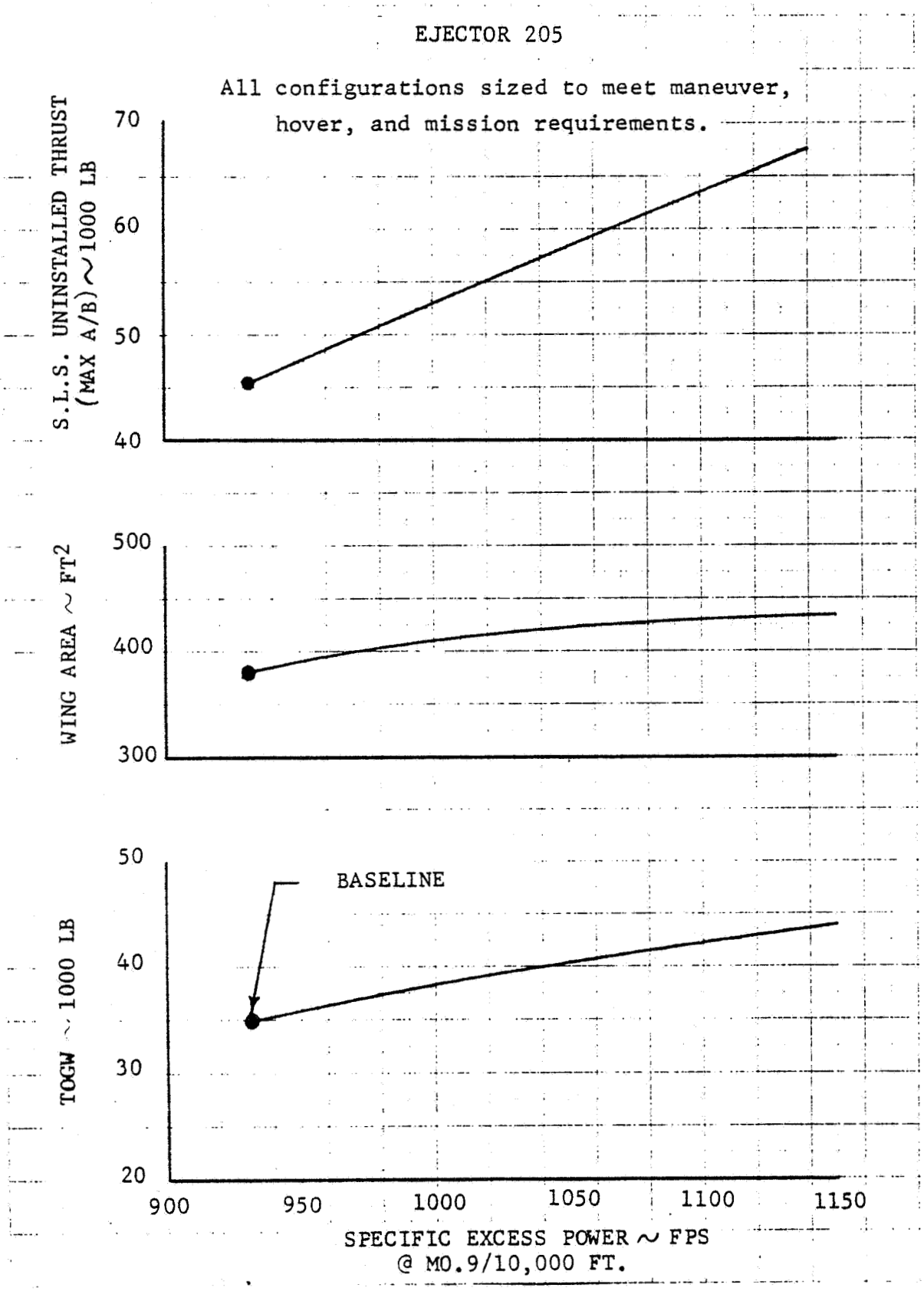

Figure 7-25 Specific Excess Power Sensitivy, Ps, at Mach 0.9, 10,000 Ft

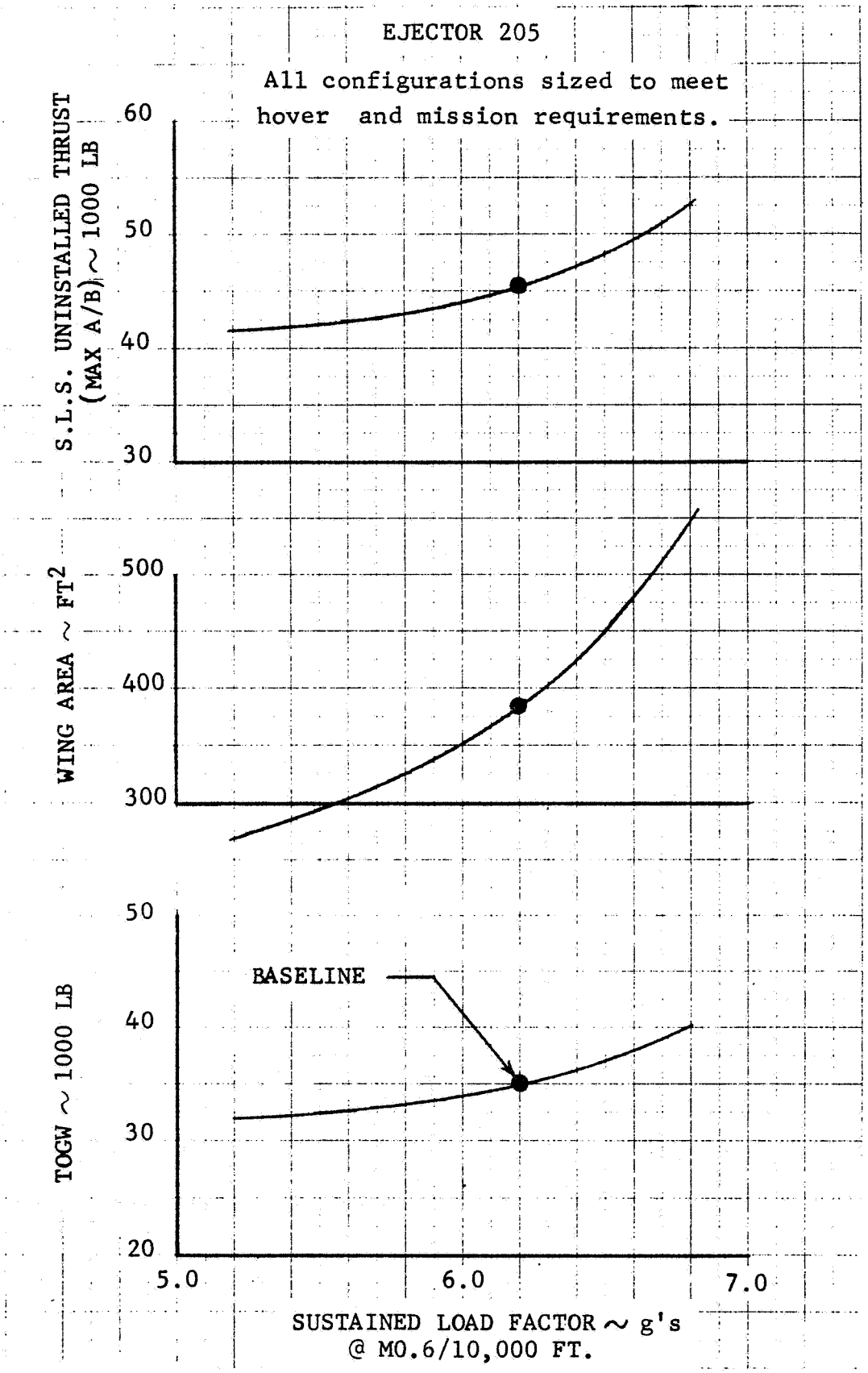

Figure 7-26 Sustained Load Factor Sensitivity, Nz at Mach 0.6, 10,000 ft

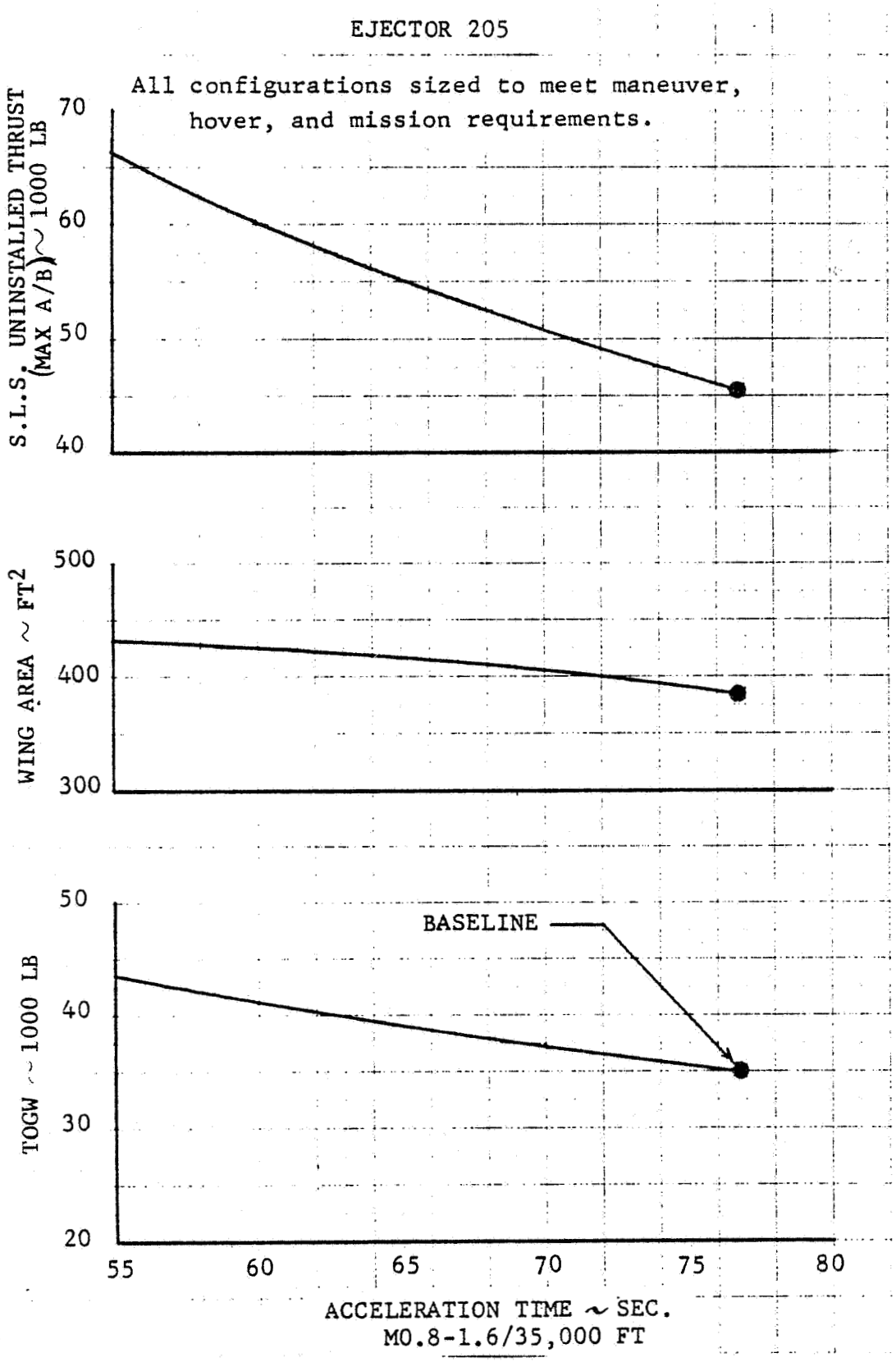

Figure 7-27 Acceleration Time Sensitivity, Time from Mach 0.8 to 1.6, 35,000 ft

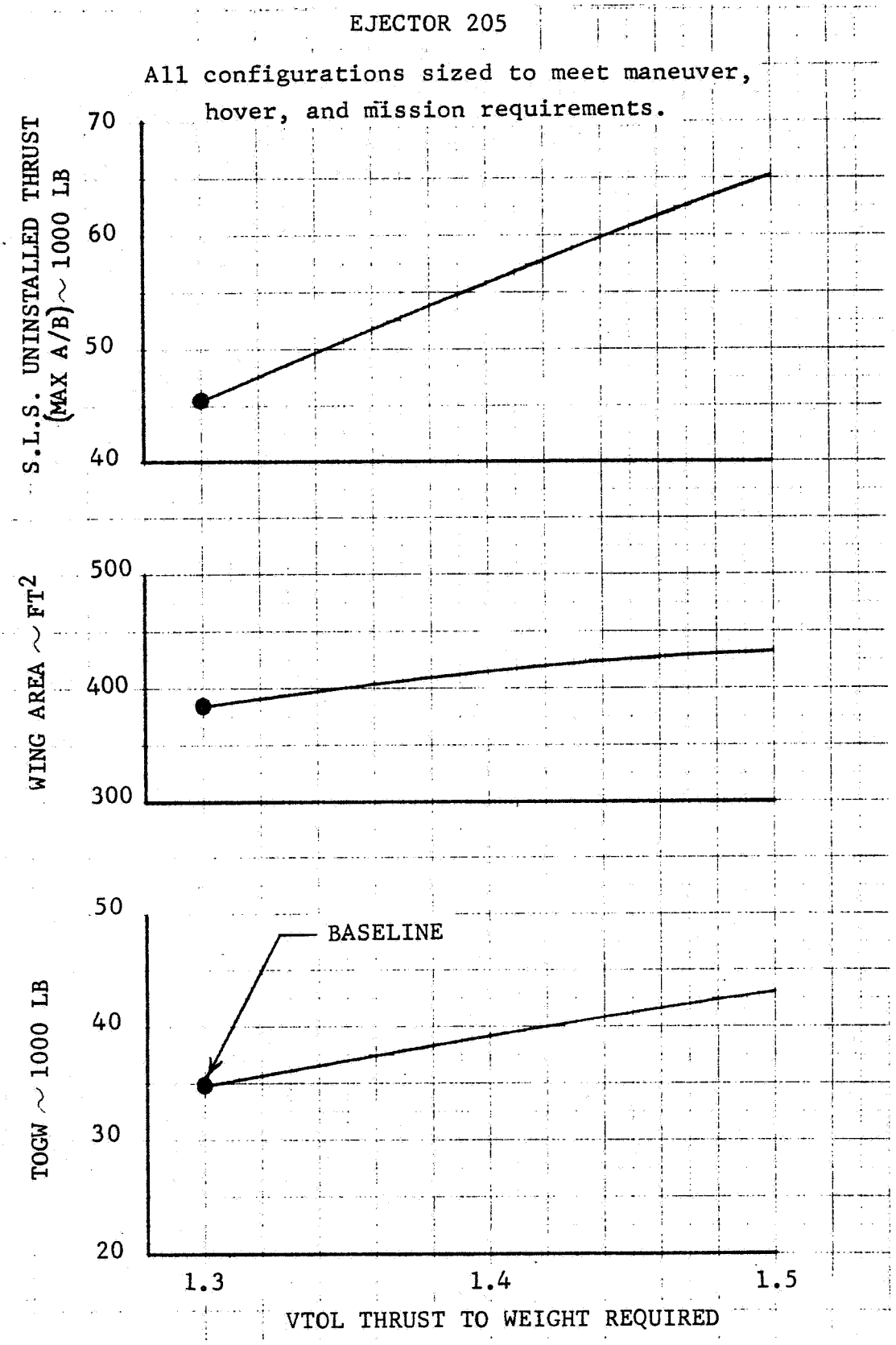

Figure 7-28 Sensitivities to Max A/B, S. L., Static, Uninstalled Thrust/Weight Required for Hover in Ground Effect

Fixed-Weight Items

7-29 Sensitivity to dry-weight variations representative of changes in weight of avionics, structure, guns and ammo, payload, airframe subsystems, etc.

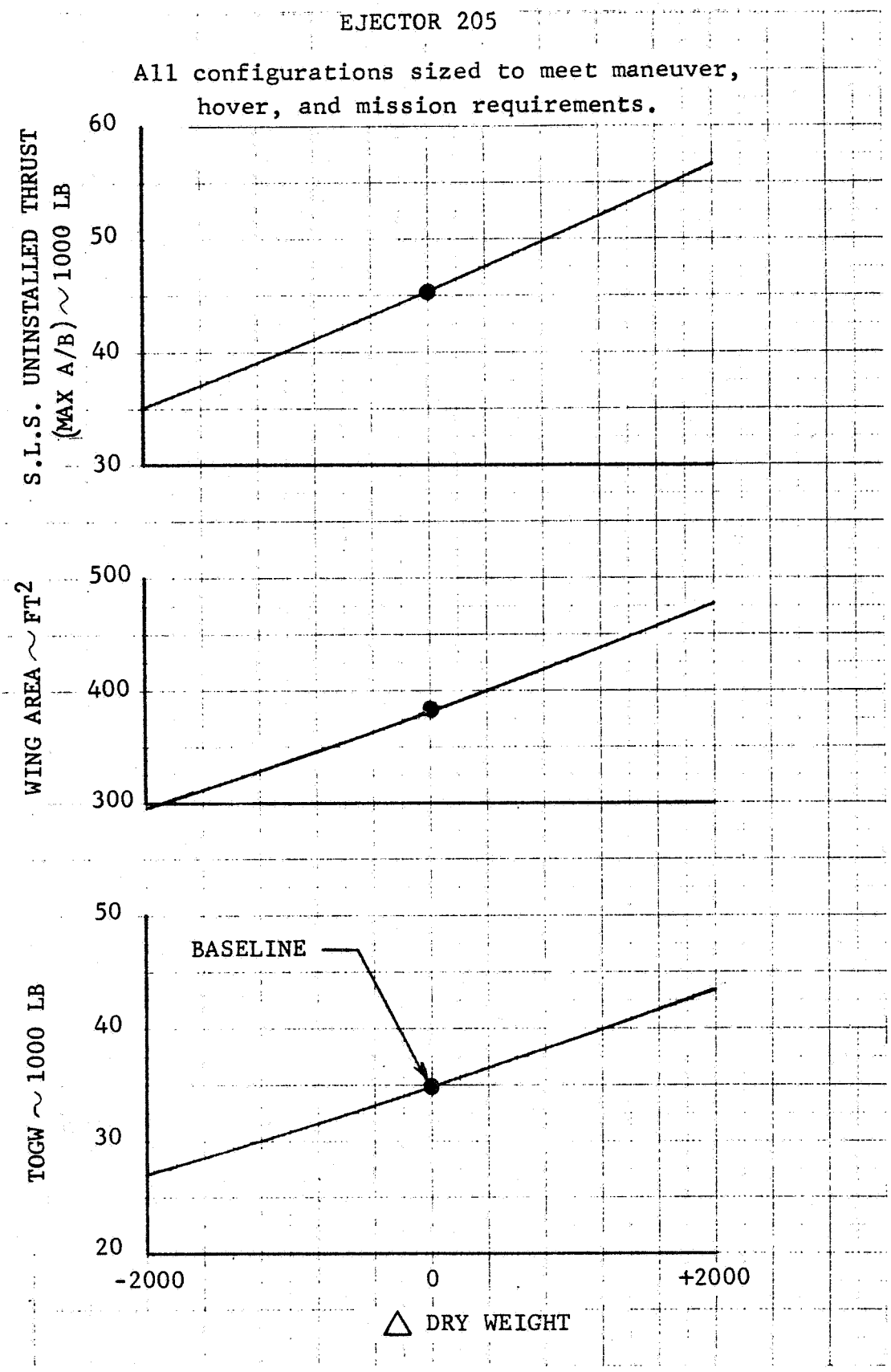

Figure 7-29 Dry Weight Sensitivity

8. AERODYNAMIC UNCERTAINTIES

8.1 Selection

The primary objectives of this study have been to (1) determine which aerodynamic parameters have the biggest effect on the design of the ejector VSTOL fighter/attack aircraft concept, (2) determine whether these parameters can be accurately predicted from analytical methods or existing experimental data and, if they cannot, (3) identify these parameters and define a wind tunnel program for Phase II, which will emphasize resolving these key areas of aerodynamic uncertainty.

The critical aerodynamic parameters that need investigation are obviously the ones that are associated with the design constraints that size the airplane and for which there is a low-confidence level in the predicted value. Table 8-1 shows which aerodynamic parameters are associated with each design requirement. Table 8-2 shows the sizing constraints for ejector/VEO-Wing fighter/attack aircraft that meet various design requirements. (The characteristics of each of these aircraft were described in Table 7-1.)

Therefore, for a given set of design requirements, the critical aerodynamic parameters associated with the sizing constraints are evident from Table 8-1.

The aircraft sensitivities to e, $C_{D_{min}}$, $C_{L_{max}}$, and trim drag for the airplane sized to meet the mission, hover, maneuver, STOL, and transition requirements (E205) presented in Section 7.7 highlight the need for resolving any uncertainties associated with these parameters. Similar sensitivities and rankings of the importance of the aerodynamic parameters could be devised for each combination of design requirements. However, since several of the aerodynamic parameters show up affecting almost all of the design requirements in Table 8-1 (i.e., they would appreciably affect the aircraft sizing no matter what combination of design constraints are selected), they will be the prime targets for the Phase II investigation. These areas of aerodynamic uncertainty are as follows:

TABLE 8-1 AERODYNAMIC PARAMETERS ASSOCIATED WITH VARIOUS DESIGN REQUIREMENTS

AERODYNAMIC PARAMETER	AERODYNAMIC PARAMETERS ASSOCIATED WITH DESIGN REQUIREMENTS						
	MISSION RADIUS	SPECIFIC EXCESS POWER	N_Z SUST	ACCEL* TIME	STO T.O.D.	TRANSITION TIME	HOVER T/W
e			√		√	√	
$C_{D_{min}}$	√	√	√	√	√	√	
Trim Drag	√	√	√	√	√	√	
$C_{L_{max}}$			√		√	√	
C_{m_o}	√	√	√	√	√	√	
a.c.	√	√	√	√	√	√	
Ground Effects					√	√	√
C_L Buffet			√		√	√	
Lateral Directional Charac.			√		√	√	
Eject Perf					√	√	√
Effect on Aero					√	√	
Eject. Ram Drag					√	√	
Supercirculation Benefits	√		√		√	√	

*NOT USED AS A SIZING REQUIREMENT FOR THIS STUDY

TABLE 8-2 SIZING CONSTRAINTS FOR VARIOUS AIRPLANE REQUIREMENTS

AIRPLANE SIZED TO MEET REQUIREMENTS	SIZING CONSTRAINTS
1. Mission	Mission (Fixed Minimum S_W)
2. Mission + Hover	Mission + Hover (Fixed Minimum S_W)
3. Mission + Hover + Maneuver (E205)	Hover + $N_{Z_{Sust}}$ (Maneuver)
4. Mission + Hover + Maneuver + STO	Hover + $N_{Z_{Sust}}$ (Maneuver)
5. Mission + Hover + Maneuver + STO + Transition	Hover + $N_{Z_{Sust}}$ (Maneuver)[1]
6. Mission + Hover + Maneuver + STO + Acceleration	$N_{Z_{Sust}}$ (Maneuver) + Acceleration

[1]Assumed based on point mass transition analysis

1. e

2. $C_{D_{min}}$

3. Trim drag

4. $C_{L_{max}}$

5. C_{m_o}

6. a.c.

7. Buffet onset

8. Lateral/directional characteristics

9. Supercirculation benefits

The Phase II investigation will be structured to determine not only the aerodynamic uncertainties of a particular configuration model but also the effects of design perturbations on these uncertainties which will allow the refinement of the configurations when an understanding and data base are available as design tools. These are the prime goals for Phase II.

8.2 Description

Both the ejector and RALS configurations have large, wide, flat fuselage/strake areas end-plated by nacelles with the primary lifting surfaces located outboard. The aerodynamics for this type of configuration are difficult to predict with existing tools. The unpowered-aerodynamic-test data base approximates the RALS much better than the ejector configuration, but no powered data exists for this separated-nacelle-type configuration.

A reiteration follows of how these areodynamic uncertainties are related to the VEO-Wing/ejector design. While the following discussion focuses primarily on the contractual ejector configuration, E205, many of the comments apply to the in-house RALS configuration due to the similarity in external arrangements.

- e - The optimum e envelopes that can be obtained with canard/VEO-Wing nozzle combinations for trim must be confirmed since the experimental data base does not exist to allow optimizing the canard/VEO-Wing nozzle deflections (especially at transonic speeds). The transonic maneuver performance (and subsequent aircraft sizing) presented in this study are predicated on the assumption that the envelope e's developed for the more stable VEO-Wing fighter configuration (Reference 4) with trim provided by the VEO-Wing nozzle only (i.e., canard fixed) can be duplicated with the canard/VEO-Wing nozzle deflections, which also provide effective augmented instability levels of -18%. The effect of canard location will be examined in this effort as well as the influence of the strake/inner-body region on aerodynamic center and the resulting trimmed e.

- Minimum Drag - Large volumes are required for installation of the vertical-lift ejector system (ejector bays and ducting). As a result, increases in wave drag and friction drag are incurred compared to a conventional takeoff-and-landing (CTOL) configuration. Minimizing the impact of increased cross-sectional area on supersonic wave drag requires considerable experimental configuration tailoring. Integration of the wing/nacelle/strake must be examined experimentally to minimize interference drag at transonic speeds because it is very difficult to predict the flow field and subsequent interference drag between the fuselage body and the nacelles.

- Trim Drag - Trim-drag penalty is critical for transonic maneuvering and the supersonic dash. The effect of canard location and schedule optimization will be investigated, as well as the effect of a.c. on trim drag.

- $C_{L_{max}}$ - Maximum lift coefficient is critical for transonic maneuvering, STOL, and VTOL transitions. The usable $C_{L_{max}}$ is determined by both longitudinal pitching moment and lateral-directional control characteristics at high α, which are virtually impossible to predict with the wide-bodied configuration being studied plus power effects.

- Body/Wing Design for C_{m_o} - During maneuver at transonic speeds, it is desirable to camber the body/wing for a positive C_{m_o} contribution to alleviate the nose-down pitching moments induced by the vectored over-wing nozzles. Without this C_{m_o} contribution, the (larger) positive canard deflections required to trim degrade the configuration transonic maneuver capability. Unfortunately, the E205 configuration, with jet diffuser ejectors installed in the fuselage, precludes the use of a design body camber. (This restriction does not exist for the RALS configuration, which has body camber incorporated.) One possible approach to obtain the desired positive C_{m_o} shift for the ejector configuration is to employ a fuselage beaver tail deflected upward during maneuvers.

- Aerodynamic Center Location - Power-off aerodynamic-center predictions versus Mach number are shown in Figure 4-15 for the ejector configuration (canard off and zero-canard deflection). The estimates are based on the Carmichael method (Reference 9), with a comparison point against the DATCOM method (Reference 10) at Mach 0.4 and zero-canard deflection. There is a significant disparity between the predicted values for the two methods, which must be resolved during Phase II testing.

  It is very difficult to predict the aerodynamic center with either of these methods because of the unusual aspects of the configuration, the wide flat body with separated nacelles, and the relatively blunt forward strake. Also, the variation of aerodynamic center with power setting, angle of attack, and trailing-edge-flap deflection is difficult to estimate with conventional methods. This variation will be investigated during testing with the engine simulators installed.

In addition, the effect of the spanwise blowing on aerodynamic center at low speeds must be investigated experimentally.

- Buffet Characteristics - The close-coupled canard of the E205 configuration is expected to delay the buffet onset to higher angles of attack in much the same way as does the forebody strake on the F-16 aircraft. However, data to substantiate this favorable effect is lacking for canard/wing configurations. An additional increase in angle of attack for buffet onset should result from power-on supercirculation effects. It is desirable to obtain root-bending-moment (C_{rms}) strain-gage data during the wind tunnel tests to verify the estimated configuration buffet characteristics.

- Lateral-Directional Characteristics - Lateral-directional characteristics determine the max and resulting usable $C_{L_{max}}$, which contributes to airplane sizing for transonic maneuvering, STO, and VTOL operations. The effectiveness of the all-moving vertical tail in preserving lateral-directional control at high angles of attack when influenced by the large side flat body and strake of the E205 (or RALS) configurations is difficult to estimate.

- Supercirculation Effects - These are one of the most critical uncertainties of the VEO-Wing/ejector design concept. All of the sizing has been based on VEO-Wing benefits extracted from a research model without widely spaced nacelles. Whether the same benefits will exist with a configuration like E205 is unknown. Powered testing must be done to confirm the expected benefits. These benefits drive the design very hard by forcing the c.g. aft and by producing large instabilities that must be compensated for by sophisticated control systems. The validity of these supercirculation benefits are critical to the transonic maneuvering and STOL performance also.

In addition to the aerodynamic uncertainties outlined above, there are two propulsion-related uncertainties that are critical to the success of this configuration: the propulsion-induced ground effects on the aerodynamics (discussed in Section 4.3) and the achievable ejector augmentation ratio (Section 5.4). Confirmation of the estimated suckdown and fountain ground effects in General Dynamics' Hover Test Facility for both configurations is expected by mid-1978. Back-pressure ground effects on the performance of an initial ejector configuration has been determined by General Dynamics in the testing discussed in Section 5.4 and has been included in this analysis. Since aircraft sizing is heavily influenced by thrust/weight for hover IGE, confirmation of the estimated ground effects is essential. Powered-configuration testing will also be required to determine ground effects with forward speed, which becomes crucial for STOL.

STOL and transition performance benefits from the VEO-Wing concept could be influenced by the ejector flowfield effect on aircraft aerodynamics. No interference effects have been assumed in the current analysis. Powered-ejector wind tunnel tests will be required to determine this influence.

9. PROPOSED RESEARCH PROGRAM

The objective of the proposed research program is to explore as many of the aerodynamic uncertainties identified in Phase I as possible. The aerodynamic uncertainties defined in Section 8.1, will be investigated in Phase II by studying the effects of variation in:

- Minimum drag
- Aerodynamic-center location
- Canard location
- Strake/inner-body region
- Buffet characteristics
- Body/wing design for C_{M_o}
- All-moving vertical tail

The wind tunnel model design and fabrication task, for which the Phase II contract funding level was established, includes the following parts:

1. One nose with built-in canopy and a nose shaft
2. One fuselage centersection
3. One set of lower nacelles
4. One set of upper nacelles
5. Two sets of nozzle plugs
6. One set of exit rakes with 30 tubes each
7. One set of exit rake supports
8. One set of horizontal canards
9. One set of horizontal-canard deflection brackets with capability of four deflections

10. One set of wing spars with provision for removable leading-edge and trailing-edge flaps

11. One set of wing leading-edge flaps

12. Three sets of wing-leading-edge-flap-deflection brackets

13. Four sets of inboard wing trailing-edge flaps

14. Four sets of outboard wing trailing-edge flaps

15. One gun-pod fairing

16. One leveling plate

17. One upper sting cover

18. One lower sting cover

19. One fuselage aft section modified for sting cover

20. One straight sting

21. One tunnel adapter

22. One vertical stabilizer bracket

23. One vertical stabilizer with provision for removable rudder

24. One rudder

25. Two rudder brackets

This parts list is based on the proposed ejector configuration shown in Reference 28. During the Phase I study, certain configuration changes were incorporated that require model parts substitutions. Also, to permit a more fruitful investigation of the aerodynamic uncertainties, a number of additions and deletions to the parts list is desirable. The approach taken is to trade parts in such a manner as to maintain the present Phase II funding level.

The recommended revisions to the parts list are detailed below:

Substitute:

- All-movable vertical tail (zero plus two deflections) for the vertical tail with rudder.

Delete:

- One set of wing leading-edge flaps.
- Three sets of wing-leading-edge-flap-deflection brackets.
- One gun-pod fairing.

Add:

- Root-bending-moment strain gages.
- Alternate forebody strake.
- Alternate forward canard location.

Although the parts mentioned above were deleted to comply with the contracted Phase II funding, it is strongly recommended that the wing leading-edge flaps (with brackets), additional alternate forebody strakes, and multiple canard locations be provided at additional cost.

On the basis of these revisions, the Phase II wind tunnel model will allow exploration of a significant number of the aerodynamic uncertainties. Specifically, these are:

Minimum Drag - Model buildup data will identify component interference drags, as well as cross-sectional-area impact.

Aerodynamic Center Location - The effects on a.c. of the basic and the smaller, alternate forebody strake will be determined. In addition, a.c. differences between the basic aft canard location and the alternate forward location will be assessed.

Canard Location - Increases in control effectiveness for a 36-inch-forward canard movement will be available.

Also, the impact of canard longitudinal movement on close-coupled-canard/wing interactions will be established to study the effects on optimum-envelope e's and trim drag.

Strake/Inner-Body Region - The alternate forebody strake will permit data to be acquired showing the effects of strake size/geometry on lateral-directional characteristics and aerodynamic-center variation with angle of attack.

Buffet Characteristics - Root-bending-moment strain-gage (C_{rms}) data will be obtained to verify buffet-onset estimates and to establish buffet-intensity levels.

All-Moving Vertical Tail - Control authority and lateral-directional effectiveness of the all-moving vertical tail will be determined. Of the three remaining areas of aerodynamic uncertainty - relaxed static stability, body/wing design for C_{MO}, and ground effects - the latter cannot be investigated directly by use of the Phase II wind tunnel model. The question to be answered regarding relaxed static stability involves the maximum instability allowable for an aircraft of the E205 type. While various levels of longitudinal instability can be demonstrated in the wind tunnel through canard movement or forebody-strake geometry changes, the extent of allowable instability will be established by control-system design considerations (response times, damping factors, etc.).

The E205 concept, with fuselage-located longitudinal jet-diffuser ejectors, does not readily permit body cambering for positive C_{MO}. One possibility is to up-rig the aft fuselage (e.g., 3 degrees) with the break between the forward and aft ejector bays. However, this effect on C_{MO} (and drag) would best be investigated by use of a vertical-tail sting mount. The current Phase II effort provides only for the fabrication of a straight sting.

The experimental determination of ground effects requires a dedicated model specifically designed for this purpose. General Dynamics' Fort Worth Division, using in-house funding, recently concluded ground-effects testing of an E205-type ejector configuration. This effort is discussed in Section 4.3.

For the follow-on powered-model tests with the XM2R engine simulator installed, a vertical-tail sting mount is preferred, although not currently funded, as noted above. The wide fuselage of the E205 configuration lessens the influence of the aft-end-modification/straight-sting presence on power-induced effects. As such, the straight sting may prove to be acceptable for the powered test phase. Another positive factor for the straight sting is that power-on effects on lateral-directional characteristics could be investigated.

Added-Cost Model Capabilities. Two additional items are attractive for testing, but the cost of required model parts is beyond the scope of the present Phase II funding. These items and approximate total implementation costs are:

- Canard leading-edge and trailing-edge flaps, $11,000
- RALS configuration simulation, $24,500

Canard leading-edge and trailing-edge flaps on the all-movable canards ($\delta_C = +20^o$) would increase the control effectiveness of these surfaces at low speeds. The flapped canard is one variable that needs to be investigated before optimization of canard/trailing-edge-flap schedules can be determined.

The approach for simulating the RALS configuration, shown in the sketch of Figure 9-1, involves the fabrication of a new fuselage center-section, a new aft fuselage section, and a set of reduced-width strakes. The forward-canard location is provided for under the present Phase II funding. The additional $24.5K required for the RALS simulation represents only 12% of the total Phase II dollars. In effect, data for a second configuration with a reduced-width nacelle could be obtained for a fraction of the cost of the E205 model. The exposed wing panels of the ejector configuration are retained for the RALS simulation.

Run Program. A recommended run program for initial unpowered testing of the Phase II E205 model (flow-through nacelles) is provided in Table 9-1. For later powered testing with the engine simulators installed, this run program would basically be repeated (except component buildup would be excluded and other reductions in scope would be made as dictated by power-conservation considerations). Three power settings (NPRs) are recommended for each test configuration

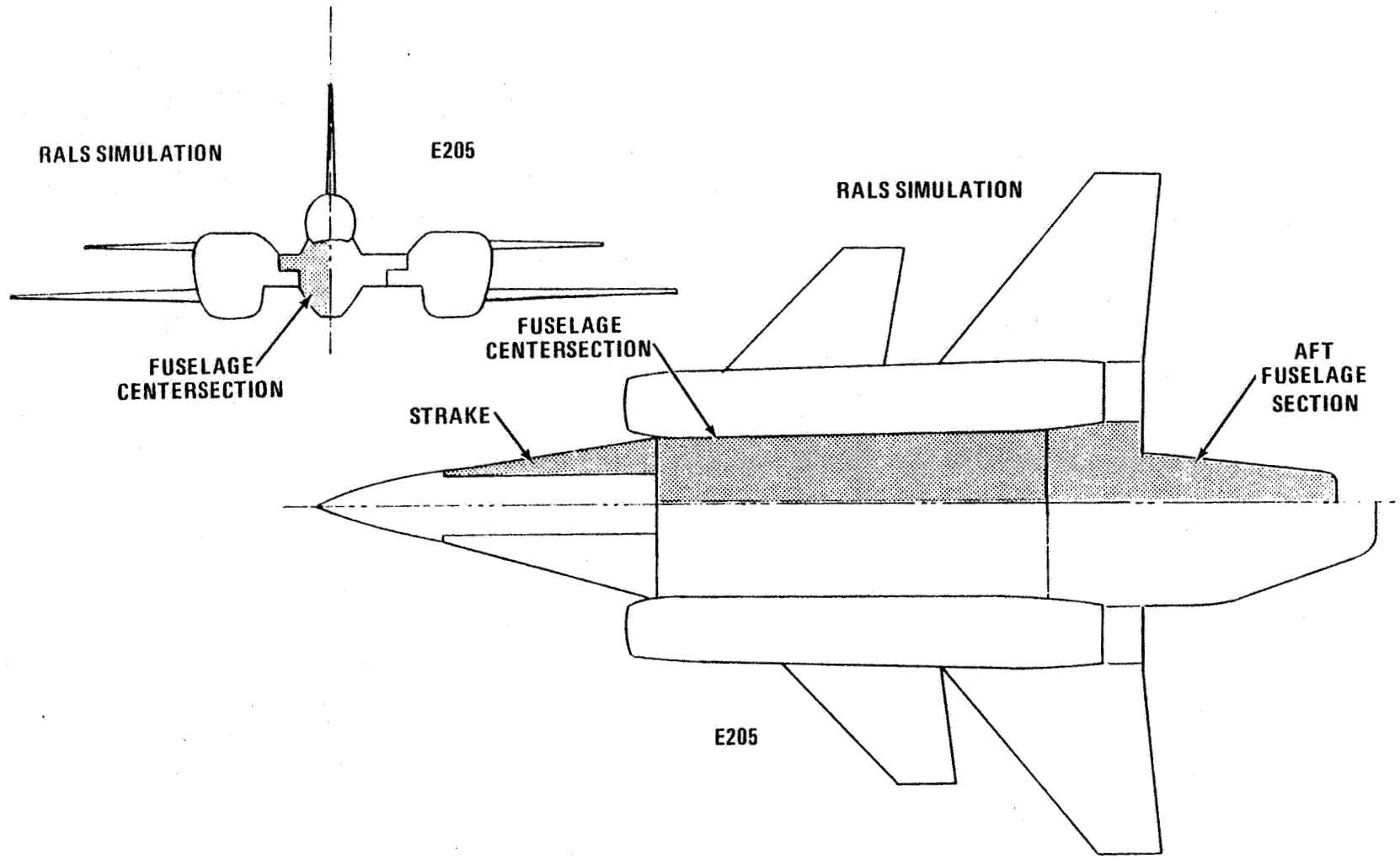

Figure 9-1 Approach for Simulating the RALS Configuration for Use of the E205 Wing Tunnel Model

Table 9-1 Proposed Wind Tunnel Test Program

CONFIGURATION	δ_{VT}	δ_{TE} INB'D	δ_{TE} OUTB'D	δ_C	α	β	12-FT .2	12-FT .4	11-FT MACH NUMBER .6	.8	.85	.9	.95	1.1	1.2	9x7-FT 1.6	1.8	2.0	REMARKS
Basic	0	0	0	0	V	0	P	P	P	P	P	P	P	P	P	P	P	P	Rake
					V	0	P	P	P	P	P	P	P	P	P	P	P	P	inverted
					V	0	P	P	P,B	P,B,O	P,B	P,B,O	P,B,O	P,B	P,B,O	P	P	P	
				0	0,10,15	A	Y	Y		Y		Y			Y	Y		Y	
Canard Off				OFF	V	0	P	P	P,B	P,B,O	P,B	P,B,O	P,B,O	P,B	P,B,O	P	P	P	
				OFF	0,10,15	A	Y	Y		Y		Y			Y	Y		Y	
Basic				10	V	0	P	P	P	P		P			P	P		P	
				20			P	P	P	P		P			P				
				-10			P	P	P	P		P			P	P		P	
				-20			P	P	P	P		P			P				
Canard Forward 36"	0	0	0	0	V	0	P	P	P,B	P,B	P,B	P,B,O	P,B	P,B	P,B	P		P	
				0	0,10,15	A	Y	Y		Y		Y			Y	Y		Y	
				10	V	0	P	P	P	P		P			P	P		P	
				20			P	P	P	P		P			P				
				-10			P	P	P	P		P			P	P		P	
				-20			P	P	P	P		P			P				
Basic	0	5	5	OFF	V	0			P	P		P			P				TE Flap Effects
				0					P	P		P			P				
				10					P	P		P			P				
				20					P	P		P							
				-10					P	P		P			P				
				-20					P	P		P							
		15	15	OFF			P	P	P	P		P							
		15	15	OFF	0,10,15	A	Y	Y		Y		Y							
Basic	0	15	15	0	V	0	P	P	P	P		P							
				0	0,10,15	A	Y	Y		Y		Y							
				10	V	0	P	P	P	P		P							
				20	V	0	P	P	P	P		P							
				20	0,10,15	A	Y	Y		Y		Y							
				-10	V	0	P	P	P	P		P							
				-20	V	0	P	P	P	P		P							
				-20	0,10,15	A	Y	Y		Y		Y							
		30	30	OFF	V	0	P	P	P	P									
				0			P	P	P	P									
				10			P	P	P	P									
				20			P	P	P	P									
				-10			P	P	P	P									
				-20			P	P	P	P									
Vert. Tail Off	OFF	0	0	0			P	P	P	P		P			P	P		P	
	OFF				0,10,15	A	Y	Y	Y	Y		Y			Y	Y		Y	
Basic	5				V	0	P	P	P	P		P			P	P		P	
	5				0,10,15	A	Y	Y	Y	Y		Y			Y	Y		Y	
	10				V	0	P	P	P	P		P			P	P		P	
	10				0,10,15	A	Y	Y	Y	Y		Y			Y	Y		Y	
Alt. Forebody Strake	0	0	0	0	V	0	P	P	P	P		P			P	P		P	
					0,10,15	A	Y	Y	Y	Y		Y			Y	Y		Y	
Body + Nacelles	0	0	0	OFF	V	0	P	P	P	P		P			P	P		P	Wing Off
					0,10,15	A	Y	Y	Y	Y		Y			Y	Y		Y	
Body Only					V	0	P	P	P	P		P			P	P		P	
					0,10,15	A	Y	Y	Y	Y		Y			Y	Y		Y	
Basic	0	0	30/0	0	V	0	P	P	P	P		P			P	P		P	Roll Control
			30/15				P	P	P	P		P			P	P		P	
			30/-30				P	P	P	P		P			P	P		P	
				+10/-10			P	P	P	P		P							
				0			P	P	P	P		P			P	P		P	

DATA TYPE BEING TAKEN: P = pitch, Y = yaw, O = oil flow, B = buffet

v = variable

variation. Detailed angle-of-attack and sideslip-angle schedules would be determined at the time of tunnel entry.

10. CONCLUSIONS

An ejector-VEO-Wing VSTOL fighter/attack aircraft has been designed and analyzed to assess the important aerodynamic uncertainties associated with this VSTOL concept. The most important aerodynamic uncertainties, determined as those which most affected the sizing of the aircraft to meet a selected set of ground rules, are as follows:

1. e
2. $C_{D_{min}}$
3. Trim drag
4. $C_{L_{max}}$
5. C_{m_o}
6. a.c.
7. Buffet onset
8. Lateral-directional characteristics
9. Supercirculation benefits

A wind tunnel program has been recommended that will allow investigation of these uncertainties. Modifications to the proposed model have also been suggested that will allow an investigation of a RALS/VEO concept for little additional funding. A comparison of the ejector and RALS configuration has also been suggested.

Significant conclusions of this analysis are:

1. The ejector/VEO-Wing VSTOL configuration presented in this study is a feasible cold-deck-environment concept for attaining the performance levels sought for a 1990 IOC Navy fighter/attack aircraft. The configuration is <u>very</u> complex requiring blending of the aerodynamic, propulsion, and control systems to provide the necessary characteristics to

achieve the desired performance. This is, however, characteristic of <u>any</u> VSTOL airplane capable of providing acceptable VTOL, mission, maneuver, and STOL performance.

As indicated above, there are a great number of aerodynamic uncertainties associated with this concept that have significantly affected the design and sizing and that should be investigated in a wind tunnel test program. There are also a number of other key uncertainties that cannot be investigated in a wind tunnel test program but that will have pronounced effects on the success of this concept. Most notable among these are induced ground effects and installed ejector performance including effects of forward speed and angle of attack.

2. Combining the VEO-Wing and ejector concepts forces the airplane to have a c.g. very far aft (to minimize the moment produced by the VEO-Wing nozzle) while the real estate required to house the ejectors (lying ahead of the c.g.) produces a very unstable airplane at low speeds; this instability is reduced to an acceptable level by use of the FCS, which schedules the canard and VEO-Wing nozzle deflections with angle of attack and Mach number.

3. Since VEO-Wing configurations are basic thrust elements to control attitude, the total control system integrates the propulsive elements and the aerodynamic control elements into the basic control system. The airplane, thus controlled, must meet the performance goals as well as exhibit satisfactory flying qualities. This requires analysis in both the frequency and time domain to ensure that the optimum control-system configuration results.

4. The STO analysis performed in the study indicates that dynamic effects and trim characteristics are critical to an accurate determination of performance. Required takeoff distances and times are so short (400 ft in 5 seconds) that the dynamics of the control systems, landing gear, aerodynamic, and propulsion responses

must be included to obtain accurate results.

5. Although a point-mass analysis of the VEO transition indicated the transition was well within the targeted time of 60 seconds, the detailed STOL analysis has revealed that the VTO transition should be re-examined, paying close attention to trim requirements. It is expected that transition can be demonstrated with this more rigorous analysis.

6. Comparisons between the RALS and ejector VEO-Wing VSTOL fighter/attack concepts sized to do the mission, hover, and maneuver-performance requirements indicate that the ejector airplane VTOGW may be about 7% greater than the RALS. Considering the magnitude of the hot-footprint problems associated with the RALS (and other afterburning VTOL concepts), the moderate ejector weight penalty may prove to be a favorable trade.

7. The VEO-Wing configuration general arrangement applies to several types of vertical-lift systems, i.e., lift plus lift cruise as well as ejector or RALS. The use of the VEO-Wing concept in conjunction with a forward-located vertical-propulsive/lift system yields a configuration with a superior STOL performance capability.

11. REFERENCES

1. Advanced V/STOL Fighter/Attack Aircraft Pre-Concept Formulation Study, General Dynamics Fort Worth Division Report NAV-GD-006, March 1978.

2. Alperin M., Wu, J.J., and Smith, C.A., The Alperin Jet-Diffuser Ejector. Testing and Performance Verification Report, NWC TP 5853, February 1976.

3. Woodrey, R.W., et al. An Experimental Investigation of a Vectored-Engine-Over-Wing Powered-Lift Concept, AFFDL-TR-76-92, Volumes I and II, September 1976.

4. Heim, E.R., Basic Aerodynamic Data for a Vectored-Engine-Over-Wing Configuration, AEDC-TR-78-1, February 1978

5. Schemensky, R.T., Development of an Empirically Based Computer Program to Predict the Aerodynamic Characteristics of Aircraft, AFFDL-TR-73-144, Vols. 1 and 2, November 1973.

6. Komar, James, Skin Friction Prediction in Turbulent Compressible Flow, AIAA Journal, Vol 4, No. 7, July 1966.

7. Sherrer, H.J., Semi-Empirical Methods for Predicting the Installed Drag of External Stores, General Dynamics Fort Worth Division Report FZA-480, October 1976.

8. Smith, C.W., ed., Aerospace Handbook, General Dynamics Fort Worth Division Report FZA-381-II, October 1972.

9. Carmichael, R.L., Castellano, C.R., and Chen, F.C., "The Use of Finite Element Methods for Predicting the Aerodynamics of Wing-Body Combinations," Analytical Methods in Aircraft Aerodynamics, NASA SP-228, October 1969.

10. Hoak, D.E., USAF Stability and Control DATCOM, October 1960.

11. Ray, Edward J., Techniques for Determining Buffet Onset, NASA TMX2103, November 1970.

12. Dennis, R.J., Transonic Wind Tunnel Tests of a 1/5-Scale Advanced Day Fighter Airplane Configurations ADF401F-5, -5A, -10A, -16, Cornell Aeronautical Laboratory Report No. AA-403-W-15 May 1972.

13. Benepe, D.B., Further Analysis of Buffet Characteristics of a Canard-Delta Aircraft Configuration Based on Wing Bending and Wing Tip Accelerometer Data, General Dynamics Fort Worth Division ARM No. 088, 9 June 1972.

14. Fox, J.K., Analysis of Buffet Characterisics of the YF-16 Aircraft Configuration Based on Wind Tunnel Test Data, General Dynamics Fort Worth Division, AIM No. LWF-020, 10 April 1973.

15. Benepe, D.B., High Angle of Attack Aerodynamics, Part 1: Investigations of YF-16 Lightweight Fighter Prototype Buffet Characteristics, General Dynamics Fort Worth Division Report, ERR-FW-1654, 15 December 1975.

16. Yoshihara, H., Benepe, D.B., and Whitten, P.D., Transonic Performance of Jet Flaps on an Advanced Fighter Configuration, AFFDL TR-73-97, September 1973.

17. Howell, G.A., Further Conceptual Studies of Longitudinal Blowing for Leading-Edge Vortex Enhancement, General Dynamics Fort Worth Division Report, ARM No.104, 29 December 1972.

18. Smith, C.W., et al., The Aerodynamic and Thermodynamic Characteristics of Fountains and Near and Far Field Reingestion Characteristics, To Be Published.

19. Karemaa, A., and Ramsey, J.C., Aerodynamic Methodology for the Prediction of Jet-Induced Lift in Hover, General Dynamics Convair Division Report CASD-ERR-73-012, December 1973.

20. Karemaa, A., Abbreviated Methodology for the Prediction of Jet-Induced Lift in Hover, General Dynamics Convair Division CASD-ERR-74-024, December 1974.

21. Bevilaqua, P.M., Capt., USAF and Toms, H.L., Jr., A Comparison Test of the Hypermixing Nozzle, ARL TR 74-0006, January 1974.

22. Quinn, B., "Recent Developments in Large Area Ratio Thrust Augmentors," AIAA Paper No. 72-1174, November 1972.

23. Bergman, D., A Nozzle/Afterbody Drag Prediction Technique for Isolated Bodies of Revolution at Subsonic Speeds, General Dynamics Fort Worth Division Report ERR-FW-1634, December 1974.

24. Bergman, D., Twin-Engine Nozzle/Afterbody Drag Prediction Procedure, General Dynamics Fort Worth Division Report ERR-FW-1767, December 1976.

25. Whitten, P.D., Kennon, I.G., and Stumpfl, S.C., "Experimental Investigation of a Nozzle/Wing Propulsive Lift Concept," AIAA Paper No. 76-625, July 1976.

26. Jackson, S.K., Jr., Parametric and Point Design Studies of an Advanced Tactical Fighter (U), ASD/XR 72-32, July 1972. (Secret)

27. Stewart, V.R., A Study of Scale Effects on Thrust Augmenting Ejectors, Rockwell International Final Report prepared for NADC, NR76H-2, 1976.

28. Whitten, P.D., Technical Proposal for a Study of Aerodynamic Technology for VSTOL Fighter/Attack Aircraft, General Dynamics Fort Worth Division Report FZP-1871, 25 July 1977.

12. APPENDICES

APPENDIX A

RALS V/STOL FIGHTER/ATTACK

AIRCRAFT CONCEPT

GENERAL DYNAMICS PROPRIETARY INFORMATION

See Volume II

GENERAL DYNAMICS PROPRIETARY INFORMATION

See Volume II

TABLE AA-1 RALS SIZED AIRPLANE CHARACTERISTICS

GENERAL DYNAMICS PROPRIETARY INFORMATION

See Volume II

TABLE AA-2 COMPARISON OF DLI MISSION FUEL USAGE FOR RALS AND EJECTOR CONFIGURATION

APPENDIX B
Aero-Only Aerodynamic Coefficient Prediction

This appendix displays and explains the equations used to estimate the STOL/VTOL aero-only aerodynamic coefficients for the E205 configuration, discussed in Subsection 4.1.2.

These aero-only coefficients were estimated starting with the power-off, wing-body lift, drag, and pitching-moment coefficients of the AFFDL VEO-Wing fighter model (Figure 3-3, Reference 4), are shown in Figure BB-1. Corrections for differences in model and E205 geometry are accounted for in the "change" increments and include effects of body camber and nacelle incidence. The increments for canard deflection and supercirculation due to the powered VEO-Wing flap (and flaperon), derived from General Dynamics Research powered model data of Reference 3, are displayed in Figures BB-2 and BB-3. These increments are applied in the equations below to produce aerodynamic coefficients that do not include any thrust increments[1]. Supercirculation increments for a 30° VEO-Wing flap deflection with spanwise blowing are also shown to illustrate the effects of spanwise blowing.

---

[1] For $\delta_{TE}=0^{\circ}$, $\bar{x}_{cp_{\Gamma}}=.53\bar{c}$ was used for all C_T's

AERO-ONLY COEFFICIENTS BUILDUP

$$C_{L_{AERO}} = C_{L_{WB_{TEST}}} \cdot \frac{S_{W_{E205}}}{S_{W_{TEST}}} \cdot \frac{S_{REF_{TEST}}}{S_{REF_{E205}}} + \Delta C_{L_{CHANGE}} \frac{S_{REF_{TEST}}}{S_{REF_{E205}}} + \Delta C_{L_{CANARD}} \frac{S_{C_{E205}}}{S_{C_{TEST}}} \frac{S_{REF_{TEST}}}{S_{REF_{E205}}} + \Delta C_{L_{FLAP}} \cdot \frac{S_{W_{E205}}}{S_{W_{TEST}}} \cdot \frac{S_{REF_{TEST}}}{S_{REF_{E205}}}$$

$$C_{D_{AERO}} = C_{D_{WB_{TEST}}} \cdot \frac{S_{W_{E205}}}{S_{W_{TEST}}} \cdot \frac{S_{REF_{TEST}}}{S_{REF_{E205}}} + \Delta C_{D_{CHANGE}} \frac{S_{REF_{TEST}}}{S_{REF_{E205}}} + \Delta C_{D_{CANARD}} \frac{S_{C_{E205}}}{S_{C_{TEST}}} \frac{S_{REF_{TEST}}}{S_{REF_{E250}}} + \Delta C_{D_{FLAP}} \frac{S_{W_{E205}}}{S_{W_{TEST}}} \frac{S_{REF_{TEST}}}{S_{REF_{E205}}}$$

$$C_{M_{AERO}} = C_{M_{WB_{TEST}}} \cdot \frac{S_{W_{E205}}}{S_{W_{TEST}}} \cdot \frac{S_{REF_{TEST}} \cdot \bar{c}_{TEST}}{S_{REF_{E205}} \cdot \bar{c}_{E205}} + \Delta C_{M_{CHANGE}} \cdot \frac{S_{REF_{TEST}} \cdot \bar{c}_{TEST}}{S_{REF_{E205}} \cdot \bar{c}_{E205}} + \Delta C_{M_{CANARD}} \frac{S_{C_{E205}}}{S_{C_{TEST}}} \cdot \frac{S_{REF_{TEST}} \cdot \bar{c}_{TEST}}{S_{REF_{E205}} \cdot \bar{c}_{E205}}$$

$$+ \Delta C_{L_{CANARD_{E205}}} \frac{X_{C_{TEST}} - X_{C_{E205}}}{\bar{c}_{REF_{TEST}}} \frac{\bar{c}_{REF_{TEST}}}{\bar{c}_{REF_{E205}}} + \Delta C_{L_{FLAP}} \cdot \frac{X_{CP}}{\bar{c}_{TEST}} \cdot \frac{\bar{c}_{REF_{TEST}}}{\bar{c}_{REF_{E205}}} + C_{L_{AERO}} \cdot \left(cg_{E205} - \text{moment ref.}_{TEST} \right)$$

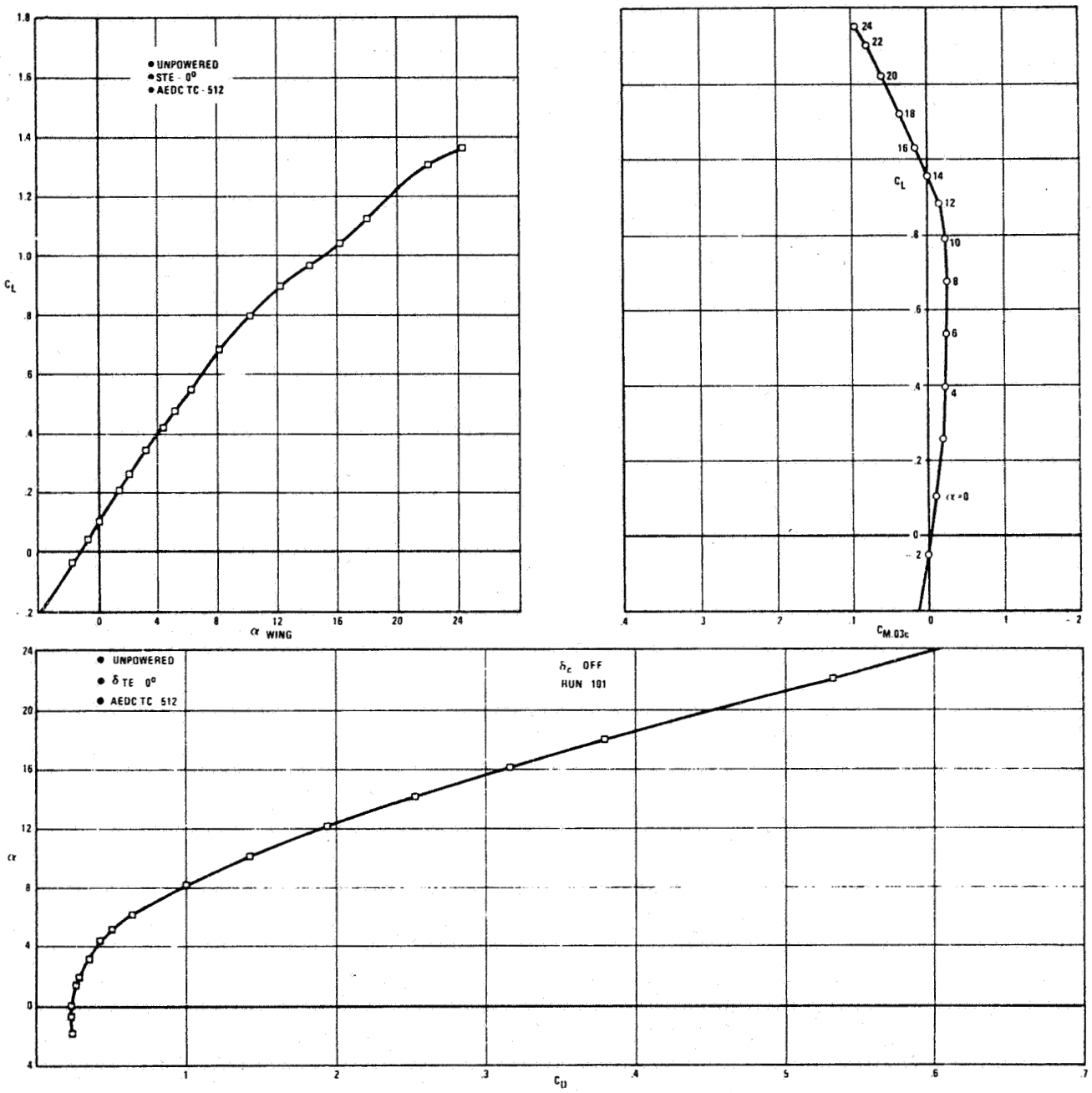

Figure BB-1 Power-Off Wing Body Lift, Drag, and Pitching Moment Characteristics for the VEO-Wing Fighter Model of Reference 4 , Mach = .2

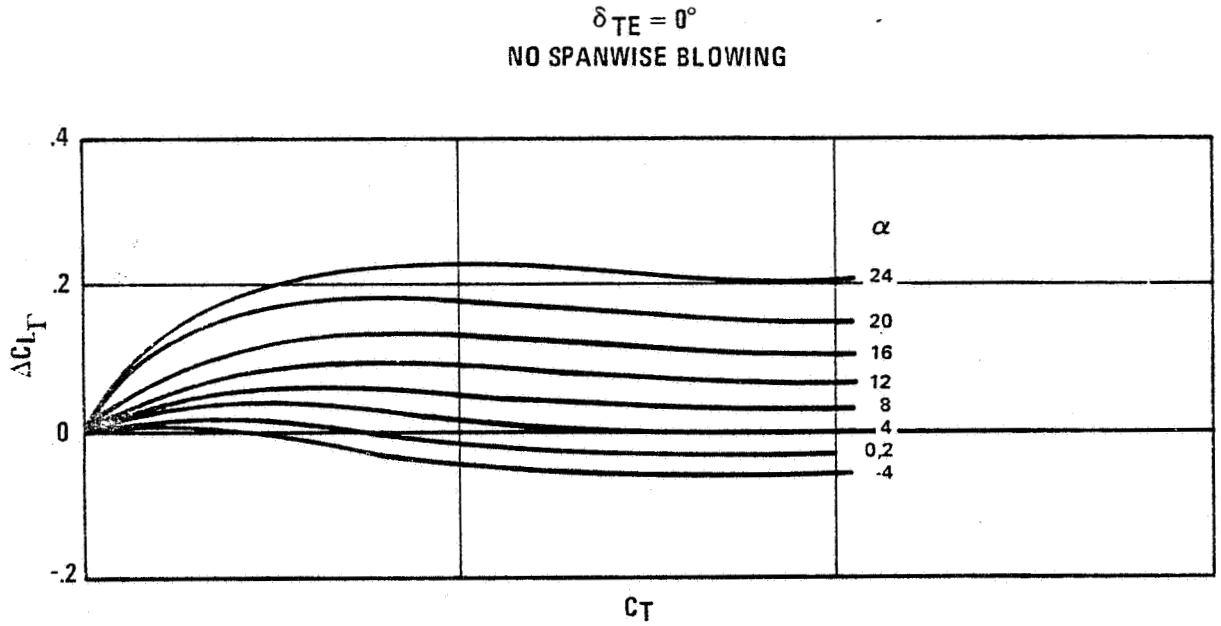

a. ΔC_L vs. C_T $\delta_{TE} = 0°$

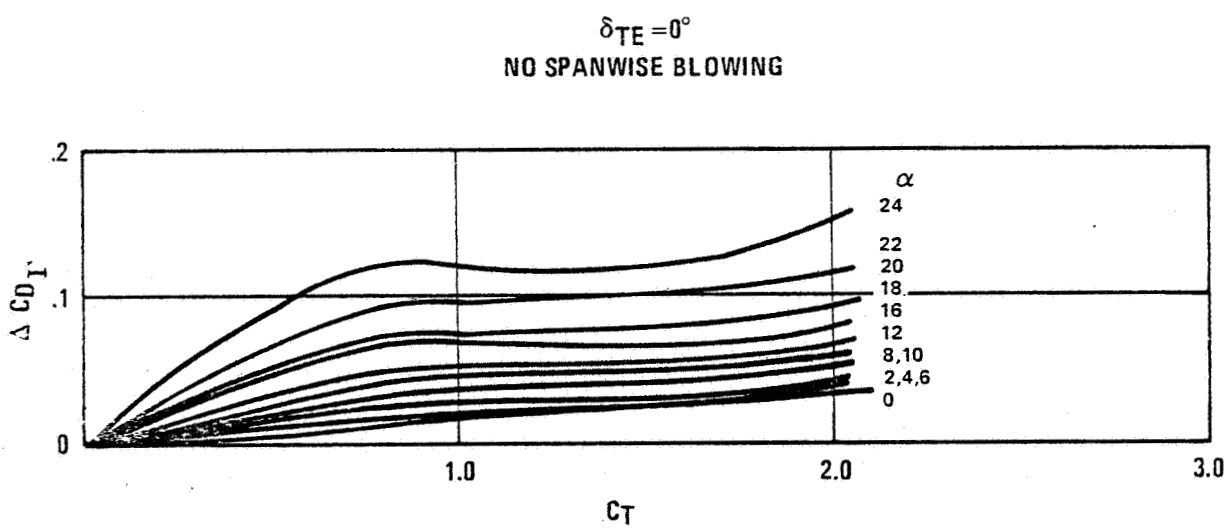

$\bar{X}_{CP_T} = .53\bar{c}$

b. ΔC_D vs. C_T $\delta_{TE} = 0°$

Figure BB-2 Supercirculation Lift, Drag, and Center-of-Pressure-Location Increments Due to VEO-Wing Flap Deflection and Blowing from General Dynamics Powered Research Model of Reference 3, Mach = .2

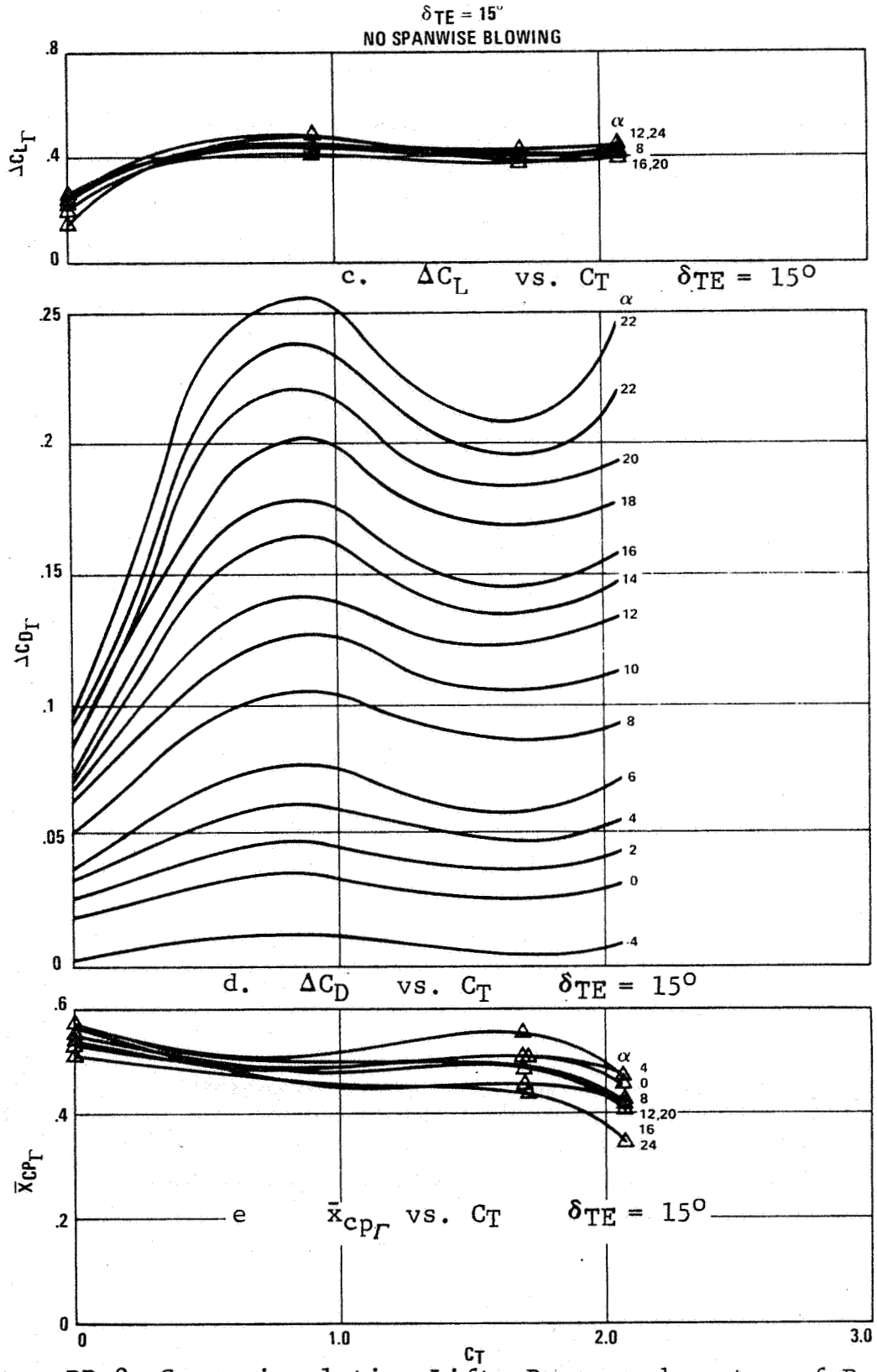

Figure BB-2 Supercirculation Lift, Drag, and center-of-Pressure-Location Increments due to VEO-wing Flap Deflection and Blowing from General Dynamics' Powered Research Model of Reference 3, Mach = .2

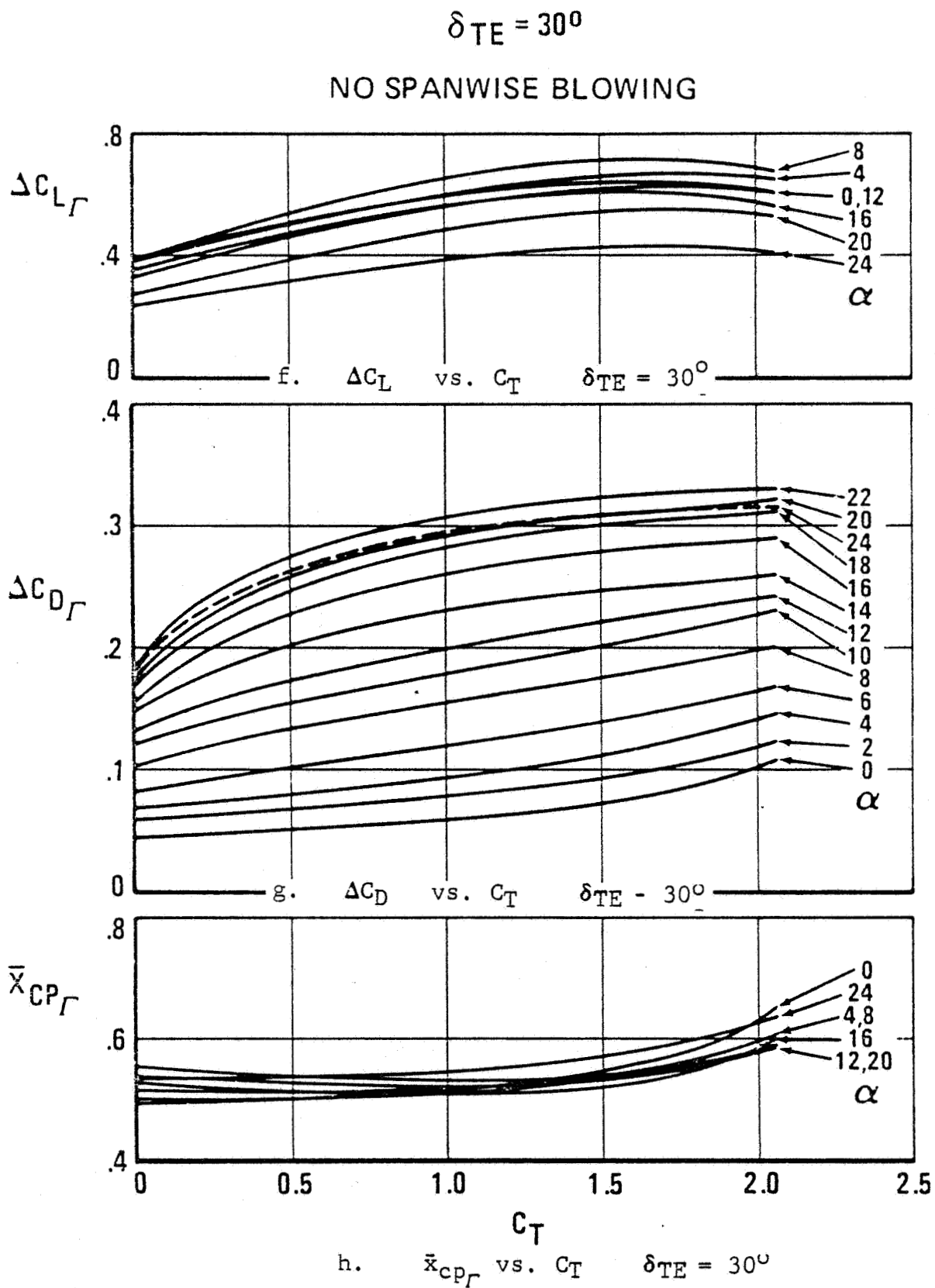

h. $\bar{x}_{cp_\Gamma}$ vs. C_T $\delta_{TE} = 30^\circ$

Figure BB-2 Supercirculation Lift, Drag, and center-of-Pressure-Location Increments due to VEO-wing Flap Deflection and Blowing from General Dynamics' Powered Research Model of Reference 3, Mach = .2

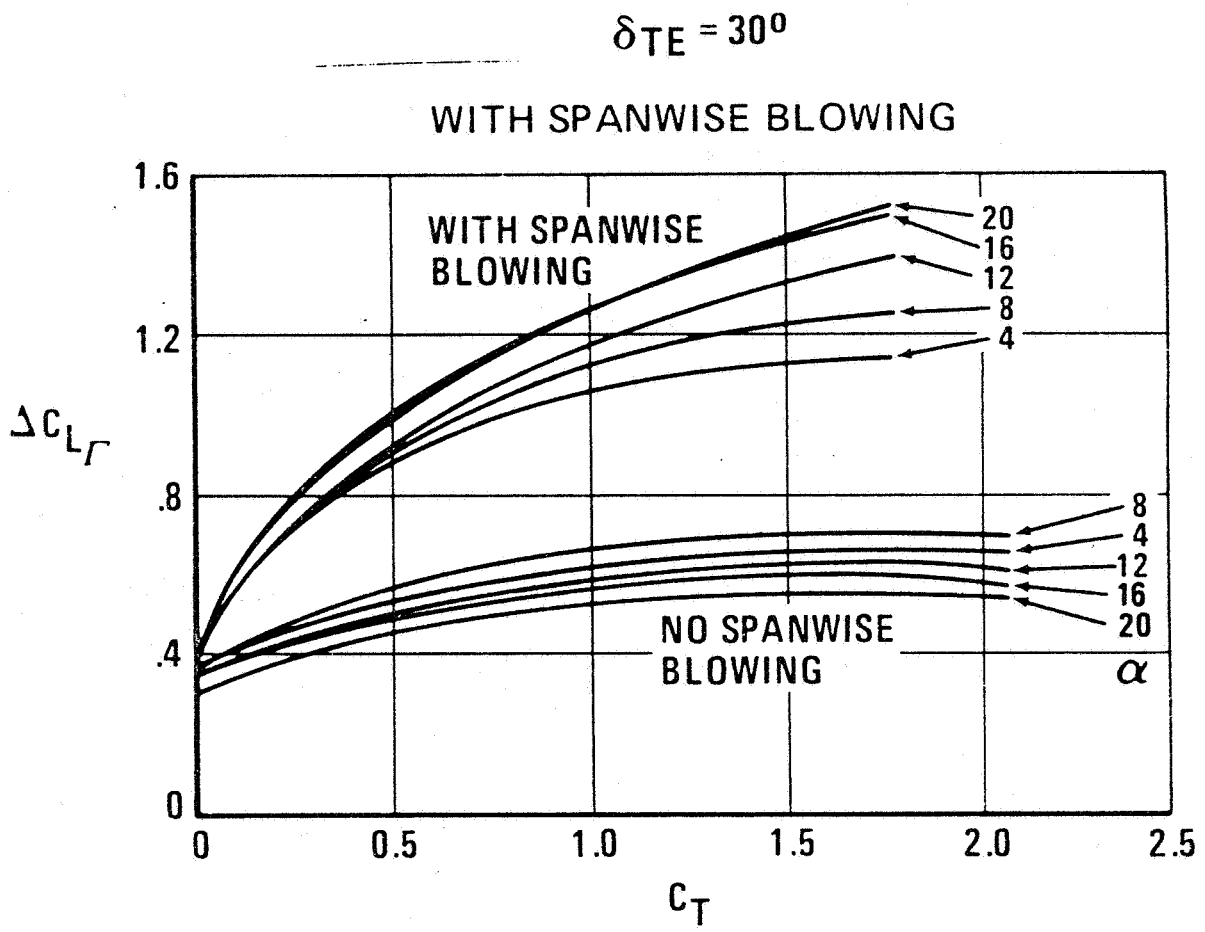

i. ΔC_L vs. C_T $\delta_{TE} = 30^o$ with Spanwise Blowing

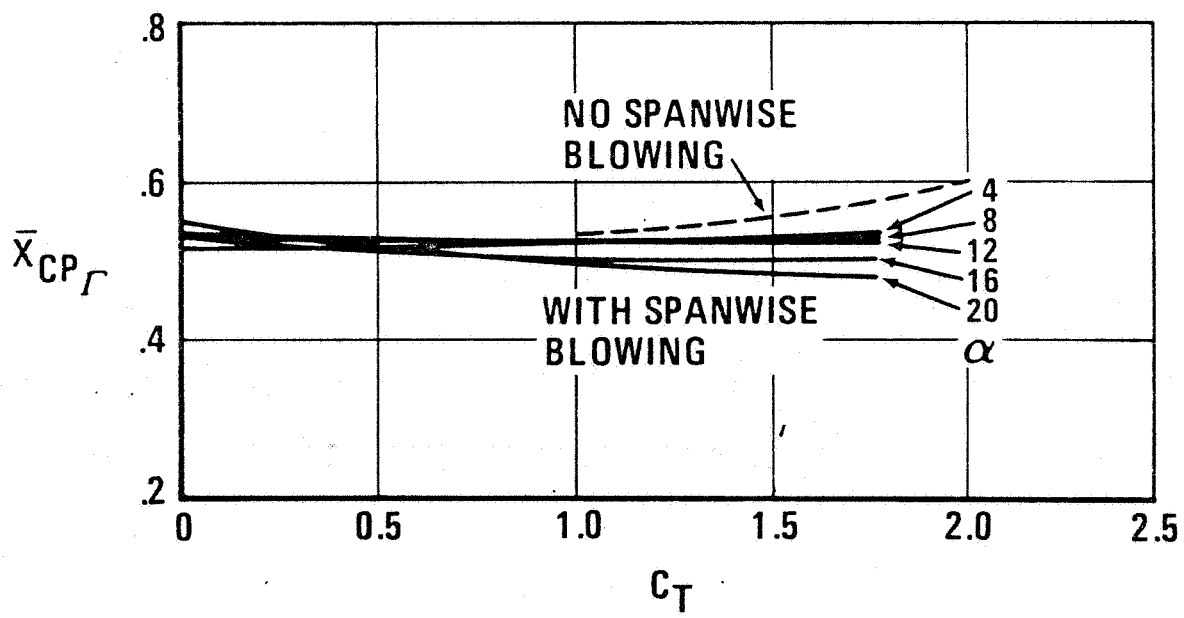

j. $\bar{X}_{cp_\Gamma}$ vs C_T $\delta_{TE} = 30^o$ with Spanwise Blowing

Figure BB-2 Supercirculation Lift, Drag, and center-of-Pressure-Location Increments due to VEO-wing Flap Deflection and Blowing from General Dynamics' Powered Research Model of Reference 3. Mach = .2

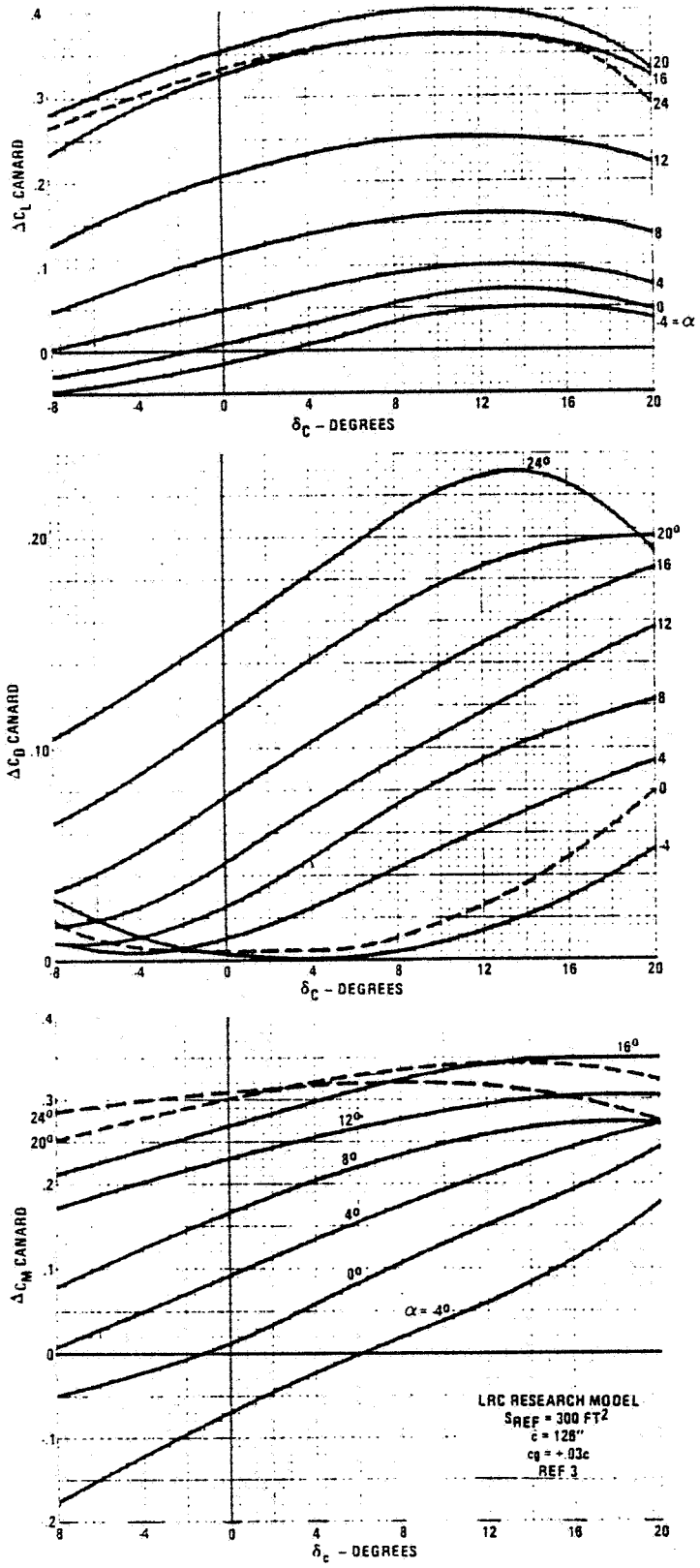

Figure BB-3 Lift, Drag, and Pitching-Moment Increments Due to Canard Deflection from General Dynamics Powered Research Model of Reference 3, Mach = .2